SILK BIOMATERIALS FOR CONTROLLED DRUG DELIVERY

A dissertation submitted by

Eleanor M. Pritchard

in partial fulfillment of the requirements for the degree of

Doctor of Philosophy
in
Biomedical Engineering

TUFTS UNIVERSITY
Medford, MA, USA

May 2011

Advisor: David Kaplan

Silk Biomaterials for Controlled Drug Delivery

by

Eleanor M. Pritchard

Submitted in partial fulfillment of the requirements for the degree of Doctor of Philosophy in Biomedical Engineering

Abstract

Despite the multitude of applications, no system currently exists for controllable, sustained, long-term drug delivery via fully degradable implants. To address this need, polymeric systems have been studied and while there are a number of biomaterials available for drug delivery devices, purified silk fibroin protein is a unique material particularly well suited to controlled release applications. Implants derived from silk exhibit the requisite biocompatibility and degradation profile for implantable applications, but also possess the necessary material properties to provide a sufficient diffusion barriers (even for small molecule drugs) and highly-controllable material features that can in turn be used to precisely tailor drug release behavior.

Studies have suggested that a particular desired release profile adapted to the target drug delivery application can be obtained by varying polymer coating formulation and processing parameters, but the systematic characterization of these effects necessary to achieve tight control has never been undertaken. Release of the small molecule adenosine from a variety of silk-based drug delivery systems was examined to correlate fundamental relationships between material features (e.g., processing conditions, crystallinity, degumming time, layer thickness, etc.) and resulting release kinetics. Characterizing and modeling these effects led to development of an integrated model that incorporated multiple control points that could be modulated to achieve specific target release profiles. The predictive accuracy of the model was confirmed by comparing theoretical release predictions to experimental release behavior.

Degradation also played a role in drug release both in cases of freely diffusible drugs and for drugs bound to the silk matrix. Degumming time, film fabrication process and coating thickness impacted degradation of the silk carriers and release kinetics. Strategies to control local proteolytic degradation via proteinase inhibitors and proteolytic enzymes were demonstrated.

Silk drug delivery implants have significant potential clinical applications due to the features above, including treatment of neurological disorders, stabilization and delivery of antibiotics and incorporation of signaling molecules into tissue engineering scaffolds. These fundamental and application-driven *in vitro* and *in vivo* studies showed that hydrophobic, hydrophilic, small and large molecule drugs can be entrapped and released from silk-based devices with tight control of the release kinetics through manipulation of the implant processing and material properties.

Acknowledgements

This project was supported by grant R01NS058780 from the National Institute of Neurological Disorders and Stroke and by the Epilepsy Research Foundation through the generous support of the Arlene and Arnold Goldstein Family Foundation.

I would like to thank my research committee, David Kaplan, Sergio Fantini, Catherine Kuo, James E. Schwob and Anthony Barry for all of their guidance, support and inspiration. I am especially grateful to David for challenging and supporting me and giving me the opportunity to work on such a range of exciting projects. I am also grateful to Anthony for offering me such excellent and thought-provoking discussions every time I asked for advice.

I would like to thank my colleagues at Tufts and wonderful collaborators, especially Andrew Wilz, Cory Szybala, Tianfu Li and Detlev Boison at the R.S. Dow Neurobiology Laboratory. I would like to thank Xiao Hu for his assistance with FTIR and DSC and the drug delivery mini-group (Dan Hines, Nick Guziewicz and Jeney Zhang) for all their advice, feedback and guidance. I would also like to thank Lindsay Wray for her assistance with SDS-PAGE, Lee Tien, Biman Mandal, Danielle Rockwood and Evangelia Bellas for advice on bone tissue engineering, and Michaela Reagan for assistance and advice on chemotherapy delivery and cancer cell culture. I would like to thank Xiaoqin Wang for teaching me to fabricate silk microspheres and guidance on silk drug delivery and Bruce Panilaitis for his advice on numerous projects.

I would like to offer special thanks to my undergraduate students, especially Tom Valentin for his assistance on many projects.

Finally, I would like to thank my family for their tireless love and support, especially my Aunt Dana and Uncle Edward, my step-father George, my sister Elizabeth and above all my mother Sarah.

Table of Contents

List of Tables and Figures

SILK BIOMATERIALS FOR CONTROLLED DRUG DELIVERY

1. Silk fibroin biomaterials for controlled release drug delivery

1.1. Introduction

The systemic periodic administration of drugs, such as via oral delivery or repeated injections, has been the primary mode of drug delivery for decades. However, this approach suffers from many disadvantages. One of the major disadvantages of periodic, systemic delivery is its inability to achieve sustained zero order release, a term that signifies that at the steady state, the rate of drug release remains constant (Acharya and Park, 2006). Sustained zero order release is critical as therapeutic efficacy and safety are dependent on maintaining a drug concentration within the range specified by the maximum safe concentration (C_{max}) and the minimum effective concentration (C_{min}). For drugs with a narrow therapeutic index (the ratio of C_{max}/C_{min}), a tightly controlled, nearly constant release rate is necessary (Langer, 1980).

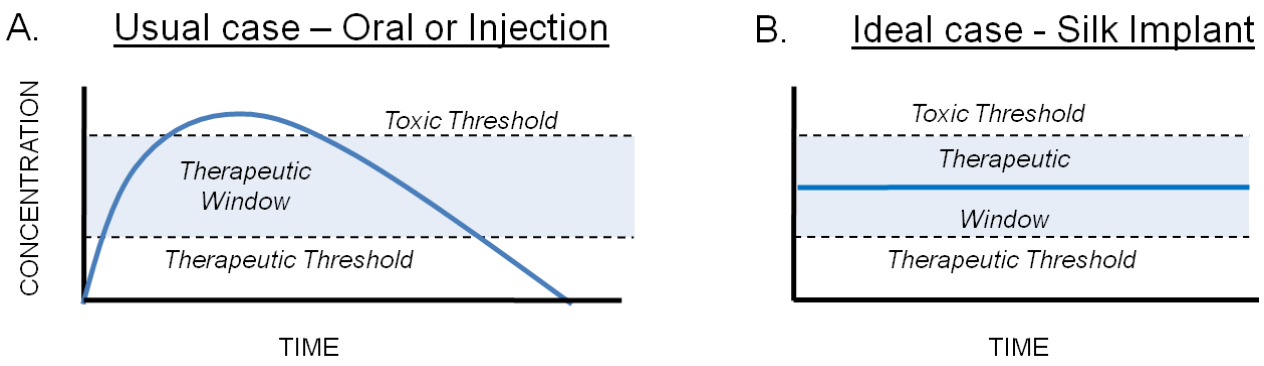

Figure 1.1. Plasma drug levels as a function of time for the usual and ideal case of drug administration. Dashed lines indicate the toxic threshold (concentration at which the maximum safe concentration (C_{max}) is exceeded), therapeutic threshold (concentration at which the minimum effective concentration (C_{min}) is exceeded) and therapeutic window (range of plasma concentrations between C_{max} and C_{min}). (A) Usual systemic administration (for example, subcutaneous bolus injection, oral administration via pill, etc.): drug concentration at the target site increases and reaches a peak as drug passes from the injection site or GI tract into the bloodstream and reaches the target site, but drops off as the drug is metabolized, eliminated from the bloodstream, etc. Once the local concentration drops below the therapeutic threshold, it no longer elicits a therapeutic effect. In order to enable re-entry into the therapeutic range, repeated drug administration is necessary and results in a sawtooth pattern of plasma drug levels. (B) Ideal case: a controlled, sustained release silk drug carrier is implanted or injected at the target site of therapeutic effect and the encapsulated drug is engineered to release within the target therapeutic window for the desired time frame (days, weeks, months, etc.) (Modified from Langer, 1980)

Systemically administered drugs must be distributed throughout the entire body and large doses are usually required to maintain sufficient drug concentration at the target site, resulting in unwanted side effects (Langer, 1980). Issues of patient compliance (Lebovits *et al*., 1990), convenience (Danckwerts and Fassih, 1991) and cost (Daugherty and Mrsny, 2006) also suggest that alternatives to systemic periodic administration of drugs would be attractive. Controlled, sustained drug delivery from implanted polymer drug depots offers numerous advantages over traditional periodic systemic administration including enhanced efficacy and cost-efficiency, reduction or elimination of unwanted side effects, increased patient convenience and compliance, and drug levels that are continuously maintained in a therapeutically desirable range without

peaks and valleys (Langer, 1980). “Sustained release” is defined as “prolonging the action of a single dose,” while “controlled release” is defined as “capable of releasing drugs by reproducible and predictable kinetics” (Heller and Hoffman, 2004).

To meet this need, many synthetic non-degradable materials or implantable pumps have been proposed, but biodegradable implants alleviate the need for surgical removal of the materials after the conclusion of therapy (Danckwerts and Fassih, 1991). Polylactide-co-glycolide (PLGA) systems have received considerable attention due to their ability to degrade *in vivo* and their customizable degradation rates and properties. PLGA implants can be easily processed and their degradation rate and physical and mechanical properties are adjustable over a wide range by changing the polymer molecular weight or copolymer ratio. However, PLGA suffers from numerous severe disadvantages (see Table 1.1). Degradation of PLGA implants proceeds via a random, bulk hydrolysis of ester bonds in the polymer chain with subsequent possible premature scaffold failure. In addition, release of acidic degradation products can cause local irritation and drug instability. Not only does PLGA incite local inflammation, the material has been shown to stimulate an immune response against incorporated proteins (Gupta *et al*., 1998, Lavelle *et al*., 1999, O’Hagan *et al*., 1991), a serious concern for therapeutic protein delivery. Many PLGA material formats require harsh processing conditions that might inactivate sensitive drugs during device loading.

Table 1.1. Comparison of the Properties of Silk Fibroin and PLGA for Biomedical Implants

	Silk	**PLGA**
Safety	FDA approved	FDA approved
Controllability	Degradation rate and physical and mechanical properties controllable via regulation of molecular weight or beta sheet content (crystallinity) (Wenk *et al*., 2010-2)	Degradation rate and physical and mechanical properties controllable via changing of molecular weight or copolymer ratio (Puppi *et al*., 2010)
Biodegradation	Biodegrades *in vivo* via proteolysis to non-toxic products (Horan *et al*., 2005; Wang *et al*., 2008-1)	Biodegrades *in vivo* via random, bulk hydrolysis to acidic products which can cause adverse tissue reactions (Puppi *et al*., 2010) and drug degradation (Varde and Pack, 2007)
Degradation Lifetimes	Weeks to years depending on material format, processing and beta-sheet content (Horan *et al*., 2005; Wang *et al*., 2008-1)	Degradation lifetimes 2-5 months depending on copolymer ratio (Hicker *et al.*, 2002)
Biocompatibility	- Less inflammation than PLGA or collagen (Meinel *et al*., 2005) - Well tolerated by immune system (Seo *et al*., 2009, Panilaitis *et al., 2003*) - Supports cell growth, proliferation and differentiation (Acharya *et al.*,2008; Wang *et al*., 2006)	- PLGA incites local inflammation (Daugherty *et al*., 1997) - Encapsulation in PLGA stimulates immune response against incorporated proteins (Gupta *et al.*, 1998, Lavelle *et al*., 1999, O'Hagan *et al*., 1991) - Lack of cellular adhesion and interaction (Puppi *et al*., 2010)
Processing	Entirely aqueous processing or organic solvent processing options (Vepari and Kaplan, 2007; Lawrence *et al.*, 2008)	Harsh processing: typically organic solvent evaporation or hot-melt processing (Jain, 2000)
Stabilizing Effects	Enzymes stored in silk films retained significant activity over 10 months, even stored at 37^{o}C (Lu *et al*., 2009)	Potential protein damage from : - Organic solvents used in processing (Bilati *et al.*, 2005) - Local acidity during degradation (Varde and Pack, 2007) - Aggregation during encapsulation (Wang *et al*., 2004)
Sterilization	Numerous sterilization options including gamma radiation, ethylene oxide and autoclaving (Omenetto and Kaplan, 2010-1)	Few suitable sterilization techniques - PLGA scaffolds susceptible to degradation and/or morphological degeneration by high temperature and pressure (Holy *et al*., 2001)

Naturally derived biodegradable materials generally offer superior biocompatibility and cell support compared with synthetic degradable materials like PLGA (Panilaitis *et al*., 2003). However, these naturally derived materials frequently lack the necessary controllability and material properties needed for long-term sustained release applications. Drug carriers made from naturally derived polymers tend to degrade rapidly and become highly permeable or disintegrate upon exposure to aqueous body fluids, releasing drug loads over short time frame (Puppi *et al*., 2010; Siepmann *et al*., 2008; Abletshauser *et al*., 1993). The advantages and disadvantages of commonly used naturally-derived biodegradable polymers are summarized in Table 1.2.

Table 1.2. Pros and cons of naturally derived biodegradable polymers under investigation for biomedical applications (Puppi *et al*., 2010)

Polymer	**Advantages**	**Disadvantages**
Collagen	• Low antigenicity • Good cell-binding properties (natural extracellular matrix (ECM) component)	• Low biomechanical stiffness and rapid degradation • Some crosslinking agents are associated with toxicity
Chitosan	• Good cell adhesion, proliferation and differentiation • Good biocompatibility • Antibacterial activity • Acceptable host response	• Mechanically weak and unstable • Incapable of maintaining a predefined shape • Material properties are highly influenced by impurities (purification requirements)
Hyaluronic Acid	• No host immune response • Ease of chain size manipulation and large scale production • Natural ECM component • Good biocompatibility and viscoelastic properties	• Water soluble • Rapid resorption and short residence time in the tissue
Alginates	• Crosslinking under very mild condiditons • Injectable gel format for minimally invasive administration	• Mechanical weakness • Difficult to sterilize and to handle • Material properties are highly influenced by impurities (purification requirements)
Starch-based materials	• Inexpensive • Diversity of material properties	• Unknown *in vivo* degradation behavior (specific enzymes required may be absent from target implantation sites)
Bacterial cellulose	• High purity	• Difficult to sterilize and to handle

	• High tensile strength • Good biocompatibility • Good host immune tolerance	• Mechanical weakness • Further investigations of *in vivo* behavior needed
Dextrans	• Many hydroxyl groups available for chemical modification	• Resistant both to protein adsorption and cell adhesion (modification required to enhance cell adhesion) • Mechanical weakness • Further investigations of *in vivo* behavior needed

Silk fibroin is a biologically derived protein polymer isolated from domestic silkworm (*Bombyx mori*) cocoons that possesses unique properties that me*et al*l the requirements for implantable drug delivery applications (Table 1.3). Silk exhibits excellent biocompatibility (Leal-Egaña and Scheibel, 2010, Tang *et al*., 2009, Meinel *et al*., 2005, Panilaitis *et al*., 2003) and tunable, robust mechanical properties (Altman *et al*, 2003). Silk degrades to non-toxic products *in vivo* and the degradation time course of silk implants can be controlled from weeks to years via regulation of beta sheet content (crystallinity) during processing (Horan *et al*., 2005; Wang *et al*., 2008-1). While many polymer drug carrier systems require harsh manufacturing conditions that can degrade or denature incorporated therapeutics (shear, heat, exposure to organic solvents or extreme pH, etc.), silk can be entirely aqueously processed using mild, ambient manufacturing conditions (Vepari and Kaplan, 2007, Lawrence *et al*., 2008). Silk has also been found to exert a stabilizing effect on encapsulated enzymes, even at elevated temperatures (Lu *et al*., 2009, Lu *et al*., 2010-1). A comparison of the features of silk with the features of PLGA (Table 1.1) and the features of other natural biodegradable polymers (Table 1.2) shows that silk combines the advantages of both, exhibiting the controllability and mechanical strength of PLGA with the biocompatibility and mild processing options of naturally derived polymers.

Table 1.3 Summary of the Advantages of Silk Fibroin for Drug Delivery

Properties of silk fibroin
• Biocompatible – FDA approved, little to no immunogenicity, cytotoxicity or inflammation • Biodegradable – Degradation lifetimes controllable via beta-sheet content/crystallinity • Excellent mechanical properties • Aqueous and ambient processing or solvent processing options • Stabilizing effects on incorporated drugs • Facile chemical functionalization • Diverse material formats • Highly controllable material properties and release kinetics

Silk has been processed into a variety of useful material formats including porous tissue scaffolds that structurally mimic extracellular matrix (ECM) (Sofia *et al*., 2001) and sustained release drug carriers (Numata and Kaplan, 2010-1; Wenk *et al.*, 2010). In addition, the material properties of silk biomaterials can be tightly controlled during processing and fabrication (Vepari and Kaplan, 2007). The combined diversity of material formats available for drug delivery and tight controllability of the various drug carriers result in a broad range of possible silk-based systems available for clinical and scientific applications (Omenetto and Kaplan, 2010-2).

While other silk based drug-delivery material formats will be mentioned, emphasis will be placed on implantable or injectable silk drug delivery systems capable of functioning as long-term, sustained release depots (i.e. release duration lasting days to weeks). Particular emphasis will be placed on the controllability of the silk drug delivery systems reviewed to demonstrate how the tunability of silk material properties can be used to achieve specific target release profiles.

1.2. Silk Fibroin Biomaterials for Drug Delivery

For use in biomedical applications, silk fibroin must be purified from the glue-like sericin (which causes an immune response in humans) by degumming in boiling alkaline solution (most

commonly sodium carbonate) (Altman *et al*., 2003, Vepari and Kaplan, 2007). Degummed fibers can be used to manufacture fiber biomaterials including yarns, sutures, rope and woven fabrics (Horan *et al.,* 2006). However, most drug carriers are prepared from regenerated silk fibroin, which is prepared by solubilizing the degummed silk fibroin in hot salt solution (dissolution temperatures vary; typically range from 50-70^{o}C), then dialyzing out the salt to obtain an aqueous solution. While materials fabricated from regenerated silk fibroin can be mechanically inferior to the native silk fiber, they exhibit superior mechanical properties compared with similar scaffolds or drug carriers prepared from other biomaterials (Kim *et al.*, 2005-1; Kluge *et al*., 2010).

Silk solution can be processed into porous silk sponges, silk films, nano- or microscale coatings, hydrogels and nano- and microparticles (Figure 1.2). For solvent processing, regenerated silk fibroin solution can be lyophilized and then dissolved in solvent (usually 1,1,1,3,3,3-hexafluoro-2-propanol (HFIP)). Depending on the intended application and the properties of the active compound to be delivered, drug loading of silk biomaterials is typically achieved by: (1) "bulk loading" (i.e. mixing drug and silk solutions prior to material fabrication) (2) surface decoration with the drug(s) of interest (either via chemical coupling or adsorption) or (3) use of composite systems.

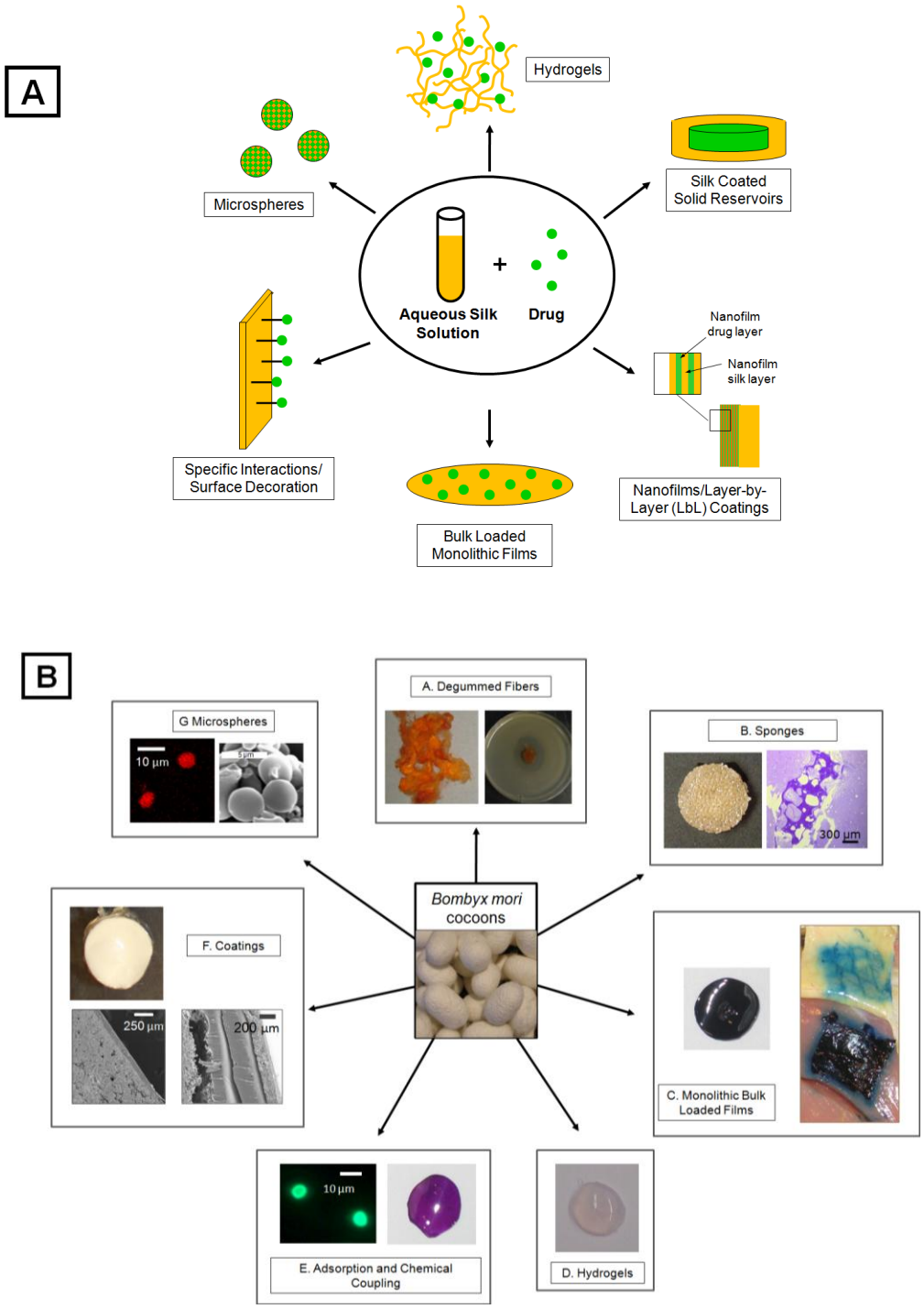

Figure 1.2. Silk material formats for drug delivery (A) schematic representations of silk drug carriers (B) examples of silk drug delivery biomaterials (a) degummed silk fibers loaded with the antibiotic rifampicin inhibit growth of a bacterial lawn (b) porous sponges and histology sections of silk sponges implanted in rat brains (crystal violet stain) (c) bulk loaded film containing indigo carmine dye (d) sonication induced gel contained phycoerythrin (e) microspheres coated with fluorescein-coupled silk and silk film loaded with nile red via adsorption (f) silk encapsulated reservoir and scanning electron microscope (SEM) images of single and multiple coatings (g) red fluorescent bead loaded silk microspheres and SEM of silk microspheres.

Biodegradable drug carriers like silk exhibit release rates dependent on diffusion of drug through the silk, degradation of the silk polymer carrier, or a combination of both mechanisms (Luo *et al*., 2000). The contribution that degradation plays in the overall release profiles depends on the diffusivity of the drug through the polymer carrier as well as the rate of degradation of the carrier. For low molecular weight drugs free diffusion results in rapid release while higher molecular weight molecules or bound/adsorbed proteins are less able to diffuse and rely more on degradation to liberate the entrapped drug (Luo *et al*., 2000).

Diffusion can be controlled via carrier morphology (geometry, number/thickness of coating, porosity) and manipulation of polymer properties including degumming time and crystallinity/beta-sheet content. Degradation behavior of silk is dependent on many factors including silk processing and material properties (organic solvent vs. aqueous processing, crystalline content, silk concentration and porosity (Horan *et al*., 2005)), silk material format (Arai *et al*., 2004, Yang *et al*., 2009), type and concentration of enzyme (Arai *et al*., 2004) and immune system response (Horan *et al*., 2005)

1.2.1 Degummed Silk Fibers and Fabrics

Degummed silk fibers have been processed into various material formats (including woven fabric, yarns, ropes and knitted scaffolds) for a range of biomedical applications including, soft-tissue reinforcement meshes (Horan *et al*., 2006), sutures (Altman *et al*., 2003) and tissue engineered ligaments (Liu *et al*., 2008), tendons (Chen *et al*., 2010-1) and blood vessels (Enomoto *et al*., 2010). Notably, Altman *et al*. confirmed the utility of silk for ligament tissue engineering by matching the complex and demanding mechanical requirements of a native

human ACL and demonstrating support of cell attachment, expansion and differentiation (Altman *et al.,* 2002).

Drug eluting silk fibers could be used to enhance the therapeutic efficacy of biomedical fabrics, yarns and knitted contructs. Choi *et al*. "dyed" silk fibers with two antibiotics (doxycycline and ciprofloxacin) using a range of conditions, including varied dyeing temperature, time, and dyebath pH and treatment of silk with NaOH for varied times to induce chemical and conformational changes. Varied processing and differences in the antibiotic properties affected the total drug loading and release behavior. Fibers loaded with doxycycline and ciprofloxacin were able to inhibit local growth of *Staphylococcus epidermis* (measured using a zone of inhibition assay compared with a standard antibiotic-impregnated Sensi-Disc) for at least 48 hours and 24 hours, respectively (Choi *et al.,* 2004).

1.2.2. Tissue engineering scaffolds

1.2.2.1. Porous 3D sponges

3D porous silk sponge scaffolds can be prepared from silk solution using either aqueous or organic solvent (HFIP) processing. The necessary interconnected pores in the sponges can be generated using salt leaching, gas foaming or freeze-drying (Nazarov *et al*., 2004, Hardy *et al*., 2008). The morphological and structural features of the scaffolds produced by salt leaching depend on a number of variables including silk fibroin concentration, solid salt particle loading, salt particle size, and the use of aqueous- or HFIP-derived process (Wang *et al.,* 2006). Degradation behavior of silk sponges is also affected by processing (pore size, aqueous- or HFIP-derived, silk concentration, etc.) (Wang *et al*., 2008-1, Park *et al*., 2010, Makaya *et al*.,

2009). The pore size of sponges made from lyophilized hydrogels is dependent on silk fibroin concentration, gelation temperature and Ca^{2+} concentration (Kim *et al*., 2004).

Incorporation of drug carriers into porous tissue engineering scaffolds can provide high local concentrations and spatiotemporal control of signaling growth factors. While sponges have predominantly been studied as tissue engineering scaffolds, the diversity of processing options and tight control of the resulting structural and mechanical properties suggests silk sponges might exhibit a similar degree of controllability as a drug carrier.

Demura and Asakura successfully immobilized glucose oxidase in porous silk membranes (approx. 50-300 μm thick, depending on porogen concentration and swelling) using polyethylene glycol (PEG) as a porogen (Demura and Asakura, 1991) and reported that porosity increased with PEG concentration and increased membrane permeability to glucose and NaCl. Aspirin loaded silk foams prepared by freeze-drying an aqueous solution of silk and aspirin exhibited burst release followed by constant release lasting approximately 2.5 days. Average pore size and morphology of the silk foam was dependent on freezing temperature, pH and methanol treatment (Tsukada *et al*., 1994). Lyophilized silk fibroin hydrogel matrices loaded with monoclonal antibodies exhibited sustained release for up to 38 days. Antibody release was primary governed by hydrophobic/hydrophilic silk-antibody interactions and secondarily altered by hydration resistance related to beta-sheet (crystalline) density of the matrix (Guziewicz et al., 2011).

Highly porous 3D silk scaffolds loaded with insulin growth factor I (IGF-I) were fabricated using freeze drying and porogen leaching, achieving sustained release of bioactive growth factor from a substrate suitable for tissue growth. Methanol treatment after freeze-drying increased β-sheet content in the scaffolds, reduced initial burst, achieved higher total cumulative

IGF-I release and increased release duration. The bioactivity of the released IGF-I was validated both with an MG-63 proliferation assay and by chondrogenic differentiation of hMSCs (Uebersax *et al*., 2008). NGF-loaded porous tube-shaped scaffolds for nerve guides were prepared by filling molds with an aqueous solution of NGF and silk, freezing drying (freezing at -20 or -196^{o}C) and methanol treating to induce β-sheet formation and water insolubility of the silk matrices. Methanol treatment did not appear to alter NGF bioactivity and increased the proportion of bound NGF. NGF release was prolonged over 3 weeks and supported PC12 cell differentiation with neurite outgrowth. Freezing temperature (-20 or -196^{o}C) influenced carrier porosity, morphology, release rate and absolute cumulative NGF release (Uebersax *et al*., 2007).

1.2.2.2. Electrospun nanofiber mats

Electrospinning is a process which produces nanoscale fibers (diameters from 50–500 nm) with microscale-interconnected pores (Zhang *et al*., 2009). Nanofiber mat scaffold properties (geometry, fiber diameter, orientation and porosity) can be controlled via manipulation of the solution properties and operating parameters (Zhang *et al*., 2009). This controllability and the structural similarity to native ECM make electrospun silk biomaterials excellent substrates for tissue engineering (Jin *et al*., 2004).

Electrospun silk nanofiber mats were bulk-loaded with BMP-2 and/or hydroxyapatite nanoparticles (nHAP) by mixing the growth factor and nanoparticles into the aqueous silk solution prior to electrospinning. The mild aqueous processing resulted in retention of the encapsulated BMP-2's bioactivity, as evidenced by increased osteogenesis of hMSCs cultured for 31 days on BMP-2 loaded scaffolds compared to empty control scaffolds (Li *et al*., 2006).

1.2.3. Silk fibroin films

1.2.3.1 Bulk loaded monolithic silk films

Bulk loading of silk films represents a very simple, straightforward method for preparing monolithic drug delivery implants: silk solution is mixed with the drug solution of interest, films of the desired thickness and surface area are cast, dried, then treated to produce the desired material and release properties. Silk film processing options include controlled slow drying (Lu *et al.*, 2010-2), water annealing (Jin *et al*., 2005), stretching, compressing (Demura *et al*., 1989), and solvent immersion (including methanol (Hofmann *et al*., 2006), ethanol (Miyairi *et al*., 1978), glutaraldehyde (Acharya *et al*., 2008-2), 1-ethyl-3-(3-dimethyl aminopropyl) carbodiimide (EDC) ((Bayraktar *et al.*, 2005). Silk films can also be dried at ambient conditions and left untreated to retain their water solubility. These films dissolve rapidly upon exposure to an aqueous environment (Figure 1.3).

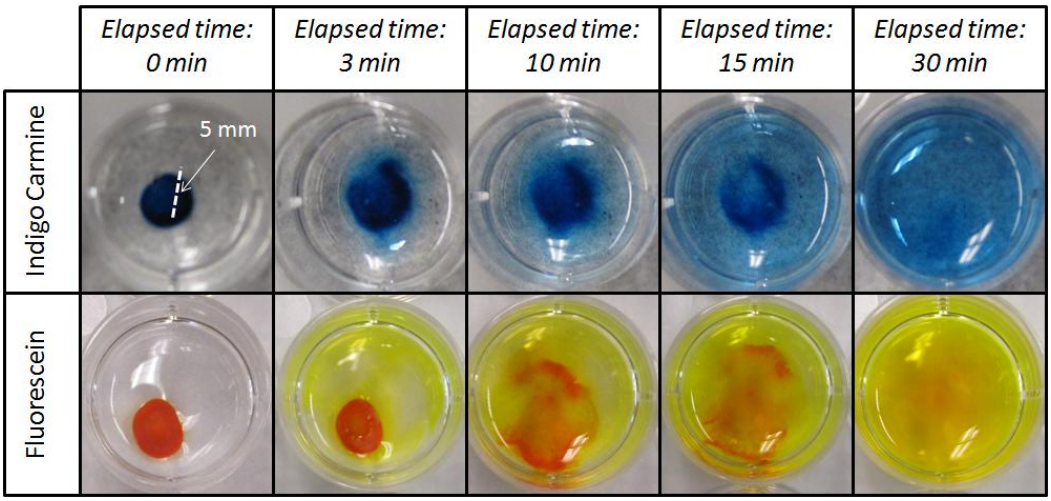

Figure 1.3. Time-course of untreated, dye-loaded silk film dissolution in water. Untreated silk films loaded with indigo carmine (top row) and fluorescein (bottom row) begin dissolving within 3 minutes of exposure to 37^{o}C water and are fully dissolved after 30 minutes of immersion.

Permeability of silk films to small molecule pharmaceuticals (5-fluorouracil, vitamin C, resorcinol, sodium phenolsulfonate and benzyltrimethylammonium chloride) was found to be dependent on release buffer pH and drug properties (Chen *et al*., 1994). Hofmann *et al*. prepared monolithic bulk loaded films from aqueous silk solution containing dextrans of different molecular weights (4, 10, 20 and 40 kDa) and horseradish peroxidase (HRP) and lysozyme (Lys) as model proteins. Release from the films was sustained approx. 4 weeks and release behavior was related to film crystallinity and drug properties (including molecular weight and adsorption to the silk) (Hofmann *et al*., 2006). The release of FITC-labeled dextrans of varying sizes (4, 10, 20, 40 kDa) from methanol-treated and untreated silk fibroin films has also been reported. For a mechanism-based semiempirical model derived from Fickian diffusion, the estimated diffusion coefficient was smaller for the methanol-treated films than for the untreated films and decreased linearly with increasing analyte molecular weight (Hines and Kaplan, 2011). Blended polyurethane-silk films loading with heparin exhibited sustained release over 24 hours and high controllability (release rate and total cumulative heparin release could be controlled via total heparin load in the film, composition ratio of silk fibroin to polyurethane, and film thickness (Liu *et al*., 2009).

The effects of various post-drying treatments (water annealing for 6 hours, methanol treating for 8 min, stretching) on stabilization and release of horseradish peroxidase (HRP) loaded silk fibroin films and silk films prepared with 30% glycerol were examined. HRP release was linearly related to silk degradation, which can be controlled through manipulation of the silk film structure (in this case, beta-sheet content related to type and duration of post-drying treatment). The effects of various post-drying treatments (water annealing for 6 hours, methanol treating for 8 min, stretching) on stabilization and release of horseradish peroxidase (HRP)

loaded silk films and silk films prepared with 30% glycerol were examined. HRP release was found to be linearly related to silk degradation, which could be controlled by modifying the silk material properties. Along with material properties and degradation behavior, processing conditions also determined ratio of untrapped (readily released by diffusion) and trapped protein (bound and inactive until released by proteolytic degradation). The authors also reported that, due to the unique periodic hydrophobic-hydrophilic domains of silk's structure, HRP in films retained more than 90% of the initial activity after two months at 37^{o}C. This study demonstrates that silk films are capable of both retention of enzyme activity and controllable release kinetics (Lu *et al*., 2010-2).

It is worth noting that numerous studies have demonstrated that silk films can be used as a stabilizing immobilization matrix for proteins and enzymes that reduces their sensitivity to pH, temperature and proteinase-induced degradation. Proteins stabilized in silk films include glucose oxidase (Lu *et al*., 2009), immunoglobulin G-binding *Staphylococcal* protein A (Kikuchi *et al.*, 1999), uricase (Zhang *et al*., 1998), tyrosinase (Acharya *et al*., 2008-2), lipase (Lu *et al*., 2009), β-glucosidase (Miyairi *et al*., 1978), horseradish peroxidase (Lu *et al*., 2009, Lawrence *et al*., 2008, Wu *et al*., 2006), myoglobin (Wu *et al*., 2006) hemoglobin (Wu *et al*., 2006, Lawrence *et al*., 2008), catalase (Wu *et al*., 2006) and green fluorescent protein (GFP) (Putthanarat *et al.*, 2004).

1.2.3.2. Silk Coatings

The addition of silk fibroin film coatings offers many potential advantages including controlled release drug delivery (Wang *et al*., 2007-1, Wang *et al*., 2008-2), improved release kinetics (increased diffusion barrier to drug release, decreased carrier degradation, enhanced

controllability, etc. (Wang *et al*., 2007-1, Wang *et al*., 2007-2, Gobin *et al*., 2006)), added mechanical strength (Wang *et al*., 2007-2) and improved cell-biomaterial interfaces (Mathur and Gupta, 2010, Gobin *et al*., 2006, Wang *et al*., 2008-2, Nathwani *et al.,* 2009, Chang *et al.,* 2009).

Wang *et al*. developed a simple, entirely aqueous layer-by-layer (LbL) assembly technique for applying nanoscale silk film coatings to solid substrates. This stepwise deposition process resulted in robust, stable material coatings that were highly controllable. Film thickness increased linearly with the number of silk fibroin layers deposited, and control of individual layer thickness (ranging from a few to tens of nanometers) could be achieved via manipulation of the concentrations of silk and salt and the rinsing method (Wang *et al.,* 2005).

Later studies validated the use of silk nanofilm coatings as a delivery vehicle for various bioactive drugs, including small molecules and proteins. Wang *et al*. prepared silk nanofilm coatings loaded with model drugs Rhodamine B, Even Blue and Azoalbumin and found that control of β-sheet crystal content and the multilayer structure of the silk coatings could be used to effectively regulate the release kinetics of the incorporated compounds (Wang *et al*., 2007-1). Silk nanofilm coatings loaded with heparin, paclitaxel, and clopidogrel were validated as stent coating materials both *in vitro* and *in vivo* (Wang *et al.,* 2008-1).

Wang *et al*. demonstrated that ultrathin silk coatings applied to PLGA and alginate microspheres significantly retarded release of model drugs (horseradish peroxidase and bovine serum albumin), particularly when the silk coatings were methanol treated. Along with increasing the diffusion barrier, silk coatings provided mechanically stable shells and delayed degradation. Further, the process could be carried out aqueously, did not alter protein loading or microsphere morphology, and was characterized by controllable coating thickness and crystalline content (Wang *et al*., 2007-2).

Silk fibroin coatings on liposomes have also been shown to improve release kinetics, cell targeting and liposome uptake (Gobin *et al*., 2006, Cheema *et al*., 2007). Silk coatings on quantum dots reduced particle aggregation and improved their water solubility, clearance and biocompatibility (Nathwani *et al.,* 2009, Chang *et al.,* 2009).

Silk coatings can also be applied to solid drug dosage formats, including pills for oral delivery and dry powder reservoirs for long-term release. Bayraktar *et al*. examined tablets of theophylline dip-coated with thin silk films containing different amounts of polyethylene glycol (PEG) and silk films cross-linked with EDC. Silk films prepared with 17% PEG or cross-linked with EDC produced zero-order release of theophylline over 5 and 7 hours, respectively. Varied PEG concentration and use of multiple EDC cross-linked coatings allowed tuning of drug release kinetics (Bayraktar *et al.,* 2005). Press-fit tablets prepared from blends of silk powder and theophylline for oral delivery exhibited decreasing release rate as the fibroin content in the tablets increased (Katayama et al., 2000).

1.2.4. Microspheres and nanoparticles

Silk fibroin microspheres have been prepared using a variety of methods, including use of lipid template (Wang *et al*., 2007-3), spray-drying (Hino *et al.,* 2000; Hino *et al*., 2003; Yeo *et al*., 2003), ethanol and freezing-induced self-assembly (Cao *et al*., 2007, Bessa *et al.,* 2010-1, Bessa *et al.,* 2010-2), salting out (Lammel *et al.,* 2010), water-in-oil emulsification (Imsombut *et al*., 2010), laminar jet break-up of an aqueous silk solution (Wenk *et al*., 2008) and casting and dissolution of PVA-silk blend films (Wang *et al*., 2010). Though silk nanoparticles have been successfully fabricated (Mathur and Gupta, 2010; Numata and Kaplan, 2010; Kundu et al.,

2010), nanoparticles are less well-suited to depot applications as their small size and high surface area to volume ratio leads to rapid drug release.

Wang *et al*. developed a method to prepare silk fibroin microspheres less than 2 μm in diameter by adding aqueous silk solution to phospholipid, freeze-drying and treating with methanol or sodium chloride to remove the lipid vesicle template and induce beta-sheet formation in the silk. Release duration of enzymatically active horseradish peroxidase from these microspheres varied from 10 to 15 days depending on duration of sodium chloride treatment, demonstrating that release kinetics can be controlled via processing and that bioactivity of loaded drugs is maintained during encapsulation (Wang *et al.,* 2007-3).

Silk microspheres produced by ethanol precipitation exhibited predictable sizes (ranging from 0.2 - 1.5 μm) and size distributions that could be controlled through manipulation of preparation conditions, including amount of ethanol additive, freezing temperature and concentration of silk fibroin solution (Cao *et al*., 2007). Bessa *et al*. took advantage of the mild processing conditions associated with this approach to encapsulate growth factors. They demonstrated successful loading and sustained release of therapeutically relevant amounts of BMP2, BMP9 and BMP14 over 14 days (Bessa *et al*., 2010-1). In a later study, the authors confirmed the bioactivity of the BMP2 released from these silk microspheres *in vitro* and *in vivo* (Bessa *et al.,* 2010-2).

Salting out represents another simple aqueous preparation method for silk microparticles. Lammel *et al*. used potassium phosphate salting out to prepare smaller silk fibroin particles (approx 0.5- 2 μm). Secondary structure and particle size could be controlled via pH and protein concentration, respectively. Particles were loaded post-fabrication with small molecule model drugs (alcian blue, rhodamine B, and crystal violet) by simple absorption (Lammel *et al.,* 2010).

Wenk *et al*. fabricated drug loaded silk fibroin spheres using the laminar jet break-up of an aqueous silk solution (induced by nozzle vibration at controlled frequency and amplitude) followed by methanol treatment or water vapor annealing to increase β-sheet content. The resulting spheres were 101 – 440 μm in diameter with sizes dependent on nozzle diameter and processing conditions. Salicyclic acid, propanolol hydrochloride and insulin-like growth factor I (IGF-I) loaded microsphere exhibited release durations of 1 day, 20 days and >7 weeks, respectively. This process was characterized by high encapsulation efficiency (close to 100% prior to methanol treatment), retention of bioactivity and controllable release kinetics that were tunable via silk concentration (Wenk *et al.,* 2008).

Recently, Wang *et al*. developed an easy, efficient, aqueous-based method for micro- and nanosphere preparation based on the phase separation of blended silk fibroin and polyvinyl alcohol (PVA) (Wang *et al*., 2010). Size (ranging from 300 nm up to 20 μm) and polydispersity could be controlled via manipulation of the silk to PVA ratio or the application of ultrasonication. In addition, they demonstrated loading and release of model drugs spanning a broad range of sizes, hydrophobicities and charges (BSA, dextran and rhodamine B) from their silk particles, demonstrating their broad utility as drug delivery vehicles (Wang *et al.,* 2010).

1.2.5. Hydrogels

Beta sheet rich, physically crosslinked hydrogels have been formed from silk fibroin solution by sol-gel transition (Wang *et al*., 2008-3). Gelation is affected by temperature, silk fibroin concentration, and pH (Kim *et al*., 2004; Wang *et al*., 2006) and can be accelerated by additives (Wang *et al*., 2006), sonication (Wang *et al*., 2008-3) or vortexing (Yucel *et al*., 2009). Mechanical properties (Kim *et al*., 2004), porosity (Kim *et al.,* 2004; Wang *et al.*, 2008-3) drug

release behavior (Hanawa *et al*., 1995) and gelation time can be tightly controlled through manipulation of the processing conditions. In addition, sonication and vortex induced silk hydrogels both exhibit a useful range of timeframes for cell, drug or microsphere encapsulation prior to final gel-setting (Wang *et al*., 2008-3; Yucel *et al*., 2009). Gelation conditions can be selected to ensure silk solution remains in a liquid state long enough to mix in other components and inject, then completes gelling *in vivo* at the injection site.

Hanawa *et al*. prepared silk fibroin hydrogels loaded with the vitamin B_1 derivative benfotiamine (BTMP) and studied release behavior as a function of silk fibroin and glycerol content and the presence of BTMP-solubilizing β-cyclodextrin. The authors found that BTMP release from the silk hydrogels decreased with increasing silk fibroin concentration, firmness and glycerol concentration. The addition of β-cyclodextrin increased BTMP release and silk hydrogel firmness (Hanawa *et al*., 1995).

Fang *et al*. investigated rapid release of buprenorphine (a morphine-like analgesic) from silk fibroin hydrogels prepared from varied silk concentrations and molecular weight silk proteins and found that material properties and drug release rate could be controlled via manipulation of the concentration of silk and by blending of silks of different molecular weights. Zero-order release was observed for the 4 hour duration studied (Fang *et al*., 2006).

Hydrogels made from a genetically modified version of recombinant silk containing periodic incorporation of elastin-like blocks (for increased solubility and gelation rate and decreased total crystallinity and bioresorption rate) termed silk-elastinlike polymer (SELP) hydrogels have been applied to a wide range of drug delivery applications, including delivery of plasmid DNA (Megeed *et al*., 2004), adenovirus (Megeed *et al*., 2004, Greish *et al*., 2009, Gustafson *et al*., 2009), fluorescently labeled probes (Cappello *et al*., 1998), cytochrome C,

vitamin B 12, theophylline (Dinerman *et al*., 2002) and recombinant protein mitotoxin (Cappello *et al*., 1998). For reviews of synthesis, characterization and drug delivery from silk-elastinlike polymers, see Haider *et al*., 2004 and Gustafson and Ghandehari, 2010.

1.2.6. Surface Modification

Surface modification is frequently used in silk tissue engineering scaffolds to alter cell attachment and proliferation, especially attachment of the asp-gly-asp (RGD) peptide to various silk biomaterial surfaces to increase cell attachment (including films (Sofia *et al*., 2001), fibers (Chen *et al*., 2003) and sponges (Meinel *et al*., 2004)). Surface modification (including physical adsorption or chemical immobilization) can also be used to attach therapeutics of interest to silk implants. Because free diffusion of adsorbed or chemically coupled drugs is limited, drug release from these silk implants is more dependent on silk degradation-rate.

1.2.6.1 Adsorption

Due to the hydrophobicity of silk surfaces, proteins and other molecules can be attracted or repelled depending upon the pI and hydrophobicity of the protein and pH of the solution. Attraction between silk and other proteins can be used to decorate silk biomaterials by simple absorption.

Lipase immobilized via adsorption on silk fibers exhibited enhanced pH and temperature stability and increased enzymatic activity (Chen *et al*., 2010-2). 3D porous silk sponges fabricated using either the aqueous or HFIP salt-leeching technique were loaded with basic fibroblast growth factor (bFGF) by dropping bFGF solution onto the sponges and allowing adsorption to occur overnight at 4^{o}C. The affinity between the bFGF and the silk substrate

resulted in incomplete drug release *in vitro* (approx. 30% over 3 days), but exposure to proteinase induced silk matrix degradation, increasing total cumulative release and release duration (approx. 85-90% over 8 days). When immersed in proteinase the HFIP-derived scaffolds degraded (and thus released bFGF) more slowly than the aqueous-derived scaffolds. *In vivo,* injected bFGF disappeared within 24 hours of administration while implanted bFGF-loaded silk sponges sustained release over 14 days (Wongpanit *et al*., 2010). Karageorgiou *et al*. adsorbed BMP-2 onto silk films by covering the silk films with a BMP-2 solution for 2 hours at room temperature followed by rinsing and drying. Adsorbed BMP-2 on silk films caused an increase in hMSC osteogenesis compared with controls, though less of an increase in hMSC osteogenesis than covalently coupled BMP-2 on silk films (Karageorgiou *et al*., 2004).

1.2.6.2. Chemical Immobilization

Silk fibroin can be functionalized using the amino acid side chain chemistry, particularly carbodiimide chemistry, which uses amine or carboxyl groups on silk for modification.

Karageorgiou *et al*. used carbodiimide chemistry to directly immobilize BMP-2 onto silk fibroin films. Covalently coupled BMP-2 remained bioactive and was retained on the film surface longer than adsorbed BMP2 (50% remaining bound after 4 weeks in culture media, compared with only 10%). Increased osteogenesis was observed for hMSCs seeded on the surface of BMP-2 decorated films compared with hMSCs exposed to similar amounts of soluble BMP-2 supplementation in the media, which the authors attribute to enhanced stability and higher protein concentrations in the local microenvironment (Karageorgiou *et al*., 2004). Wenk *et al*. used diazonium coupling to decorate silk fibroin films with a sulfonated moiety to bind fibroblast growth factor 2 (FGF-2) and found that silk films decorated with sulfonic acid

exhibited high, controllable binding of bioactive FGF-2 (Wenk *et al*., 2010-1). NeutrAvidin was coupled to silk fibroin in solution and the silk retained its self-assembly features post-reaction. NeutrAvidin was also coupled to silk microspheres and then further functionalized with biotinylated anti-CD3 antibody, resulting in specific binding of the functionalized microspheres to CD3 positive T-lymphocytic cells (Wang and Kaplan, 2011).

Vepari and Kaplan generated stable immobilized HRP gradient patterns within 3D silk fibroin sponges by activating the HRP with carbodiimide then distributing the activated HRP using either diffusion or convection coupled with diffusion. Slope and activity of the immobilized HRP gradients were controlled by varying the volume and starting concentration of activated HRP solution. Covalent immobilization of HRP increased enzyme stability versus time and temperature compared to adsorbed HRP. This simple, mild process could be extended to gradient immobilization of a variety of proteins or small molecules (Vepari and Kaplan, 2006).

For additional information on conjugation of drugs to silk fibroin biomaterials and chemical modification of silk fibroin for biomedical applications, see Murphy and Kaplan, 2009.

1.2.7. Composite Materials

Biomaterials fabricated by integrating multiple different material formats (composite materials) offer numerous advantages, including enhanced control of release kinetics and the possibility to combine both precise control of temporal and spatial biological signals and physical/mechanical cues in a single construct. For an excellent review of silk composite biomaterials, see Hardy and Scheibel, 2010.

Silk microspheres suspended in silk hydrogel (sometimes called "plum pudding hydrogels") provide minimally invasive injectable delivery that restricts drug delivery to the target site (Figure 1.4).

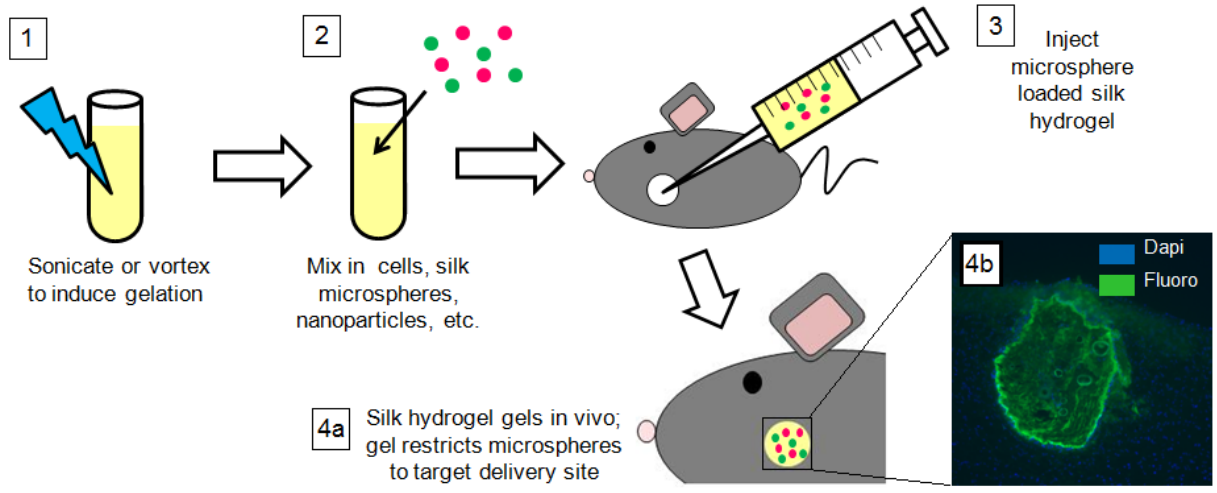

Figure 1.4. Schematic of injectable drug delivery based on silk microspheres suspended in silk hydrogel. (1) Gelation of silk solution is induced via sonication or vortexing (2) While the silk solution is still in the solution state, micropsheres (or cells, nanoparticles, protein, etc.) are mixed in. (3) The microsphere loaded hydrogel is injected at a desired target site and completes the gelling process *in vivo* (4a) Silk hydrogel restricts drug-releasing microspheres at the delivery site of choice, then degrades after therapy is completed. (4b) Frozen histology cross section of a 1 µL silk hydrogel containing fluorescein-labeled silk microspheres injected into a mouse brain. Green fluorescence shows fluorescein and blue fluorescence indicates 4',6-diamidino-2-phenylindole (DAPI) staining of local brain tissue nuclei. 14 days post injection, hydrogel restricts microspheres to injection site (microscope image courtesy of Abraham Boskovitz, Charest Lab).

Madduri *et al*. prepared silk films to release glial cell line-derived neurotrophic factor (GDNF) and nerve growth factor (NGF) and incorporated them into nerve guidance conduits. The conduits exhibited sustained release of bioactive GDNF and NGF *in vitro* over 4 weeks and when cultured with various neuronal cells from chicken embryos induced an augmented length and rate of axonal outgrowth parallel to the aligned nanofibers (Madduri *et al*., 2010). To achieve controlled spatial distribution of multiple growth factors in a tissue engineering scaffold, Wang

et al. prepared silk microspheres loaded with bone morphogenetic protein 2 (BMP-2) and insulin-like growth factor I (IGF-I) using the lipid-template technique and incorporated them into aqueous-derived silk porous scaffolds using a gradient process. Both growth factors formed deep and linear concentration gradients in the scaffolds and were shown to induce and control hMSC differentiation (Wang *et al*., 2009).

Numerous composite biomaterial scaffolds based on combining silk biomaterials with other polymer drug delivery systems have also been developed. Wenk *et al*. prepared silk fibroin sponges carrying embedded poly(lactide-co-glycolide) microparticles (PLGA) microspheres to release insulin-like growth factor I (IGF-I) and found that embedment into the silk scaffolds led to slower release rates (approx. 80-100% total IGF-I release after 50 days from free microspheres, compared with approx. 20-40% from composite scaffolds) (Wenk *et al*., 2009). Mandal and Kundu prepared porous silk scaffolds (using the freeze-drying method and silk from the Indian non-mulberry tropical tasar silkworm, *Antheraea mylitta*) embedded with calcium alginate microspheres and calcium alginate/silk fibroin blended microspheres for controllable, dual protein release. Release behavior of the model proteins tested (bovine serum albumin and FITC–Inulin) was dependent on composition of the microspheres and silk content (in weight %) of the scaffold, suggesting release kinetics can be tightly controlled. Embedding microspheres in silk sponges provided a mechanically stable shell and increased the diffusion barrier to the encapsulated protein drugs (Mandal and Kundu, 2009). Controlled drug release from multilayer films based on a blend of silk fibroin and self-degradable gelatin have been studied. Release of model compounds (trypan blue, FITC-inulin and FITC-BSA) was dependent on the ratio of silk fibroin to gelatin and the buildup of layers. Modeling of release behavior suggested a combined mechanism of Fick's diffusion and polymer degradation (Mandal *et al.*, 2009).

Because of the ability of silk to support cell-growth, silk biomaterials are also useful for cell-mediated drug delivery. Modified bone marrow stromal cells (hMSCs) transduced with an adenovirus overexpressing BMP-2 were seeded on premineralized aqueous derived silk scaffolds to repair mandibular defects in a rat model. The premineralized scaffold alone alone did not result in repair, while the premineralized scaffolds seeded with BMP-2 expressing hMSCs increased new bone formation and local bone mineral density. Silk fibroin films were shown to be suitable substrates for adenosine releasing adenosine kinase deficient (Adk -/-) embryonic stem cells. Differentiation of Adk -/- ESC-derived glial precursor cells was efficient on silk films and the amounts of adenosine released by the cell cultures on silk substrates (420 ng/mL) were considered to be of therapeutic relevance (Uebersax *et al*., 2006).

1.3. Conclusions

Silk exhibits attractive properties for controlled, sustained release. Silk can be aqueously processed into a diverse range of material formats for implantable or injectable sustained release drug depots, possesses remarkable mechanical properties, biodegrades over controllable timeframes and preserves stability during encapsulation and storage. Silk biomaterials, with their excellent material properties, unique and versatile processing options, biocompatibility and highly tunable material properties, are poised to significantly impact not only drug delivery, but also many other biomedical applications including tissue engineering, implant coating, imaging and diagnostics. Implantable polymer systems capable of achieving controlled, sustained release of drugs locally have the potential not only to improve existing therapies, but also to deliver drugs that previously have been impossible to administer due to rapid clearance, poor stability or failure to reach the site of action via systemic delivery.

Thus far, research in the field of silk-based drug delivery has demonstrated the exceptional potential of this unique biomaterial to overcome the limitations that have prevented other polymer controlled release implants from achieving widespread medical utility. The diversity of drugs and silk material formats reported in the literature suggests that these properties can be exploited to meet a multitude of urgent clinical needs. Further, numerous control points have been identified for each of the silk material formats described in this review, suggesting that with sufficient characterization, release behavior will eventually be highly tunable.

Though many promising control points have been identified, further work is needed to characterize the relationships between silk processing and/or material properties and resulting drug loading and release kinetics. Chapter 2 of this thesis describes control points used to manipulate drug release from silk encapsulated reservoir, including material diffusivity and coating thickness, and describes an integrated model to predict outcomes from manipulation of multiple control points to achieve different target release kinetics.

As with any implantable drug delivery system, there is a critical need to relate *in vitro* release behavior with *in vivo* performance. Because silk degrades via proteolysis and local enzymatic activity may vary from implantation site to implantation site, the effects of *in vivo* degradation and strategies to control local degradation will be especially important to investigate. Chapter 3 of this thesis discusses the effect of degradation rate on release behavior. Potential strategies to manipulate local degradation (via material properties and processing and via controlled release of proteinases and inhibitors from the drug carriers) are also discussed in Chapter 3.

Following the chapters on characterization and manipulation of the fundamental driving forces behind drug release from silk biomaterials, specific applications of controlled release silk implants that have shown promise *in vitro* and *in vivo* are presented, including localized delivery of the small-molecule anticonvulsant adenosine for the prevention of epileptic seizures (Chapter 4), delivery and stabilization of antibiotics for prevention of infection and treatment of infectious disease (Chapter 5) and incorporation of small molecule drug delivery into silk scaffolds for tissue engineering (Chapter 6).

2. Basic material features of silk implants as control points for tunable diffusion driven drug release from silk biomaterials

2.1 Introduction

2.1.1. Fundamentals of silk fibroin structure and assembly

Bombyx mori cocoon silk consists of hydrophilic "glue-like" sericin proteins and the hydrophobic structural protein fibroin, which is comprised of a heavy chain (approximately 390 kDa) and a light chain (approximately 25 kDa) bonded together via disulfide bond (Kaplan *et al.*, 1997; Matsumoto *et al.*, 2006). Silk fibroin's heavy chain is a natural block copolymer composed of large hydrophobic blocks, much smaller hydrophilic blocks and two large hydrophilic blocks at the chain ends at the N and C termini (Kim *et al.*, 2004, Matsumoto *et al.*, 2006)

Silk fibroin's primary structure is dominated by the amino acids glycine, alanine, serine, valine and tyrosine with characteristic repetitive sequences of GAGAGS, GAGAGY and GAGAGVGY (Matsumoto *et al.*, 2006). These structural elements (large hydrophobic domains consisting of short side chain amino acids) permit tight packing of stacked sheets of hydrogen bonded anti-parallel chains, forming the characteristic anti-parallel beta-sheet secondary structure that gives silk fibroin its strength and resilience (Vepari and Kaplan, 2007).

Beta-sheet stacking occurs such that methyl groups and hydrogen groups of opposing sheets interact to form the inter-sheet stacking in the crystals. Strong hydrogen bonds and Van der Waals forces generate a structure that is thermodynamically stable. The inter- and intra-chain hydrogen bonds form between amino acids perpendicular to the axis of the chains and the fiber (Vepari and Kaplan, 2007, Kaplan *et al.*, 1997)

Silk in its prespun water soluble state (referred to as silk I) is relatively unstable, and when converted to the more energetically stable, β-sheet rich silk II (via shearing, drawing,

heating, spinning, exposure to solvent, etc.) the transition is considered essentially irreversible (Kaplan *et al.*, 1997). *In vivo*, glandular silk is assembled into highly ordered, β-sheet rich fibers via extraction of water, changes in pH and salt concentration and mechanical stresses during fiber spinning that induce chain alignment (Hofmann *et al.*, 2006). These processes (along with others that manipulate the factors involved in the assembly process) have been biomimetically exploited *in vitro*. For example, silk films that are cast and air-dried overnight at ambient conditions retain their silk I conformation (and water solubility) (Kaplan *et al.*, 1997). Once the films are treated with methanol, localized dehydration results in β-sheet formation by pulling off the ordered water molecules that surround fibroin's hydrophobic moieties in the solution state (Matsumoto *et al.*, 2006). Stretching of the films mimics the stresses encountered in the spinning process, forming β sheet by inducing chain alignment.

These approaches to controlling assembly *in vitro* have also been successfully applied to fibroin hydrogels. In solution, the hydrophobic regions of the silk assemble physically, and then eventually organize into β-sheet rich crosslinked hydrogels (Matsumoto *et al.*, 2006) with homogenous crosslinking distribution (Nagarkar *et al.*, 2010). Following degumming, dissolution and dialysis, regenerated silk fibroin solution is predominantly in the random coil conformation with a small amount of β-sheet (Nagarkar *et al.*, 2010). When gelation occurs, a conformational transition from a predominantly random coil state to a predominantly β sheet is induced that renders the silk hydrogel network stable and water insoluble (Kim *et al.*, 2004). This process, including the transition from the random coil-dominated solution state to the physically assembled pre-crosslinked early gel state to the stable, β-sheet rich hydrogel state is represented schematically in Figure 2.1.

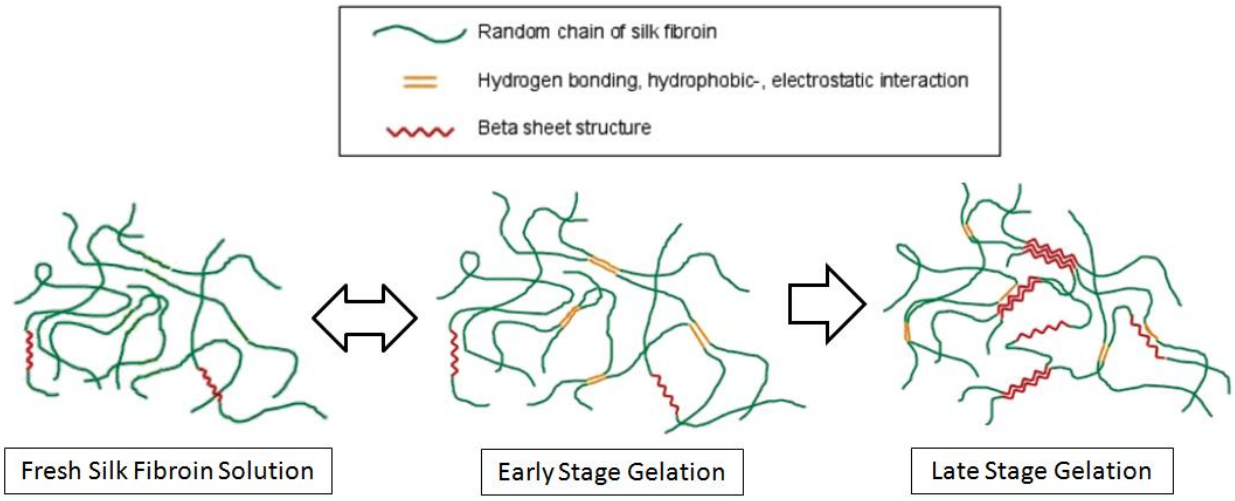

Figure 2.1. Schematic of silk fibroin hydrogel assembly process. After dialysis, silk fibroin proteins are in the solution state with a relatively small amount of β-sheet and little to no intermolecular bindings. During early stage gelation, weaker interchain interactions occur which do not involve significant changes in secondary structure (such as non-β-sheet forming hydrogen bonding, hydrophobic interactions, electrostatic interactions, etc.). The transition from solution to this early stage of gelation may be reversible. These interactions weaker interchain interactions lead to formation of a permanent, physical hydrogel (i.e. late stage gelation) which is characterized by stable, irreversible β-sheet formation (adapted from Matsumoto *et al.*, 2006).

Because gelation occurs due to the formation of inter- and intramolecular interactions among the fibroin protein chains (including hydrophobic interactions and hydrogen bonds), manipulations that increase the ability of the fibroin chains to interact (inputting energy into the solution, reducing repulsion among the chains or dehydrating to remove the water molecules that stabilize the hydrophobic moieties in solution) leads to increased physical crosslinking and shorter gelation times (Kim *et al.*, 2004).

2.1.2. Controlling drug release from silk drug delivery biomaterials

In the field of drug delivery, constant, sustained, tightly controlled release from fully degradable implants remains a major unmet challenge. Target ideal release profiles vary greatly

amongst different drug delivery applications. As such, it is critical that any polymer system proposed for drug delivery applications exhibit release behavior that is highly controllable so that target release rates can be precisely dialed in. This is particularly important for drugs with narrow therapeutic indexes (the ratio of the maximum safe concentration (C_{max}) and the minimum effective concentration (C_{min})). For these drugs, achieving a tightly controlled release rate is essential to achieving maximum safety and efficacy.

It is also essential that a polymer drug delivery system be not only controllable, but versatile: multiple control points must be understood so that certain constraints can be preset as needed. For many applications, several of the material parameters will be fixed and unavailable as control points for release manipulation. For example, an implant may need to be a certain geometry and size based on the target implantation site or a tissue engineered construct may need to degrade at a certain rate that's been optimized for new tissue ingrowth and scaffold remodeling. An understanding of how numerous relevant material features of silk biomaterials affect release would allow target release rates to be achieved without compromising other necessary implant specifications.

Rate of drug release from implantable biodegradable systems like silk is dependent on diffusion of drug through the polymer, degradation of the polymer carrier, or a combination of both mechanisms (Luo *et al*., 2000). The contribution that degradation plays in the overall release profiles depends on the diffusivity of the drug through the polymer carrier as well as the rate of degradation of the carrier. For low molecular weight drugs free diffusion results in rapid release while higher molecular weight molecules or bound/adsorbed proteins are less able to diffuse and rely more on enzymatic degradation or chemical hydrolysis to liberate the entrapped drug (Luo *et al*., 2000). The rates of drug diffusion from a polymer carrier and degradation of the

polymer carrier are affected by both the intrinsic properties of the drug and the polymer carrier and the external environment (see Figure 2.2) (Yoshioka *et al*., 2008).

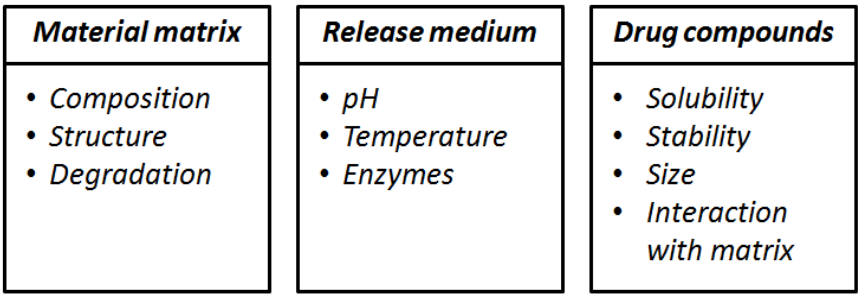

Figure 2.2. Factors that influence drug release from degradable polymer delivery devices with key examples of each category: Factors relating to the matrix material, factors relating to the release medium (i.e., site of implantation or injection) and factors relating to the drugs being released (adapted from Fu and Kao, 2010)

Each of the factors that can impact drug release can potentially be manipulated to control release behavior, though some are more practical to manipulate than others. Manipulation of drug properties (for example, PEGylation to increase apparent drug size (Roberts *et al*., 2002) or manipulation of aqueous solubility through salt formation (Østergaard *et al*., 2005)) can be effective, but increase system complexity and must be thoroughly screened to ensure they do not diminish or alter efficacy. Release rate can also be controlled via carrier morphology [(geometry, number/thickness of coating, etc. (Dorta *et al*., 2002, Zhang *et al*., 1995)], but for some applications implant geometry may be constrained.

Manipulation of polymer properties to control release is one of the most popular approaches because these manipulations are relatively simple yet effective *in vitro* and result in systems with constant, predictable, easily controlled release behavior. A huge body of work has been published characterizing material features and their effect on release for many natural and synthetic implantable polymers. Some qualitative results have been published on the

relationships between processing conditions and release in silk based biomaterials; however a rigorous, quantitative review of the relevant parameters comparable to existing literature for other implantable polymers is still needed.

External environmental properties including pH, temperature and enzymes (Yoshioka *et al*., 2008) can also impact drug release kinetics and polymer degradation *in vivo*. This is particularly true of natural biomaterials like silk, collagen and HA that are subject to enzymatic degradation. Previous studies suggest local enzyme manipulation through controlled-release could also be effective in modulating the environmental conditions at the site of implantation.

2.1.3. Controlling drug diffusion from silk encapsulated reservoirs

A critical problem, from a pharmaceutical standpoint, is the ability to achieve zero-order release rates. Based on geometry and diffusion-driven release mechanisms, cumulative drug release from rectangular slab polymer devices is inversely proportional to the square root of time (Higuchi, 1963). These monolithic drug delivery devices are frequently criticized for their inability to achieve zero-order release. Reservoir systems (comprised of a drug core surrounded by polymer film) also exhibit drug release rates dependent on the rate of drug diffusion through the polymer membrane, but are easier to engineer to produce zero order release kinetics (Langer and Peppas, 1981). Use of dry powder drug reservoirs allows reservoir loading far above the drug's solubility. Drug concentration at the internal wall is continuously maintained above the saturation concentration of the drug, resulting in near zero-order release (Langer and Peppas, 1981) followed by a phase of first-order release once the concentration of drug in the core drops below the saturation concentration (Zhou *et al*., 2010). Reservoir systems typically use non-degradable polymers, including silicone rubber and ethylene-vinyl acetate copolymer. Studies

have shown that a particular, desired release profile adapted to the target drug delivery application can be obtained by varying the polymer coating formulation and processing parameters (Siepmann *et al.*, 2008).

Though these non-degradable reservoir systems offer the great advantage of producing near zero-order release kinetics (a constant rate of drug diffusion across the polymer membrane is maintained due to the coating's nondegradability), they also have several disadvantages. They are generally permeable only to low molecular weight drugs (MW < 600), carry the risk of "dose dumping" in the event of membrane ripping and can be more expensive to make than other types of controlled release systems (Langer and Peppas, 1981). They require surgical removal at the end of therapy, and the necessary retrieval operation can be much more traumatic that the original insertion (Ma *et al*., 2006). The hormone-releasing implantable contraceptive device Norplant, for example, was approved for use by the Food and Drug Administration (FDA) in 1990, but was withdrawn in 2002 due to complications associated with implant removal (The Practice Committee of the American Society for Reproductive Medicine, 2004).

Several natural and synthetic degradable polymers have been studied as coating materials, but they generally fail to produce zero-order release kinetics or sustained release durations due to their material properties. Most studies that investigate natural polymers for pill encapsulation focus on delivery of total drug load within short time frames corresponding to residence times in the target gastro-intestinal organs (on the order of hours) for improved oral delivery. However, given its unique material properties, silk fibroin encapsulated reservoirs are expected to achieve the controllable, zero-order, sustained release behavior characteristic of synthetic, non-degradable polymer coated reservoirs while maintaining biocompatibility and degrading after the completion of therapy.

The polymer coated solid reservoir drug delivery device was selected for studies investigating silk material formats for controllable release based on its potential to achieve zero-order release and because this system biased control of the release rate in favor of the polymer coating, maximizes drug loading relative to total implant volume and total drug loading is easy to accurately assess.

The predominant model drug in these studies is the brain's endogenous anticonvulsant, adenosine. Adenosine has therapeutic potential in a range of disorders (described at greater length in Chapter 5), but is rapidly metabolized, causes severe systemic side effects and has difficultly crossing the blood-brain barrier. Other model dyes and proteins are also included in some studies, including azoalbumin, reactive-red 120, rifampicin, and indigo carmine (Figure 2.3). These model compounds were selected to span a broad range of potential therapeutics and due to their ease of quantification.

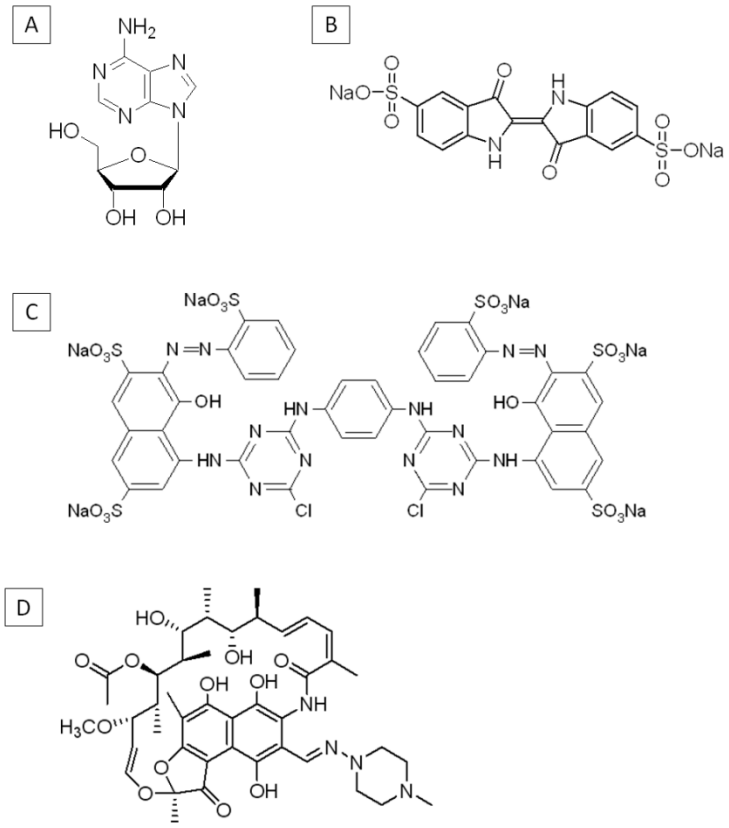

Figure 2.3. Model drugs used in studies of controllable diffusion-driven drug delivery from silk biomaterials (A) adenosine (MW=267.24), (B) indigo carmine (MW = 466.35), (C) reactive red 120 (MW = 1469.98), (D) rifampicin (MW = 822.94).

For simplicity of device design, adenosine release from silk encapsulated reservoirs is assumed to be purely diffusion driven. Literature on biodegradable polymer reservoirs recommends that these systems be designed to degrade following, but not during, therapeutic delivery (Langer and Peppas, 1981; Stamatialis *et al*., 2008). This alleviates the need for retrieval while maintaining a simple, diffusion-driven release mechanism. Silk is ideally suited to this approach, as it has been processed into extremely slow-degrading material formats. Note that specific, practical strategies for delaying degradation until completion of therapy (via sustained inhibitor release or manipulation of material properties) are discussed in Chapter 3.

The following model describes purely diffusional drug release from an encapsulated reservoir based on an early time approximation ($M_t/M_\infty \leq 0.6$) of Fick's second law (Saltzman, 2001):

$$M_t \approx \frac{AD_iC_0}{L}\left(t - \frac{L^2}{6D_i}\right) \qquad \textit{Equation 2.1.}$$

Where: M_t = amount of drug released at time t
D_i = Diffusion coefficient of species i (units: [cm^2/hr])
A = Surface area of the slab (units: [cm^2])
L = thickness of the membrane (units: [cm])
C_o = Initial concentration of species i in reservoir (units: [g/cm^3])

Taking the derivative of M_t with respect to time (in order to obtain an equation describing release rate, dM_t/dt), for the early time approximation ($M_t/M_\infty \leq 0.6$) we obtain the following equation:

$$\frac{dM_t}{dt} \approx \frac{AD_iC_0}{L} \qquad \textit{Equation 2.2.}$$

Because this model is derived from the underlying drug release mechanisms, it includes relevant parameters to test and provides predicted relationships between release profiles and the parameters represented in the model. The physicochemical properties of the silk material directly involved in the mechanisms of drug release represented in models of drug release from polymer coated reservoirs suggest specific control points of interest, especially diffusivity of the polymer (D_i) and path length (L). Fitting experimental data to these models can enhance understanding of the system and, in cases where the predictions of the model are matched to the collected data, less empirical data collection could ultimately be required to make predictions of drug release. In other words, to achieve a specific target release profile for a given application, the implant could

be designed based on predictions of a model that has been previously confirmed as valid. Release testing could then be performed on a much more limited number of samples than would be required to pursue a guess-and-check empirical approach. When quantitative relationships are characterized, they can be used to predict the effect of the individual variables on release rates.

The hypothesis tested is that predictable, consistent, quantitative relationships between individual material features and drug release parameters will be observed. Thickness of coating is predicted to scale inversely with release rate (as predicted by the Fickian diffusion model). B-sheet content and degumming time of the silk in the reservoir coating are predicted to alter diffusivity of the silk coating, thereby impacting release rate (as diffusivity is predicted to be directly related to release rate). In addition, since all variables may not impact drug release equally, these studies will help identify practical strategies for controlled small molecule release. Tunable material features will be reviewed individually (with particular emphasis on degumming time and path length) then an integrated model will be proposed.

2.2. Geometry - Path length/ silk coating thickness

Equation 2.2 suggests that implant geometry (both thickness of polymer coating and implant surface area) can be used to control release behavior and the literature provides several examples of this strategy. For example, Zhang *et al*. reported that antibiotic delivery from poly(d,l-lactide) cylinder-shaped reservoirs was dependent on drug loading, drug particle size and cylinder length. Increasing cylinder length increased release duration and decreased release rate, providing a convenient method for controlling release properties (Zhang *et al*., 1995). Woolfson *et al*. characterized drug release from torus shaped reservoir silicon reservoirs (intravaginal rings or IVRs) and reported that release characteristics could be readily modified

either by changing the thickness of the silicone sheath layer or the implant geometry. Decreasing sheath thickness decreased the diffusional pathway for the drug, increasing release rate (Woolfson *et al*., 2003).

While surface area manipulations would require use of different molds, coating thickness represents a potentially very simple, easy-to-manipulate system parameter that has been successfully employed in previous silk drug carriers. Coating thickness of silk nanofilm caps has been shown to increase with the number of silk fibroin layers deposited and silk solution dipping concentration (Wang *et al.,* 2005). Wang *et al*. prepared silk nanofilm coatings on glass substrates loaded with model compounds Rhodamine B and Azoalbumin and found that the addition of several silk capping layers significantly suppressed burst and prolonged release duration due to the increased barrier to diffusion (Wang *et al*., 2007-1). Wang *et al*. demonstrated that ultrathin silk coatings applied to PLGA and alginate microspheres significantly retarded release of model proteins (horseradish peroxidase and bovine serum albumin) by increasing the diffusion barrier (Wang *et al*., 2007-2). Bayraktar *et al*. dip-coated theophylline tablets with thin silk films for improved oral delivery. In release studies of single coated, double coated and triple coated tablets (corresponding to 26, 57, 83 μm silk coating thicknesses, respectively), the increasing barrier hindrance from the thicker coating materials significantly decreased the release rate of theophylline (Bayraktar *et al*., 2005).

Release of adenosine from silk encapsulated solid press-fit dry powder reservoirs with varying coating thickness was studied to assess the relationship between processing and coating thickness and coating thickness and release behavior.

2.2.1. Aqueous silk solution dip coating method of adenosine reservoir encapsulation

2.2.1.1 Introduction

Dip coating in aqueous silk solution represents a simple, mild method for coating a substrate of interest with silk. This strategy has been applied to the application of layer by layer (LbL) nanofilm deposition ((Wang *et al.*, 2005, Wang *et al*., 2007-1) and to delay release from theophylline tablets for oral delivery (Bayraktar *et al*., 2005), as described above. Dip coating has also been used to develop silk microtubes for blood vessel engineering (Lovett *et al*., 2007) and to coat other 3D polymer scaffolds (Petrini *et al*., 2001). We hypothesized that increasing solution concentration and increasing the number of coatings added would both linearly increase reservoir coating thickness.

2.2.1.2. Materials and Methods

2.2.1.2.1. Materials

Cocoons of *Bombyx mori* silkworm silk were purchased from Tajima Shoji Co., LTD (Sumiyoshicho, Naka-ku, Yokohama, Japan). All other chemicals including adenosine and indigo carmine were purchased from Sigma-Aldrich (St. Louis, MO).

2.2.1.2.2. Silk fibroin solution preparation

Silk fibroin was prepared from the cocoons as we have previously described (Sofia *et al*., 2001). Briefly, cocoons were boiled for the 40 minutes in a solution of 0.02 M Na_2CO_3 and rinsed, then dried at ambient conditions overnight. The dried fibroin was solubilized in a 9 M aqueous LiBr solution at 60^{o}C for 4 hours, yielding a 20% (w/v) solution. LiBr was then removed from the solution by dialyzing the solution against distilled water for 2.5 days using

Slide-a-Lyzer dialysis cassettes (MWCO 3,500, Pierce) (Figure 2.4). Silk fibroin concentration was determined by evaporating water from a solution sample of known volume and massing using an analytical balance. The silk solution was concentrated by osmotic stress as previously described (Kim *et al*., 2004). Briefly, silk fibroin aqueous solution (8% (w/v), 10 mL) was dialyzed against a 10-25% w/v PEG (10,000 g/mol) solution at ambient conditions, causing water molecules to move from the silk fibroin solution into the PEG solution through the dialysis membrane. A final concentration of silk in water of 8% (w/v) was diluted with distilled water to obtain the 4% (w/v) and 2% (w/v) solutions. All solutions were stored at 4-7^{o}C before use.

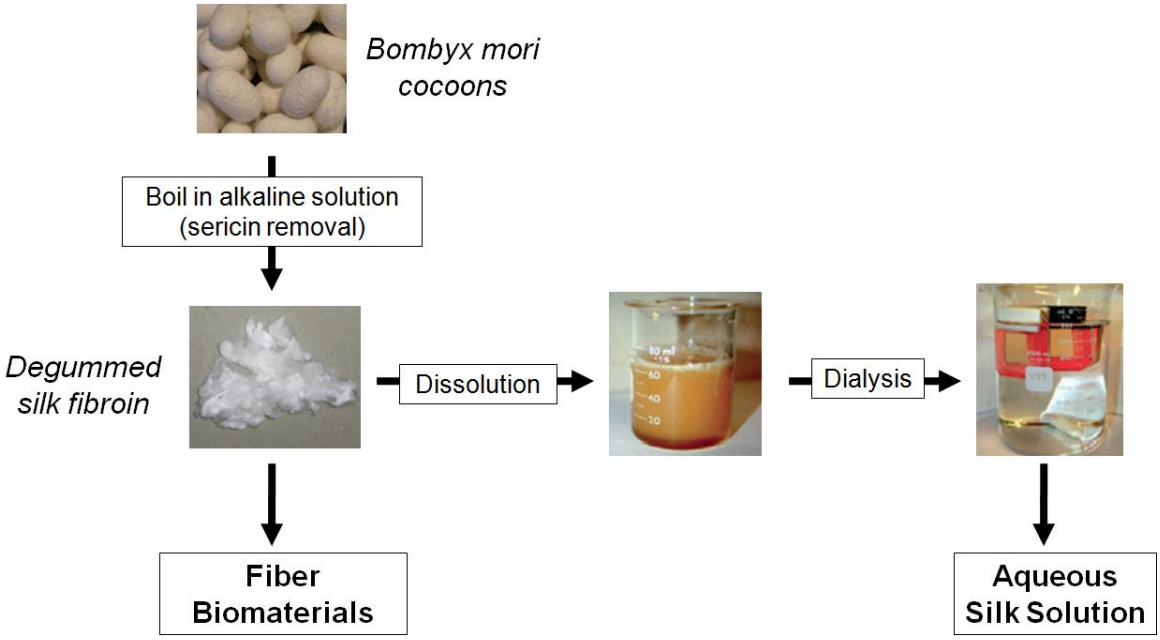

Figure 2.4. Silk fibroin preparation. *Bombyx mori* cocoons are purified from sericin via boiling in an alkaline solution. Degummed silk fibroin can be processed into fiber biomaterials including sutures, meshes, woven fabrics, yarns and ropes. To prepare aqueous silk solution, degummed silk fibroin is dissolved in lithium bromide then the lithium bromide is removed with dialysis. The aqueous silk solution can then be processed into various material formats for drug delivery.

2.2.1.2.3. Adenosine powder reservoir preparation and encapsulation

Press-fit adenosine reservoirs were prepared using an Econopress (Sigma-Aldrich, St. Louis, MO). One bolt was positioned in the press-fit chamber, approximately 100 mg of powdered adenosine was loaded into the chamber, then the second bolt was added and both bolts were manually tightened to compress the powder into solid powder reservoir form. Finished solid powder reservoirs for this study were approximately 10 mm in diameter, and 2 mm in height (these dimensions can be easily modified for future studies). Following a 15 minute incubation at -20^{o}C, the solid adenosine tablet was removed from the press (incubation at cold temperatures served to minimize drug sticking to the bolt surface thereby yielding a more smooth even surface for coating, but had no noticeable effect on drug reservoir mechanical integrity). Reservoirs selected for study were all within ± 5 mg of 70 mg. Mannitol reservoirs were fabricated for controls. Mannitol is a commonly used chemically inert filler material for compressed tablets (Ward *et al*., 1969) and has been used as a placebo for orally administered adenosine tablet studies (Graven-Nielsen *et al*., 2003). Total silk coating mass was determined by measuring the weight of the press-fit adenosine powder reservoirs with an analytical balance before and after coating.

Adenosine reservoirs were coated by dipping in aqueous silk solution at the desired protein concentration, drying for 30 min at 60^{o}C, then immersing in methanol for 5 minutes to increase β sheet content for aqueous-insolubility. No occlusion was observed where the forceps held the reservoir, as the aqueous silk solution was sufficiently non-viscous to seep into this small area during drying. Following treatment, methanol was evaporated and the residue was resuspended in PBS and assayed for adenosine content. For the study of the silk coatings, 8% (w/v) aqueous silk fibroin solution was used and the process of dipping, drying and methanol treatment was repeated until the desired number of layers was achieved (1x, 2x, 4x or 8x). For

the varied silk concentration study, the silk concentrations (in w/v) tested were 2%, 4%, 8%, 16% and 20%. For studies in which the silk concentration/coating thickness or number of silk coating layers were varied, n = 3. Uncoated adenosine tablets were tested to ensure rapid reservoir dissolution in the absence of a silk coating.

2.2.1.2.4. Release studies in phosphate buffered saline (PBS)

To determine drug release, drug loaded material formats were immersed in Dulbecco's PBS (DPBS) at 37°C. Typically, 1-2 mL of buffer was used to ensure detectable drug concentrations. At desired time points, the buffer was removed and replaced with fresh buffer to approximate infinite sink conditions (i.e., modeling immediate clearance of adenosine released from systems implanted *in vivo* into the brain parenchyma (Lesniak *et al*., 2005)). The frequent buffer replacement coupled with the 1-2 mL volume was designed to represent sink without diluting the drug concentration in the buffer below detection limits. This process is represented schematically in Figure 2.5.

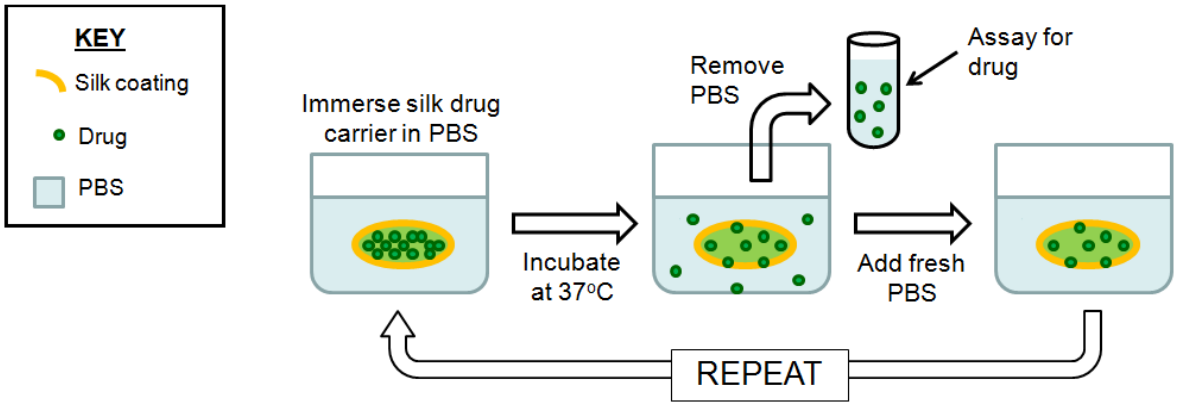

Figure 2.5. Diagram of the release study process. Material format is immersed in phosphate buffered saline (PBS) which is removed and replaced with fresh buffer at desired time points. The removed buffer is assayed for drug content.

The buffer removed periodically from the system was assayed for adenosine content by measuring absorbance at 260 nm using a UV spectrophotometer and by using a modified fluorescence assay as previously described (Wojcik and Neff, 1982). Briefly, collected PBS sample was transferred to a 1.5 mL Eppendorf tube and chloroacetaldehyde was added to a final concentration of 220 mM chloroacetaldehyde. These tubes were capped and boiled for 20 min. Boiling of mixed adenosine and chloroacetaldehyde yields the fluorescent derivative $1,N^6$-ethenoadenosine. The fluorescence of the sample was measured with a plate reader (excitation = 310 nm, emission = 410 nm) (Rosenfeld and Taylor, 1984).

At the end of the study when no additional drug was detected in the release buffer, the residual biomaterials were degraded overnight in a 1.0 mg/mL proteinase K solution at 37^{o}C and then assayed for any residual trapped drug that had not diffused from the reservoirs into the PBS.

2.2.1.2.5. Release kinetics

The release profiles were characterized by linear regression analysis by determination of regression coefficients, R^2, as zero order release is expected to correspond to constant drug release with respect to time. Values of t_{50} were taken as the time at which 50% of the drug was released from the reservoir. The data for release of drug from encapsulated reservoirs was fit using Eq. (2.3) in order to assess possible release mechanisms. M_t/M_∞ corresponds to the percent of adenosine released at time t relative to the total amount of drug in the tablet; K is a release constant and n is the release exponent indicating the type of drug release mechanism (Ritger and Peppas, 1987). The term t_0 corresponding to one unit of time t (i.e., if time is reported in hours, t_0 = 1 hour, if time is reported in minutes, t_0 = 1 minute, etc.) has been included in order to produce unitless values of K and n when the data is fitted:

$$M_t/M_\infty = K(t/t_0)^n \qquad [equation\ 2.3]$$

A fit to this equation (referred to as the Siepmann Peppas Power Law) is traditionally used to assess the relative importance of Fickian and zero order mechanisms in drug diffusion. When n=0.5, pure diffusion for drug release is present, when n=1 swelling-controlled drug release or Case II transport is indicated. Other values for n suggest anomalous transport kinetics from combined mechanisms of pure diffusion and Case II transport.

The theory behind fitting data to this equation to assess mechanism is based on the observation that, graphically, a cumulative release curve that is purely diffusion-driven will be related to the square root of time [$M_t/M_\infty = K\sqrt{t}$, as described by Higuchi (Higuchi, 1963)], while linear release curve will be described by an n of 1 because, by definition, drug release versus time is constant. However, experimental values frequently fell between 0.5 and 1, and values outside the theoretical limits (i.e, n<0.5 or n>1) were often encountered. Given the complexity of release mechanism observed experimentally (neither pure diffusion nor pure Case II release), rather than draw conclusions about release mechanisms based on n, values of n were instead applied to empirical observations about release (i.e., with increasing silk coating thickness an increase in n would suggest that the release profile from the reservoir was becoming increasingly more linear with increasing film thickness).

For linear fit, Eq. 2.3 is modified to Eq. 2.4. In this case, n is obtained from the slope of the plot of log(released%) versus log t.

$$\log(\text{released}\%) = \log(Mt/M\infty) = \log K + n \log(t/ \qquad [equation\ 2.4]$$

2.2.1.2.6. Characterization

The surface and cross-sectional morphology of the silk encapsulated reservoirs was examined by scanning electron microscopy (SEM). Cross-sectional SEM images of the coated tablets were analyzed with Image J imaging software to determine the coating thickness. For each coating thickness determination, n = 3. Specimens were directly mounted and Au sputter-coated using a Ploaron SC502 Sputter Coater (Fison Instruments, UK). Samples were examined using a JEOL JSM 840A Scanning Electron Microscope (Peabody, MA) at 15 kV.

2.2.1.3. Results

2.2.1.3.1. Effect of silk fibroin coating solution concentration and number of silk coatings applied on coating thickness

Examination of the surface morphology of 8% (w/v) silk coated adenosine reservoirs by scanning electron microscopy (SEM) revealed smooth, constant coating with no observed defects or cracks. Examination of cross sections of silk fibroin coated adenosine reservoirs revealed increasing film thickness with increasing silk concentration and increasing number of coatings. The cross sections showed good packing of adenosine into the tablets and consistent, smooth silk coatings that exhibited constant thickness across the entire surface of the encapsulated reservoir. Sample SEM cross sections from a 4% (w/v) silk coated adenosine reservoirs (coating thickness = approximately 100 μm) are shown in Figure 2.6 to demonstrate the evenness of the silk coating.

Examination of cross-sections of silk fibroin coated adenosine reservoirs revealed increasing film thickness with increasing silk concentration and increasing number of coatings. Figure 2.7 shows sample SEM cross-sections from reservoirs coated with 4% (w/v) (Figure

2.7C–D), 8% (w/v) (Figure 2.7E–F), 16% (w/v) (Figure 2.7G–H) and 20% (w/v) silk (Figure 2.7I–J). 2% (w/v) coatings were too thin to measure. The thickness of the film coating was determined by SEM and Image J software analysis and was found to increase with increasing silk concentration (reported in weight/volume percent) (Figure 2.7A). The thickness of the film coating also increased with the mass of silk coating added (in milligrams) (Figure 2.7B). The proportionality of coating thickness to mass of silk added suggests evenness of coating deposition and the proportionality of coating thickness relative to silk concentration suggests a controllable relationship exists between silk coating processing and final coating thickness.

Figure 2.8 shows a comparison of encapsulated reservoirs coated with single and multiple coatings of 8% (w/v) silk. An unmagnified single coated reservoir and an unmagnified reservoir coated with eight 8% (w/v) silk layers are shown in Figure 2.8A and B, respectively. Figure 2.8C–F show SEM images of cross-sections of a reservoir coated with a single silk layer (3C and 3D) and a reservoir coated with multiple silk layers (3E and 3F). Mass of coating relative to number of coatings applied is shown in Figure 2.8G (due to the inhomogeneity and variability of multiple dip coatings, thickness in this case is more difficult to measure via SEM, making mass a more accurate reflection of the effects of the multi-layer coating process).

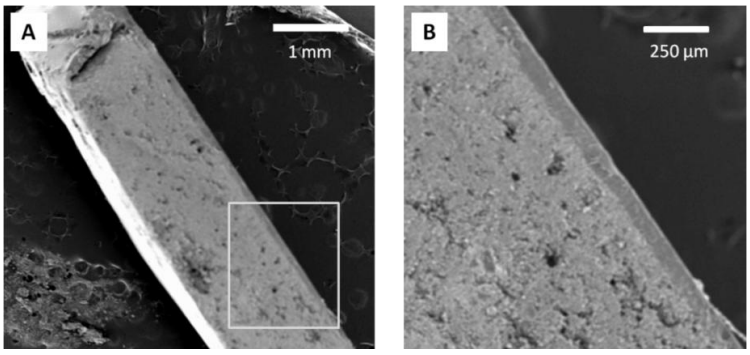

Figure 2.6. SEM images of cross-sections of encapsulated reservoirs coated with 4% (w/v) silk fibroin solution. Coating layer thickness is consistent over the entire cross-section.

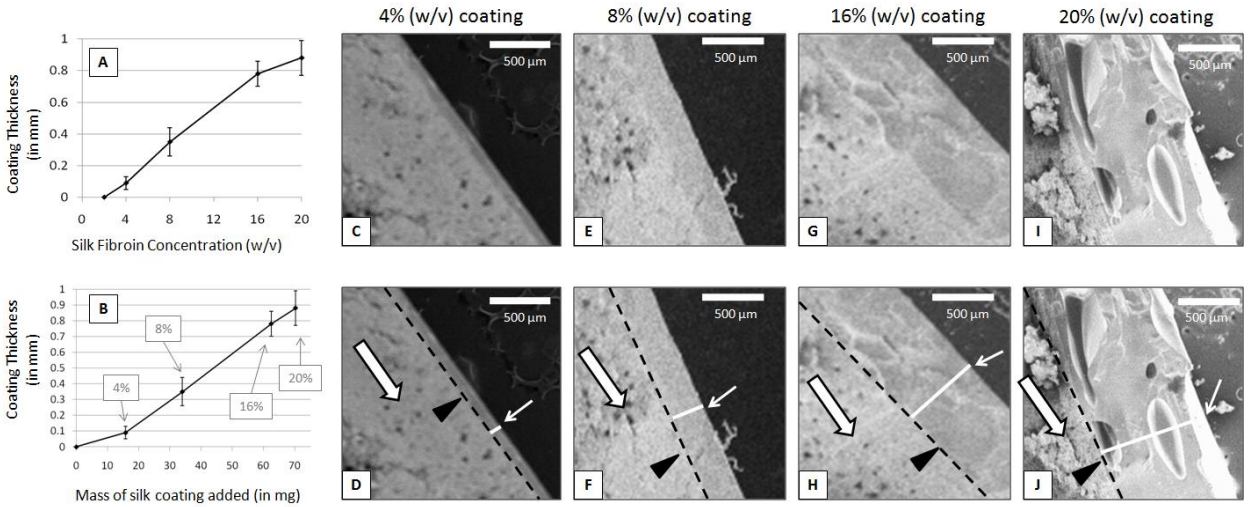

Figure 2.7. Silk fibroin coating thickness relative to silk fibroin coating concentration (A) Average thickness of silk fibroin coating relative to silk fibroin solution concentration (n= 3, error bars represent standard deviation. (B) Average thickness of silk fibroin coating relative to mass of silk coating added (n= 3, error bars represent standard deviation). (C), (E), (G), and (I) SEM cross-sections of encapsulated reservoirs coated with 4% (w/v), 8% (w/v), 16% (w/v) and 20% (w/v) silk, respectively. (D), (F), (H) and (J) are the same SEM images as (C), (E), (G), and (I) but with additional markings to aid in distinguishing features present in the encapsulated reservoir cross-sections: black outlined empty white arrows indicate the adenosine reservoir, black triangles with black dotted lines indicate the interface between the silk coating and the adenosine reservoir. White lines accompanied by small white arrows mark the width of the coating film thickness. Scale bars are all 500 µm.

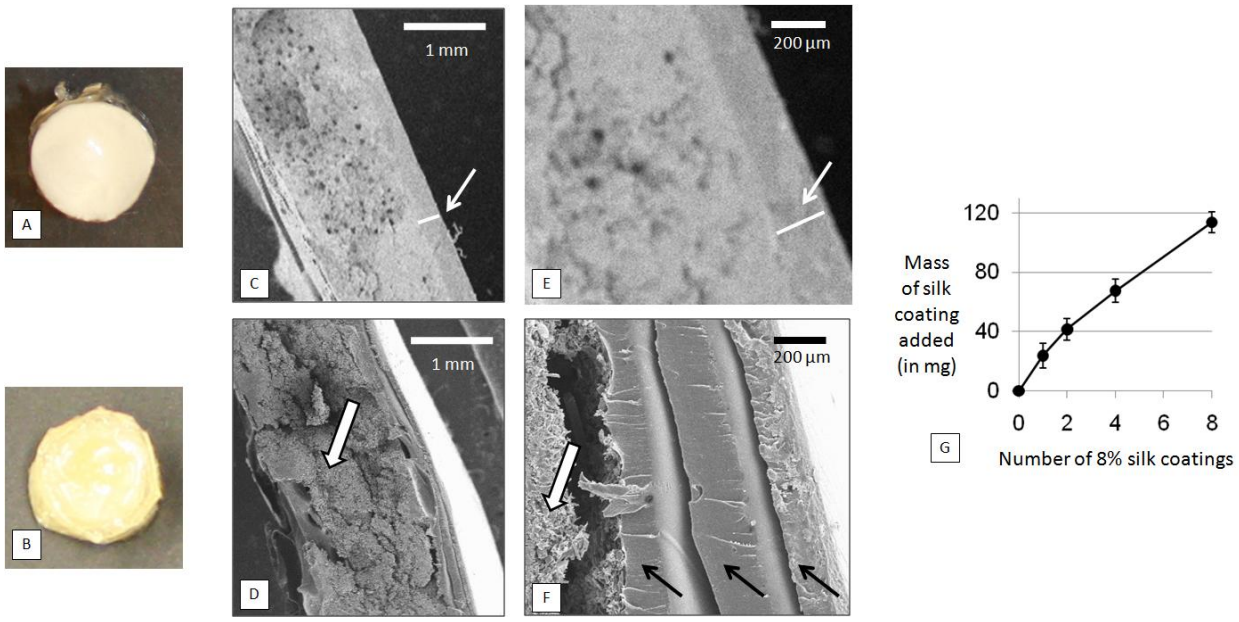

Figure 2.8. Comparison of reservoir coated with single 8% (w/v) silk coating with an encapsulated reservoir coated with multiple 8% (w/v) coatings (A) gross morphology of single 8% (w/v) silk coated reservoir. (B) Gross morphology of reservoir coated with eight 8% (w/v) silk coatings (C) and (E) SEM images of cross section of single 8% (w/v) silk coated reservoir. (D) and (F) SEM cross section of multiple 8% (w/v) silk layer coated reservoir. (E) Graph of mass of coating added relatively to increasing number of 8% (w/v) silk coatings. Scale bars in (C) and (D) are 1 mm. Scale bars in (E) and (F) are 200 µm.

2.2.1.3.2. Effect of silk fibroin coating concentration/film thickness on adenosine release in PBS

Uncoated adenosine reservoirs dissolved immediately upon immersion in PBS and 100% of the drug load was recovered when the first sample was collected at 12 hours. Due to the insolubility of adenosine in methanol, no significant drug loss occurs during methanol treatment of the silk coatings to stabilize the β sheet physical cross links. Less than 0.001 mg of adenosine out of an average total mass of approximately 70 mg (or 0.0014%) was recovered from the methanol residue. At the end of all release studies, when the encapsulated reservoirs had released their full adenosine drug load (i.e., adenosine was no longer detected in the release study buffer) the systems were degraded by protease and no residual adenosine was found. Binding studies have shown that adenosine exhibits little to no affinity for silk substrates (data not shown).

The linearity of release increased and average release rate slowed with increasing silk concentration used in the coatings, up through 16% w/v silk (Figure 2.9). The only deviation from this trend was the 20% (w/v) silk coated reservoirs which showed more rapid release kinetics and decreased linearity compared to the 16% (w/v) release curve. Potential explanations for this discrepancy include cracking of thicker films during methanol treatment or uneven drying of the films due to the high silk concentration in the coating solution resulting in inhomogeneous films (Figure 2.10). These phenomena have also been observed when thick (high concentration) silk films were cast on flat surfaces (Sofia *et al.*, 2001).

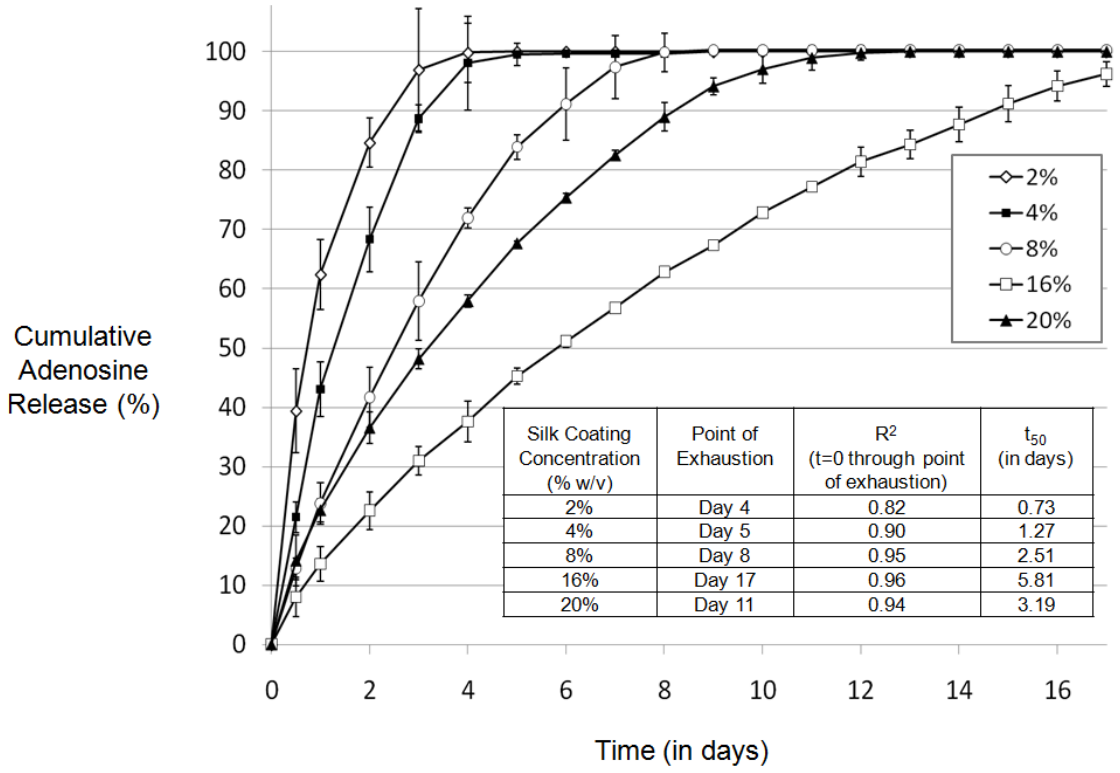

Silk Coating Concentration (% w/v)	Point of Exhaustion	R^2 (t=0 through point of exhaustion)	t_{50} (in days)
2%	Day 4	0.82	0.73
4%	Day 5	0.90	1.27
8%	Day 8	0.95	2.51
16%	Day 17	0.96	5.81
20%	Day 11	0.94	3.19

Figure 2.9. Cumulative adenosine release from encapsulated adenosine reservoirs coated in silk of varying concentration over time in PBS at 37° C. N=3, error bars represent standard deviations (where error bars aren't shown they fall into background).

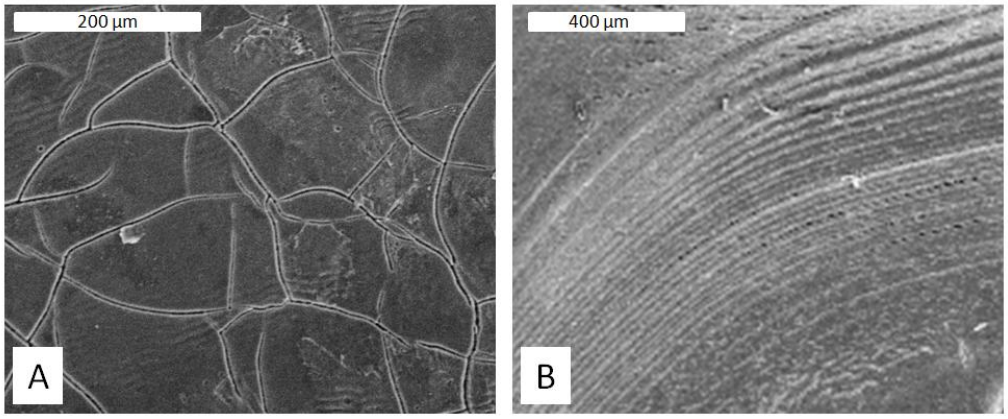

Figure 2.10. Microscopic surface defects observed on 20% (w/v) silk encapsulated reservoir coating surface (A) Surface cracking, scale bar = 200 µm (B) Uneveness/rippling of the film surface towards the reservoir edge, scale bar = 400 µm.

Values of t_{50}, or the time at which 50% of the total drug load was released from the reservoir, and regression coefficients (R^2) are reported in the Table inset in Figure 2.9. The release profile closest to the zero-order target was observed in encapsulated reservoirs coated with the 16% w/v silk, which sustained release through day 17 with a regression coefficient (R^2) of 0.96. Values for t_{50} for 2%, 4%, 8%, 16% and 20% w/v silk fibroin coating concentrations were 0.73 days, 1.27 days, 2.51 days, 5.81 days and 3.19 days, respectively. The n values of the log (release%) versus log(t) curves for 2%, 4%, 8%, 16% and 20% (w/v) silk fibroin coating concentrations were 0.35, 0.54, 0.71, 0.70 and 0.53, respectively. In this case the Siepmann–Peppas models suggest complexity of release mechanism (i.e., neither pure diffusion nor pure Case II release), so the results of the fit do not allow us to characterize release mechanism. However, the results of the fit do allow empirical observation of increased linearity at higher silk coating concentrations (i.e., as silk coating thickness increases, n increases, suggesting that the release profile from the reservoir becomes increasingly more linear with increasing film thickness).

2.2.1.3.3. Effect of number of silk fibroin coatings on release of adenosine

Encapsulated reservoirs coated with 8 layers of 8% (w/v) silk fibroin exhibited a zero order release with a regression coefficient (R^2) of 0.999 (Figure 2.11). Reservoirs coated with 4 layers of 8% (w/v) silk fibroin exhibited near zero-order release (R^2=0.98). Reservoirs with 4 coatings released continuously for 13 days at an average release rate of 7.03 $\pm$ 2.83% of the total adenosine mass (average total adenosine mass = 71.5 mg) per day and encapsulated reservoirs with 8 coatings continued to release for 14 days at an average release of 6.53 $\pm$ 2.26% of the total reservoir mass per day. Values of t_{50} for 1x, 2x, 4x and 8x encapsulated reservoirs were 3.3 days, 4.3 days, 5.3 days and 7.1 days, respectively. Regression coefficients, release durations, values of t_{50} and average release rates are reported in the Table inset in Figure 2.11.

The n values of the log(release%) versus log(t) curves were 0.70 for 1 coating, 0.87 for 2 coatings, 0.89 for 4 coatings and 1.15 for 8 coatings. Encapsulated reservoirs coated with 8 layers of silk had an n>1, suggesting zero order release. The other reservoirs (1x, 2x and 4x) all had 0.5<n<1, suggesting a complex (i.e., neither pure diffusion nor pure Case II release) release mechanism ((Ritger and Peppas, 1987). As before, with increasing number of silk coatings and increasing thickness, n increases, suggesting that the release profile from the reservoir becomes increasingly more linear with increasing number of coatings.

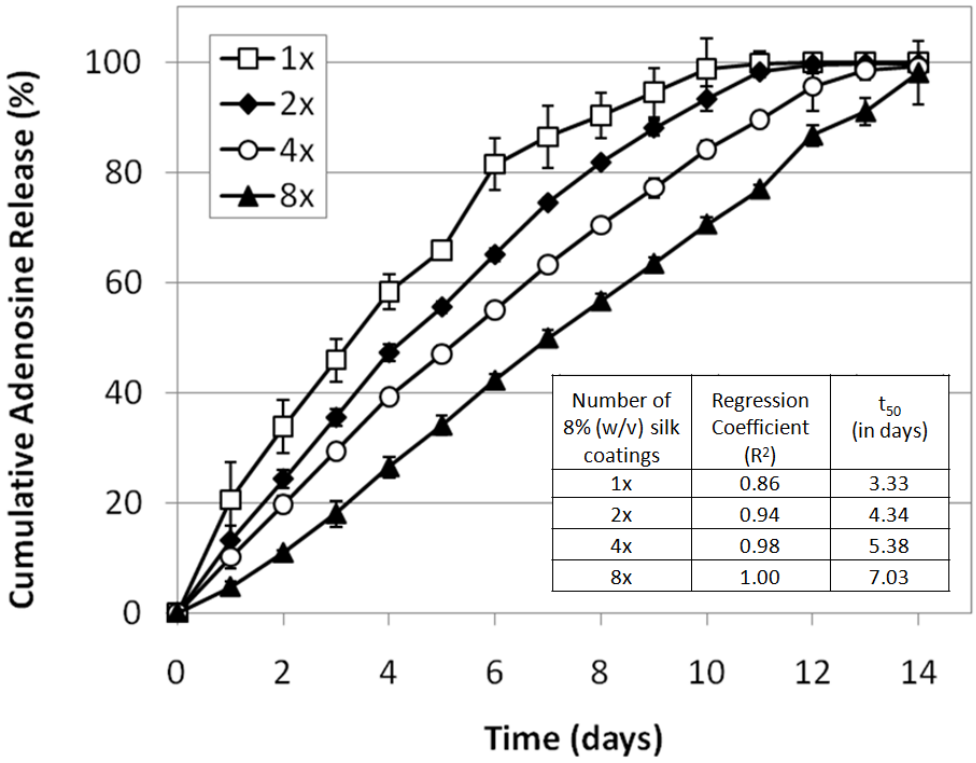

Figure 2.11. Cumulative adenosine release from encapsulated adenosine reservoir coated in varied number of 8% (w/v) silk coatings in PBS at 37°C. 1x = one coating, 2x = two coatings, 4x = four coatings, 8x = 8 coatings. N = 3, error bars represent standard deviations (where error bars aren't shown they fall into background).

Figure 2.12 shows cumulative release for a reservoir coated with sixteen layers of 8% (w/v) silk (16x). Constant release is sustained from 16x coated reservoirs approximately 40 days ($R^2 = 0.992$).

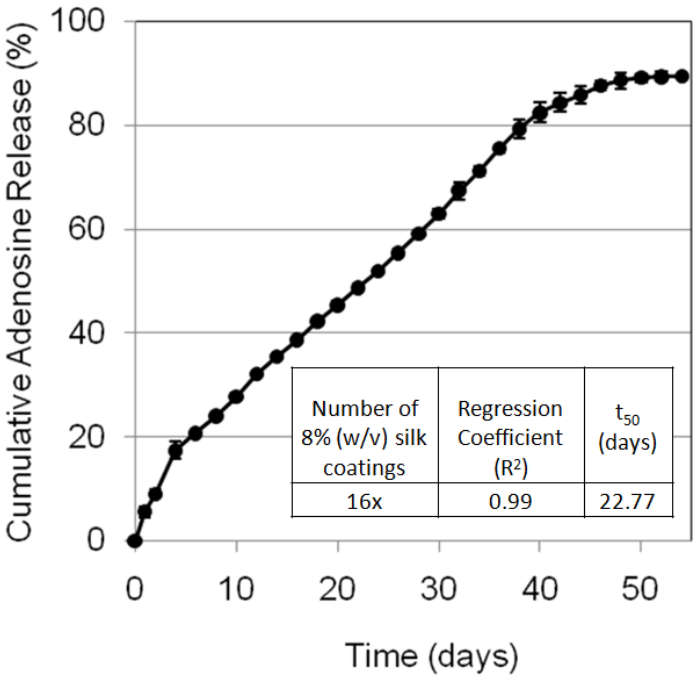

Figure 2.12. Cumulative adenosine release from encapsulated adenosine reservoir coated with 16 8% (w/v) silk coatings in PBS at 37° C. N = 3, error bars represent standard deviations (where error bars aren't shown they fall into background).

The use of multiple coatings increased the mass of silk that could be added to the reservoir without compromising zero-order release (Figure 2.11). An average mass of 62.50±3.40 mg of silk coating was added to the adenosine reservoirs coated with 1 layer of 16% (w/v) silk, while an average of 113.58±4.21 and 188.99±22.30 mg of total silk was added to the adenosine reservoirs coated with 8 layers and 16 layers of 8% (w/v) silk, respectively.

2.2.1.3.4. Relationship between release rate and path length

According to the early time approximation of Fick's second law ($dM_t/dt \approx AD_iC_o/L$), for $M_t/M_\infty \leq 0.6$), release rate for the first 60% of the release curve is expected to be proportional to the inverse of path length. For increasing silk concentration, this relationship holds, suggesting that the model accurately describes the system (Figure 2.13).

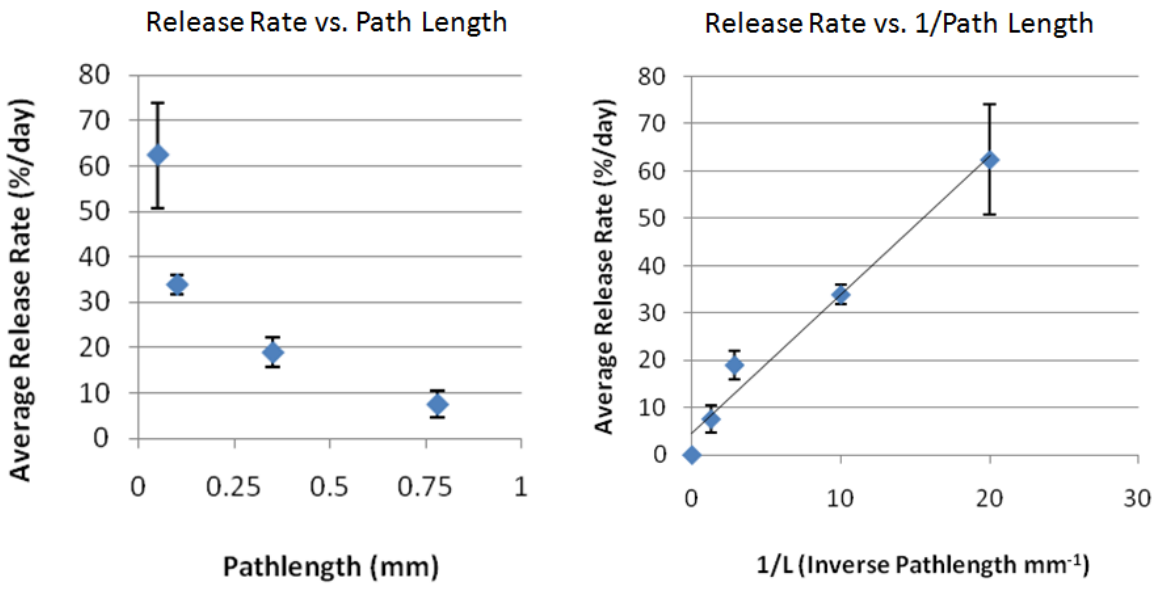

Figure 2.13. Average release rate (through M_t/M_∞ =0.6 release) versus path length (L) and inverse path length (1/L).

However, for multiple coatings release rate is linearly proportional to path length (Figures 2. 14 and 2.15), resulting in a non-linear relationship with inverse of path length (Figure 2.15).

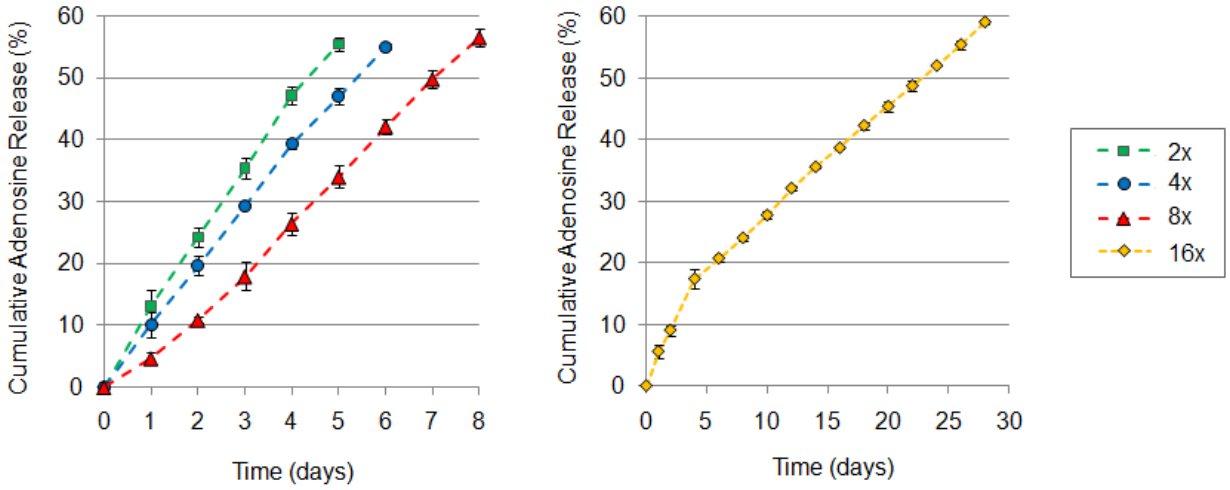

Figure 2.14. Cumulative adenosine release from encapsulated adenosine reservoir coated in varied number of 8% (w/v) silk coatings in PBS at 37°C through 60% cumulative release. 2x = two coatings, 4x = four coatings, 8x = 8 coatings, 16x = 16 coatings. N = 3, error bars represent standard deviations (where error bars aren't shown they fall into background).

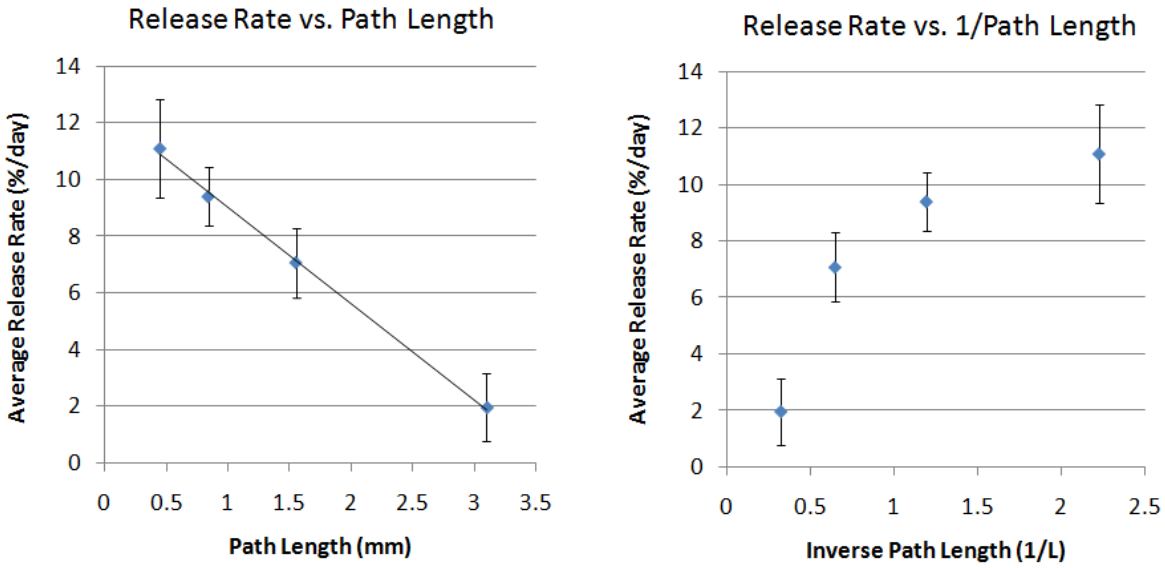

Figure 2.15. Average release rate (through $M_t/M_\infty = 0.6$) versus path length (L) and inverse path length (1/L).

In the case of multiple coatings, release rate (dMt/dt) is linearly related to the path length, resulting in a non-linear relationship between release rate and inverse path length. Fick's second law no longer appears to accurately describe the system, meaning an assumption about the system or the model is invalid. Ratio of release rate to inverse path length is decreasing with inverse path length, meaning release rate slows relative to path length less than the model predicts (apparent diffusivity increases with path length, rather than remaining constant as the model predicts it should).

Diffusivity might for some reason be increasing with path length (outer layers might be packing differently than inner layers). Alternately, path length might be underestimated: thickness for single varied concentration coatings was determined by examining SEM cross-sections, however the process of applying multiple coatings results in a less homogenous coating than single dip processes, making it difficult to accurately assess thickness via SEM. Therefore

coating mass added (which for single varied concentration coatings is proportional to thickness) is tracked as a function of coating cycle, and layer thickness is estimated by measuring total construct height, subtracting the pill height and dividing by two. This approach assumes equal coating distribution, but during the drying step of the coating process, some of the silk solution might be pooling on the bottom surface. Pooling would result in slightly thinner top layers than bottom layers, but neither measuring mass added nor total implant height would indicate the difference. If the coating is not homogenous, then release will be dominated by the thinner layer and release rate will be faster than predicted. Additionally, the single varied-concentration coatings and multiple coatings results in different scales, so the difference in release behavior might be related to the increase in length rather than a function of the coating process (Figure 2.16).

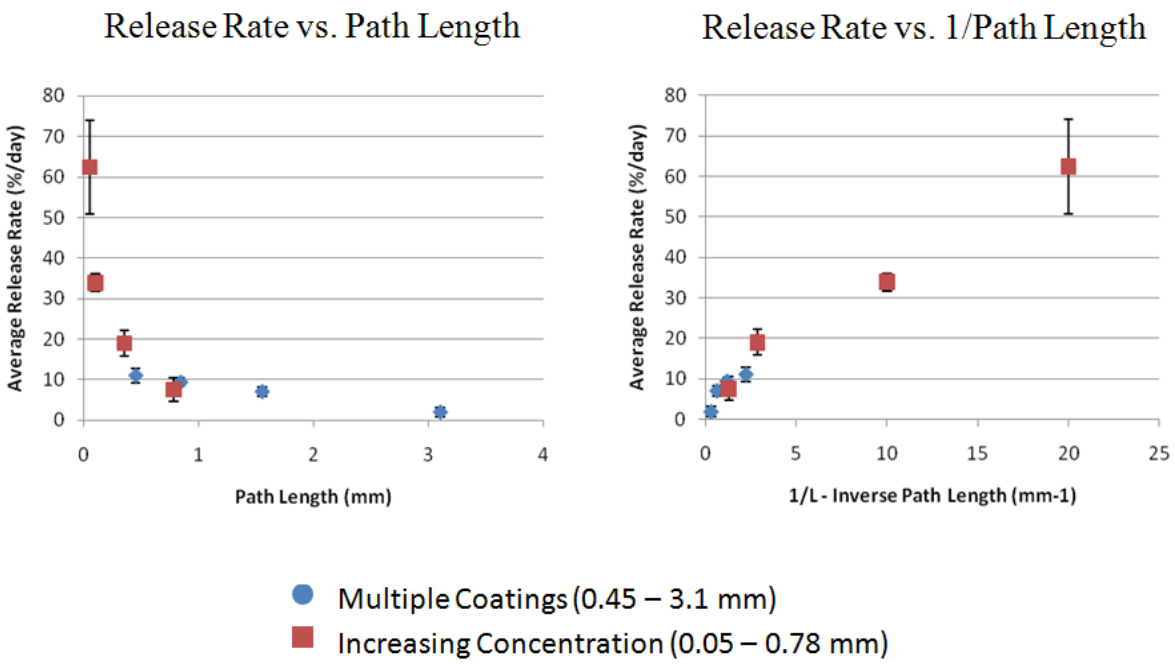

Figure 2.16. Average release rate (through M_t/M_∞ =0.6 release) versus path length (L) and inverse path length (1/L) for both encapsulated reservoirs coated with multiple 8% (w/v) silk coatings and single silk coatings of varied silk concentration for comparison of scale.

2.2.1.4. Conclusions

Increasing the thickness of the silk coating (either by increasing the silk concentration or increasing the number of coatings added) decreased release rate, increased release duration (as evidenced by increases in t_{50}) and increased release linearly (as evidenced by increases in the Siepmann-Peppas release exponent, n). However, the relationship between inverse path length and release rate for multiple coatings was found to be non-linear, inconsistent with the predictions of Fickian diffusion. Specifically, increases in path length produce less of a decrease in release rate than predicted. The shape of the release rate versus inverse path length curve suggests that either the outer layers are somehow more diffusive that the inner layers (the model predicts consistent diffusivity, but experimental data suggests that the silk becomes more permeable as more coatings are added) or that the path lengths are being overestimated (possibly due to pooling). Fitting release behavior to the Fickian diffusion model informed our understanding of the system by identifying which assumption might be invalid (homogeneity of the individual layers, consistent capping thickness, etc.).

Future work requires a more consistent coating process to elucidate the relationship between silk coating thickness and diffusion-driven release. In addition to lacking sufficient control and consistency, the process described here (repeated dipping, drying and methanol treating) is also time consuming. A new, more rapid, more consistent process was therefore developed for future encapsulation studies.

2.2.2. Dehydrated silk hydrogel encapsulated reservoirs

2.2.2.1. Introduction

The aqueous silk reservoir coating process confirmed that increasing path length decreased release rate, decreased burst and increased release duration (t_{50}). However, attempts to fit to the early time approximation for diffusion from encapsulated reservoirs suggested a modified encapsulation approach was needed to determine whether disparities between experimental release profiles and predicted model release profiles revealed false assumptions about the material (i.e., that material diffusivity is constant with length) or false assumptions about the coating process (i.e. that each layer deposited coats the reservoir evenly).

An alternate coating process was developed based on the observation that silk hydrogels compact into films when dehydrated. Encapsulation is performed by embedding press-fit pills in crosslinked silk hydrogel then drying the hydrogel into a film-like coating at ambient conditions (Figure 2.17).

2.2.2.2. Materials and methods

2.2.2.2.1. Adenosine powder reservoir encapsulation and characterization

Adenosine reservoirs and silk solution were fabricated as previously described, except the silk fibroin was degummed for 30 minutes. Adenosine reservoirs were encapsulated by sonicating 8% (w/v) silk solution for 30-45 seconds at amplitude 15% then aliquoting the liquid silk solution into Peel-A-Way histology molds (22 mm square, 20 mm deep). Once the bottom layer completed gelling, a press-fit adenosine reservoir was added and another aliquot of sonicated silk was added and allowed to gel, resulting in an adenosine reservoir at the center of a hydrogel cube. The hydrogel cube is then dried overnight at ambient conditions and the dried hydrogel forms a film envelope that coats the adenosine reservoirs with films of equal thickness

on either side. This process is shown schematically with representative photographs in Figure 2.17. Volume of hydrogel (1 mL, 2 mL, 3 mL) on either side determines thickness of coating. For each coating thickness tested n = 3.

Path_length was determined by breaking the completed, dried reservoir in half, dissolving the adenosine reservoir in water, re-drying the reservoir halves and measuring film thickness using a Mitutoyo absolute digimatic caliper with a 0.01 mm resolution (Mitutoyo America Corporation, Aurora, IL)

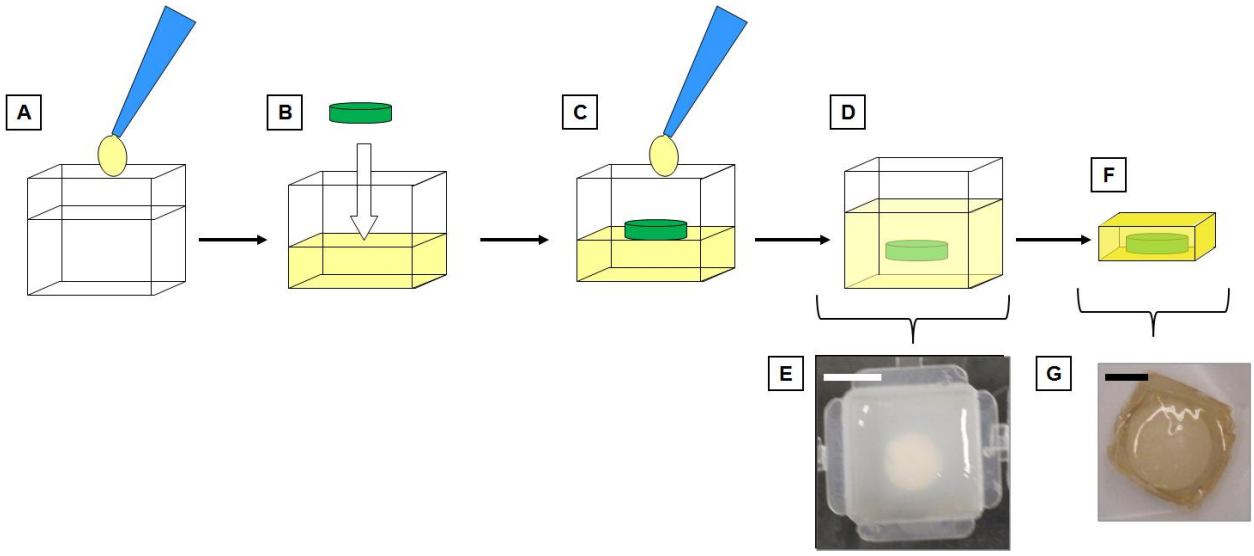

Figure 2.17. Schematic of the dehydrated silk hydrogel encapsulation method. (A) molds are partially filled with the desired volume of sonicated silk solution. (B) The sonicated silk solution is allowed to gel, then a press-fit tablet of drug is added. (C) Another aliquot of sonicated silk solution is added and allowed to gel, (D-E) resulting in a solid press-fit reservoir embedded in the center of a hydrogel cube (white scale bar = 10 mm). (F-G) When the hydrogel is air-dried, the reservoir is coated with film of equal thickness on either side (black scale bar = 5 mm). No additional methanol treatment is needed because the silk crosslinking during gelation renders the resulting film water insoluble.

2.2.2.3. Results

2.2.2.3.1. Effect of silk fibroin hydrogel volume on coating thickness

As expected, a linear relationship is observed between mass of silk coating added and volume of silk hydrogel added to the molds and the total mass of silk coatings. 1, 2 and 3 mL of 8% (w/v) on either side (corresponding to a theoretical mass added of 160, 320 and 480 mg, respectively) and an actual mass added of 172.80 ± 14.45, 321.13 ± 17.77 and 492.67 ± 19.22 mg, respectively (Figure 2.18A). Path lengths also exhibited a linear relationship with mass added/volume of hydrogel used for encapsulation: 1, 2 and 3 mL of 8% (w/v) produced coating thicknesses of 14.45 ± 0.13, 17.77 ± 0.23 and 19.22 ± 0.12 mm, respectively (Figure 2.18B). Note that one iteration of this process produces a total coating thickness equivalent to sixteen dips of the aqueous process. Total mass added in the hydrogel process results in a thinner path length compared to an equivalent mass added for the aqueous silk coating process due to the use of a cube-shaped mold (though a more efficient mold could ultimately be used).

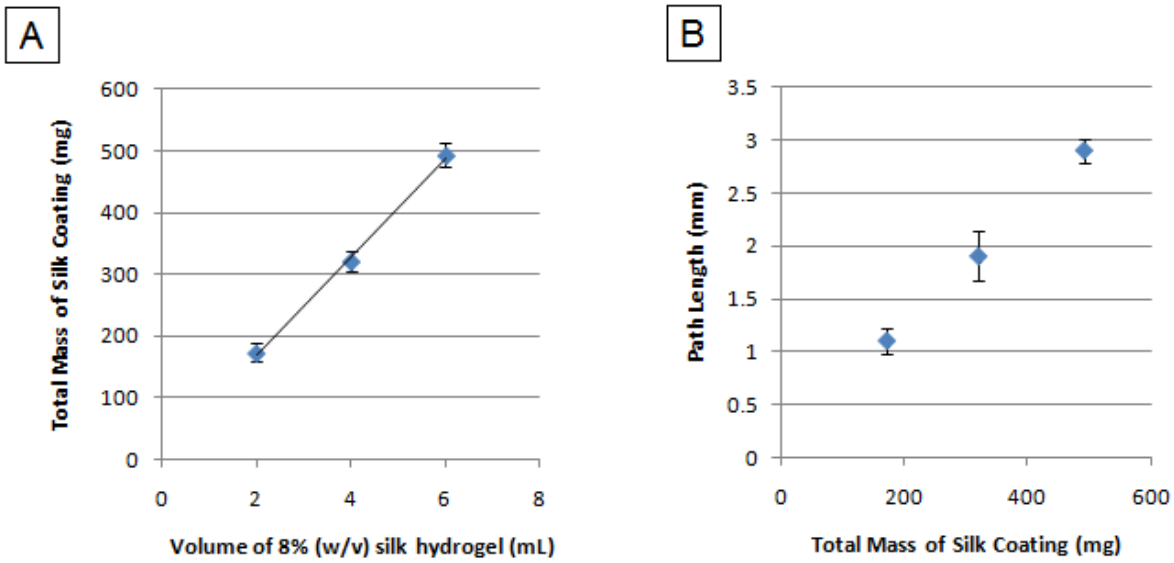

Figure 2.18. Hydrogel volume added determines mass of coating added and path length (A) Average total silk coating mass added to adenosine reservoir versus volume of 8% (w/v) silk hydrogel used for encapsulation N = 3, error bars represent standard deviations (where error bars aren't shown they fall into background). (B) Path length (i.e. coating thickness) verses total mass of silk coating.

2.2.2.3.2. Effect of dehydrated silk hydrogel coating thickness on release of adenosine

Encapsulated reservoirs coated with silk hydrogel exhibited constant, fairly linear release profiles through $M_t/M_\infty = 0.6$: regression coefficient (R^2) for reservoirs with average coating thicknesses of 1.08, 1.91 and 2.93 mm of 0.99, 1.00 and 1.00 (Figure 2.19). Reservoirs with 1 mL of 8% (w/v) hydrogel on either side (coating thickness = 1.1 mm) released continuously for 7 days and the average release rate for $M_t/M_\infty \leq 0.6$ was 15.47 ± 1.9 % of the total adenosine mass (approx. 75 mg) per day. Reservoirs with 2 mL of 8% (w/v) hydrogel on either side (coating thickness = 1.89 mm) released continuously for 11 days and the average release rate ($M_t/M_\infty \leq 0.6$) was 8.16 ± 1.18 % per day. Reservoirs with 3 mL of 8% (w/v) hydrogel on either side (coating thickness = 2.93 mm) released continuously for 14 days and the average release rate ($M_t/M_\infty \leq 0.6$) was 3.72 ± 1.44 % per day. Values of t_{50} for 1.08, 1.91 and 2.93 mm coating thicknesses were 3.26 days, 5.98 days, 12.08 days, respectively. Regression coefficients and values of t_{50} are reported in the table inset in Figure 2.19.

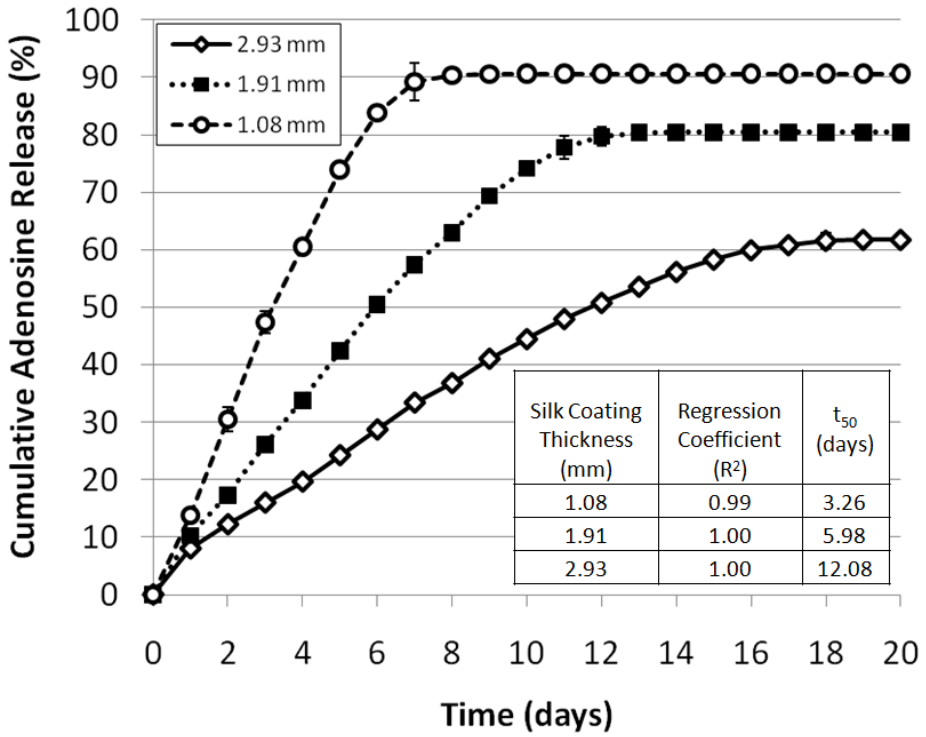

Silk Coating Thickness (mm)	Regression Coefficient (R^2)	t_{50} (days)
1.08	0.99	3.26
1.91	1.00	5.98
2.93	1.00	12.08

Figure 2.19. Cumulative adenosine release from encapsulated adenosine reservoir coated in varied thicknesses of dehydrated silk hydrogel in PBS at 37° C. N = 3, error bars represent standard deviations (where error bars aren't shown they fall into background).

Strangely, the total cumulative adenosine recovery (in percentage of the total initial load) appears to decrease with increasing thickness/release duration, a phenomenon that was not observed for reservoirs coated with aqueous silk solution-derived films. Unreleased drug might be getting trapped in the silk coating. As increasing the silk coating would increase the total amount of silk present to trap drug, this might explain the trend of decreasing total recovery with increasing coating thickness. However, since adenosine doesn't bind aqueous silk films or become entrapped in aqueous solution-derived coatings, this explanation seems unlikely.

Another potential explanation might be that when an adenosine reservoir is coated with an aqueous silk solution some of the liquid silk soaks into the adenosine tablet and forms an immobilization matrix. When drug diffuses out of the matrix, any drug remaining in the reservoir

is unaffected by the loss. However, the hydrogel encapsulation method forms an envelope around the reservoir, such that when adenosine diffuses out and water diffuses into the vacated space, the dry solid powder reservoir becomes a high-concentration 37^{o}C liquid reservoir. Degradation of the encapsulated adenosine might result in decreased total adenosine recovery, and prolonging release duration would result in decreasing recoveries. Future work will include improving stability of the reservoir (reservoirs could potentially be dipped in an aqueous silk solution for a stabilizing coating prior to hydrogel encapsulation) and studies with fluorescent models drugs or small molecule dyes to determine if drug is becoming trapped in the silk coating.

Figure 2.20 shows average release rate for the first 60% of M_t/M_∞ versus path length and inverse path length. As shown, a proportional relationship is observed between release rate and inverse path length, as predicted by the early time approximation of Fick's second law. Further, when comparing the release rates and path lengths for encapsulated reservoirs coated with multiple aqueous-derived silk films and encapsulated reservoirs coated with dehydrated silk hydrogel (Figure 2.21), the length scales are comparable.

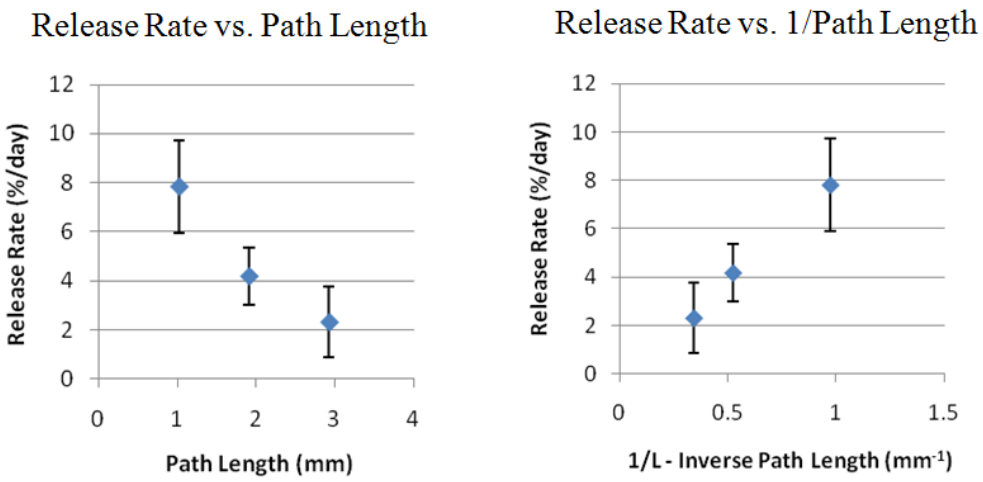

Figure 2.20. Average release rate (through $M_t/M_\infty = 0.6$) versus path length (L) and inverse path length (1/L).

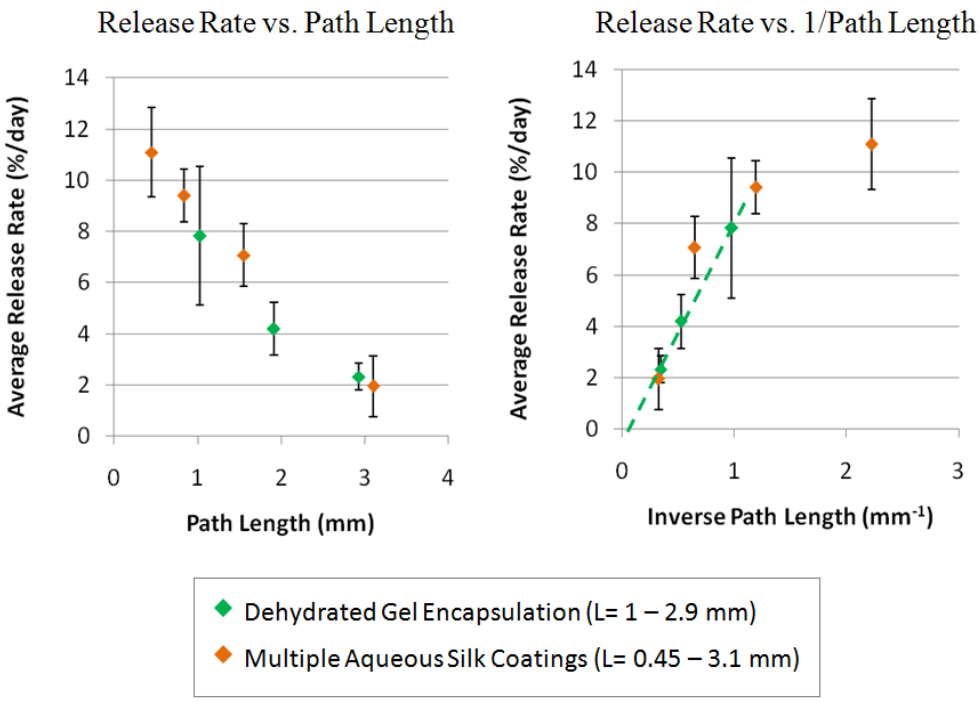

Figure 2.21. Average release rate (through M_t/M_∞ =0.6 release) versus path length (L) and inverse path length (1/L) for both encapsulated reservoirs coated with multiple 8% (w/v) silk coatings and single silk coatings of varied silk concentration for comparison of scale.

2.2.2.3. Conclusions

The dehydrated hydrogel encapsulation process described produced more controlled, consistent coating thickness compared with the aqueous solution dipping process. Once path length control was improved, release rate was found to scale linearly with inverse path length, as predicted by the early time approximation model of Fick's second law. This suggests that the diffusivity of the silk capsule is consistent (i.e., does not decrease or increase with increasing path length). Unfortunately, dehydrated hydrogel encapsulation resulted in incomplete drug recovery, but we anticipate this could possibly be overcome by improving reservoir stabilization.

2.3 Material Diffusivity

Rate of diffusion from polymer drug carriers can be controlled via carrier morphology (as described in the previous section) and manipulation of polymer properties including porosity, molecular weight and crystallinity/β-sheet content. In the case of PLGA, properties are usually controlled via manipulation molecular weight or copolymer (PGA:PLA) ratio (Puppi *et al*., 2010). For silk films, material diffusivity can be controlled through porosity, degumming time and β sheet content. Increasing porosity has been shown to increase membrane permeability and increase drug release rate (Lin and Lee, 2003), which might be a useful control point for relatively slow diffusing drugs like proteins. However, as small molecule drug release is already fairly rapid in non-porous silk membranes and our goal is long term release (days to weeks), β sheet content and degumming time were selected for study.

2.3.1 Beta sheet content

2.3.1.1 Introduction

Beta sheet content has been shown to decrease the permeability of silk to incorporated drugs (for a detailed description of silk beta sheet structure and assembly, please refer to section 2.1.1.). Uebersax *et al*., 2008 found that methanol treatment of insulin growth factor I (IGF-I) releasing lyophilized silk scaffolds increased β-sheet content in the scaffolds, reduced initial burst, achieved higher total cumulative IGF-I release and increased release duration (Uebersax *et al*., 2008). Hofmann *et al*. found drug release from bulk loaded silk films was related to film crystallinity. (Hofmann *et al*., 2006). Wang *et al*. reported that β-sheet crystalline content could be used to effectively regulate the release kinetics of the incorporated compounds from silk nanofilm coatings (Wang *et al*., 2007-1). Similarly, methanol treatment of ultrathin silk coatings

applied to PLGA and alginate microspheres decreased release rate of encapsulated model compounds (Wang *et al*., 2007-2). Wang *et al*. demonstrated that increasing duration of sodium chloride treatment decreased release rate and increased release duration of horseradish peroxidase (HRP) from silk microspheres (Wang *et al.*, 2007-3). Beta-sheet content for this study was controlled via concentration of methanol in the post-film-drying treatment solution and duration of treatment.

The objective of this study was therefore to determine whether β sheet content of silk in drug carriers could be controlled during processing (via concentration of methanol in the solution or methanol treatment duration) and to determine what effect β sheet content has on drug diffusion through silk films.

2.3.1.2. Materials and Methods

2.3.1.2.1. Preparation of model dye loaded films

Silk solution was prepared as previously described (2.2.1.2.2.), using a 60 minute degumming time. For degradation studies, the dyes reactive red 120 (MW = 1469.98) and indigo carmine (MW= 466.35) were used. For varied concentration proteinase release studies, films were prepared from 8% (w/v) silk containing either 1 mg of reactive red 120 or indigo carmine (see Figure 2.3 for model compound chemical structures) per film and 24 mg of silk (0.3 mL of 8% (w/v) silk per film). Films were cast by aliquoting into Teflon coated molds, then dried overnight at ambient conditions. Following dying, films were treated with solutions of 50%/50% (v/v) methanol/water, 75%/25% (v/v) methanol/water, or 90%/10% (v/v) methanol/water (referred to as 50%, 75% and 90% methanol, respectively) for either 30 seconds or 5 minutes.

Solutions with a methanol content lower than 50% (i.e. more than 50% H_2O) were found to dissolve silk films during treatment.

2.3.1.2.2. Reservoir fabrication and encapsulation

Adenosine reservoirs were coated by dipping in aqueous silk solution at the desired protein concentration, drying for 30 min at 60^{o}C, then immersing in methanol for 5 minutes to increase β sheet content for aqueous-insolubility. Following treatment, methanol was evaporated and the residue was resuspended in PBS and assayed for adenosine content. Adenosine and control/mannitol pills for the comparison of methanol treated versus untreated coatings were coated with 8% (w/v) silk fibroin solution and treated with a solution of 90% MeOH/10% H_2O or left untreated. For the comparison study of methanol treated 8% (w/v) coatings versus untreated 8% (w/v) coatings, n = 4.

2.3.1.2.3 Release studies

To determine dye release from films and adenosine release from encapsulated reservoirs, the silk material systems were immersed in 1 mL of Dulbecco's PBS and at desired time points, the buffer was removed and replaced with fresh buffer. The amount of released dye was determined using UV-Vis spectroscopy at 535 nm and 610 nm for reactive red 120 and indigo carmine, respectively, and compared to standard curves. Adenosine content was determined as previously described. The amount of released compound in each sample was summed with the amounts at each previous time point and divided by the total amount to obtain cumulative release values. Four film samples were tested (n=4) and each sample was assayed in triplicate.

2.3.1.2.4. Film characterization - FTIR

FTIR analysis was performed using a Bruker Equinox 55 FTIR spectrometer to confirm the structural changes for the coatings treated with methanol or left untreated. Beta sheet structure was represented by curves with absorption bands in the frequency range of 1620–1630 cm^{-1} and 1695–1700 cm^{-1} (Ishida *et al.*, 1990).

2.3.1.2.5. Film characterization – permeability and diffusion coefficient

Fickian diffusional release from a thin polymer film has been represented by a mathematical equation given appropriate initial and boundary conditions:

$$\frac{M_t}{M_\infty} = 1 - \sum_{n=0}^{\infty} \frac{8}{(2n+1)^2\pi^2} exp\left[\frac{-D(2n+1)^2\pi^2}{l^2} t\right] \qquad [Equation\ 2.5]$$

Where M_t is the mass released at time t (mg), M_∞ is the mass released as $t \to \infty$ (mg), D is the diffusion coefficient (mm^2/day), assuming one-dimensional diffusion in the x direction and l^2 is the square of the thickness of the film (mm^2) (Ritger & Peppas, 1986).

This equation was encoded into MATLAB to produce models of release based on Fickian diffusion. The MATLAB statistics toolbox was used to non-linearly fit the parameters of the Fickian film diffusion model. Values of D and l^2 were grouped together to form the new value p ($days^{-1}$) where:

$$p = \frac{D}{l^2} \qquad [Equation\ 2.6]$$

Once values of p were obtained using MATLAB, the diffusion coefficient (D) was solved for based on the measured length values.

2.3.1.3. Results

2.3.1.3.1. Effect of methanol treatment on indigo carmine release from silk films

Cumulative release of indigo carmine from dye-loaded films treated for 5 minutes with solutions of varying methanol concentration is shown in Figure 2.22.

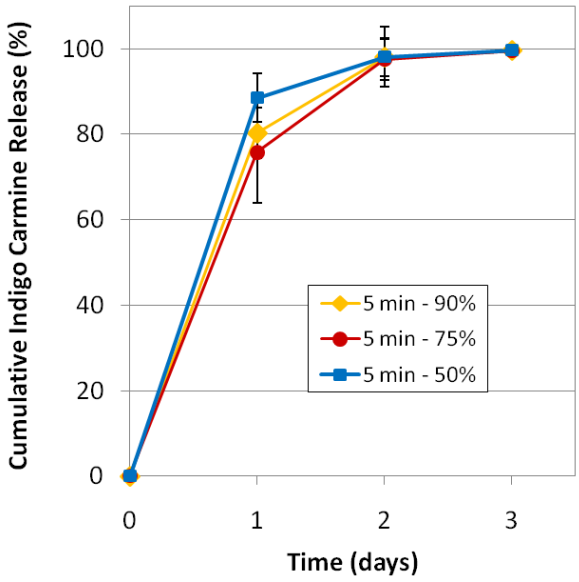

Figure 2.22. Cumulative indigo carmine release from silk films treated with 50%, 75% or 90% methanol solution for 5 minutes. N=4, error bars represent standard deviation.

Despite testing nearly the full range of feasible/practical methanol concentrations (less than 50% methanol dissolves the film, more than 90% can result in cracking), no real difference in release behavior is observed between the different treatment groups. This can be attributed to the small size of the indigo carmine. Diffusivity (D_i) of a drug through a polymer film will be determined by both the properties of the drug and the properties of the polymer (Lieb and Stein, 1969). In particular, D_i is expected to be inversely related to size of the drug (i.e., the smaller the drug the more quickly it will diffuse through polymer). If the drug is small and highly water

soluble, the contribution of the polymer properties will be masked and the effects of moderate changes in D_i may be difficult to detect.

2.3.1.3.2. Effect of methanol treatment of silk fibroin coatings on release of adenosine from silk encapsulated reservoirs

Methanol treatment of the 8% (w/v) silk reservoir coatings slowed release compared to the untreated 8% (w/v) silk coatings (Figure 2.23A). FTIR confirmed that increasing the concentration of methanol during treatment increased the crystallinity of the silk coating (Figure 2.23B). As seen in Figure 2.23B, silk coatings that received methanol treatment show an increase in the absorbance in the 1620-1630 cm^{-1} range (amide I region), which indicates an increase in the β sheet content of methanol treated films compared to untreated films. The methanol treated coatings exhibit a characteristic peak at around 1625 cm^{-1} (indicative of β sheet conformation) while the untreated films only exhibit a peak at around 1645 cm^{-1}. In the amide II region, methanol treated coatings also exhibit increased absorbance at 1515 cm^{-1} compared to untreated coatings, another indication that these coatings have increased β-sheet conformation. Values of t_{50} for pills coated with untreated silk films and 90% methanol treated films were 2.10 days and 3.34 days, respectively.

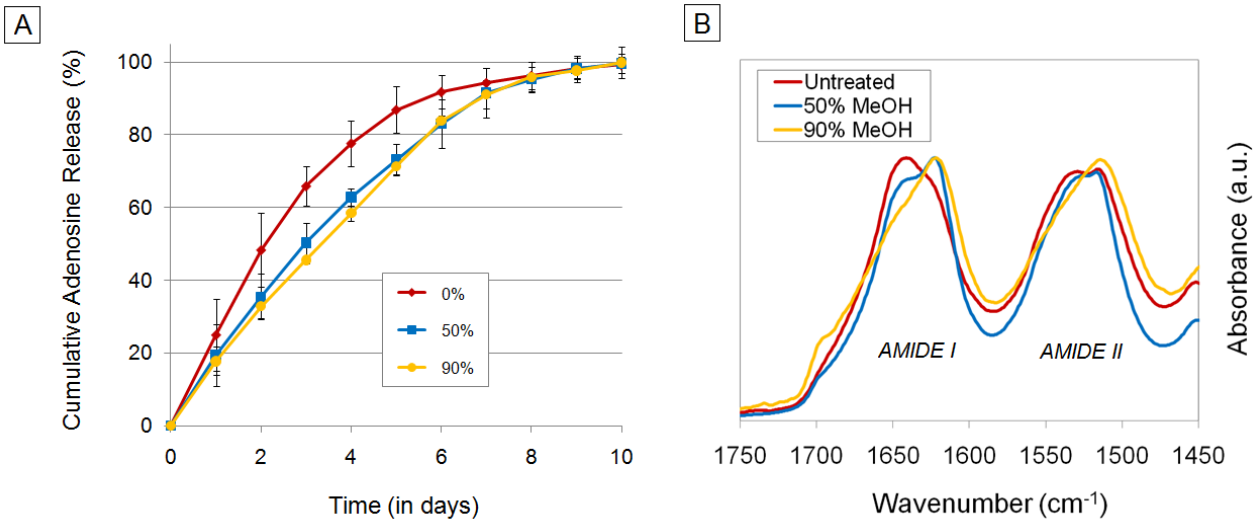

Figure 2.23. Adenosine release and FTIR of encapsulated reservoirs treated with varying methanol concentration (A) Cumulative adenosine release from adenosine pills coated in 8% w/v silk treated with methanol or left untreated. N=4, error bars represent standard deviations (where error bars aren't shown they fall into background). Percentages in the key represent methanol content in the treatment solution (B) FTIR spectra (amide I and amide II bands) of silk fibroin pill coatings comparing methanol treated silk coatings to untreated silk coatings.

As seen in Figure 2.23, methanol treatment of the pill coatings (with either 50% methanol or 90% methanol) appears to slow release slightly compared to leaving pill coatings untreated (untreated = 0% methanol). A slight delay in release from pills coated with 90% methanol treated coatings compared to 50% methanol treated coatings was observed from days 2 to 5, but very little overall difference was observed between the release profiles resulting from these two treatments. Values of t_{50} for pills coated with silk films treated with 0%, 50% and 90% methanol were 2.10 days, 2.98 days and 3.34 days respectively. Though methanol treatment appears to slow release slightly compared with untreated films, when daily release rates were compared, the difference was not statistically significantly difference (two tailed t-test, df = 6, $p > 0.05$).

2.3.1.3.3. Effect of methanol treatment on reactive red 120 release from silk films

While varied methanol treatment did not produce a significant difference in the release behavior of indigo carmine films, both concentration and duration of treatment had a significant effect on the drug release of reactive red 120. Figure 2.24 shows images of reactive red 120 loaded silk films treated with varying concentration methanol solutions.

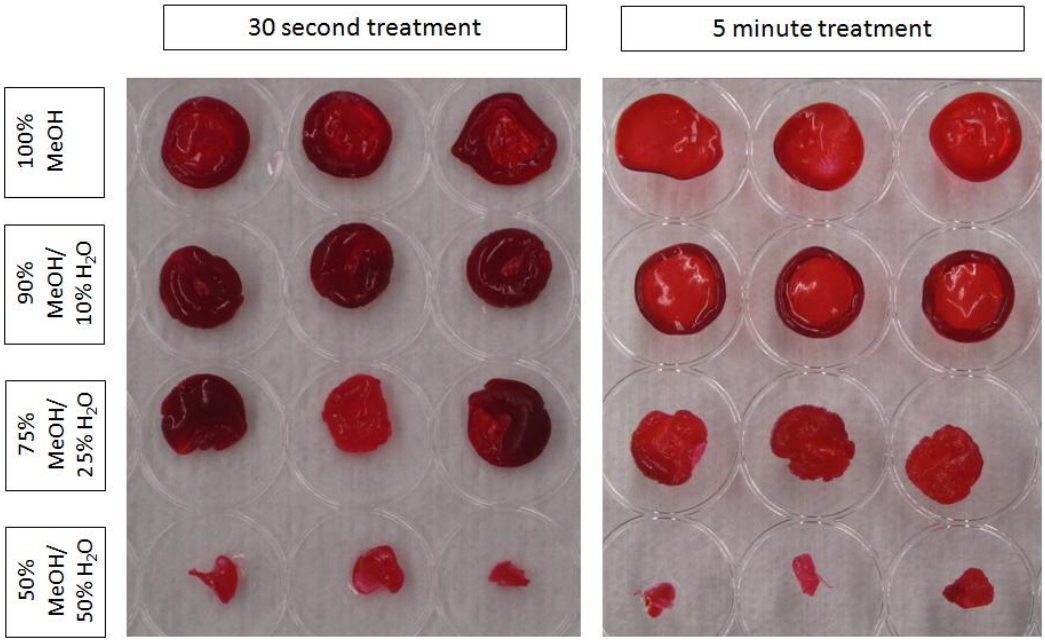

Figure 2.24. Swelling behavior of reactive red 120 loaded silk films soaked in PBS for 72 for varied methanol concentration and methanol treatment durations.

Films treated with 50% methanol for both 30 seconds and 5 minutes are mostly dissolved after 72 hours, suggesting that the low methanol content in this treatment solution is insufficient to fully crosslink the silk in the films and therefore they are still partially (but not completely) water soluble. Increasing treatment duration and methanol concentration in the treatment solution both appear to decrease swelling. In the samples treated with 75%, 90% and 100% methanol for 30 seconds and 90% methanol for 50 minutes, swelling is more pronounced around the edges. During drying, films form that are thinnest at the center with increasing thickness towards the outer edge. This suggests that, due to film thickness and short treatment durations, methanol may

not have fully penetrated the entire thickness of the films. Once hydrated, the crosslinked water insoluble shell on the exterior of the film restricts diffusion of the uncrosslinked silk out of the interior of the film and it forms hydrogel (see samples treated with 75% methanol for 5 minutes and the center sample treated with 75% methanol for 20 seconds; these samples appear to have ruptured their methanol crosslinked shells and appear as hydrogel masses). The thin region in the center of the film does not swell because the films are sufficiently thin in this area to allow complete permeation of the methanol through the film within the limited treatment time. In the case of films treated with 90% and 100% methanol solution, increasing the treatment time increases the size of the central non-swelling region. As film thickness will increase with distance from the center, longer treatment times allow complete methanol penetration for the larger thicknesses corresponding to the increasing distance from the center. This suggests that response to methanol treatment (both concentration of the treatment solution and duration of treatment) depend on material thickness. Further work is needed to investigate this relationship.

Figure 2.25 shows cumulative release of reactive red 120 from films treated with various concentrations (50% 75% or 90%) of methanol for either 30 seconds or 5 minutes.

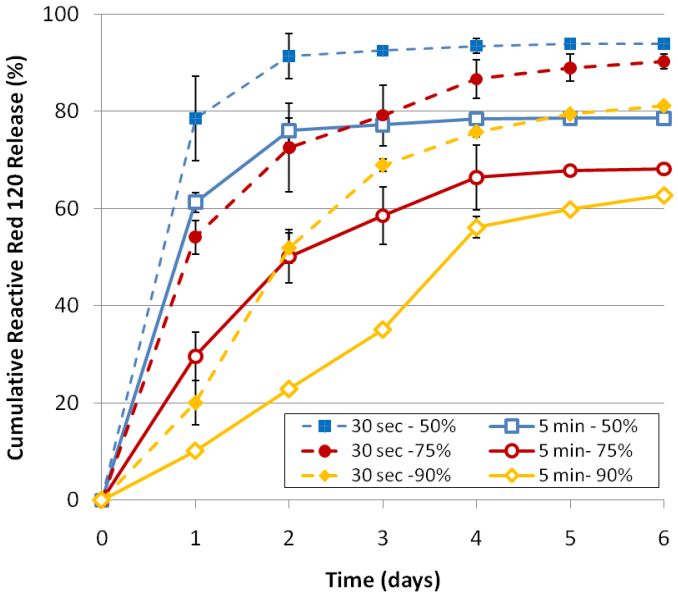

Figure 2.25. Cumulative reactive red 120 release from silk films treated with 50% (blue), 75% (red) or 90% (yellow) methanol solution for either 30 seconds (dotted lines) or 5 minutes (solid lines). N=4, error bars represent standard deviation (where error bars aren't shown they fall into background).

Increasing duration of treatment and methanol concentration in the treatment solution both result in decreased release rate. The most rapid release rate is observed for films treated with 50% methanol for 30 seconds (the shortest, lowest concentration methanol treatment tested) and the slowest release rate is observed for films treated with 90% methanol for 5 minutes (the longest, highest concentration methanol treatment tested). The difference in release rate on Day 1 is statistically significant for all treatment groups (two tailed t-test, df = 6: 5 minute treatment duration, 75% MeOH compared with 30 second treatment duration, 90% MeOH= $p < 0.05$, all other comparisons = $p<0.01$).

Values of n (the Siepmann-Peppas release coefficient) obtained by fitting the cumulative release data through Day 6 to equation 2.4 are listed in Table 2.1. With increasing treatment duration and increasing methanol content in the treatment solution, n increases. This suggests that release behavior becomes increasingly linear (i.e. closer to zero-order release) with increasing treatment duration or increasing methanol concentration in the treatment solution.

Estimated values of D/l^2 obtained by fitting experimental release data to equation 2.5 using MATLAB are also listed in Table 2.1. Permeability of the material (D/l^2) decreases with increasing treatment duration or methanol concentration in the treatment solution, suggesting that, as predicted, the increased cross linking that results from increased solution exposure or increased methanol in the treatment solution renders the silk increasingly less permeable to loaded drugs. Permeability (D/l^2) relative to methanol concentration in the post-drying treatment solution for the two treatment durations tested is shown in Figure 2.26.

Table 2.1. Parameters of release of reactive red 120 from silk films treated with varying concentrations of methanol solution for either 30 seconds or 5 minutes

		50% MeOH 50% H_2O	75% MeOH 25% H_2O	90% MeOH 10% H_2O
Treatment duration = 30 seconds	Siepmann Peppas Release Coefficient (n)	0.09	0.29	0.77
	Permeability (D/l^2)	1.66×10^{-1}	6.82×10^{-2}	2.26×10^{-2}
Treatment duration = 5 minutes	Siepmann Peppas Release Coefficient (n)	0.13	0.47	1.07
	Permeability (D/l^2)	1.36×10^{-1}	4.14×10^{-2}	1.30×10^{-3}

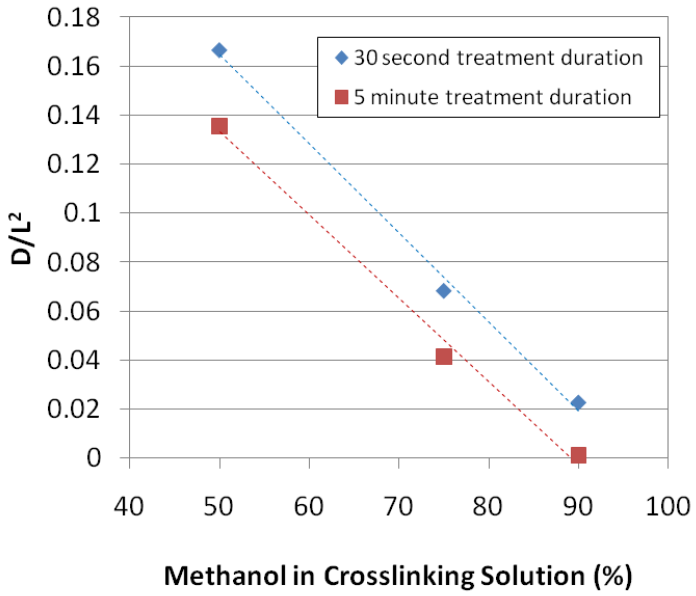

Figure 2.26. Diffusivity of reactive red 120 through silk films treated with varying ratios of methanol to water for either 30 seconds (blue diamonds) or 5 minutes (red squares). Values of D/L^2 (*p*) obtained by fitting a film diffusion model to cumulative release data using MATLAB.

Diffusivity decreases linearly with methanol concentration in the crosslinking solution: the correlation coefficients, R^2, for the 30 second and 5 minute treatment duration were 0.99 and 1.00, respectively. The different treatment durations also produced similar slopes: -3.63×10^{-3} and 3.40×10^{-3} for the 30 second and 5 minute treatment durations, respectively. This suggests that, for larger drugs like reactive red 120, duration of methanol treatment and concentration of methanol in the treatment solution could potentially provide tunable control of silk coating diffusivity.

2.3.1.3. Conclusions

While methanol treatment does not appear to significantly impact diffusion of small molecule drugs through silk films, β sheet content manipulation does appear to have potential as a control point for larger drugs. This approach to manipulating silk film permeability may prove

useful for controlling release of proteins, large molecule drugs and drugs with limited water solubility. Future work will include studies of other mild post-drying cross-linking strategies, including controlled slow drying (Lu *et al.*, 2010-2), water annealing (Jin *et al*., 2005) and stretching (Demura *et al*., 1989).

2.3.2. Degumming time

2.3.2.1. Introduction

As previously mentioned, degumming of silk to remove the inflammatory glue-like sericin is an essential step in preparing fibroin for implantable biomedical applications. However, the effects of this critical processing step on silk properties have not been extensively investigated. Vepari and Kaplan report that treatment of silk fibroin under alkaline conditions and heat (as encountered during degumming) will produce changes in the average molecular weight of silk. The authors also speculate that degumming time could impact degradation rate as decreased molecular weight might disrupt ordered structures and reduce cross-links, but these effects have never been studied (Vepari and Kaplan, 2007). Pandit *et al.* characterized silk solutions prepared by degumming cocoons for 30, 60, 90, 120, 150 and 180 minutes and found that degumming time affected average molecular weight and solution viscosity (Pandit *et al.*, 1972). Yamada *et al.* also reported decreased average molecular weight with increased degumming time (Yamada *et al*., 2001) and Jiang *et al*. found that different degumming treatments produced clearly visible effects on the tensile behavior, mechanical properties and morphology of cocoon silk (Jiang *et al*., 2006). Rajkhowa et al. report that an increase in *Philosomia cynthia ricinieri* non-mulberry silk degumming intensity (through increased alkali

concentration, treatment temperature or time) reduced the average molecular weight and increased the fraction of β-sheet (Rajkhowa *et al*., 2011). However, the effects of degumming on the degradation and drug release behavior of *B. mori* fibroin based materials have not been characterized.

If degumming time affects the resulting silk implant material properties (particularly average molecular weight) it could provide a useful control point. For many biodegradable polymers, molecular weight is one of the key factors in controlling degradation and drug release (Mittal *et al.*, 2007; Jain, 2000). Jain reports that increased polymer molecular weight corresponds to increased chain length (which can impact rate of diffusion through polymer matrices) and increased lipophilicity (which can decrease the rate of polymer degradation) (Jain, 2000). Varying the molecular weight of a polymer can therefore theoretically be used to control the degradation rate of a polymer and the release kinetics of drug from the polymer (Jain, 2000). Molecular weight has been reported to impact rates of drug release and degradation for several biodegradable polymer delivery systems including PLGA (Mittal *et al*., 2007), poly(D,L-lactic acid) (PDLA) (Park, 1994), *N*-isopropylacrylamide (NIPAAm) (Ramkissoon-Ganorkar *et al.*, 1999) and polycaprolactone (PCL) (Vandamme and Ngombo Mukendi, 1996).

Mittal *et al.* (2007) found that increasing the molecular weight of PLGA from 14.5 to 213 kDa significantly decreased the release rate of estradiol from PLGA nanoparticles. Further, they observed that the low molecular weight PLGA nanoparticles (14.5 and 45 kDa) released over 90% of total drug, while the higher molecular weight PLGA nanoparticles (85 and 213 kDa) released only 54.5 and 26.6% of their total drug load, respectively. Park (1994) reported that a relatively small difference in MW (17 versus 41 kDa) played a critical role in the degradation profile of PDLA microspheres (lower MW polymer exhibited significant degradation while the

higher molecular weight polymer showed no detectable degradation for 53 days). Ramkissoon-Ganorkar *et al*. (1999) studied release of insulin from NIPAAm beads and found that release rate was a function of the polymer's molecular weight, which they suggest could be exploited for targeted delivery (the low, intermediate and high MW beads dissolved within 2h (immediate delivery to the duodenum), 4h (lower small intestine) and 8h (colon), respectively). Vandamme and Mukendi observed increased release of levamisole from PCL matrix systems with a molecular weight of 53.5 kDa compared to systems with a molecular weight of 101.1 or 147 kDa.

Molecular weight has been shown to have a significant impact on drug release from other biodegradable systems, but as the degradation of silk is dependent on enzymatic proteolysis rather than hydrolysis, it is unclear whether degumming-induced changes in average molecular weight will have a similar effect on drug release or material degradation. In addition, Dang *et al*. (1996) report that the rate of release of carmustine (BCNU) from GLIADEL® wafers (copolymer matrix consisting of 1,3-bis(p-carboxyphenoxy)propane (CPP) and sebacic acid (SA)) and the rate of wafer erosion are both independent of the initial molecular weight. The objective of this study was therefore to determine what effect degumming time has on silk properties (including average molecular weight) and silk film material properties and diffusivity.

2.3.3.2. Materials and methods

2.3.3.2.1. Materials

Cocoons of *Bombyx mori* silkworm silk were purchased from Tajima Shoji Co., LTD (Sumiyoshicho, Naka-ku, Yokohama, Japan). Protease type XIV (3.5 units/mg) from *Streptomyces griseus* and all chemicals were purchased from Sigma-Aldrich (St. Louis, MO).

2.3.3.2.2. Silk fibroin solution preparation

Silk fibroin was prepared from *B. mori* cocoons as we have previously described (Sofia *et al*., 2001). Briefly, cocoons were boiled for 10, 30, 60 or 90 minutes in a solution of 0.02 M Na_2CO_3 and rinsed, then dried at ambient conditions overnight. Degumming times were varied (10 min, 30 min, 60 min and 90 min) to confirm that increased exposure to heat and alkaline conditions would decrease average molecular weight, as predicted (Vepari and Kaplan, 2007). The dried fibroin was solubilized in a 9.3 M aqueous LiBr solution at 60^{o}C for 4 hours, yielding a 20% (w/v) solution. LiBr was then removed from the silk solution via dialysis against distilled water for 2.5 days using Slide-a-Lyzer dialysis cassettes (MWCO 3,500, Pierce Thermo Scientific Inc., Rockford, IL). Silk fibroin concentration was determined by evaporating water from a solution sample of known volume and massing using an analytical balance. All solutions were stored at 4-7^{o}C before use.

2.3.3.2.3. SDS-PAGE gel electrophoresis

Samples of silk prepared using varied degumming times were analyzed by SDS-PAGE using NuPAGE Novex 3-8% Tris-Acetate pre-cast gels and Tris-acetate running buffer. 5 micrograms of protein per well were run as denaturing, reduced samples according to manufacturer's instructions (150 V constant for 1 hour). Separated proteins were detected with Colloidal Blue staining kit according to manufacturer's instructions. Molecular weight was

estimated from HiMark unstained protein standard. All SDS-PAGE gel materials were purchased from Invitrogen, Carlsbad, CA.

2.3.3.2.4. Aqueous silk film preparation and capping

Drug loaded silk fibroin films were prepared as we have previously described (Hofmann *et al*., 2006). Briefly, drug solution was mixed with silk that was degummed for 60 minutes to a final concentration of 6% (w/v) silk and aliquoted into 24 well plate wells (0.5 mL per well). Controls were prepared using silk diluted with water containing no drug. Films were dried overnight at ambient conditions then treated with methanol for 5 minutes to increase β sheet content and render the films water insoluble. Once dried, 0.5 mL of 6% silk that had been degummed for varied times (10, 30, 60, 90 min) was added to each drug loaded film, forming a capping layer. Capping layers were dried overnight at ambient conditions then treated with methanol for 5 minutes. For the purposes of comparison, samples of each drug loaded film were also left uncapped.

To characterize the effects of varied degumming on a range of different potential therapeutics, multiple different model dyes and proteins were studied, including azoalbumin, reactive-red 120, rifampicin, and indigo carmine (Figure 2.2), which are 66.4 kilodaltons, 1469.98 g/mol, 822.94 g/mol and 466.35 g/mol, respectively. Azoalbumin, rifampicin and reactive-red 120 loaded films all received only one capping layer. Due to its relatively small molecular weight, indigo carmine films received either two or four capping layers (abbreviated 2x or 4x). For multiple capping layers, each layer was dried and methanol treated prior to the addition of the next layer.

2.3.3.2.5. Dehydrated hydrogel silk film preparation and capping

Due to its limited solubility in water, bulk loaded rifampicin film reservoirs were prepared using an alternative protocol: 0.25 mL of 8% (w/v) silk was aliquoted into each well of a 24 well plate, then 0.25 mL of 10 mg/mL rifampicin suspended in methanol was added and mixed into each well (resulting in 0.5 mL of 4% (w/v) silk gel containing 2.5 mg of rifampicin per gel). The addition of methanol to silk induced gelation, and the resulting gel was dehydrated to a film overnight at ambient conditions. The dried film was not subjected to any addition methanol treatment, as the necessary cross-linking occurs during gelation and methanol treatment could potentially leech the alcohol-soluble rifampicin from the film. Once dried, the rifampicin loaded silk films were capped with one silk capping layer as described above (0.5 mL of 6% silk degummed for varied times was added to each drug loaded film, dried and methanol treated for 5 minutes).

2.3.3.2.6. Release testing

To determine drug release from the capped silk films, 1 mL of PBS was added to each well and sampled were incubated at 37^{o}C. At desired time points, the buffer was removed and replaced with fresh buffer. The amount of released dye was determined using UV-Vis spectroscopy at 358 nm, 475 nm, 535 nm and 610 nm, for azoalbumin, rifampicin, reactive red 120 and indigo carmine, respectively. The amount of released compound in each sample was summed with the amounts at each previous time point and divided by the total amount to obtain cumulative release values. Four samples were tested per release buffer type (n=4) and each sample was assayed in triplicate.

2.3.3.2.7. Film characterization – Differential Scanning Calorimetry (DSC)

Differential Scanning Calorimetry (DSC) studies were carried out using TA Instruments Q100 DSC (New Castle, DE), and equipped with a refrigerated cooling system. Indium was employed for the temperature and heat flow calibration. The heat capacity was evaluated with respect to sapphire standard. Dry nitrogen gas was purged into the DSC cell with a flow rate of 50 mL/min. Five mg of each silk sample were encapsulated in aluminum pans and first heated to 140^{o}C to remove the bound water in the materials ((Hu *et al*., 2006; Hu *et al*., 2010-1; Hu *et al*., 2010-2), and then standard mode DSC measurements were performed at a heating rate of 2^{o}C/min, from -40^{o}C to 350^{o}C. Endotherms are presented with downward deflection in scans.

2.3.3.2.8. Film characterization – Fourier Transform Infrared spectroscopy (FTIR) analysis

Fourier Transform Infrared spectroscopy (FTIR) analysis of the silk samples was performed with a Jasco FT/IR-6200 Spectrometer, equipped with a multiple reflection, horizontal MIRacle^{TM} Attenuated Total Reflectance (ATR) attachment (Pike Tech., Madison, WI). 128 scans were co-added for each measurement and Fourier transformed employing a Genzel-Happ apodization function to yield spectra with a nominal resolution of 4 cm^{-1}. The wavenumber ranged from 400 to 4000 cm^{-1}. Secondary structures in silk protein samples can be identified from the absorption spectra of the Amide I region (1595~1705 cm^{-1}). The peak absorption bands in the frequency range of 1610~1625cm^{-1} represent β-sheet structure (Hu *et al*., 2006; Hu *et al*., 2010-1; Hu *et al*., 2010-2). The peak absorption bands around the frequency 1640~1660cm^{-1} were ascribed to the random-coil and alpha-helix spectrum (Hu *et al*., 2006; Hu *et al*., 2010-1; Hu *et al*., 2010-2). The peaks above 1660 cm^{-1} were ascribed to beta turns (Hu *et al*., 2006; Hu *et al*., 2010-1; Hu *et al*., 2010-2).

2.3.3.2.9. Film characterization – packing density

Packing density was determined by measuring mass using an analytical balance, and measuring film thickness using a using a Mitutoyo absolute digimatic caliper with a 0.01 mm resolution (Mitutoyo America Corporation, Aurora, IL). Density (in mg/mm^3) was determined by dividing the total film mass (in mg) by the total film volume (surface area of the mold in mm^2 multiplied by film thickness in mm). For the packing density studies, n =5.

2.3.3.2.10. Film characterization – diffusivity

Values of p (D/l^2, units of $days^{-1}$) were obtained using MATLAB as described previously (section 2.3.1.2.5**)**, the diffusion coefficient (D) was solved for using the measured length values determined in section 2.3.3.2.9.

2.3.3.3. Results and discussion

2.3.3.3.1. Effect of degumming time on silk molecular weight

Figure 2.27 show silk prepared using 90 minute and 10 minute degumming times in dialysis cassettes and the result of SDS PAGE analysis of silk degummed for 10, 30, 60 and 90 minutes.

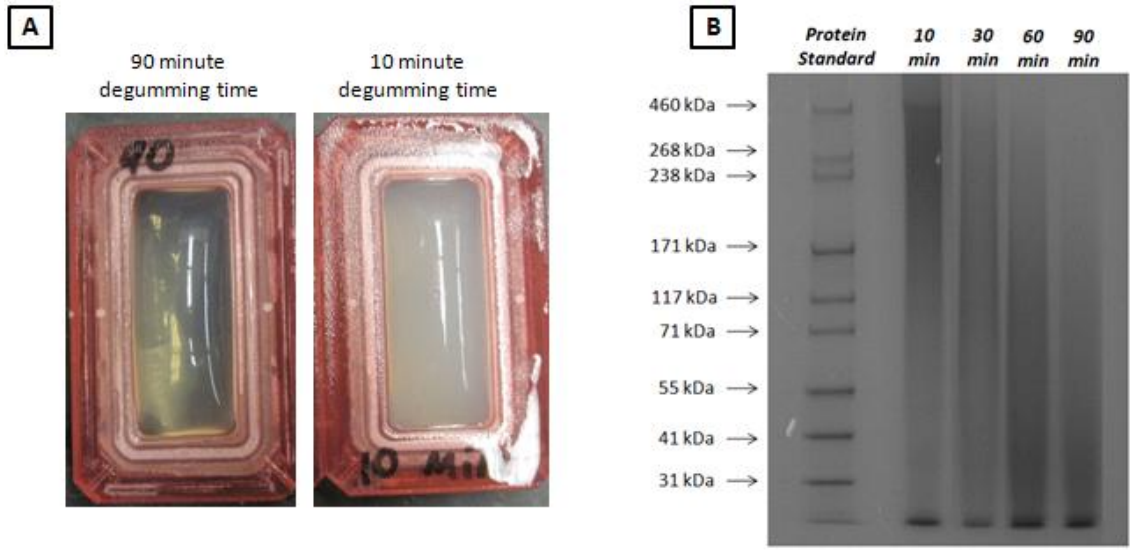

Figure 2.27. Effect of varied degumming time on silk solution. (A) Appearance of aqueous silk solutions in dialysis cassettes prepared from fibroin degummed for 90 minutes (left) and 10 minutes (right) (B) SDS-PAGE analysis of silk subjected to various degumming times and stained with colloidal blue. Lane 1: HiMark high molecular weight protein standard; lane 2: empty; lane 3: silk degummed for 10 minutes; lane 4: silk degummed for 30 minutes; lane 5: silk degummed for 60 minutes; lane 6: silk degummed for 90 minutes.

Decreasing degumming time produced an increasingly more opaque/less clear post-dialysis silk solution (Figure 2.27A). In addition, a qualitative decrease in viscosity was observed with increasing degumming time. Though quantitative viscosity measurement to confirm this observation is still needed, this observed relationship is consistent with the Mark-Houwink equation which predicts that viscosity (η) will increase proportionally with weight-average molecular weight (M_w) (Omelczuk and McGinity, 1992).

Figure 2.27B shows that increased degumming time resulted in a decrease in the degummed silk's MWD. Silk degummed for 10 minutes had a molecular weight distribution predominantly contained in the 171 kDa to 460 kDa range. 30 minute degumming produced silk with a broad molecular weight distribution from approximately 31 kDa to 268 kDa (the lightness of the 30 minute well is likely due to the even distribution of the protein over a larger range than the 90 minute, 60 minute or 10 minute treatment groups). The majority of the silk protein

produced by the 60 minute degumming time was less than 171 kDa. 90 minute degumming time produced silk proteins that were predominantly 71 kDa or smaller. This confirms that treating silk fibroin under the heated alkaline conditions encountered during degumming impacts the molecular weight as reported by Vepari and Kaplan (Vepari and Kaplan, 2007). This suggests that degumming time can potentially be used to manipulate silk properties like average molecular weight and viscosity, which may in turn affect silk drug carrier and scaffold material properties.

2.3.3.3.2. Effect of degumming time on silk beta sheet content and glass transition temperature

β-sheet content of silk fibroin films prepared using silk solutions of varied degumming times was assessed using FTIR (Figure 2.28). Results of DSC analysis are shown in Figure 2.29.

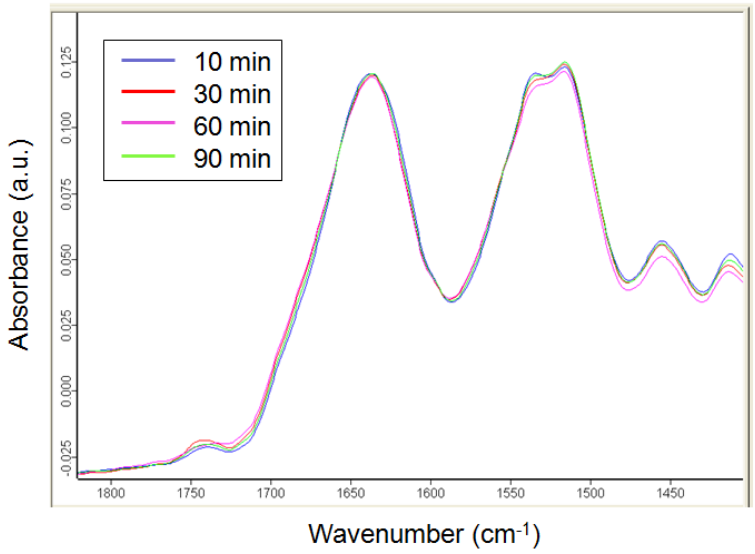

Figure 2.28. Effect of degumming time on the β-sheet content of silk films: FTIR spectra (amide I and amide II bands) of silk films prepared from silk degummed for 10, 30, 60 and 90 minutes. There are no discernable differences between the four FTIR spectra.

Despite the decrease in molecular weight produced by increased degumming time, no difference in the β-sheet content of the silk films was observed. This suggests that degumming time (up to 90 minutes) does not impact the β-sheet crystal assembly of silk films, and that the difference in molecular weight is produced by degradation of other regions of the silk protein.

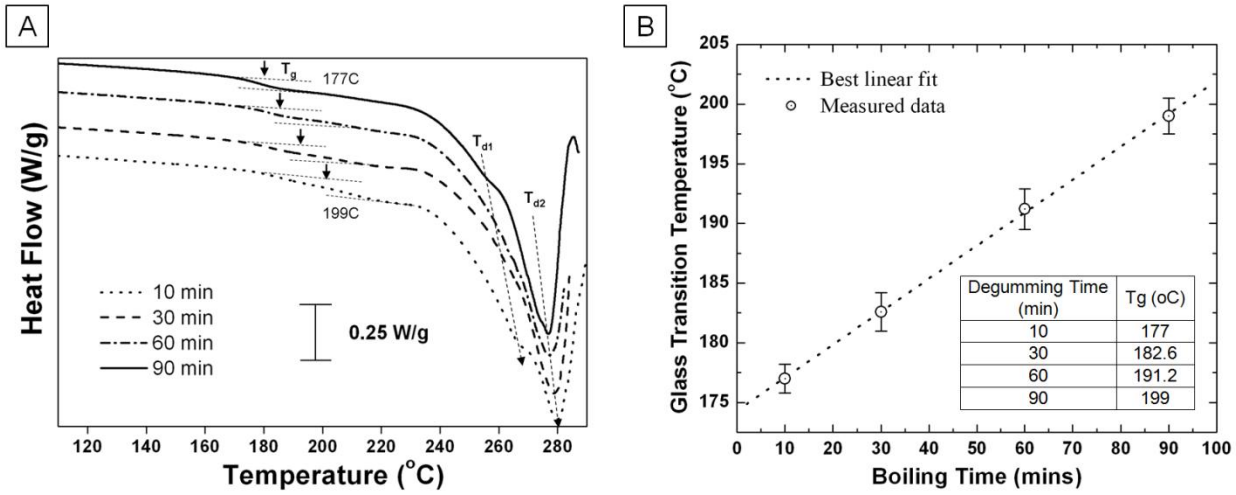

Figure 2.29. (A) Effect of degumming time on the glass transition temperature of silk films: TGA analysis of silk films prepared from silk degummed for 10, 30, 60 and 90 minutes. (B) Glass transition temperature versus degumming time.

Glass transition temperature was found to linearly increase with degumming time. This is consistent with literature on the relationship between Tg and molecular weight for PLGA (Omelczuk and McGinity, 1992; Steendam *et al*., 2001). According to Omelczuk and McGinity, this change in Tg arises from the fact that as the polymer molecular weight increases, there are fewer chains ends which have less free volume than the same number of atoms in the middle of the chain (Omelczuk and McGinity, 1992).

2.3.3.3.3. Effect of degumming time on silk film packing density

Average packing densities for films cast from silk solutions of equal concentrations prepared using varied degumming times are shown in Figure 2.30.

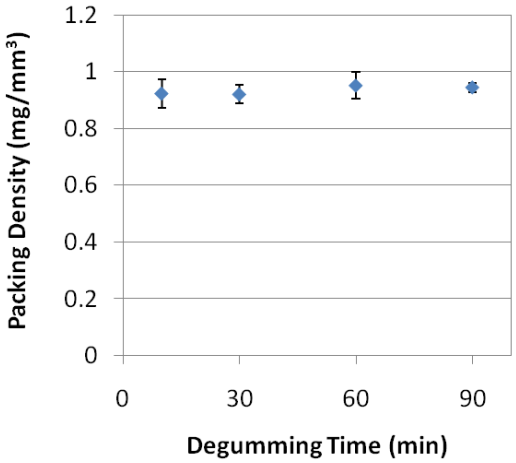

Figure 2.30. Packing density measurements of films prepared from silk degummed for 10, 30, 60 and 90 minutes. N=5, error bars represent standard deviations.

Films prepared from silk degummed for 10, 30, 60 and 90 minutes were found to have packing densities of 0.92 ± 0.05, 0.92 ± 0.03, 0.95 ± 0.05 and 0.94 ± 0.02 mg/mm^3, respectively. It appears as though the 60 and 90 minute silk films might be slightly more dense than the 10 and 30 minute silk films, but statistical analysis reveals no significant difference in packing density among the different degumming times (two tailed t-test, df = 8, $p < 0.01$). This suggests that degumming time does not affect initial packing density or film thickness.

2.3.3.3.4. Effect of varied degumming time on indigo carmine release through silk capping layers

Figure 2.31 shows cumulative release behavior for films loaded with indigo carmine, then capped with either two or four capping layers of silk prepared using varied degumming times.

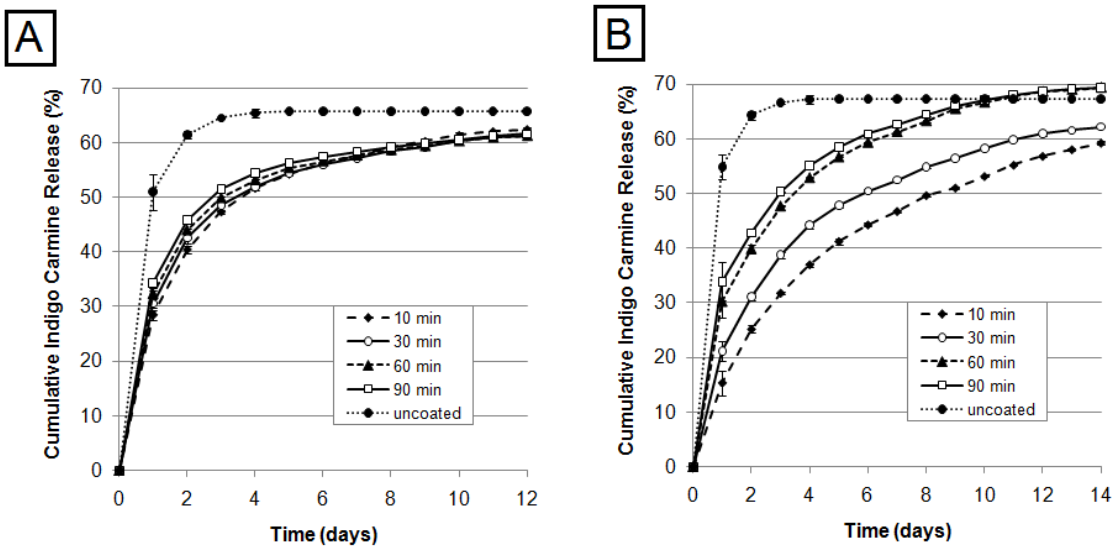

Figure 2.31. Cumulative indigo carmine release from films (A) capped with two silk layers and (B) capped with four silk layers with silk prepared using varied degumming times. N=4, error bars represent standard deviations (where error bars aren't shown they fall into background).

As seen in Figure 2.31A, when indigo films are coated with only two capping layers, the difference in release profile among the different degumming times is slight. However, when the number of capping layers is increased to four (Figure 2.31B), a difference is observed. For four capping layers, release rate decreases with decreasing degumming time.

To determine the relationship between path length, permeability and diffusion coefficient, indigo carmine cumulative release data was fitted to equation 2.5 using MATLAB. Fitted data is shown in Figure 2.32.

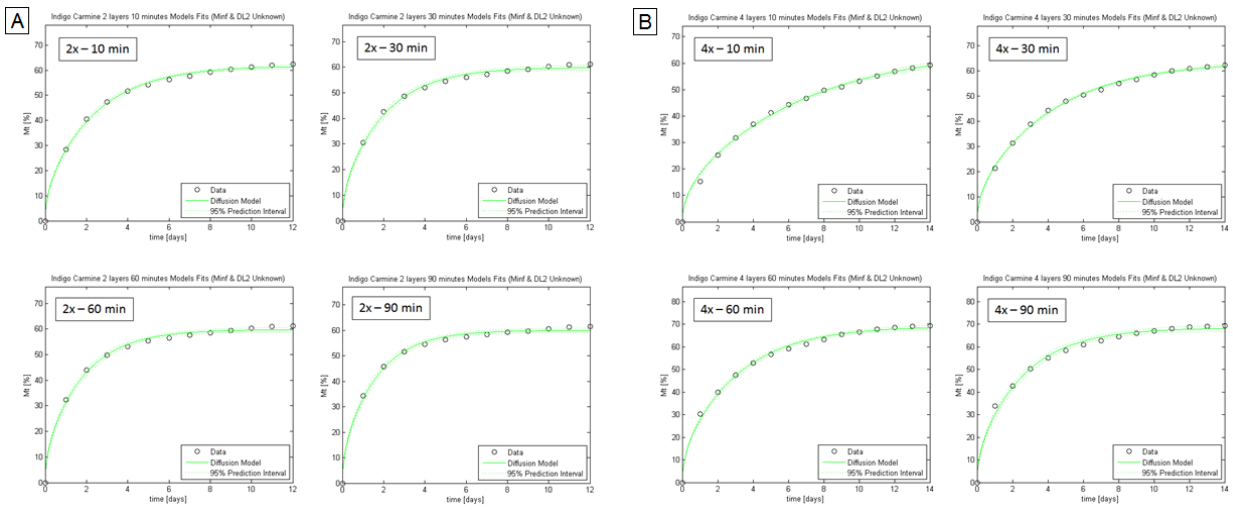

Figure 2.32. Sample diffusion based model fits to (A) 2x and (B) 4x indigo carmine cumulative release data.

Figure 2.32 shows that the experimental data fits the model well (green release curves predicted by the model intersect the black circles representing experimental data). Values of p ($p= D/L^2$, equation 2.6) were obtained from this fitting. Values of D/L^2 are shown relative to degumming times in Figure 2.33A. Thickness measurements were used to solve for diffusion coefficients, D, which are shown relative to degumming time in Figure 2.33B.

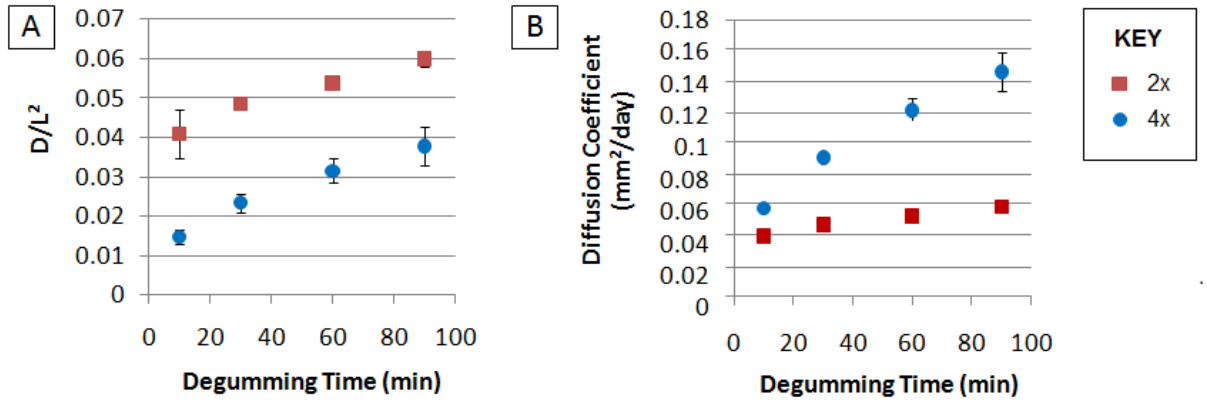

Figure 2.33. Diffusivity of indigo carmine through silk films. (A) Values of D/L^2 (*p*) obtained by fitting a film diffusion model to cumulative release data using MATLAB relative to degumming time for two silk capping layers (2x, red squares) and four silk capping layers (4x, blue circles). N=4, error bars represent standard deviations (where error bars aren't shown they fall into background). (B) Values of diffusion coefficient

Strangely, when solving for diffusion coefficient, diffusivity appears to increase with path length. This suggest that, as described in the previous section on path length, the assumptions of the model are not upheld (diffusion coefficient is not constant, path length is shorter than predicted, etc.). Solving for the ratio of path lengths assuming constant D, the ratio of 4x to 2x is approximately 1.4 to 1, rather than the expected 2 to 1. Uneven film drying (thinner in the center, thicker around the edges, as described in section 2.3.1.3.3.) might be compounded by multiple coatings, causing overestimation of film thickness. Further work is needed: if path length is controlled (as in the case of dehydrated hydrogel encapsulation), diffusivity might be constant.

2.3.3.3.5. Effect of varied degumming time on rifampicin release through silk capping layers

Figure 2.34 shows cumulative release behavior over two weeks for dehydrated gel films loaded with rifampicin, then capped with a single layer of silk prepared using varied degumming times.

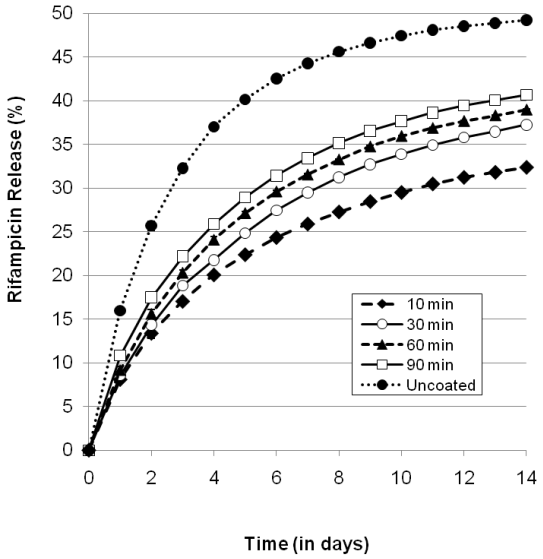

Figure 2.34. Cumulative rifampicin release from dehydrated gel films capped with silk prepared using varied degumming times. N=4, error bars represent standard deviations (where error bars aren't shown they fall into background).

As with indigo carmine release through four capping silk layers, release of rifampicin through one silk capping film increases with increasing degumming time, suggesting the barrier to diffusion increased with decreasing degumming time. The fact that the difference in rate of drug diffusion through the silk is observable for rifampicin compared to indigo carmine even though the capping thickness is thinner can be attributed to rifampicin being larger and less water soluble than indigo carmine.

2.3.3.3.6. Effect of varied degumming time on reactive red 120 release through silk capping layers

Figure 2.35 shows cumulative release behavior over seven days for films loaded with reactive red 120, then capped with a single layer of silk prepared using varied degumming times.

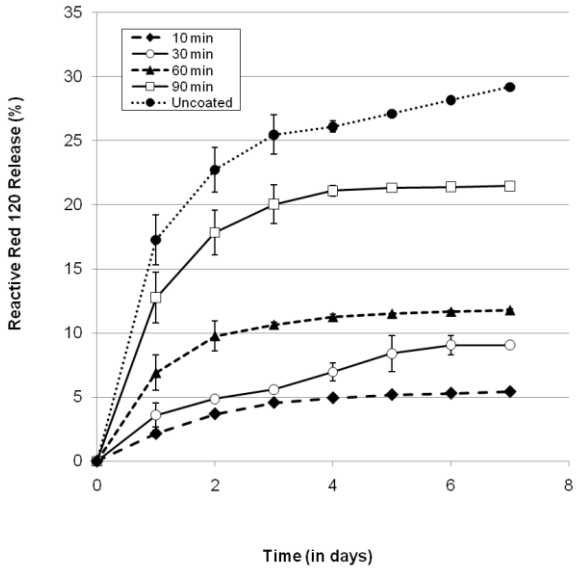

Figure 2.35. Cumulative reactive red 120 release from films capped with silk prepared using varied degumming times. N=4, error bars represent standard deviations (where error bars aren't shown they fall into background).

Again, increased degumming times results in an increased rate of drug diffusion through the capping layer. The difference in release is particularly pronounced when the degumming time of the silk used for the capping film increases from 60 minutes to 90 minutes. Further study is needed to investigate the cause of this disproportionate increase.

2.3.3.3.7. Effect of varied degumming time on azoalbumin release through silk capping layers

Figure 2.36 shows cumulative release behavior over 30 days for films loaded with azoalbumin, then capped with a single layer of silk prepared using varied degumming times.

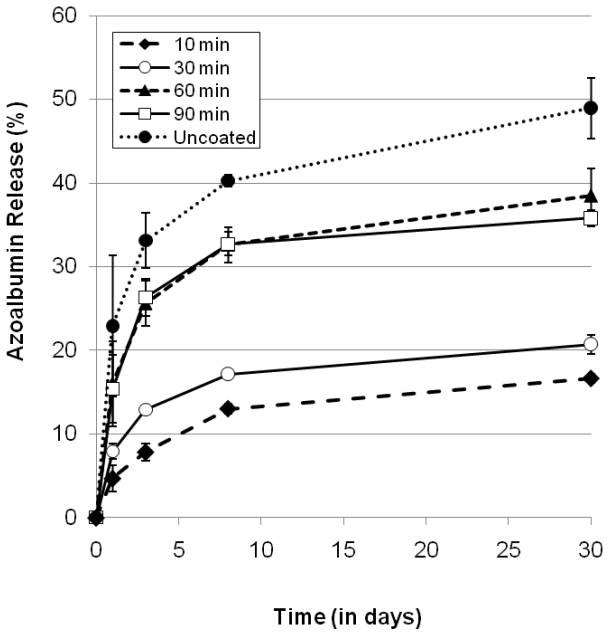

Figure 2.36. Cumulative release of azoalbumin from films capped with silk prepared using varied degumming times. N=4, error bars represent standard deviations (where error bars aren't shown they fall into background).

In this case, increased degumming times only result in an observable increase in the rate of drug diffusion through the capping layer up to a 60 minute degumming time (no difference is seen between the release curves for the films capped with 60 and 90 minute degumming time silk films).

2.3.3.3.8. Discussion

Results of the SDS-PAGE analysis demonstrate that, as predicted, increased degumming times decrease the average molecular weight of silk. The increased exposure to heat and alkalinity break down the protein into smaller and smaller fragments. Release studies demonstrate that increased degumming time using in preparing the silk consistently increased rate of release of various drugs through silk capping layers (i.e., increased degumming time decreases the diffusivity of the silk films.

Though longer degumming durations degraded the silk protein into increasing smaller fragments, and silk films cast from silk prepared using longer degumming times are increasingly permeable to drugs, FTIR analysis shows that degumming time has no effect on β sheet content. A potential explanation for this observation (represented schematically in Figure 2.37) is that the hydrophobic domains of silk involved in β-sheet secondary structure are unaffected by increased degumming, while the other regions of the silk protein are increasingly degraded during degumming. When films are prepared from silk solution prepared with varied degumming times, β-sheet content remains constant but films prepared from longer degumming time silks are less organized and more permeable.

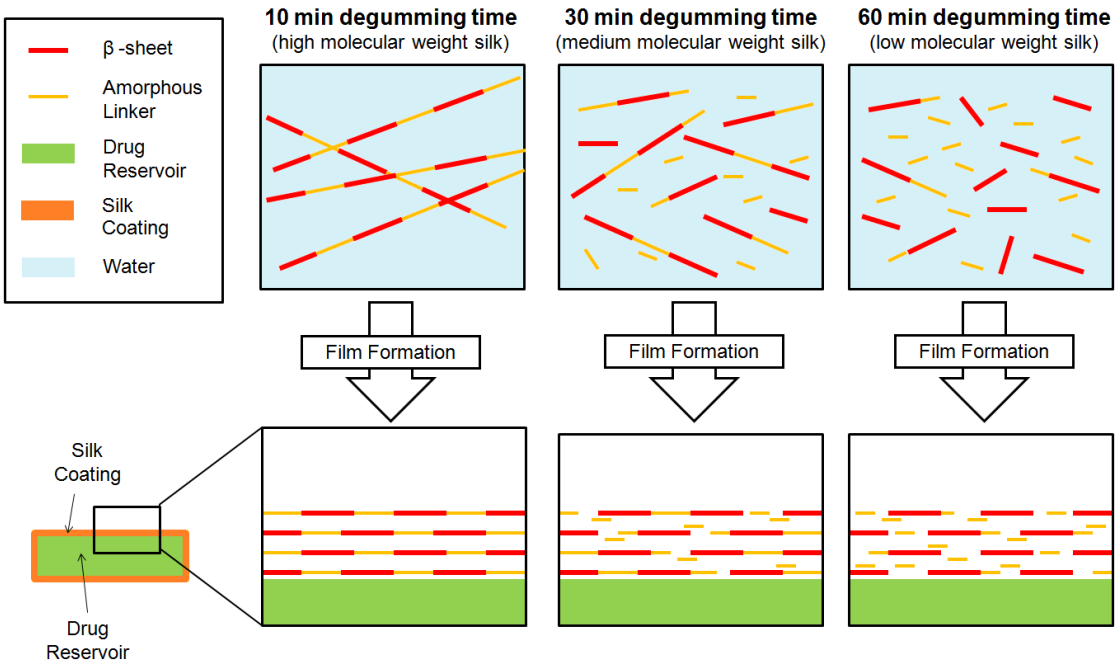

Figure 2.37. Schematic representation of the relationship between β-sheet content, fragment size and diffusivity of silk films. At the beginning, all three aqueous silk solutions produced by the different degumming times have the same total amount of red bars (representing the domains involved in β sheet formation) but with increasing degumming time the other regions of the silk protein like the amorphous linkers (represented by gold bars) are increasingly degraded. When silk films are formed around the drug reservoir (silk coating in orange, drug reservoir in green), all the films have the same β sheet content. However, the increasing degumming time that produced increasingly smaller molecular weight fragments results in formation of a less organized, more permeable polymer membrane for the drug to diffuse through.

Uncrosslinked silk fragments (which are expected to be increasingly prevalent with increasing degumming time based on the decreasing average molecular weight) are also expected to dissolve out of the films during methanol treatment and subsequent immersion in release buffer (films prepared from 10 minute, 30 minute, 60 minute and 90 minute degumming time silk lost 5.6, 6.6, 9.1 and 13.9% of their mass in PBS within 24 hours). Since the initial pre-treatment packing densities and film masses are equal, the initial film thicknesses are the same. Once unequal amounts of silk film diffuse out of the films, the thickness presumably does not change so as mass loss increases with decreasing fragment size, the apparent packing density must decrease.

2.3.2.4. Conclusions

This study confirms that degumming time can be used to manipulate average molecular weight and demonstrates for the first time that the degumming process can affect the rate of drug diffusion through silk films. Degumming time represents a new, previously unexploited control point for manipulating silk material properties with great potential utility in designing silk biomaterials for controlled drug delivery. The observation that β sheet content is unaffected by degumming time is particularly exciting, as it suggests that additional release rate control could be achieved by manipulating both the β sheet content and molecular weight of the silk solution used for coating.

2.4. Integrated Model: controlled diffusion of adenosine from silk encapsulated reservoirs

In the previous studies we demonstrated that release rate was proportionally related to inverse path length in a dehydrated hydrogel encapsulation system (i.e., as the amount of silk hydrogel was added, path length increased and release rate decreased). We also showed that diffusivity of silk films to drugs could be controlled via degumming time. Cumulative adenosine release from dehydrated silk hydrogel encapsulated reservoirs (section 2.2.2.3.2, Figure 2.19) and the early time approximation of Fickian diffusion (equation 2.2) together provide a model for controlling release rate via path length for 30 minute degumming time silk (Figure 2.20; path length is varied while diffusivity is held constant). Based on this model, we predicted the release rate of adenosine from a reservoir encapsulated in a 1.47 mm thick coating (corresponding to 120 mg or 1.5 mL of 8% (w/v) silk hydrogel per side) would result in a release rate of approximately 10.2% per day.

To manipulate diffusion coefficient, cumulative release data was collected for adenosine films coated with capping layers of silk prepared using varied degumming times was collected (Figure 2.38A), fitted to equation 2.5 using MATLAB as previously described (section 2.3.3.3.4.) Values of p ($p= D/L^2$, equation 2.6) obtained from this fitting and measured thicknesses were used to solve for diffusion coefficients, which are shown relative to degumming time in Figure 2.38B.

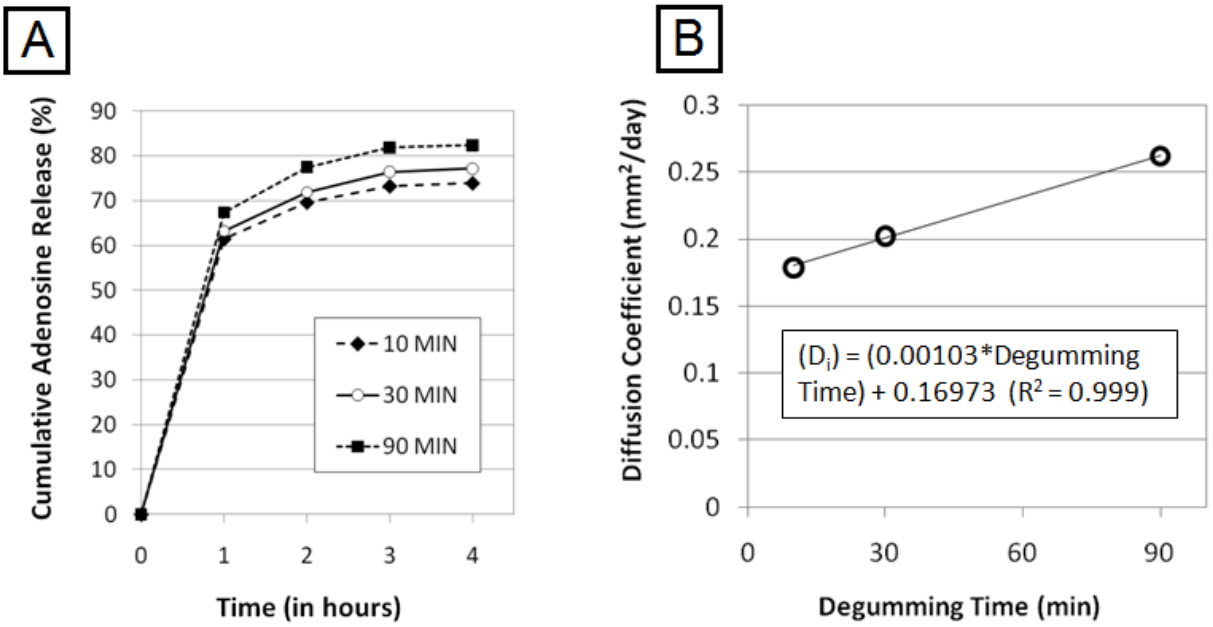

Figure 2.38. Degumming time controlled diffusion of adenosine through silk films. (A) Cumulative release of adenosine from films capped with silk prepared using varied degumming times N=4, error bars represent standard deviations (where error bars aren't shown they fall into background). (B) Diffusion coefficient relative to degumming time. Linear relationship is observed (equation inset in graph).

An equation was fit to the linear relationship between degumming time and diffusion coefficient, shown as an inset in Figure 2.38. This allowed us to predict the diffusion coefficient of adenosine through silk films prepared using any degumming time from 10 to 90 minutes (increases above 90 minutes would need further study to confirm that the proportional relationship between degumming time and diffusion coefficient is maintained). Again, data was used for cumulative adenosine release from dehydrated silk hydrogel encapsulated reservoirs (section 2.2.2.3.2, Figure 2.19) and the early time approximation of Fickian diffusion (equation 2.2), but this time diffusivity was also varied by solving for AC_o (assumed to be constant) using known values of $D_{i,30min}$, release rate and path length (theoretical AC_o was calculated to check that values of AC_o derived from experimental data were reasonable, and excellent agreement was found between the two values). With the AC_o constant known, path length controllable via mass

of hydrogel coating added, and diffusion coefficient controllable via degumming time (and calculated using the equation shown in Figure 2.38), release rates could be predicted for reservoirs in which both path length and silk degumming time were manipulated. The predicted release rates for varied path length and varied silk degumming time (10, 30, 60 and 90 minutes) are shown in Figure 2.39.

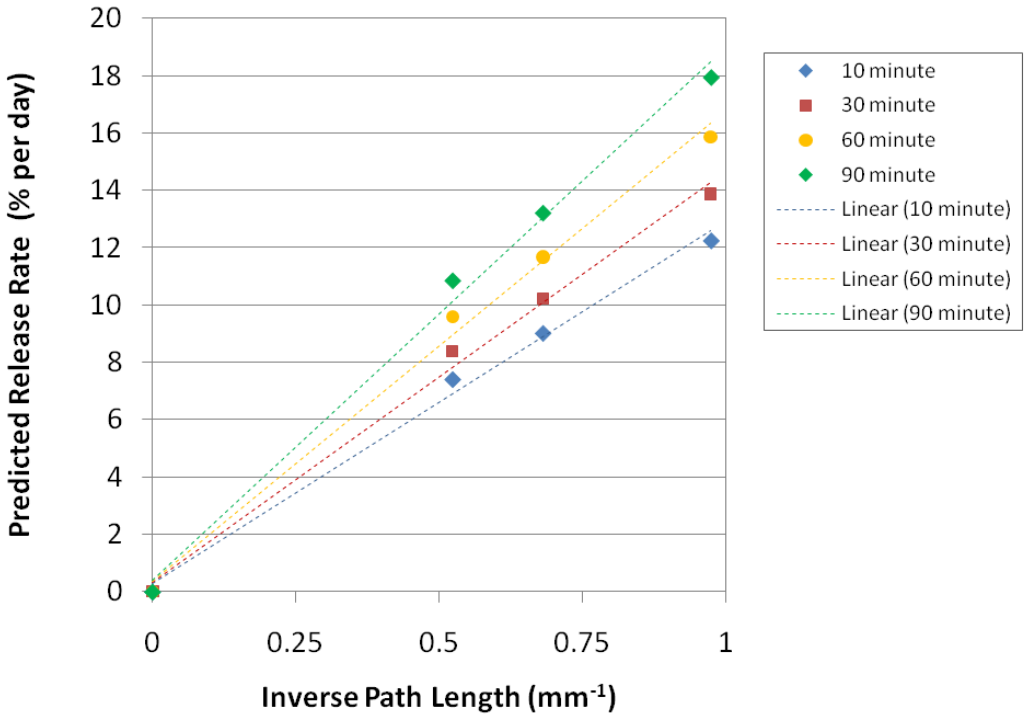

Figure 2.39. Model predictions of adenosine release rate from silk encapsulated reservoirs versus inverse path length for varied silk degumming times (10, 30, 60 and 90 minutes).

To check the predictive accuracy of this model, encapsulated reservoirs were prepared using 30 minute and 60 minute degumming time silk. Path length was again controlled via mass of silk hydrogel added. The only difference between these encapsulated reservoirs and the reservoirs prepared in section 2.2.2.3.2, was that prior to hydrogel encapsulation the reservoirs were dipped in 8% (w/v) aqueous silk solution, dried, and methanol treated to preserve the drug

stability in the reservoir during release. Experimental cumulative release curves and release curves predicted by this model are shown in Figure 2.40 and 2.41 (Figure 2.41 presents the same data as Figure 2.39, broken down by the characteristics of the silk coating for easier comparison).

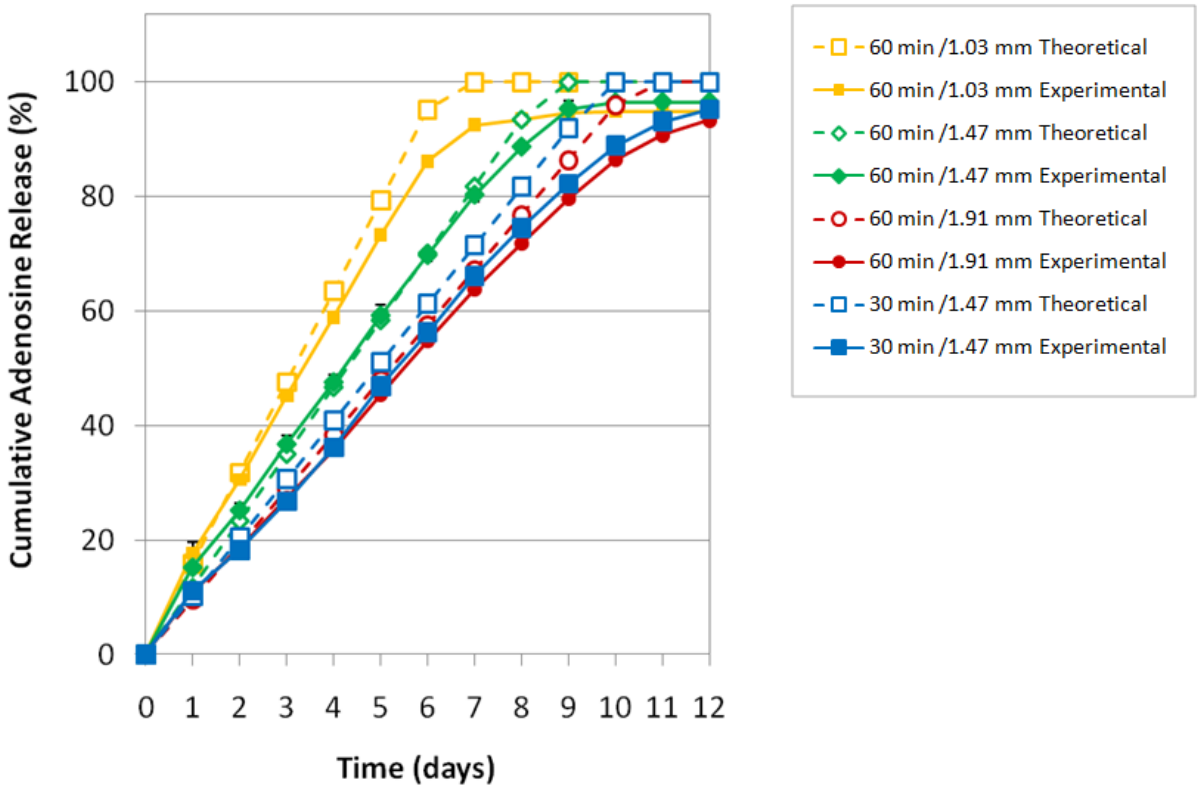

Figure 2.40 Cumulative release of adenosine from silk encapsulated reservoirs of varying path length and diffusivity (degumming time). Collected experimental release curves are shown in solid lines with filled markers, theoretical release curves predicted by the model are shown in dotted lined with empty markers. N=3, error bars represent standard deviations (where error bars aren't shown, they fall into background).

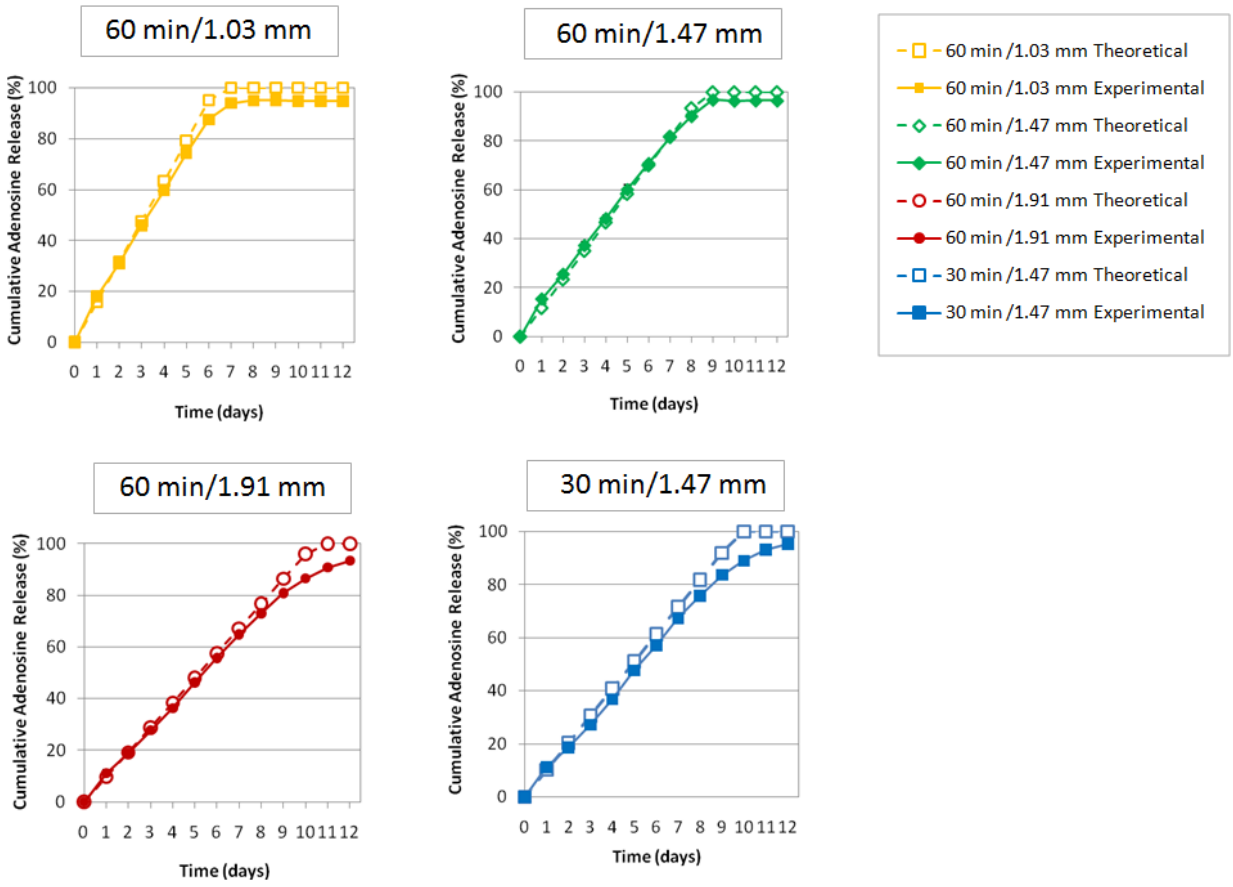

Figure 2.41 Cumulative release of adenosine from silk encapsulated reservoirs of varying path length and diffusivity (degumming time) broken down by characteristics of the silk coating. Collected experimental release curves are shown in solid lines with filled markers, theoretical release curves predicted by the model are shown in dotted lined with empty markers. N=3, error bars represent standard deviations (where error bars aren't shown, they fall into background).

Generally, rate of release is slightly slower than predicted, but overall excellent agreement is observed between the predicted release behavior and the experimental data, especially within the first 60% of the release curve. Note that an aqueous dip-coating prior to hydrogel encapsulation improves stability, but longer time frames will need to be investigated to confirm that stabilization improves long term recovery.

Average release rates were calculated for the first 60% of drug release for the experimental samples, and compared to predicted release rates. These comparisons are shown in

Figures 2.32 (30 minute degumming time, varied path length) and 2.33 (60 minute degumming time, varied path length).

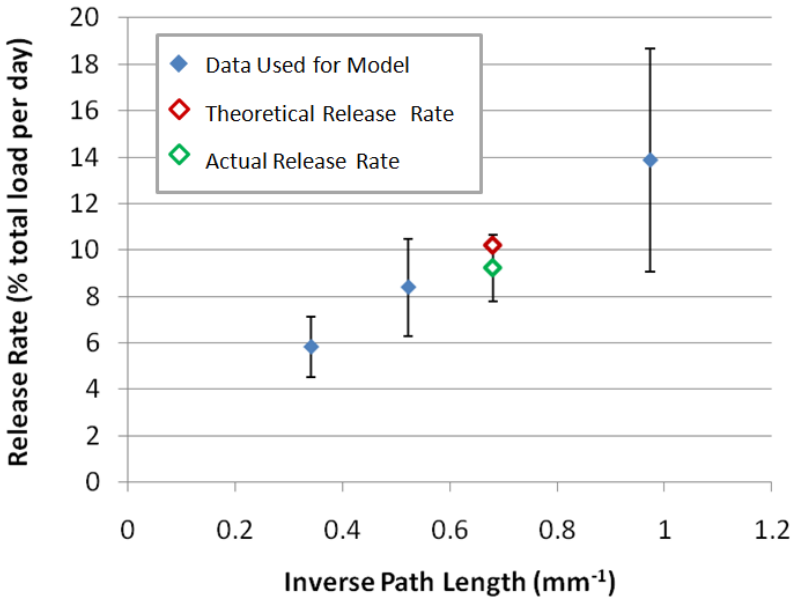

Figure 2.42. Average adenosine release from 30 minute-degumming time silk encapsulated reservoirs. Blue diamonds represent data used to develop the predictive model (i.e., data from section 2.2.2.3.2, Figure 2.18), the red diamond represents theoretical release extrapolated based on the linear relationship between release rate and inverse path length, the green diamond represents the average release rate of the experimental samples (n=3, error bar represents standard deviation).

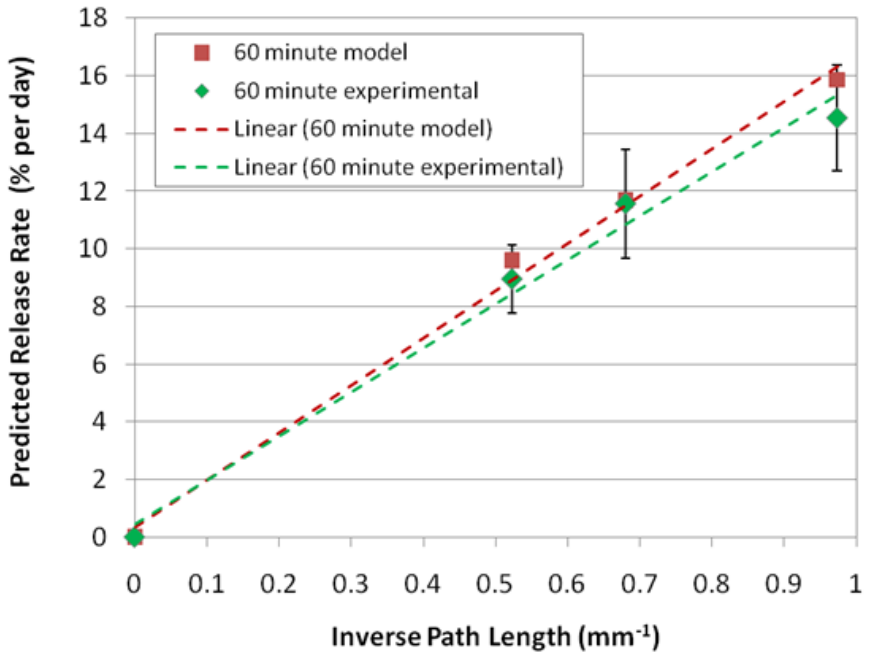

Figure 2.43. Comparison of predicted adenosine release behavior and experimental adenosine release from 60 minute-degumming time silk encapsulated reservoirs. Red indicated the theoretical release rates predicted by the proposed model, green indicates average adenosine release rate for the experimental samples (n=3, error bars represent standard deviations).

Figures 2.31 and 2.32 confirm the predictive capabilities of the proposed model. Excellent agreement is once again observed between the predicted release rates and experimentally determined release rate averages.

2.5. Conclusions and Future Directions

These studies demonstrate that multiple control points exist through which drug release from silk biomaterials can be controlled. While methanol treatment was not found to have a significant effect on small molecule diffusion through silk films, we present a thorough characterization of two promising control points related to geometry and diffusivity: path length

and degumming time. Manipulations of these properties through processing were shown to yield controllable, quantifiable effects on release behavior.

A model based on Fickian diffusion that predicts release rate based on manipulation of diffusivity and path length of the silk coating is proposed. Though the applicability of this particular model is very limited (it is only able to predict adenosine release from dehydrated hydrogel encapsulated reservoirs and assumes that degradation can be prevented until after diffusion-driven release is exhausted), it exhibited excellent agreement with experimental data and shows how multiple control points can be integrated into a single model. This demonstrates that processing and fabrication can be used to precisely control release for highly tunable, customizable drug delivery implants.

We anticipate that this approach could be successfully applied to other therapeutics. Future work will include investigating more complex systems (such as protein release), which are impacted by degradation and adsorption to the silk carrier. In addition, this model will be applied to develop systems for sustained small molecule release for long-term therapeutic delivery (3-6 months).

3. Strategies for controlling degradation-driven drug release from silk biomaterials

As a protein, silk fibroin is susceptible to biological degradation by proteolytic enzymes such as chymotrypsin, actinase, and carboxylase. The final degradation products of silk digestion are often amino acids which are easily absorbed *in vivo* (Cao and Wang, 2009). Silk degradation has been studied (see Table 3.1A and 1B), but the effect of the degradation process on drug release has not been extensively characterized. Understanding and controlling the degradation behavior of silk is important to implantable medical applications. The degradation behavior has been studied *in vitro* and *in vivo* studies (Table 3.1A,B) and reviews of silk degradation have also been published (Altman *et al*., 2003, Cao and Wang, 2009). These studies have shown that degradation behavior of silk is dependent on many factors including silk processing (organic solvent vs. aqueous processing related to crystalline content, silk concentration and porosity (Wang *et al*., 2008)), silk material format (Arai *et al*., 2004; Yang *et al*., 2009), type and concentration of enzyme (Arai *et al*., 2004) and immune system response (Wang *et al*., 2008-1).

Table 3.1A. Degradation behavior of silk *in vitro*

Proteinase	Material Format	Degree and Measure of Degradation	Ref.
Collagenase type F	Silk film	3.8% and 10.7% mass loss at days 1 and 17, respectively	Arai *et al*., 2004
	0.5 mm thick freeze-dried hydrogel sheet	Mass loss of ~52% after 15 days (compared to ~32% mass loss in PBS); internal pore size increased with increasing degradation time (SEM)	Li *et al*., 2003
Collegenase IA	Silk coating on polyester prosthesis	30% mass loss in 15 days	Huang *et al*., 2008
α-chymotrypsin	Silk film	9% and 16.5% mass loss at days 1 and 17, respectively	Arai *et al*., 2004
	Silk coating on polyester prosthesis	45% mass loss in 15 days	Huang *et al*., 2008
Protease Type XIV from *Streptomyces*	0.5 mm thick freeze-dried hydrogel sheet	Mass loss of ~70% after 15 days (compared to ~32% mass loss in PBS); internal pore size increased with increasing degradation time (SEM)	Li *et al*., 2003

griseus	Silk coating on polyester prosthesis	70% mass loss in 15 days	Huang *et al*., 2008
	Water annealed silk film	>80% mass loss by Day 6, approx. 100% by day 10	Jin *et al*. 2005
	Silk sponge 4% (dried/methanol treated)	Total degradation in 10 days	Kim *et al*., 2005-1
	Silk sponge 6-8% (dried/methanol treated)	80-70% loss after 22 days	Kim *et al*., 2005-1
	Methanol treated silk film	<60% mass loss by Day 6, approx. 80% mass loss at Day 14	Jin *et al*. 2005
	Slow drying predominantly silk I silk films	Approx. 40% mass loss within 1 day in proteinase buffer, compared with approx. 10% loss in PBS (<35% loss over 14 days in PBS)	Lu *et al*. 2010-2
	Silk encapsulated solid reservoirs (silk film)	Extensive degradation of ~ 0.3 mm thick silk coating by day 5, total degradation by day 7; increased surface roughness for both ~0.3 mm and~ 0.8 mm coatings (SEM)	Pritchard *et al*., 2010
	Silk yarn	Fibroin filament diameter decreased exponentially with time in protease to 66% of initial diameter at 10 weeks; greater than 50% mass loss after 42 days	Horan *et al*., 2005
	Silk nerve guide conduits	~60% mass loss after 9 days, ~70% mass loss after 18 days	Yang *et al*., 2009
	Degummed silk fibers	No mass loss after 7 days, ~19% mass loss after 18 days	Yang *et al*., 2009
	Aqueous/NaCl derived porous sponges	~54.5% and ~88.6% mass loss by day 1 and day 4, respectively	Makaya *et al*., 2009
		~95% mass loss by day 7	Park *et al*., 2010
		Total mass loss within 5 days in 0.5 mg/mL; >80% mass loss after 17 days (>50% after 5 days) in 0.05 mg/mL proteinase	Wongpanit *et al*. 2010
	HFIP/sucrose-derived porous sponges	~17.8% and ~ 35.2% mass loss by day 1 and day 4, respectively	Makaya *et al*., 2009
		>50% mass loss after 17 days, ~5% mass loss after 17 days in 0.05 mg/mL proteinase,	Wongpanit *et al*. 2010
	Autoclaved HFIP/sucrose-derived porous sponges	~7% mass loss by day 7	Park *et al*., 2010
	Sonication-induced hydrogel	Concentration dependent degradation; Mass loss of approx. 80% within the first four days followed by slower degradation; when concentration increased from 4% to 12% (w/v), degradation time to reach 50% mass loss in the experiment increased from 1.5 to 3 days	Wang *et al*. 2008-3
Protease type XXI from *S. griseus*	Silk film	35% and 64.3% mass loss at days 1 and 17 respectively	Arai *et al*., 2004
	Silk fiber	Negligible mass loss, but drop in strength and elongation observed relative to increased degradation time	Arai *et al*., 2004

Protease type XXIII from *S. griseus*	Silk film	Evidence of proteolytic degradation (decreasing thermal stability and change in secondary structure with incubation time)	Nuanchai *et al*., 2009
Protease type XXV from *S. griseus*	Silk film	~10% weight loss over 5 days (compared to approx. 2% loss in PBS); increased surface roughness (SEM)	Minoura *et al*., 1990
Crude papain	Freeze-dried regenerated fibroin solution	Degradation after 60 minute incubation confirmed by tricine SDS-PAGE	Jeong and Hur, 2010

Table 3.1B. Degradation behavior of silk *in vivo*

Implantation Site	Material Format	Degree and Measure of Degradation	Ref.
Rat; brain (hippocampus)	Silk-coated porous sponges imbedded with microspheres	Histology sections of silk sponges exhibited on average 9.8% more surface area after 4 weeks *in vivo*	Szybala *et al*., 2009
Rabbit; subcutaneous near the spinal column	Silk nerve guide conduits	25, 65.4 and 79% mass loss at 8-, 12- and 24-weeks post implantation, respectively	Yang *et al*., 2009
	Degummed fibers	10 and 34% mass loss at 12- and 24- weeks post-implantation, respectively	Yang *et al*., 2009
Lewis rats, subcutaneous	Aqueous/NaCl derived porous sponges	Degraded to completion between 2 and 6 months	Wang *et al*., 2008-1
	HFIP-derived porous sponges	Degradation visible in histology sections after 6 and 12 months of implantation	Wang *et al*., 2008-1
Lewis rats and nude rats, intramuscular	Aqueous/NaCl derived porous sponges	After 8 weeks, loss of structural integrity, most pores collapsed; cross-sectional area of scaffolds in Lewis rats ~1/3 of that in nude rats (indicating immune-system mediated degradation)	Wang *et al*., 2008-1

As previously mentioned, drug release from implantable biodegradable systems is dependent on diffusion of drug through the polymer, degradation of the polymer carrier, or a combination of both mechanisms. Control of diffusion rate through manipulation of the implant properties (geometry and diffusivity) was discussed in the previous section. Silk material properties can also be manipulated to control degradation rate, however, external environmental properties including pH, temperature and enzymes (Yoshioka *et al*., 2008) can also impact drug release kinetics and polymer degradation *in vivo*. This is particularly true of natural biomaterials like silk, collagen and HA that are subject to enzymatic degradation (unlike PLGA, which

degrades via hydrolysis). Despite the substantial potential impact of the external environment, manipulation of environmental properties to control drug delivery has not been explored.

In part 1 of this chapter, studies are presented investigating the relationship between silk degradation and drug release, and silk material features which can be manipulated to impact degradation behavior. In parts 2 and 3 of this chapter, controlled release of enzyme inhibitors and proteolytic enzymes are proposed for added control of local proteolytic degradation.

3.1 Effect of degradation rate on drug release from silk biomaterials

3.1.1 Introduction

The biodegradation of other protein-based delivery systems, such as collagen and gelatin have been reported to be related to drug release rate (Friess, 1998; Young *et al*., 2005). Degradable drug carriers including silk, poly(lactic-co-glycolic acid) (PLGA), collagen, gelatin and hyaluronic acid (HA) release drugs dependent on diffusion, degradation or a combination of both release mechanisms. The contribution that degradation plays in the overall release profiles depends on the diffusivity of the drug through the polymer carrier as well as the rate of degradation of the carrier. For low molecular weight drugs free diffusion results in rapid release while higher molecular weight molecules are less able to diffuse and rely more on enzymatic degradation or chemical hydrolysis to liberate the entrapped drug (Luo *et al*., 2000). Proteolytic degradation of collagen carriers (often simulated *in vitro* by incubation with bacterial collagenase, cathepsin, pepsin or trypsin (Friess, 1998)) has been reported to impact drug release. More rapid release of fluorescein isothiocyanate (FITC) from crosslinked collagen hydrogels incubated with *Clostridium histolyticum* collagenase type I was found when compared to

incubation in PBS alone (De Paoli Lacerda *et al*., 2005). The importance of accounting for the effect of the therapeutic release on cellular responses in designing drug releasing collagen systems has also been stressed (Friess, 1998). For example, steroids modify the immune response, potentially slowing degradation (Kincl and Ciaccio, 1980) and growth factors or immunostimulants can impact cellular responses, potentially altering degradation rates (Friess *et al*., 1996). In addition, disease states can be associated with increased or decreased proteolytic activity at implantation sites. For example, increased matrix metalloproteinase activity in and around chondrocytes in osteoartritic cartilage (Aigner er al., 2003), increased extracellular matrix (ECM) degrading proteinase activity in glioma tissue (Chintala *et al*., 1999), and increased alpha-chymotrypsin inhibitor activity in the cerebrospinal fluid of patients with Alzheimer's disease (Licastro *et al*., 1994) have been reported. Young *et al*. reported that crosslinking density correlated with the rate of gelatin carrier degradation, which in turn controlled the release of growth factors from gelatin hydrogels (Young *et al*., 2005). These studies suggest that release rate from gelatin hydrogels can be controlled by manipulation of the rate of carrier degradation. Kurisawa *et al*. found that increasing hyaluronidase concentration increased degradation rate of hyaluronic acid (HA) hydrogels (Kurisawa *et al*., 2005). Luo *et al*. found that FITC loaded HA hydrogels incubated with hyaluronidase exhibited increased release rates compared to controls without enzyme (Luo *et al*., 2000).

Poly(lactic-co-glycolic acid) (PLGA) systems which are degraded via chemical hydrolysis rather than enzymes also exhibit increased rates of drug release with increased degradation rate. The degradation of PLGA has been manipulated by buffer pH (Zolnik and Burgess, 2007), temperature (Zolnik *et al*., 2006) and monomer ratio (Uhrich *et al*., 1999, Schmitt *et al*., 1994; Zhou *et al*., 2004, Moioli *et al*., 2006). In temperature-induced degradation

of the PLGA drug carrier, both release and degradation rate were almost ten times faster at 60^{o}C versus 37^{o}C (Zolnik *et al*., 2006). These studies demonstrate that increased polymer carrier degradation rate can increase drug release.

Lu *et al*. prepared horseradish peroxidase (HRP) loaded silk films and silk films blended with 30% glycerol and tested the effects of various post-drying treatments (water annealing for 6 hours, methanol treating for 8 min, stretching) on enzyme stabilization and release. They found that HRP release was linearly related to silk degradation in protease XIV (4U/mL), which could be controlled by modifying the silk material properties. Along with material properties and degradation behavior, processing conditions also determined ratio of untrapped (readily released by diffusion) and trapped protein (bound and inactive until released by proteolytic degradation). kinetics (Lu *et al*., 2010-1).

3D porous silk sponges fabricated using either the aqueous or HFIP salt-leeching technique were loaded with basic fibroblast growth factor (bFGF) by dropping bFGF solution onto the sponges and allowing adsorption to occur overnight at 4^{o}C. The affinity between the bFGF and the silk substrate resulted in incomplete drug release *in vitro* (approx. 30% over 3 days), but exposure to proteinase induced silk matrix degradation, increasing total cumulative release and release duration (approx. 85-90% over 8 days). When immersed in proteinase the HFIP-derived scaffolds degraded (and thus released bFGF) more slowly than the aqueous-derived scaffolds. (Wongpanit *et al*., 2010).

The objective of the present study was to investigate the effect of degradation of silk on drug release from silk carriers and the relationships between various silk material features and degradation behavior to determine potential degradation rate control points.

3.1.2. Materials and Methods

3.1.2.1. Materials

Reactive red 120, indigo carmine and recombinant human insulin expressed in yeast were purchased from Sigma Aldrich (St. Louis, MO). 1,2-Dioleoyl-*sn*-glycero-3-phosphocholine (DOPC) was purchased from Avanti Polar Lipids (Alabaster, AL).

3.1.2.2. Silk fibroin solution preparation

Silk fibroin was prepared from *B. mori* cocoons as we have previously described (Sofia *et al*., 2001) using varied degumming times (10 min, 30 min, 60 min and 90 min). Briefly, cocoons were boiled for 10, 30, 60 or 90 minutes in a solution of 0.02 M Na_2CO_3 and rinsed, then dried at ambient conditions overnight. The dried fibroin was solubilized in a 9.3 M aqueous LiBr solution at 60^{o}C for 4 hours, yielding a 20% (w/v) solution. LiBr was then removed from the silk solution via dialysis against distilled water for 2.5 days using Slide-a-Lyzer dialysis cassettes (MWCO 3,500, Pierce Thermo Scientific Inc., Rockford, IL). Silk fibroin concentration was determined by evaporating water from a solution sample of known volume and massing using an analytical balance. All solutions were stored at 4-7^{o}C before use.

3.1.2.3. Mass loss degradation study

To determine the effect of degumming time on film degradation, films were prepared from 6% (w/v) silk that had been degummed for various times (10, 30, 60 or 90 min). Prior to study film masses were determined using an analytical balance. Films were then immersed in 1 mL of PBS or 1 mL of 0.1 mg/mL protease type XIV solution for 5 days. Every 24 hours, a

subset (n=3) of the films was removed, dried overnight at ambient conditions and reweighed. Protease solution and PBS were replaced every 24 hours to account for proteinase activity loss due to 37^{o}C incubation (Horan *et al*., 2005). The fraction of remaining mass was determined by dividing the mass at each time point by the initial mass values.

To determine the effect of different silk film processing approaches on degradation behavior, silk films were prepared from aqueous silk solution as previously described. Briefly, 6% (w/v) silk solution prepared using a 30 minute degumming time was aliquoted into Teflon molds (250 µL per film), dried overnight at ambient conditions, and treated with 90% methanol for 5 minutes to induce β sheet formation. For comparison, aliquots of 6% (w/v) silk solution were sonicated for 60 seconds at an amplitude of 15% to induce gelation, aliquoted into Teflon molds (same volume as the aqueous-derived films, 250 µL per film), allowed to complete gelation and dried overnight at ambient conditions (no methanol treatment followed drying). Mass loss studies were then carried out as described for the varied degumming time silk films.

3.1.2.4. Reactive red 120 and indigo carmine film preparation and release studies in phosphate buffered saline (PBS) and proteinase type XIV

Silk solution was prepared as previously described. For degradation studies, the dyes reactive red 120 and indigo carmine were used (Figure 3.1). For varied concentration proteinase release studies, films were prepared from 8% (w/v) silk containing either 1 mg of reactive red 120 or indigo carmine per film and 24 mg of silk (0.3 mL of 8% (w/v) silk per film).

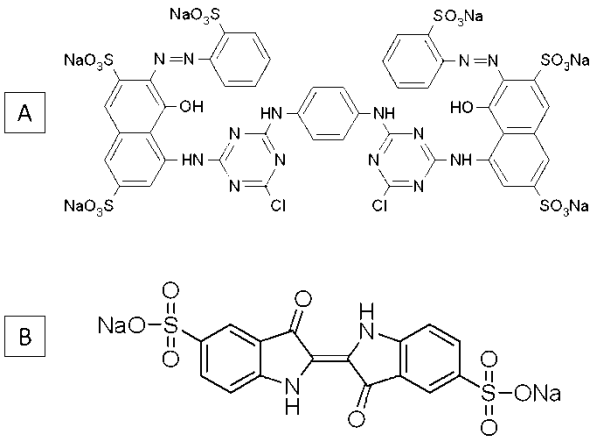

Figure 3.1. Chemical structures of (A) reactive red 120 (MW = 1469.98) (B) indigo carmine (MW = 466.35)

To determine dye release from encapsulated reservoirs, the silk films were immersed in 1 mL of Dulbecco's PBS at 37^{o}C or a 0.025 mg/mL, 0.05 mg/mL, or 0.5 mg/mL protease type XIV solution. At desired time points, the buffer was removed and replaced with fresh buffer. The amount of released dye was determined using UV-Vis spectroscopy at 535 nm and 610 nm for reactive red 120 and indigo carmine, respectively, and compared to standard curves. The amount of released compound in each sample was summed with the amounts at each previous time point and divided by the total amount to obtain cumulative release values. Four samples were tested per release buffer type (n=4) and each sample was assayed in triplicate.

3.1.2.5. Insulin releasing silk microsphere preparation

Microspheres were prepared according to the phospholipid template protocol previously described (Wang *et al*., 2007-3). Briefly, 200 mg of 1,2-dioleoyl-sn-glycero-3-phosphocholine (DOPC) phospholipid was dissolved in 1 mL of chloroform, then dried under N_2 to a film on the interior of a glass test tube. 2 mL of drug solution in 8% (w/v) silk containing 16.7 mg/mL insulin were added to hydrate the phospholipid film, which forms microspheres upon exposure to

the aqueous solution. Microspheres prepared with 8% (w/v) silk with no drug added served as controls. The suspension of microspheres was repeatedly freeze-thawed, diluted in distilled water, then lyophilized. Once lyophilized, the material was treated with methanol (MeOH) for 30 minutes to remove the lipid templates and induce β-sheet physical crosslinks to stabilize the structure. Methanol and microspheres were separated by centrifugation at 10,000 rpm for 5 min at 4^{o}C. The pellet was dried overnight at ambient conditions. Prior to release testing, the microsphere pellet was resuspended in the desired buffer and any clustered microspheres were dispersed by brief ultrasonication (5-10 seconds at 20% amplitude) using a Branson 450 ultrasonicator (Branson Ultrasonics Co., Danbury, CN). Microspheres were not characterized physically, as microspheres produces using the lipid template have been extensively characterized previously (Wang et al., 2007-3) and consistently produces microspheres with average diameters of approx. 2 μm.

3.1.2.6. Insulin-loaded silk microsphere release testing

To determine insulin release from silk microspheres, microspheres were resupended in Dulbecco's PBS at 37^{o}C with shaking. At desired time points, the microspheres were centrifuged at 10,000 RPM for 5 minutes and the buffer was removed and replaced with fresh buffer. After 30 days, when release from the microspheres leveled off, the release buffer was changed to a 0.1 mg/mL solution of protease type XIV.

The buffer removed periodically from the system was assayed for insulin content using an ELISA kit (Calbiotech, Inc., Spring Valley, CA). To determine loading, the microspheres were treated with hexafluoroisopropanol (HFIP) to dissolve the silk, dried to films and re-

dissolved in PBS as previously described (Wang *et al*., 2009). Release kinetics were assessed as described in the previous chapter.

3.1.2.7. Silk encapsulated adenosine reservoir release studies in proteinase type XIV

Silk encapsulated adenosine reservoirs were prepared and coated as previously described (see section 2.3.1.2.2). Proteinase release studies were performed as previously described (Chapter 2) using a 0.1 mg/mL proteinase type XIV solution in place of PBS. This choice of proteinase and concentration is intended to mimic *in vivo* proteolytic degradation of the silk coatings (Horan *et al*., 2005; Li *et al*., 2003). Silk coating concentrations tested included 4% (w/v), 8% (w/v) and 16% (w/v) due to abnormalities in the silk coatings and reservoir release behavior above 16% (w/v) and below 4% (w/v) in the previous PBS release studies.

3.1.2.8. Characterization of silk encapsulated adenosine reservoir degradation

Photographs of 8% (w/v) or 16% (w/v) silk encapsulated adenosine reservoirs in PBS or proteinase buffer were taken every other day to compare gross morphological differences between the two buffers and the two difference coating thicknesses.

The microscopic surface morphology of the degradation study silk encapsulated reservoirs was examined by scanning electron microscopy (SEM). Specimens were directly mounted and Au sputter-coated using a Ploaron SC502 Sputter Coater (Fison Instruments, UK). Samples were examined using a JEOL JSM 840A Scanning Electron Microscope (Peabody, MA) at 15 kV.

3.1.3. Results

3.1.3.1 Effect of degumming time on silk film degradation

Mass loss of films prepared from varied degumming time silk solutions was studied in PBS and protease type XIV solutions to determine the effect of degumming time on degradation. The results of the mass loss study are shown in Figure 3.2.

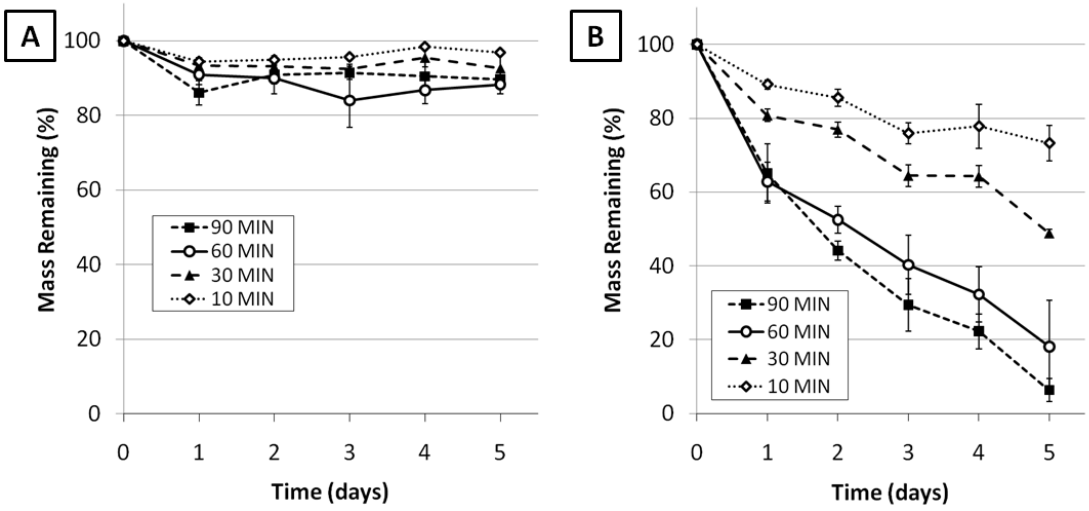

Figure 3.2. Mass loss over 5 days of silk films cast from silk prepared using varied degumming times immersed in (A) PBS or (B) 0.1 mg/mL protease type XIV solution. N=3, error bars represent standard deviation. Where error bars are not shown, the standard deviation falls into the background.

As expected, very little mass loss occurs for films in PBS (approx. 5-20%) due to the absence of proteinase (mass loss that occurs in PBS is the result of uncrosslinked silk diffusing out of the film, as proteinase is required for actual carrier degradation). In protease type XIV solution, a clear relationship is observed between degumming time and degradation rate: the longer the degumming (and the smaller the average fragment size), the more rapidly degradation occurs. After 5 days in protease solution, films cast from silk degummed for 90 minutes have

almost entirely degraded, while approx. 20%, 50% and 70% of the films initial mass still remains for films cast from 60 minute, 30 minute and 10 minute degummed silk respectively.

3.1.3.2 Effect of fabrication on silk film degradation

Mass loss of films prepared using different fabrication approaches (aqueous solution dried to films, then methanol treated compared with dehydrated hydrogel derived films) was studied in PBS and protease type XIV solutions to determine the effect of fabrication on distribution on degradation. The results of the mass loss study are shown in Figure 3.3.

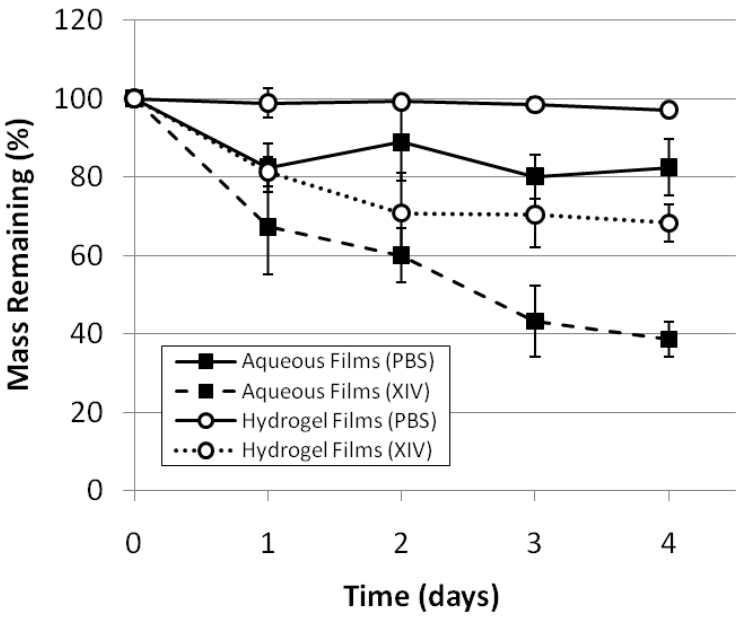

Figure 3.3. Mass loss over 4 days of silk films prepared by casting aqueous silk solution then methanol treating the dried films (designated "aqueous films;" represented by filled in squares) and silk films prepared by inducing gelation via sonication, then drying the crosslinked hydrogels to films (designated "hydrogel films;" represented by empty circles) immersed in PBS (solid lines) or 0.1 mg/mL protease type XIV solution (dashed lines). N=3, error bars represent standard deviation. Where error bars are not shown, the standard deviation falls into the background.

Despite using the same initial silk solution and film dimensions, hydrogel-derived films exhibit less mass loss compared with aqueous-derived films, both in proteinase and in PBS. The

difference in mass loss cannot be explained by differences in the silk protein, as the samples are prepared from the same initial solution. Clearly, the hydrogel gelation process ultimately produces a crosslinked silk network that is less susceptible to proteolytic degradation that crosslinking of dried films. This is supported by the reduction in mass loss in PBS observed for hydrogel derived films compared with aqueously derived films: the crosslinking gelation process is evidently more efficient at incorporating all available silk protein into the final matrix and little to no silk is available to diffuse out of the crosslinked matrix when re-hydrated. The aqueous derived films might also have regions that are insufficiently crosslinked during their exposure to methanol, while the hydrogel will not have uncrosslinked regions. Futher work is needed to investigate the structural difference between these insoluble silk networks derived from different crosslinking methods. Previous studies have demonstrated that hydrogel-derived films and aqueous-derived films have comparable drug diffusivities (see Chapter 2), so choice of fabrication might represent a promising potential strategy for manipulating degradation behavior.

3.1.3.3. Effect of silk fibroin coating concentration/film thickness on adenosine release in proteinase XIV

Morphological changes for encapsulated reservoirs coated with 8% (w/v) and 16% (w/v) silk coatings in PBS and 0.1 mg/mL proteinase type XIV solution at days 3, 5 and 7 are shown in Figure 3.4. Coatings on both 8% (w/v) and 16% (w/v) silk encapsulated reservoirs in PBS appeared unchanged over 7 days. In proteinase type XIV solution the 16% (w/v) silk encapsulated reservoirs retained their shape through the first seven days and only began to show any gross morphological signs of degradation at day 7. The 8% (w/v) silk encapsulated reservoirs showed translucence at day 3, partial degradation at day 5 and complete degradation by day 7. SEM images of the degrading encapsulated reservoir surfaces at day 0, day 3, day 5

and (in the case of 16% (w/v) silk coated reservoirs) day 7 are shown in Figure 3.5. Surface morphology changes rapidly for 8% (w/v) silk coated reservoirs. Though the progression of degradation in 16% (w/v) silk coated reservoirs is more apparent in the SEM images than in gross pill morphology, the microscopic surface changes are more subtle than the 8% (w/v) silk coated reservoirs.

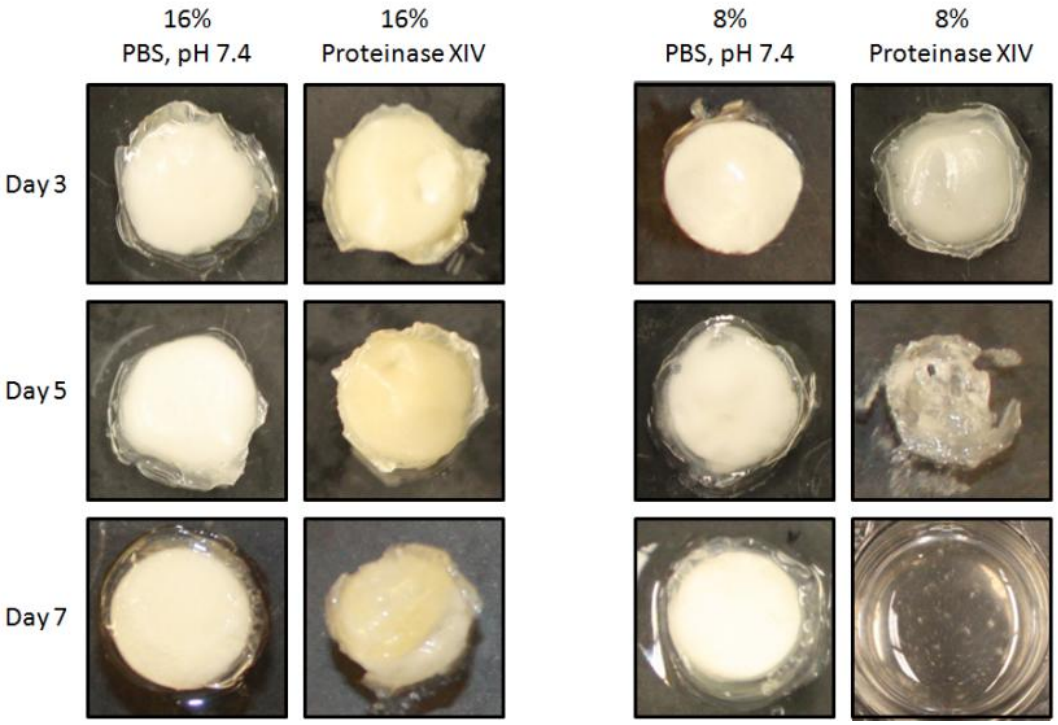

Figure 3.4. Gross morphological changes of silk coated adenosine reservoirs in PBS and proteinase type XIV solution over 7 days. The 8% (w/v) coated reservoirs in proteinase type XIV solution were beginning to become translucent at day 3 and showed extensive degradation by day 5. By day 7 in proteinase type XIV solution, 8% (w/v) encapsulated reservoirs were totally disintegrated. 16% (w/v) encapsulated reservoirs retained their shape through day 7.

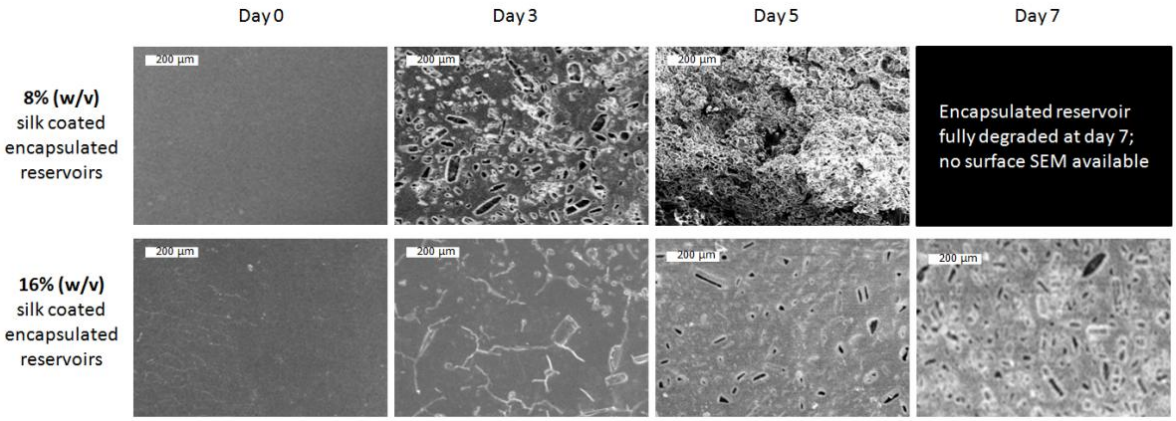

Figure 3.5. SEM of 8% (w/v) and 16% (w/v) encapsulated reservoir surfaces over the course of proteolytic degradation in 0.1 mg/mL proteinase type XIV at 37°C. Scale bars are all 200 µm.

Cumulative release profiles from silk encapsulated adenosine reservoirs in proteinase type XIV release buffer are shown in Figure 3.6A.

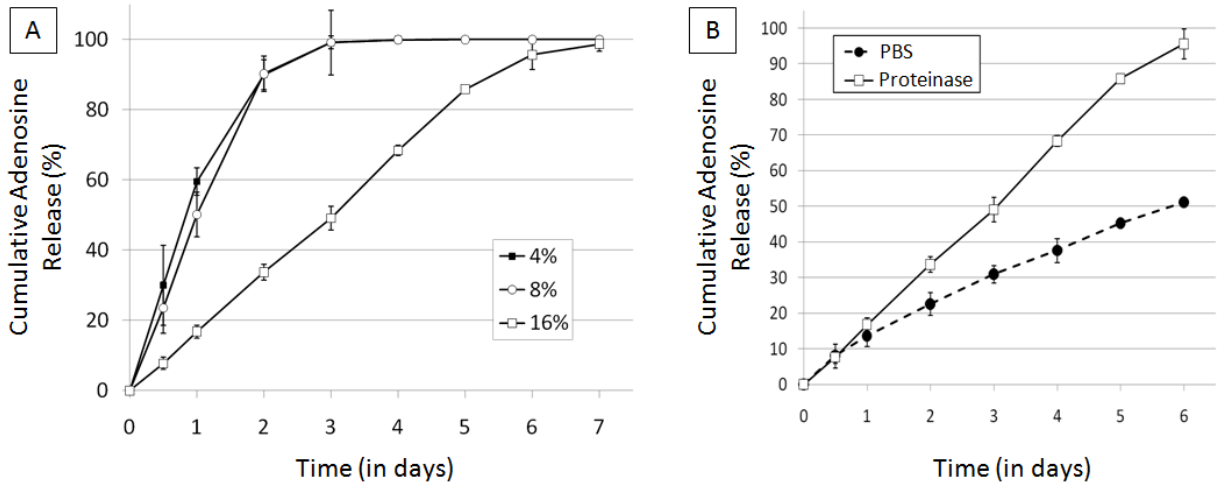

Figure 3.6. Effect of degradation on adenosine release from silk encapsulated reservoirs (A) Cumulative adenosine release from encapsulated adenosine reservoirs coated in silk of varying concentrations over time in 0.1 mg/mL proteinase type XIV solution at 37° C. N=3, error bars represent standard deviations (where error bars aren't shown they fall into background) (B) Comparison of cumulative adenosine release curves of 16% (w/v) silk encapsulated reservoirs in PBS and in 0.1 mg/mL proteinase type XIV solution at 37°C through day 6. N=3, error bars represent standard deviations (where error bars aren't shown they fall into background)

The shape of the cumulative release curve of the 16% silk coated reservoirs in the protease resembles the shape of the curve in PBS ($R^2_{Proteinase}$ = 0.98, compared to R^2_{PBS} = 0.96), but the duration of release was shorter ($t_{50,\ proteinase}$ = 3.05 days compared to $t_{50,\ PBS}$ = 5.81 days). The release curves of 4% and 8% coated reservoirs were more similar in the proteinase than in PBS. Values for t_{50} for 4%, 8% and 16% (w/v) silk fibroin coating concentration samples in proteinase type XIV were 0.84 days, 1.00 days and 3.05 days, respectively. A side by side comparison of adenosine release through day 6 from 16% (w/v) silk encapsulated reservoirs immersed in PBS versus 0.1 mg/mL proteinase type XIV is shown in Figure 3.6B. Data is shown through day 6 because this time-frame corresponds to linear release for both systems, allowing

for ease of comparison of average release rates: approx. 16.49% total adenosine load per day in proteinase type XIV and approx. 8.28% total adenosine load per day in PBS. In proteinase solution, adenosine release from silk encapsulated reservoirs (driven by diffusion and degradation) occurs at nearly double the rate observed in PBS (driven only by diffusion, as confirmed by minimal weight loss of silk films in PBS alone).

3.1.3.4. Effect of rate of proteolytic degradation on drug release from silk films

The release of reactive-red 120 and indigo carmine from silk films was characterized in buffer containing varied amounts of protease type XIV to confirm that increasing the degradation of silk films would result in increased drug release. Cumulative release profiles for the two dyes are shown in Figure 3.7A and 3.8A, respectively. Zero order release was observed for reactive-red 120 films over the first four days, likely due to the relatively high molecular weight and bulky structure of the dye. Correlation coefficients (R^2) were $\geq$0.93 for all release profiles (R^2 = 0.99, 0.95, 0.93 and 0.97 for 0, 0.025, 0.05 and 0.1 mg/mL proteinase, respectively). Therefore, daily release rates were relatively constant. Note that while general data trends can be identified in the data, even with $R^2 \geq 0.93$, the error bars on average release rates are still fairly wide due to variations in the release rate from day to day. The average daily release rate of reactive-red 120 from silk films in % total loaded drug per day was 7.62, 11.08, 13.89 and 21.42 for release buffer containing 0, 0.025, 0.05 and 0.1 mg/mL of protease type XIV, respectively. Figure 3.7B shows average daily release rate versus protease type XIV concentration in the release buffer (where PBS alone represents 0 mg/mL protease type XIV). The average release rate of reactive-red 120 increased proportionally with increased proteolytic degradation.

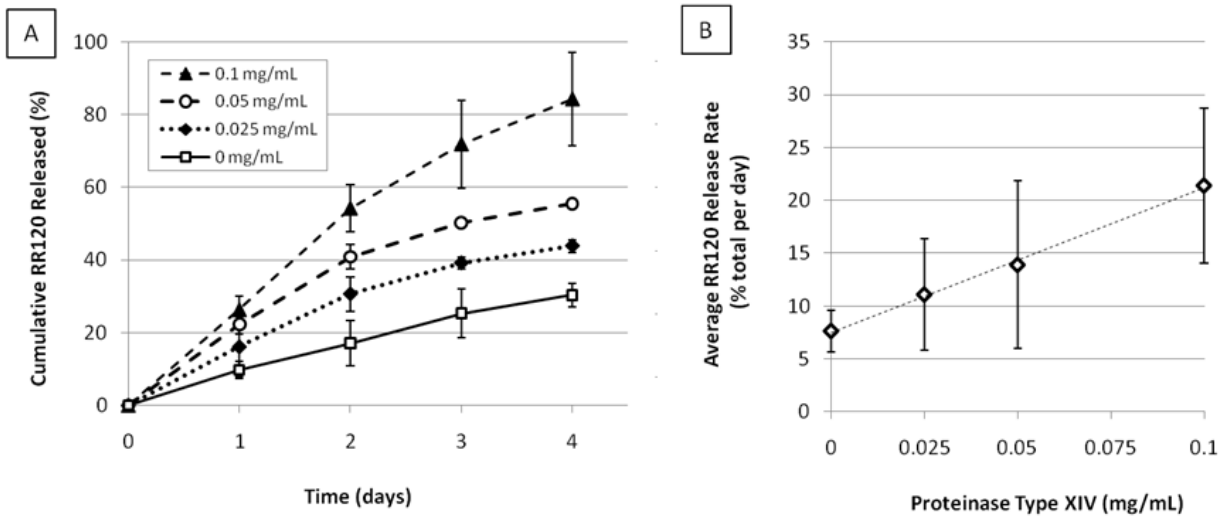

Figure 3.7. Effect of degradation on reactive red 120 release (A) Cumulative release of reactive red-120 from 8% (w/v) silk films in PBS and varying concentrations of proteinase type XIV. (B) Average daily release rate of reactive red 120 from films (in % total load per day) verses protease type XIV concentration in the release buffer. N=4, error bars represent standard deviations (where error bars aren't shown they fall into background).

Unlike the release profiles observed for reactive-red 120, the release of indigo carmine was non zero-order; burst release was observed on day 1 for all release buffers/protease type XIV concentrations, followed by decreasing daily release rates relative to time (Figure 3.8A). This is likely because indigo carmine has a relatively low molecular weight and does not chemically interact with the silk. The non zero-order release profiles and the 90%-100% total drug load released within 4 days regardless of proteinase concentration suggest that the average daily release rate was not an appropriate way to represent the release profile to assess the effects of increasing proteolysis on indigo carmine release. Therefore, the release data were fit to the modified Siepmann Peppas equation and values of the Siepmann Peppas release coefficient, n, were used to empirically compare linearity of the release profiles. The graph of fitted n values versus proteinase concentration is shown in Figure 3.8B. The n values decreased with increasing proteinase concentration in the release buffer, suggesting that in a more diffusion-driven system the increased proteolysis decreases the linearity of drug release. The increasing linearity of the

release curve suggests that since average release rates are increasingly constant, less total drug is released early in the process compared to a less linear (i.e. lower n) release curve.

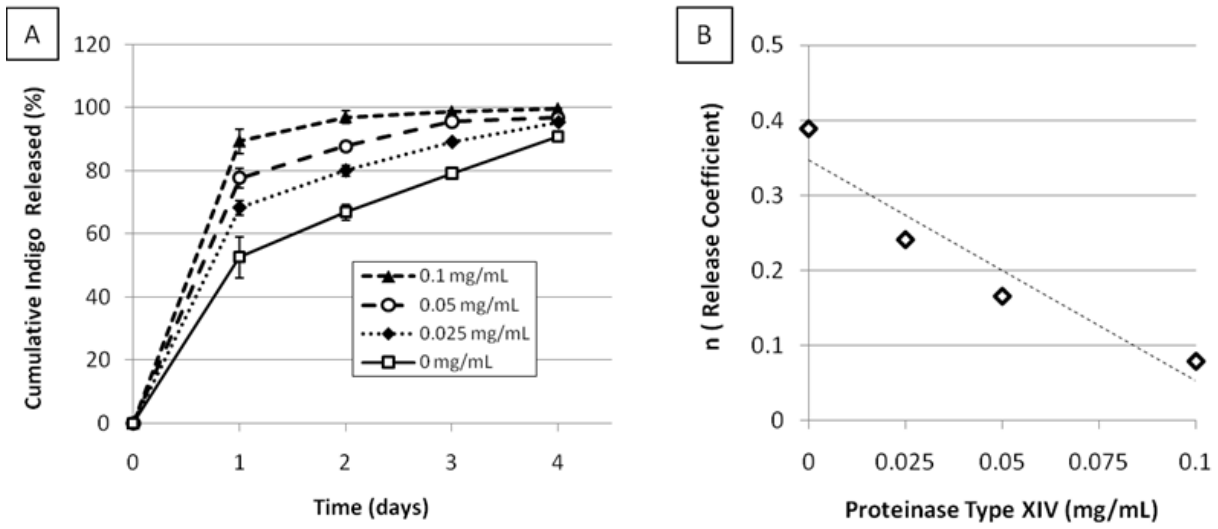

Figure 3.8. Effect of degradation on indigo carmine release (A) Cumulative release of reactive indigo carmine from 8% (w/v) silk films in PBS and varying concentrations of protease type XIV. N=4, error bars represent standard deviations (where error bars aren't shown they fall into background). (B) Siepmann-Peppas release coefficient (n) versus protease type XIV concentration in the release buffer

Increasing proteolysis results in a decrease in release coefficient n (Figure 3.8B), which shows that increasing proteolysis increases release of indigo carmine from the silk films. For both dyes and release profiles tested (reactive red 120/zero-order release and indigo carmine/diffusion-driven release), increasing the protease type XIV concentration and thus increasing proteolytic degradation of the silk film drug carrier, results in an increase in drug release (reactive red 120) or a decrease in release curve linearity (indigo carmine).

3.1.3.5. Effect of proteinase on insulin release from silk microspheres

Results of cumulative insulin release (in percent total drug load) are shown in Figure 3.9.

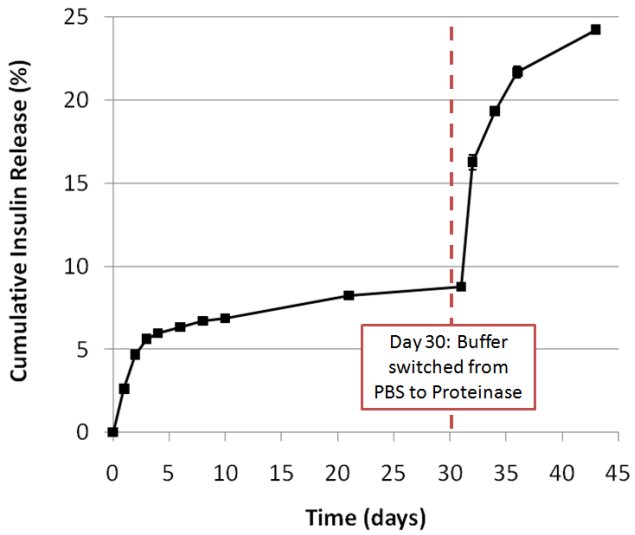

Figure 3.9. Cumulative insulin release from silk microspheres. Release buffer is PBS until day 30, at which point release buffer is switched to proteinase type XIV. N=3, error bars represent standard deviation, where error bars are not shown, they fall into background.

Total insulin loading (100%) was found to be 14.8 µg, so 7% is equivalent to approximately 1 µg. In PBS, release slowed after 10 days. Once the buffer was switched to proteinase containing buffer, drug release spiked. This suggests that while approximately 10% of the total insulin was able to freely diffuse from the microsphere, a fraction of the drug load was bound to the silk and required proteolytic degradation of the carrier to be released. Further studies of insulin binding and recovery are needed to investigate insulin loss, but the recovery below 100% might possibly due to proteolytic degradation of the drug by the proteinase in the release buffer (proteinase type XIV is fairly aggressive and non-specific), or degradation at 37^{o}C (in a previous study approximately 40% of the immunoglobulin G detectable by ELISA in an aqueous sample incubated with 0.1 mg/mL proteinase type XIV overnight at 37^{o}C was lost compared with a PBS control (data not shown)). This finding is consistent with previous studies of growth factors adsorbed to silk biomaterials (Lu *et al*., 2010-1; Wongpanit *et al*., 2010).

3.1.4. Conclusions

These studies confirm that increased proteinase concentration increased drug release from silk carriers, both in cases where drug is able to freely diffuse from the silk biomaterial and in cases where some fraction of the total drug is bound to the silk carrier. We propose several material features to potentially control degradation, which (in combination with the extensive body of literature on processing conditions that impact silk degradation) suggest that manipulation of silk processing and material features will ultimately allow tight regulation of degradation behavior and drug release.

3.2 Incorporation of Proteinase Inhibitors into Silk-Based Delivery Devices for Enhanced Control of Degradation and Drug Release

3.2.1. Introduction

Some authors have proposed inclusion of controlled drug release to mediate local immune responses to implants (Patil *et al*., 2007; Saltzman and Olbricht, 2002; Hewitt and Black, 1996), which suggests localized drug delivery can be used to modulate environmental conditions at the site of implantation. The concept of using controlled release of inhibitors to regulate proteolytic degradation and drug delivery from silk carriers was inspired in part by the natural system. The silkworm, *Bombyx mori*, produces a protease inhibitor in the silk gland which is sequestered within the cocoon to protect against premature proteolytic degradation during development (Kurioka *et al*., 1999).

EDTA was chosen as a model inhibitor for the present study due to its ability to inhibit a broad range of proteinases and general safety. EDTA inhibits a wide range of proteolytic enzymes including metalloproteinases and calcium dependent cysteine proteinases by chelating the metal-ions requires for enzymatic activity (Beynon and Bond, 2001; Sterchi and Stocker,

1999). The major disadvantage of using metal chelators for proteinase inhibition is that they are non-specific and can interfere with other metal ion-dependent biological processes. However, even though EDTA is fairly non-specific, it is suitable to demonstrate proof-of-principle and might be advantageous for implantation sites where the proteinase composition is unknown and cannot be specifically targeted.

EDTA use in humans is considered to be safe, as EDTA has been used for decades as a common additive of the food-industry to preserve freshness of products (Furia, 1964). Medically, EDTA is used for acute, high dose lead poisoning (Ellis and Kane, 2000l Gracia and Snodgrass, 2007; O'Hara *et al*., 1995). EDTA chelation has also shown promise in treating medical conditions requiring excess calcium clearance, including calcific tendinitis of the shoulder (Cacchio *et al*., 2009) and vascular disease (Price Evans *et al*., 2001; Maiscalco and Taylor, 2004; Lamas and Hussein, 2006). Chelation of Cu^{2+} and Zn^{2+} ions has been proposed as a potential treatment for Alzheimer's Disease as they are believed to contribute to amyloid β deposition (Bernstein, 2005). EDTA has also been shown to enhance the efficacy of various antimicrobials and anti-parasitics (Wooley and Jones, 1983; Lambert *et al*., 2004; Ihedioha *et al*., 2007). Several metalloproteinase inhibitors (including $CaNa_2EDTA$) have been shown to significantly reduce tissue damage caused by viper venom by inhibiting the activity of ECM-degrading enzymes present in the venom (Girish and Kemparaju, 2006, Rucavado *et al*., 2000), which demonstrates that site-specific EDTA delivery can effectively inhibit local proteinase activity.

Protease type XIV, also called Pronase E and Actinase E, is a mixture of proteolytic enzymes produced by *Streptomyces griseus*. Protease type XIV was selected for study as it is often used for *in vitro* modeling of proteolytic degradation of silk biomaterials (Table 3.1A),

degrades a broad range of protein substrates (Burrell, 1994) and degrades silk more aggressively than other candidate proteinases including collegenase and α-chymotrypsin (Minoura *et al*., 1990, Li *et al*., 2003; Arai *et al*., 2004). Because this approach was effective for one of the most aggressive silk-degrading proteinase, it could very likely also be applied to other proteinases and their inhibitors or activity enhancers.

Co-loading enzyme inhibitors into drug delivery systems allows for either non-specific suppression of local enzymatic degradation (resulting in release behavior *in vivo* that more closely resemble predictive *in vitro* models) or specific, targeted enzyme inhibition. Studies have shown that small molecule inhibitors, peptidomimetic inhibitors and proteinase-binding antibodies can effectively selectively suppress local enzymatic degradation (Girish and Kemparaju, 2006, Rucavado *et al*., 2000). Further, these different inhibitors exhibit different efficacies, suggesting that varied inhibition strategies can be used to achieve different enzymatic degradation profiles (Girish and Kemparaju, 2006, Rucavado *et al*., 2000). Previous work has also demonstrated that different proteinases achieve varied silk degradation effects (α-chymotrypsin, for example, degrades alpha-helix but leaves β-sheet intact (Numata and Kaplan, 2010-2)) Specific proteinase inhibition profiles could potentially be used to precisely control the *in vivo* degradation of silk implants by manipulating which local proteinases are active or inactive and to what extent. This strategy would be applicable to other drug carriers such as collagen and HA which, like silk, are susceptible to enzymatic degradation. However, this potential to tightly control local degradation represents a controllable feature for enzymatically degraded biomaterials that cannot be built into drug release systems based on polymers that degrade via hydrolysis (PLGA, PCL, etc.)

The objective of the present study was to investigate the effect of an enzyme inhibitor release on the proteinase/silk degradation/drug release process. The goal was to determine if inhibition of protease type XIV activity via the co-release of a small molecule inhibitor could be used as a further control point in terms of control of release of a therapeutic drug from silk. While protease concentration is important in control of drug release from silk carriers, inhibition-based control of drug release may provide both additional levels of control of the process, as well as control *in vivo*, since proteinase concentrations at the target site of carrier implantation are fixed while the loading and release of inhibitors can be modulated in the device design.

3.2.1. Materials and Methods

3.2.1.1. Materials

Cocoons of *Bombyx mori* silkworm silk were purchased from Tajima Shoji Co., LTD (Sumiyoshicho, Naka-ku, Yokohama, Japan). Phosphate buffered saline (PBS) supplemented with 100 mg/L $MgCl_2$ and 100 mg/L $CaCl_2$ was purchased from Invitrogen (Carlsbad, CA). Protease type XIV (3.5 units/mg; mixture of at least three caseinolytic activities and one aminopeptidase) from *Streptomyces griseus* and all chemicals were purchased from Sigma-Aldrich (St. Louis, MO).

3.2.1.2. Silk fibroin solution preparation

Silk fibroin solution was prepared as previously described (Sofia *et al*., 2001). The silk solution was concentrated by osmotic stress as previously described (Kim *et al*., 2004). Briefly, silk fibroin aqueous solution (8% (w/v), 10 mL) was dialyzed against a 10-25% w/v PEG

(10,000 g/mol) solution at ambient conditions, causing water molecules to move from the silk fibroin solution into the PEG solution through the dialysis membrane. All solutions were stored at 4-7^{o}C before use.

3.2.1.3. Silk film preparation

Drug loaded silk fibroin films were prepared as we have previously described (Hofmann *et al*., 2006). Briefly drug solution was mixed with silk to a final concentration of 8% (w/v) silk and aliquoted into teflon coated molds, then dried overnight at ambient conditions and removed from the molds after 24 hours, and treated with methanol for 5 minutes to increase β sheet content to render the films water insoluble.

3.2.1.4 Adenosine powder reservoir preparation and encapsulation

Press-fit adenosine reservoirs were prepared and coated as we have previously described (Pritchard *et al*., 2010). Briefly, approx. 100 mg of powder (50%/50% EDTA/adenosine, 50%/50% mannitol/adenosine or 100% mannitol) were loaded into the chamber of an Econopress (Sigma-Aldrich, St. Louis, MO) and pressed into solid tablets according to manufacturer instructions. Reservoirs were coated by dipping in a 12% (w/v) aqueous silk solution, drying for 30 min at 60^{o}C, then immersing in methanol for 5 minutes to increase β sheet content for aqueous-insolubility.

3.2.1.5 Degradation mass loss film studies

To determine the effect of EDTA release from silk films on film degradation, the films were prepared from 8% (w/v) silk containing 1 mg of EDTA, 0.5 mg of adenosine or 1 mg of

EDTA and 0.5 mg of adenosine. Prior to study the mass of the films was determined. Films were then immersed in 1 mL of PBS or 1 mL of 0.1 mg/mL protease type XIV for 5 days. At desired time points, a subset (n=3) of the films was removed, dried overnight at ambient conditions and reweighed. The fraction of remaining mass was determined by dividing the mass at each time point by the initial mass value.

3.2.1.6. Encapsulated reservoir release studies in phosphate buffered saline (PBS) and protease type XIV

To determine adenosine and EDTA release from silk coated powder reservoirs, the samples were immersed in 1.5 mL of Dulbecco's PBS at 37^{o}C or a 0.1 mg/mL protease type XIV solution [(intended to mimic *in vivo* proteolytic degradation of the silk coatings (Horan *et al*., 2005; Li *et al*., 2003)]. At selected time points the buffer was removed and replaced with fresh buffer to approximate sink conditions. Fresh protease type XIV solution was prepared for each replacement. Three samples were tested per drug loading type (EDTA + adenosine, mannitol + adenosine and mannitol alone) and each sample was assayed in triplicate for each time point. The buffer that was removed periodically from the system was assayed for adenosine content using a modified fluorescence assay as previously described.

The buffer was also assayed for EDTA content (Sorensen, 1992). Briefly, 20 µL of 1.3 mM nickel ammonium sulfate solution was added to 100 µL of sample or EDTA standard solution of known concentration. Then 50 µL of 1 mg/mL xylenol orange solution was added, the reaction was mixed and allowed to react 5 minutes and then the sample absorbance at 595 nm was determined with a UV spectrophotometer plate reader. The amount of released compound in each sample was summed with the amounts at each previous time point and divided by the half the total initial reservoir mass to obtain cumulative percent release.

3.2.1.7. Proteinase activity determination

The buffer collected from the adenosine/EDTA release studies was assayed for proteolytic activity using the Amplite™ Universal Fluorimetric red fluorescence protease activity assay kit (ABD Bioquest, Sunnyvale, CA) according to the manufacturer's instructions. Briefly, a fluorescent-casein substrate was added to samples of unknown activity and incubated 1 hour at room temperature. Following incubation, fluorescence was read at excitation/emission = 540/590 nm. Each sample was assayed in triplicate. The final fluorescence value was compared to a standard curve generated for protease type XIV. The amount of active protease type XIV in each sample was divided by the amount of active protease type XIV added to the sample every 24 hours (0.1 mg/mL) to determine what fraction of proteinase activity was retained during each 24 hour incubation with EDTA-releasing or non-EDTA-releasing silk encapsulated reservoirs.

3.2.2. Results

3.2.2.1. Effect of EDTA release on mass loss of silk films in protease type XIV

To investigate the effect of EDTA release from silk films on film degradation, mass loss was characterized for silk films loaded with drug (adenosine alone), loaded with nothing (control), loaded with inhibitor (EDTA alone) and co-loaded with both drug and inhibitor (EDTA+adenosine). Silk films were immersed in 0.1 mg/mL proteinase type XIV or in PBS (control) to account for non-proteolytic mass loss (Figure 3.10).

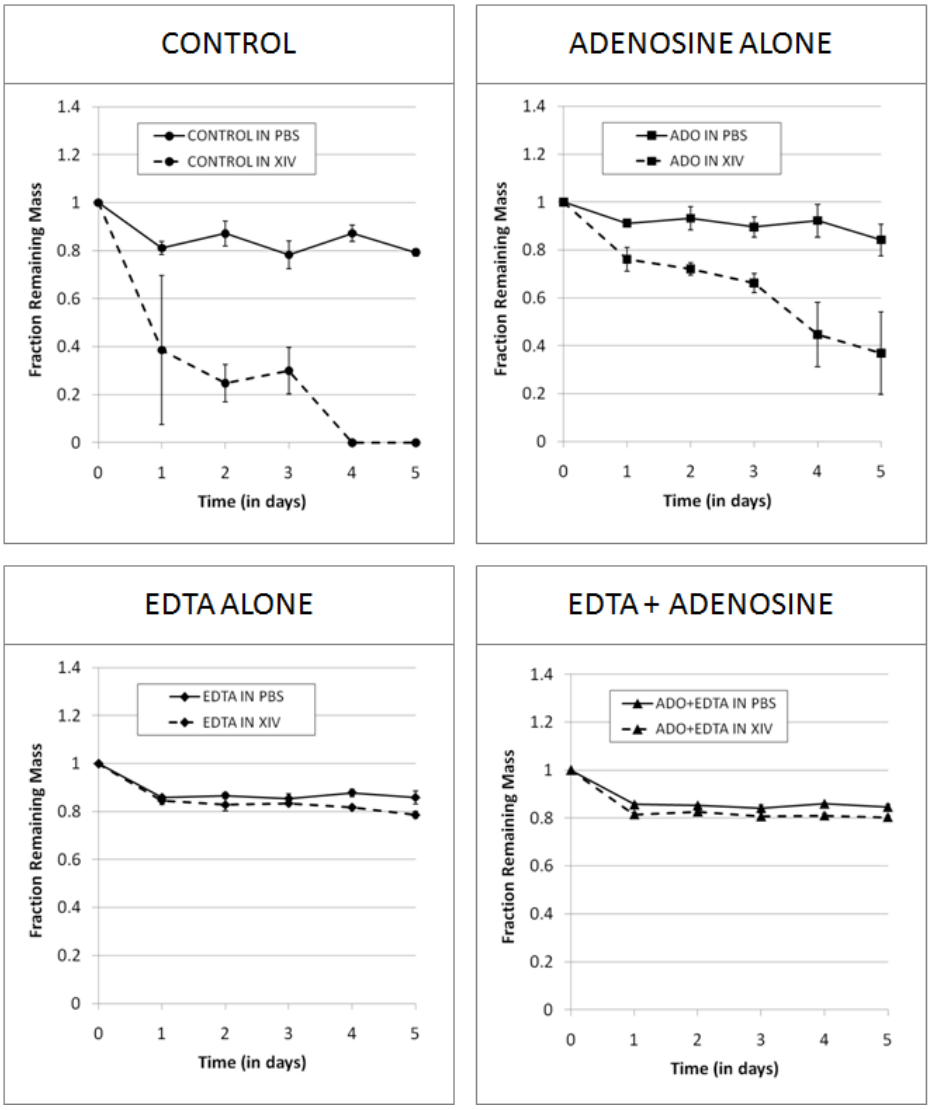

Figure 3.10. Mass loss over 5 days of silk films immersed in PBS (solid lines) or 0.1 mg/mL proteinase type XIV solution (dashed lines). N=3, error bars represent standard deviation. Where error bars are not shown, the standard deviation falls into the background.

Within the first day there was mass loss even in PBS (approx. 20%) due in part to drug elution from the films (drug loading accounts for <10%) and release of noncrystallized soluble silk into the release buffer (Figure 4). For films that are not loaded with EDTA (adenosine alone and control films), there was a significant increase in mass loss for films in protease type XIV compared to films in the PBS control. Note that the presence of adenosine in the film reduces mass loss in the film, suggesting the presence of the drug in the silk causes some decrease in the

film's susceptibility to degradation. While control films lost only 20.70% of their initial mass after 5 days in PBS, control films in protease type XIV lost an average of 61.40% of the mass within 24 hours, and were fully degraded by day 4 (100% loss of initial mass). Adenosine films lost an average of 63.10% of their mass after 5 days in protease type XIV (compared to 15.80% mass loss in PBS). Both films loaded with EDTA (EDTA alone and EDTA+adenosine) exhibited much less difference in mass lost in PBS controls compared to the proteinase type XIV treatments (Figure 3.5). After 5 days in release buffer, EDTA films lost 14.22% of their initial mass in PBS compared to 21.42% loss of initial mass in protease type XIV. After 5 days in release buffer, EDTA+adenosine films lost 15.33% of their initial mass in PBS compared to 19.68% loss of initial mass in protease type XIV. Mass loss in PBS versus proteinase type XIV was not statistically significant for EDTA alone, but was statistically significant for all other groups (two tailed t-test, $df = 4$, $p < 0.05$). Silk films loaded with EDTA that released EDTA into the buffer once the films were immersed (EDTA concentration in the buffer after 3 days was 0.58 ± 0.04 mg/mL, or approx. 2 mM, above the 1-10 μM effective concentration (Beynon and Bond, 2001)), exhibited less mass loss over 5 days in protease type XIV than films that were not loaded with EDTA. These data suggest that the EDTA-releasing silk films were capable of inhibiting proteolytic degradation in protease type XIV. Protease activity was not determined for this study (buffer was not changed during the study and thus could not be assayed until the end of the study), but was determined for the later encapsulated reservoir study.

3.2.2.2. EDTA and adenosine release from silk encapsulated reservoirs in PBS and protease type XIV release buffer

Since proteolysis increased drug release from the silk carriers and EDTA release from the silk films inhibited proteolysis, the effect of the combination of sustained EDTA release from

silk carriers on proteolytic activity and the release of the small molecule anticonvulsant adenosine from encapsulated reservoirs was investigated. The cumulative release of EDTA from encapsulated reservoirs containing 50% adenosine and 50% EDTA in PBS was assessed in 0.1 mg/mL protease type XIV (Figure 3.11).

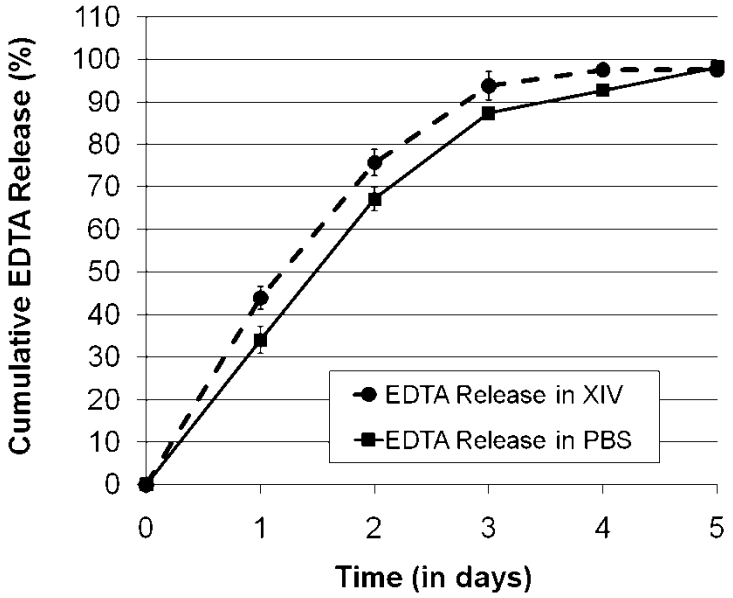

Figure 3.11. Cumulative EDTA release (in percent total load, approx. 35 mg) from silk encapsulated reservoirs in PBS (solid line) and 0.1 mg/mL proteinase type XIV (dashed line) at 37°C. N=3, error bars represent standard deviations. Where error bars are not shown they fall into background.

EDTA release was sustained for 5 days. Linear zero-order release was observed for the first three days ($R^2_{PBS} = 0.97$, $R^2_{Protease} = 0.99$) followed by decreased release for an additional two days.

The cumulative release of adenosine from encapsulated reservoirs containing 50% EDTA and 50% adenosine (ETDA + Adenosine) and encapsulated reservoirs containing 50% mannitol and 50% adenosine (Mannitol + Adenosine) was assessed in PBS (controls) and in 0.1 mg/mL protease type XIV solution (Figure 3.12).

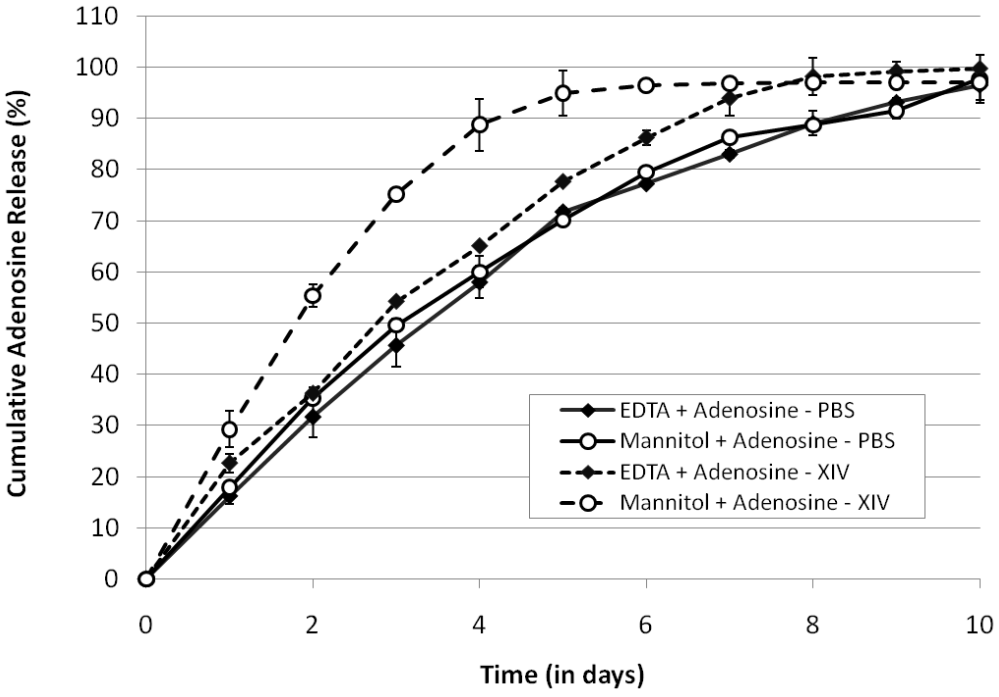

Figure 3.12. Cumulative adenosine release from silk encapsulated reservoirs in PBS (solid lines) and 0.1 mg/mL proteinase type XIV (dashed lines) at 37°C. Filled diamonds indicate release of adenosine from 50% EDTA and 50% adenosine encapsulated reservoirs; empty circles indicate release of adenosine from 50% mannitol and 50% adenosine encapsulated reservoirs. N=3, error bars represent standard deviations. Where error bars are not shown they fall into background.

The release of adenosine was slower and consequently exhibited longer release duration than EDTA (Figure 3.12) despite the same initial reservoir coatings and initial drug loading. This is attributed to the lower water solubility of adenosine compared to EDTA. The curves in Figure 3.12 show that release of adenosine from reservoirs containing 50% mannitol/50% adenosine and reservoirs containing 50% EDTA/50% adenosine were similar in PBS, suggesting that EDTA can be incorporated into reservoirs without affecting adenosine release and that any differences observed between release profiles in PBS and in 0.1 mg/mL protease type XIV are due to differences in proteolytic activity related to film degradation. The proteinase increased drug release from both types of reservoirs, while EDTA release significantly reduced the effects

of proteolysis on release rates. Even though EDTA release is only sustained for approximately 3 days, the the early effects of repressed proteolytic degradation(approx. 50% of adenosine released within 3 days from EDTA+adenosine reservoirs in proteinase, compared with approx. 75% of adenosine released within 3 days from mannitol+adenosine reservoirs) produces significant differences in the cumulative release curves. For a 10 day long release study the reservoirs comprised of EDTA+adenosine exhibited statistically significant different release rates for only 4 out of 10 days while the mannitol+adenosine reservoirs exhibited statistically significant different release rates for 8 out of 10 days (two tailed t-test, df = 4, $p < 0.05$). The increase in adenosine release rate was caused by proteolytic degradation and inhibited by sustained release of EDTA, reflected in the decrease in release duration (represented by t_{50}) and decrease in linearity of release (represented by decreased values of R^2 and n) for reservoirs containing mannitol and adenosine compared to reservoirs containing EDTA and adenosine (Table 3.3).

Table 3.3. Data for cumulative adenosine release from encapsulated reservoirs containing either 50% adenosine and 50 % mannitol or 50% EDTA and 50% adenosine in either PBS or 0.1 mg/mL protease type XIV

	Mannitol + Adenosine (no inhibition of proteolysis)			**EDTA + Adenosine (inhibition of proteolysis)**	
	PBS	0.1 mg/mL Protease type XIV		PBS	0.1 mg/mL Protease type XIV
Time at which 50% total adenosine load is released (t_{50})	3.04 days	1.80 days		3.35 days	2.77 days
Correlation Coefficent (R^2)	0.93	0.71		0.94	0.91
Siepmann-Peppas Release Coefficient (n)	0.72	0.49		0.78	0.68

3.2.2.3. Effect of EDTA release from silk encapsulated reservoirs on protease type XIV activity

To characterize the effects of sustained release of EDTA from silk encapsulated reservoirs on proteolytic activity, the enzyme activity was assayed in collected samples (Figure 3.13). PBS samples exhibited no proteolytic activity. Every 24 hours proteinase was replaced with fresh 0.1 mg/mL protease solution. Fresh, unincubated 0.1 mg/mL proteinase solution assayed prior to study was taken as the value for Day 0/100% proteinase activity.

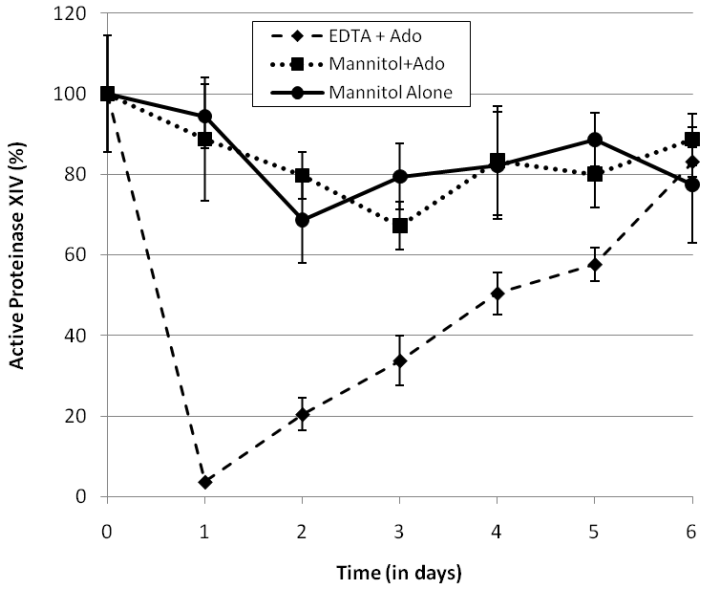

Figure 3.13. Activity of proteinase type XIV release buffers for encapsulated reservoirs containing 50% EDTA /50% adenosine (diamond with dashed line), 50% mannitol/50% (squares with dotted line) or 100% mannitol (circle with solid line). N = 3, error bars represent standard deviations. Where error bars are not shown they fall into background.

Even in the absence of inhibitor, some reduction of activity, up to 40%, was observed for encapsulated reservoirs containing 50% mannitol and 50% adenosine and reservoirs containing 100% mannitol. Some amount of activity loss is expected, as evidenced by the assertion in the literature that protease solutions must be changed daily due to activity loss at 37^{o}C incubation (Horan *et al*., 2005). The reservoirs containing 50% EDTA and 50% adenosine exhibited a

significant reduction in proteinase activity for 5 days. After 5 days, the proteinase activity returns to levels comparable to non-EDTA containing formulations. The concentration of EDTA (in mg/mL) in the release buffer versus proteinase activity (in µg/mL of active proteinase type XIV) is shown in Figure 5.14.

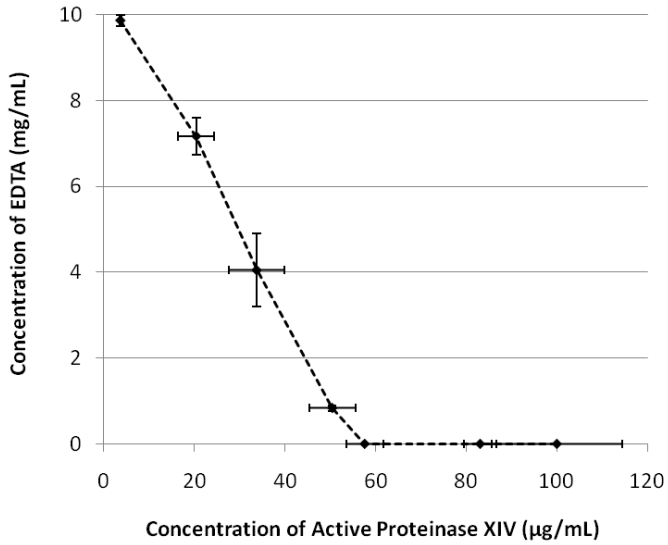

Figure 3.14. Concentration of EDTA released from 50% EDTA/50% adenosine encapsulated reservoirs (in mg/mL) versus active proteinase XIV in release buffer (in µg/mL). N=3, error bars represent standard deviations. Where error bars are not shown the standard deviation falls into background.

On day 1 when EDTA release was highest, protease type XIV was almost entirely inhibited. During the first 5 days while EDTA release was sustained, proteinase activity was reduced compared to proteinase activity levels observed when EDTA release subsided. In the absence of EDTA protease type XIV exhibited approx. 60-100% of initial activity, but overall, the concentration of EDTA released from the reservoirs proportionally inhibits the activity of protease type XIV present in the release buffer.

3.2.3. Conclusions

Loading EDTA into silk carriers inhibited proteolytic degradation of silk films and delayed drug release from silk encapsulated reservoirs immersed in proteinase solution. These studies demonstrate the effects of proteolytic degradation on drug release from silk carriers and introduce a promising strategy to control degradation rate via manipulation of local proteolytic activity. Future work includes finding strategies to achieve sustained release of silk-specific proteases or proteinase-activity enhancers from the carriers themselves to increase local degradation rates. The modulation of local enzyme function via-controlled release could be applied to a range of silk material formats, including drug delivery implants and tissue engineering scaffolds.

3.3. Controlled release of proteolytic enzymes from silk-based delivery devices

3.3.1. Introduction

Controlled release of a proteinase inhibitor (EDTA) successfully reduced local rates of degradation, but in order to increase local degradation strategies must be investigated to achieve sustained release of silk-specific proteases or proteinase-activity enhancers from the carriers themselves. Though there have been many successful studies implementing silk based biomaterials for controlled release of active enzymes (Lu *et al.*, 2010-1)), loading protein-degrading enzymes into a protein biomaterial delivery system poses new challenges. Bulk loading of silk films requires mixing proteinase into the silk solution prior to casting films (Hofman *et al.*, 2006), but during the drying phase the proteinase in the solution will degrade the silk in solution, and the degraded silk will be unable to form a film (Figure 3.15A).

Silk material format has been shown to impact degradation rate (Arai *et al.* 2004; Yang *et al.* 2009). Certain silk materials degrade more slowly, possibly due to hydration limitations and steric hindrance since densely packed silk may be less accessible to enzymes. For example, α-chymotrypsin treated silk films degrade more slowly than silk solution: films exhibit 9% mass loss at day 1 (Arai *et al.*, 2004), whereas silk in solution is totally degraded in less than 24 hours when exposed to α-chymotrypsin. A loading approach is needed that protects the silk from proteolysis while in solution during the silk film drying phase, but then releases the proteinase in active form once the film is formed. To meet this need, EDTA (a small molecule proteinase inhibitor) was added to the proteinase and silk solution prior to film casting. While in solution, the EDTA prevents proteolytic degradation of the silk, and then leeches out of the film rapidly (Figure 3.15B). The small molecule inhibitor will diffuse out of the film quickly while the proteinases, which are considerably larger, diffuse more slowly.

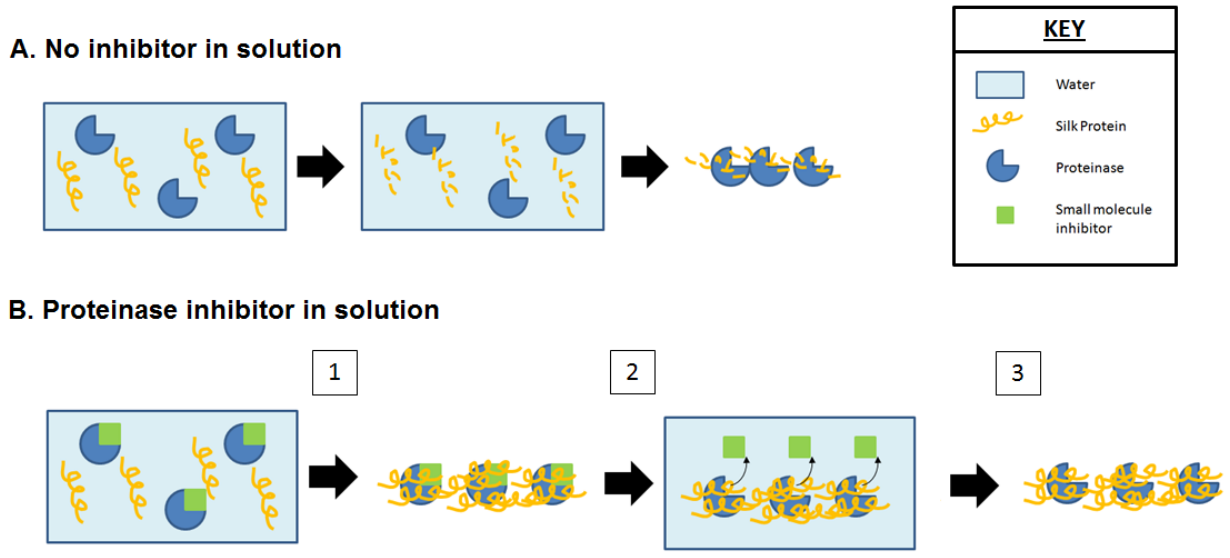

Figure 3.15. Schematic representation of proteinase loaded silk film formation in the (A) absence and (B) presence of proteinase inhibitor (1) inhibitor prevents degradation of the silk in solution, film forms and (2) inhibitor diffuses out of film, leaving (3) a proteinase loaded silk film

The model proteinases selected for controlled release from silk drug carriers have both potential utility as tools to manipulate degradation rates for control of drug release and implant degradation behavior, and therapeutic relevance in treatment of Alzheimer's Disease and biofilm infections. Protease type XIV and α-chymotrypsin were selected for study as they have been widely studied for silk degradation (Table 3.1). Protease type XIV degrades silk more aggressively than α-chymotrypsin (Arai *et al*., 2004) and cleaves different sites in the protein, so characterization of controlled release of both proteinases provides a range of potential degradation behaviors to build into implants.

Protease type XIV and α-chymotrypsin were also selected for study due to their therapeutic potential in the treatment of Alzheimer's Disease (AD). Accumulation of Aβ (which, according to the amyloid hypothesis, is central to the pathogenesis of AD) is believed to result from an imbalance between the relative rates of Aβ synthesis and clearance (Tanzi *et al*., 2004). As such, several therapies aimed at decreasing the rate of synthesis and increasing the rate of clearance have been proposed. The two major endopeptidases involved in amyloid degradation are both zinc metalloendopeptidases and are referred to as insulin degrading enzyme (IDE) or insulysin, and neprilysin (NEP) (Miners *et al*., 2008). Numerous animal-models and *in vitro* studies have demonstrated via genetic manipulations that increases in IDE and NEP activity can increase amyloid clearance via degradation of non-soluble Aβ into soluble fragments (Leissring *et al*., 2003, Vekrellis *et al.*, 2000, Farris *et al.*, 2003; Farris *et al.* 2004; Miller *et al.* 2003; Iwata *et al.*, 2004; Higuchi *et al.*, 2005).

There have been attempts to develop therapeutic interventions based on proteolytic degradation of amyloid plaques. Hemming *et al.* reported robust plaque clearance at the site of engraftment in a transgenic murine model that received NEP secreting fibroblast grafts

(Hemming *et al*., 2007). Similarly, Marr *et al.* reported that unilateral intracerebral injection of a lentiviral vector expressing human neprilysin reduced amyloid deposits by half relative to the untreated side in a transgenic mouse model of amyloidosis (Marr *et al*., 2003). Lui *et al.* demonstrated that three known Aβ-degrading peptidases (NEP, IDE and MP-1) could be coupled to erythrocytes to lower plasma Aβ levels both *in vitro* and *in vivo* (Lui *et al*., 2007). Recently, Aβ microfibrils with cross-β structures were shown to be degraded to nanospheres or nanofilaments within 24 hours of exposure to protease type XIV and α-chymotrypsin, respectively, in contrast to NEP and IDE, which were unable to digest the microfibrils after 48 hours of exposure. Protease type XIV degradation products (nanospheres) induced cytotoxicity, while the α-chymotrypsin degradation products (nanofilaments) exhibited little cytoxicity (Numata and Kaplan, 2010-2).

Another potential application of controlled release of proteolytic enzymes from silk antibiotic delivery devices is enhanced penetration through biofilms. Biofilms (discussed at greater length in Chapter 5) are complex extracellular polymer matrices secreted by a collection of micro-organisms that significantly increase the resistance of the encased micro-organisms to antibiotics. Biofilm composition is highly variable, containing various proteins, polymers, complex carbohydrates and water (Kennedy *et al*., 2010). For this application, an aggressive, non-specific protein/polymer degrading enzyme cocktail like protease type XIV would be ideal. For comparison, Lu and Collins engineered bacteriophage to express biofilm-degrading enzyme during infection to simultaneously attack the bacterial cells in the biofilm and degrade the extracellular polymeric biofilm and found that the biofilm-removal resulting from this two-pronged attack was significantly greater than nonenzymatic bacteriophage treatment (Lu and Collins, 2007).

The objective of this study was to prevent silk degradation during encapsulation to load silk-degrading proteinases (α-chymotrypsin and protease type XIV) into silk films and to recover active proteinase after film formation. Additionally, different concentrations of proteinase were studied to determine the effects of carrier degradation on proteinase loading and release.

3.3.2. Materials and Methods

3.3.2.1. Materials

Proteinases were protease type XIV (3.5 units/mg) from *Streptomyces griseus* and α-chymotrypsin Type I-S (≥40 units/mg), both from Sigma Aldrich (St. Louis, MO). The inhibitor was EDTA, which previous studies have shown effectively inhibited protease type XIV digestion of silk. Calcium also stabilizes and activates α-chymotrypsin (Castaneda-Agullom *et al.* 1962), so the presence of EDTA was predicted to also reduce digestion of the silk by α-chymotrypsin.

3.3.2.2. Proteinase-loaded silk film preparation

Silk solution was prepared and concentrated as previously described. Concentrated 20% (w/v) silk was mixed with 100 mg/mL EDTA, then proteinase solution in PBS was added. Silk, EDTA and proteinase solutions were combined in a volume:volume:volume ratio of silk:EDTA:proteinase of to 2:1:1. Initial proteinase solution concentrations tested were 10 mg/mL, 1 mg/mL and 0.1 mg/mL. Once mixed, the solution composition was 10% (w/v) silk, 25 mg/mL EDTA and 2.5, 0.25 or 0.025 mg/mL proteinase. This solution was cast into films using 100 µL aliquots in 5 mm diameter Teflon coated molds. Total EDTA loading in the films was 2.5 mg, and total proteinase loading for 10, 1 and 0.1 mg/mL initial proteinase concentrations

was 250 µg, 25 µg and 2.5 µg, respectively. Once dry, an extra silk capping layer was added to delay burst and sustain release by methanol treating the films, then dipping in 10% (w/v) silk, drying and methanol treating.

3.3.2.3. Release testing

Films were immersed in 1 mL of PBS supplemented with 100 mg/L $MgCl_2$ and 100 mg/L $CaCl_2$ (to enhance proteolytic activity). Buffer was removed and replaced every 24 hours. The removed buffer was assayed for proteolytic activity and EDTA content to track EDTA diffused from the film. Collected buffer was assayed for proteolytic activity using the Amplite™ Universal Fluorimetric red fluorescence protease activity assay kit (ABD Bioquest, Sunnyvale, CA) as previously described. EDTA content was assayed as previously described (Sorensen, 1992).

3.3.3. Results and discussion

3.3.3.1. EDTA leeching from proteinase loaded silk films

Figure 3.16 shows cumulative EDTA release from films over 4 days. In all samples, there was no EDTA detected after 2 days in PBS, and of the 2.5 mg loaded per film, 100% seems to have been recovered in all cases. This suggests that, if desired, more than 80% of the EDTA can diffuse out in 24 hours prior to implantation. Note that EDTA is released more rapidly from the films than from encapsulated reservoirs (Figure 3.11) due to the difference in material format and path length.

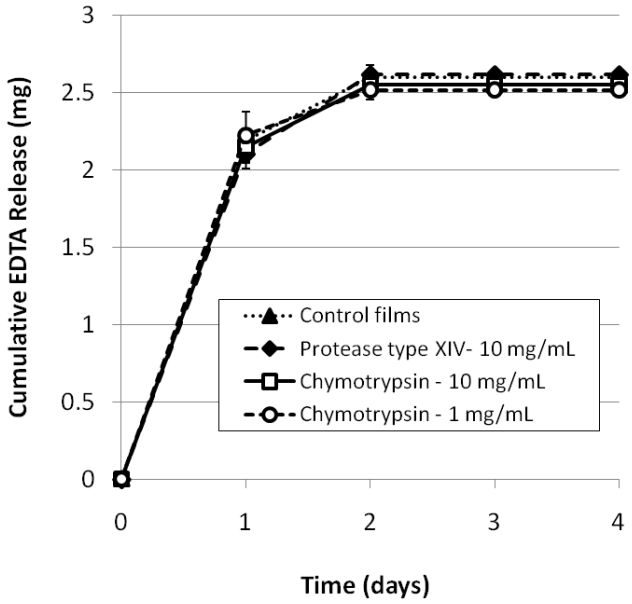

Figure 3.16. Cumulative EDTA release from various preparations of silk films loaded with protease type XIV, α-chymotrypsin or buffer (control films). N = 4, error bars represent standard deviations (where error bars aren't shown they fade into background).

3.3.3.2. Proteinase release from silk films

Figure 3.17 shows active proteinase released from the silk films over 5 days. Note that the amount of cumulative proteinase release represents only active proteinase, so proteinase that loses activity during encapsulation at room temperature or incubation in release buffer at 37^{o}C, is subject to autocatalytic degradation or is released but inhibited by the co-released EDTA is not accounted for (future work will include ELISA and release studies with fluorescently tagged proteinase to quantify total enzyme released, including inactive or degraded enzyme). Protease type XIV films loaded at 1 mg/mL or 0.1 mg/mL proteinase and α-chymotrypsin films loaded at 0.1 mg/mL proteinase exhibited no release or released enzyme at concentrations below detection limits of the assay (which in this case was approximately 3.13 µg/mL).

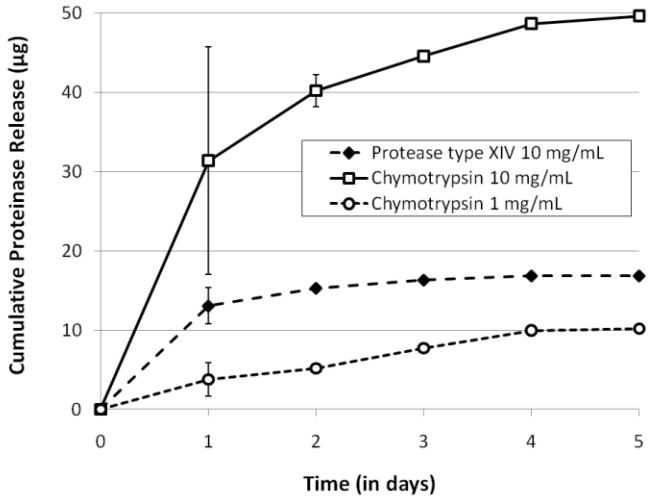

Figure 3.17. Cumulative proteinase release from various preparations of silk films loaded with protease type XIV and α-chymotrypsin. N = 4, error bars represent standard deviations (where error bars are not shown they fade into background).

Figure 3.18 shows cumulative proteinase release in percentage of total load (250 µg total for films prepared using 10 mg/mL proteinase solution and 25 µg total for films prepared using 1 mg/mL proteinase solution).

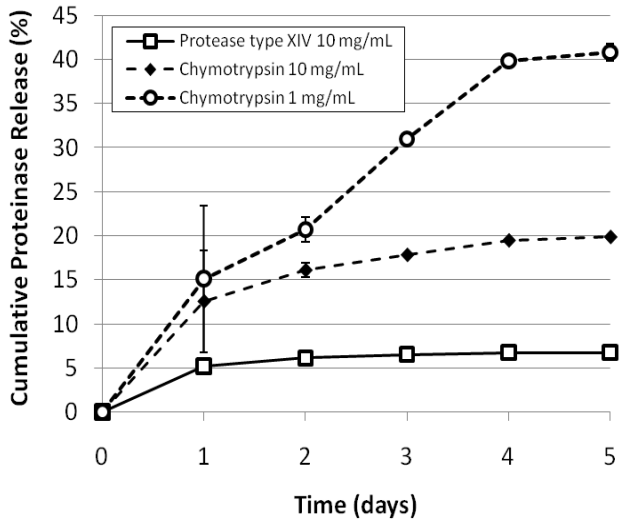

Figure 3.18. Cumulative proteinase release from various preparations of silk films loaded with protease type XIV and α-chymotrypsin in percentage total load. N = 4, error bars represent standard deviations (where error bars are not shown they fade into background).

Although the 1 mg/mL α chymotrypsin releasing silk films exhibit the lowest total proteinase release, when corrected for percentage of total drug load, these films actually exhibit the highest percentage recovery. Values of the Siepmann-Peppas release exponenent n increase (i.e., release become closer to zero-order) with decreasing proteolytic degradation (rate of proteolytic degradation: 1 mg/mL α chymotrypsin < 10 mg/mL α chymotrypsin < 10 mg/mL protease XIV). This is likely due to increasing carrier degradation as the proteinase releases causing more rapid release of the incorporated enzyme. The less aggressive the proteolytic degradation of the carrier during loading, the higher the total enzyme recovery (40.78%, 19.85% and 6.75% released over 5 days from films prepared using 1 mg/mL α chymotrypsin, 10 mg/mL α chymotrypsin and 10 mg/mL protease XIV, respectively)

Table 3.4. Loading and release behavior parameters for proteinase releasing silk films

	Protease type XIV 10 mg/mL	Chymotrypsin 10 mg/mL
Total proteinase loaded per silk film	250 µg (~0.875 U)	250 µg (~10U)
Total proteinase load recovery (%)	6.75%	19.85%
Siepmann-Peppas exponent (n)	0.17	0.29

3.3.4. Conclusions

Proteinases capable of degrading amyloid deposits responsible for the progression of Alzheimer's or enhancing penetration through biofilms were entrapped into silk films. The silk, which is degradable due to proteolysis in solution, was protected from premature degradation during film formation by the addition of EDTA, which served as a small molecule proteinase inhibitor. Once the films were prepared, EDTA diffused from the silk films rapidly, with more than 80% released over 24 hours and almost 100% in 48 hours. In contrast, the protease type XIV or α-chymotrypsin released over 5 days.

4. Silk biomaterials for local drug delivery for neurological applications

4.1 Introduction

The therapeutic application of neuroactive molecules to treat neurological disorders is currently limited, predominantly due to the problems posed by the administration of these drugs. Oral or parenteral delivery routes can be limited (as for any systemically administered therapeutic) by adverse side effects and rapid metabolism. For therapeutics designed to reach the brain, there is the added difficulty of achieving passage through the blood brain barrier (BBB). Intrathecal or intraventricular catheters suffer from drug instability in aqueous solution and fail to deliver drugs directly into the parenchyma (Menei *et al*., 1993). Although candidate compounds have been indentified for treatment of neurodegenerative conditions such as amyotrophic lateral sclerosis (ALS) and Huntington's disease, and possibly also Alzheimer's and Parkinson's diseases, an adequate means of achieving long-term delivery to the central nervous system is still lacking (Maysinger and Morinville, 1997). The effectiveness of conventional brain cancer treatment is similarly hindered: the blood–brain barrier (BBB) restricts penetration, such that only a small fraction of a systemically administered dose ultimately reaches the tumor vasculature. The high local drug concentrations necessary to eliminate brain tumors often cannot be achieved without exceeding limits of vital normal tissue toxicity (Gutman *et al.*, 2000).

One solution is the implantation in the brain of biodegradable polymer devices with controlled, localized release of a neuroactive drug. Sustained-release polymer implants consisting of biocompatible, biodegradable polymers impregnated with drugs have the potential to improve both the safety and efficacy of many neurological therapeutics. By being implanted directly, these polymeric devices eliminate the need to penetrate the BBB and sustain high

concentrations of therapeutic agents at the target site without causing systemic toxicity. (Maysinger and Morinville, 1997; Menei *et al.,* 1993; Gutman *et al*., 2000).

Several polymer implants designed for local intracerebral delivery have been proposed, particularly for the treatment of brain cancers. Brem *et al*. prepared wafers made from carmustine (BCNU) and a polyanhydride polymer (GLIADEL® wafers) to be implanted into the resected tumors of patients with recurring malignant glioma (Brem *et al.,* 1995). Poly-D-lactide-co-glycolide (PLGA) microspheres loaded with carboplatin injected into the tumors of glioma-bearing rats increased median survival and decreased weight loss compared with animals receiving systemic doses of carboplatin or empty PLGA microspheres. The authors also demonstrated highly elevated carboplatin levels in the tumors of animals receiving intratumoral injections of carboplatin-releasing PLGA microspheres compared with surrounding brain tissue (Chen *et al*., 1998). Fung *et al*. implanted polyanhydride pellets in monkey brains and found high drug concentrations within 3 mm and significant concentrations within 5 cm of the implant site as long as 30 days after implantation (Fung *et al*., 1998), an important proof-of-principle as tumor recurrence is reported to occur within 2 cm of the original tumor site in 90% of malignant gliomas (Hochberg and Pruitt., 1980). These studies have demonstrated that local drug delivery from polymer implants can effectively deliver drugs to the brain that are otherwise impossible to administer due to metabolic clearance, unwanted side-effects or limited penetration of the blood brain barrier.

Silk possesses excellent material properties for drug delivery, as previously described. The suitability of silk for central nervous systems therapies has also been investigated. Silk fibroin fiber was found to support the survival and growth of attached hippocampal neurons and neurons cultured in silk fibroin extract exhibited no significant difference in morphology or cell

viability compared to plain neuronal culture medium (Tang *et al*., 2009). Moreover, no significant difference in mRNA or protein levels of growth-associated molecules (determined via immunohistochemistry, RT-PCR and Western Blot) was detected between hippocampal neurons cultured in plain neuronal culture medium and medium containing silk fibroin extract, suggesting silk fibroin has no significant cytotoxic effects on the hippocampal neuron phenotype or function (Tang *et al*., 2009). Similar studies have demonstrated silk fibroin's biocompatibility with dorsal root ganglia and Schwann cells (Yang *et al*., 2007-1). These extensive biocompatibility studies, combined with the frequent use of silk as a suture material in brain and nerve tissue (Dehdashti *et al*., 2001 and Schmutz *et al*. 1997) and studies showing positive outcomes for silk fibroin-based nerve grafts (Yang *et al*., 2007-2, Uebersax *et al*., 2007, Madduri *et al.*, 2010), strongly suggest silk is a safe, supportive biomaterial for CNS applications including *in vitro* tissue models, drug delivery materials and therapeutic implants.

One example of a neurological therapeutic that would benefit from local, sustained delivery is the brain's endogenous anticonvulsant, adenosine. The purine ribonucleoside adenosine is an endogenous inhibitory modulator of brain activity with potent anticonvulsant and neuroprotective properties (major sources and sinks of adenosine in astrocytes are represented in Figure 4.1) (Boison, 2006; Boison *et al*., 2010). Once in the extracellular space, adenosine modifies cell function by operating G-protein-coupled receptors (A_1, A_{2A}, A_{2B}, A_3). Manipulations of adenosine receptors influence sleep and arousal, cognition and memory, neuronal damage and degeneration, as well as neuronal maturation (Ribeiro *et al*., 2003). Because adenosine is involved in many functions with consequences in the pathology of the nervous system, adenosine has therapeutic potential in a wide range of neurological diseases, including epilepsy, chronic pain and cerebral ischemia (Boison, 2007). Adenosine augmentation

therapy (AAT) represents a promising potential treatment for pharmacoresistant epilepsy. AAT is believed to act by correcting the brain's seizure generating focal adenosine deficiency, providing neurochemically relevant epilepsy therapy (Boison, 2006; Boison, 2008). Studies in animal models have shown that focal AATs can suppress individual seizures (termed ictogenesis) ((Huber *et al*., 2001; Boison *et al*., 1999) and might be capable of retarding or preventing the progression of epileptogenesis (Li *et al*., 2008; Li *et al*., 2007). These studies have also shown that focal AATs were devoid of systemic and sedative side effects (Güttinger *et al*., 2005), and produced an effect in suppressing experimental seizures that were refractory to standard antiepileptic drugs (Gouder *et al*., 2003). These proof of principle studies have demonstrated that AATs hold great promise for the therapy of refractory epilepsies, but do not themselves represent clinically suitable delivery approaches as they use animal cells or fail to achieve long term release durations. Further clinical development of AATs requires safe and biocompatible polymer brain capable of sustained adenosine release.

Unfortunately, when administered systemically, adenosine induces severe systemic side effects, including suppression of cardiac function (Dunwiddie, 1999). These peripheral side effects, along with rapid metabolic clearance and the blood brain barrier, have limited the therapeutic utility of adenosine. Adding to the complexity of attempting to administer adenosine systemically is the fact that adenosine can induce mixed responses: activation of A_1 receptors produces largely beneficial effects in epilepsy, ischemia, myelination, pain and sleep, while activation of A_{2A} receptors can have a negative impact on Alzheimer's disease, Parkinson's disease, Huntington's disease and addiction (Ribeiro *et al*., 2003, Detlev, 2007). Within the brain, adenosine receptors are distributed with varying densities through different regions of the brain (Figure 4.2), so local delivery could be expected to achieve desired therapeutic outcomes

(i.e., seizure suppression, neuroprotection, etc.) while limiting activation of adenosine receptors and minimizing negative side-effects. A system for site specific, implantable, sustained adenosine delivery is therefore essential for its therapeutic efficacy and safety.

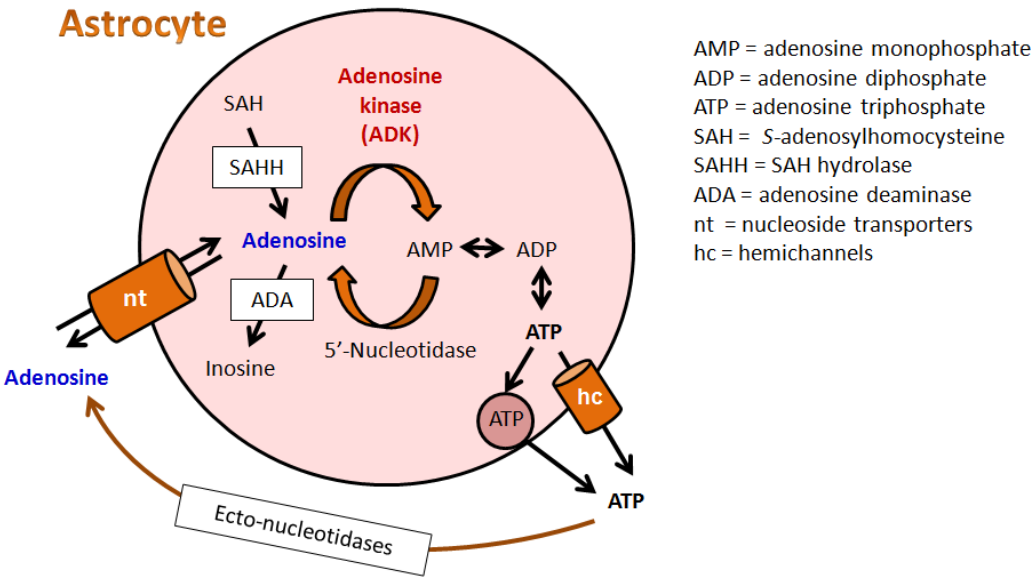

Figure 4.1 Selected mechanisms and pathways of adenosine metabolism. Extracellular adenosine levels are thought to be regulated by an astrocyte-based adenosine cycle. Astrocytes can release ATP via vesicular release and/or by direct release through hemichannels (h-ch). The extracellular cleavage of released ATP by ecto-nucleotidases (EN) contributes to the formation of adenosine. Adenosine can also be released directly via equilibrative nucleoside transporters (nt). Under physiological conditions adenosine (Ado) concentrations in adult brain depend mainly on the activity of the astrocyte-based enzyme adenosine kinase (ADK), which, together with 5′-nucleotidase, is part of a substrate cycle between AMP and adenosine. This substrate cycle is linked directly to the cellular energy pool (ATP–ADP). In the brain, alternative metabolic routes of adenosine that involve either the reversible hydrolysis of *S*-adenosylhomocysteine (SAH) by SAH hydrolase (SAHH) or the deamination of adenosine to inosine (Ino) by adenosine deaminase (ADA) constitute minor pathways for the regulation of adenosine. Intracellular and extracellular concentrations of adenosine equilibrate rapidly via nucleoside transporters (nt), which are expressed ubiquitously (Boison, 2006; Boison *et al*., 2010).

To meet this need, silk implants were designed to continuously release adenosine locally and the therapeutic potential of these novel AAT devices was tested in the rat kindling model, in which progressive seizure development could be studied and quantified as a function to different rates of adenosine release. The time-limited silk adenosine delivery system was also used to

study antiepileptic effects of focal AAT without any confounds that might be caused by cell-based brain implants.

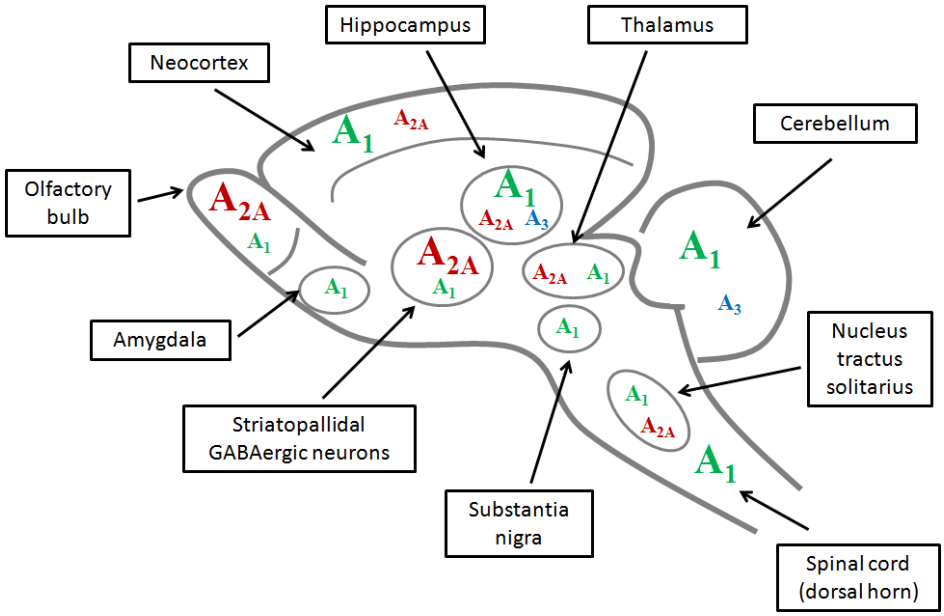

Figure 4.2. Distribution of high affinity adenosine receptors: A_1 (green), A_{2A} (red) and human A_3 (blue) in the main regions of the central nervous system where adenosine has been proposed to interfere with brain dysfunctions and disease. Higher levels of expression are indicated by larger font size. (Modified from Ribeiro *et al*., 2003).

4.2 Materials and Methods

4.2.1. Implant Design and Fabrication

For dose dependence studies, implants were designed to deliver the target doses (0, 40, 200 and 1000 ng per day). Implants were designed to split the target drug load roughly evenly between the three systems integrated into a single implantable material format: microspheres, macroscale films and nanofilms. The three variables used to control the final adenosine release rate were: (1) the concentration of microspheres in the silk solution that were formed into water based, porous scaffolds, (2) the concentration of adenosine in the adenosine plus silk solution

that the porous scaffolds were coated with to form the macroscale silk films, and (3) the number of layers of nanofilms deposited on the system (Figure 4.3).

Silk solution was prepared as previously described (Sofia *et al.*, 2001). Adenosine containing microspheres were prepared according to the MeOH-based lipid protocol described previously (Wang *et al*., 2007-3). Briefly, 200 mL of 10 mg/mL adenosine stock solution was mixed with 1 mL of 8% (w/v) silk aqueous solution, which was then added to 200 mg of 1,2-dioleoyl-sn-glycero-3-phosphocholine (DOPC) phospholipid that had been dissolved in 1 mL of chloroform, then dried under N_2 to a film on the interior of a glass test tube. The solution is diluted, then repeatedly freeze-thawed, and then lyophilized. Later, the microspheres were treated with methanol (MeOH) to remove the lipids and induce β sheet silk physical crosslinks to stabilize the structures. Water-based porous scaffolds were prepared as previously described (Kim *et al*., 2005-1) using the mixture of microspheres and silk solution to imbed the microspheres in the final porous scaffold. Briefly, 4 g of 500–600 mm granular NaCl were added to 2 mL of 6% (w/v) silk solution mixed with microspheres in a plastic container and incubated at room temperature for over 24 h. The scaffolds were then washed for 24 h to leach out the sodium chloride. To obtain the desired implant geometry (0.6–0.7 mm diameter, 3 mm length), the scaffolds were punched out with a 1 mm Miltex biopsy punch and then trimmed with a scalpel on either end. The porous scaffolds were next coated with macroscale drug-loaded silk films comparable to the films described previously (Hofmann *et al*., 2006). Implants were soaked in a mixed 8% (w/v) silk and drug solution for 5 min, then incubated at 60^{o}C for 15–20 min, and then washed in a 90% MeOH solution. Finally, nanofilm coatings were applied using our previously described protocol (Wang *et al*., 2007-2) but modified to accommodate the coating of a 3D porous scaffold. Scaffolds were first dipped in a 2 mg/mL silk fibroin solution for 2 min,

and then washed in 90:10 (v/v) MeOH/water solution for 1 min. Following the methanol wash, the scaffolds were dried at 60°C for 15 min. The dried scaffolds were then dipped in a 1 mg/mL adenosine solution for 2 min and dried at 60°C for another 15 min. These steps were repeated until the desired number of layers was achieved, ending with a silk layer. After drug loading, all implants were coated with three capping layers (three subsequent silk dips) to delay burst.

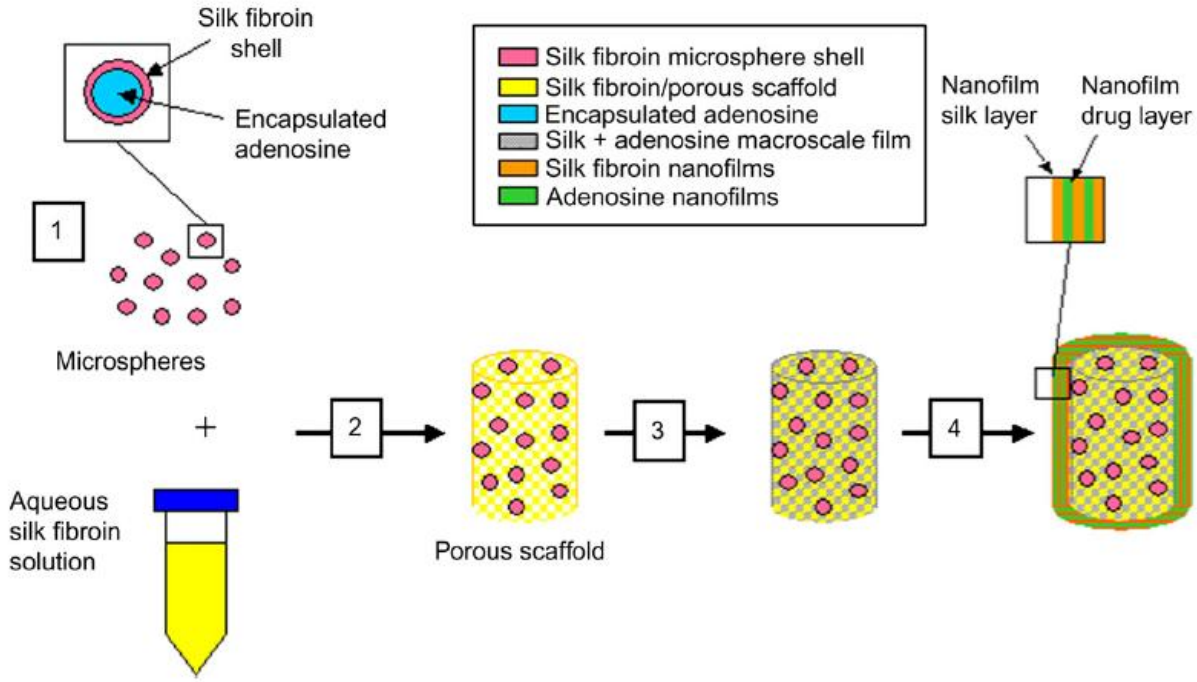

Figure 4.3. Schematic of implant fabrication showing the individual silk-based drug delivery components. (1) Adenosine encapsulating microspheres are prepared. (2) Microspheres are mixed with silk solution, and then porous scaffolds embedded with microspheres are fabricated using NaCl particulate leeching. (3) Scaffold is soaked in silk + adenosine solution, filling in pores and coating the implant with a macroscale drug-loaded film. (4) Additional adenosine is loaded with alternating nanofilm deposition.

For later studies, second generation implants designed to deliver target doses of 0 (empty/control) or 1000 ng adenosine per day were designed and fabricated as described above, with some slight modifications. Briefly, implants were designed to split the target drug load evenly between microspheres and multiple macroscale films that were integrated into a single implant and capped with additional burst-delaying silk films. Adenosine containing microspheres

were prepared according to the MeOH based lipid template protocol described previously (Wang *et al*., 2007-3). Water-based porous scaffolds were prepared as previously described (Kim *et al*., 2005-1) using the mixture of microspheres and silk solution to imbed the microspheres in the final porous scaffold. To obtain the desired implant geometry (0.6–0.7 mm diameter, 3 mm length), scaffolds were punched out with a 1 mm Miltex biopsy punch and then trimmed with a razor on either end. The porous scaffolds were next coated with multiple macroscale adenosine-loaded silk films comparable to the films described previously (Hofmann *et al*., 2006). After drug loading, all implants were coated with three silk-based capping layers to delay burst-release of adenosine.

4.2.2. *In vitro* release testing

Release studies were carried out as previously described. Briefly, implants were immersed in 1 ml of Dulbecco's phosphate buffer, pH 7.2 (PBS) at 37 °C. At desired time points PBS was removed and replaced. Adenosine content in the PBS samples removed from the system was measured using a modified fluorescence assay as previously described (Wojcik and Neff, 1982). For each device at each time point, three fluorescence readings were taken and averaged.

4.2.3. *In vivo* testing

4.2.3.1. Implantation

All animal procedures were conducted in a facility accredited by the Association for Assessment and Accreditation of Laboratory Animal Care in accordance with protocols

approved by the Institutional Animal Care and Use Committee and the principles outlined in the NIH Guide for the Care and Use of Laboratory Animals. Adult male Sprague–Dawley rats were used at a body weight of 280–300 g. All rats were acclimatized for one week before being used in the experiments. The rats were housed under a 12 h light/dark cycle (lights on from 8:00 A.M.) with food and water provided ad libitum. Anesthesia was induced with 3% isoflurane, 67% N_2O, 30% O_2 and maintained with 1.5% isoflurane, 68.5% N_2O, 30% O_2, while rats (N=22) were placed in a Kopf stereotactic frame. Polymers were implanted using a stereotactic implantation device (internal diameter 0.7 mm, external diameter 1 mm) as previously described (n=5-6 per dose) (Boison *et al*., 2002). The polymer-loaded device was stereotactically inserted into the brain using a drill hole. Upon reaching the target site the 3 mm long polymer was released and deposited within the infrahippocampal cleft by slowly retracting the outer tube of the device. Finally, the device was fully retracted as described previously. Thus, the implanted polymers were deposited within a formed cavity of 3 mm length within the right infrahippocampal cleft and adjacent to the electrode implantation site (see Figure 4.4).

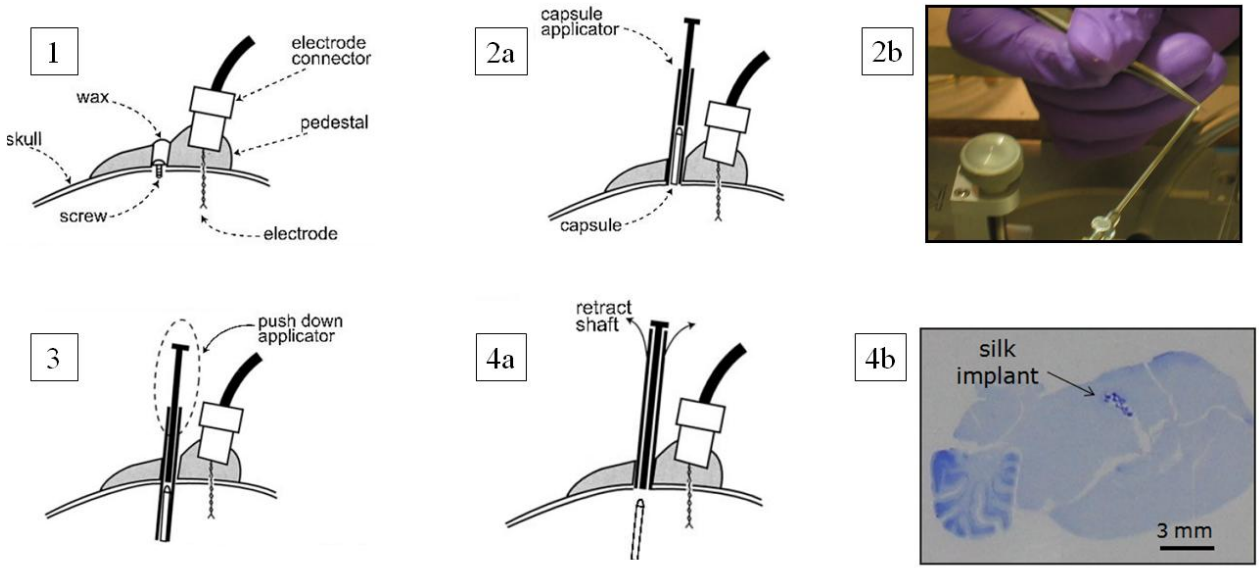

Figure 4.4. Schematic of intracranial polymer implantation procedure. (1) Longitudinal cross-section showing the location of the acrylate pedestal (in gray) at the top of the rat skull. The acrylate pedestal carries the electrode connector, which carries the electrodes used for kindling and EEG recordings. The pedestal also contains a guidance hole, which is covered with a screw and uncovered and removed prior to polymer implantation (2a) Placement of an implant containing applicator to the surface of the skull (2b) Polymer rod being inserted into the applicator for implantation (3) the whole applicator (outer shaft + implant+ inner pistil) is gently pushed down to the brain to the correct location (4a) the outer shaft is retracted first, then the inner pistil, leaving the implant in place (4b) crystal violet stain of a section of a whole rat brain confirming the correct location of the silk implant (shown stained in bright blue) (modified from Boison *et al.*, 2002).

4.2.3.2 Kindling

A bipolar, coated, stainless steel electrode (0.20 mm in diameter, Plastics One, Roanoke, VA) was implanted into the right hippocampus and fixed with a head-set of dental acrylate. Animals were stimulated unilaterally six times every second or third day with a Grass S-88 stimulator (1-ms square-wave pulses of 5 V at 50-Hz frequency for 10 s, 30-min interval between stimulations). Behavioral seizures were scored on a scale from 0 to 5 according to the scale of Racine (Racine, 1978). The electroencephalogram (EEG) was recorded for periods of 1 min before and 5 min after application of each stimulating pulse using a Nervus EEG monitoring system.

4.2.3.3 Histology

After completion of the experiments the rats were transcardially perfused with 4% paraformaldehyde in phosphate buffer (0.15 m, pH 7.4). To characterize the gross anatomy of the brain at the site of implantation and confirm implant location, whole rat brains were sectioned and stained. To characterize scaffold morphology post-implantation, scaffolds were retrieved from the brains with tweezers and sectioned or sectioned while still imbedded in the brain. To characterize scaffold morphology pre-implantation samples from batches of scaffolds intended for implantation were reserved and sectioned. The samples harvested were washed in PBS, and fixed in 10% neutral buffered formalin before histological analysis. Samples were dehydrated through a series of graded alcohols, embedded in paraffin and sectioned at 5 μm thickness. Sections were stained with either hematoxylin and eosin (H&E) or crystal violet (methyl violet 10B).

Samples of implants prior to implantation and after implantation were compared to analyze *in vivo* degradation. Sections were examined under a Zeiss Axiovert S100 light microscope with a Sony Exwave HAD 3CCD color video camera. The ratio of total surface area of pores (in pixels) to total surface area of the implant (in pixels) was evaluated using Image J image processing software (Figure 4.5). Data was analyzed with a two sample t-test: $df = 10$, $p < 0.001$. The Image J analysis results are based on $n = 6$ implants.

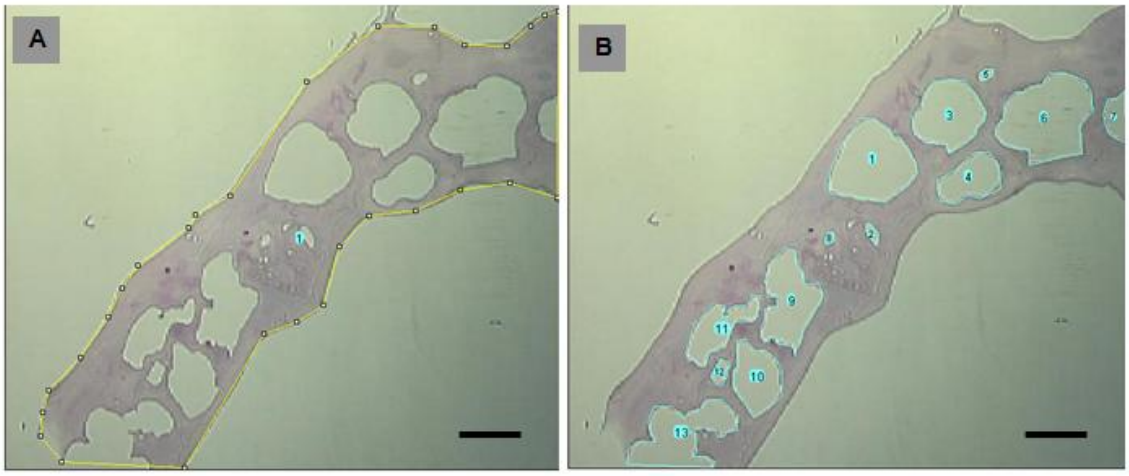

Figure 4.5. Example of Image J degradation analysis (pre-implantation sample #1): Total surface area (yellow line) in pixels in measured (A), then the sum of the surface areas of all the pores (blue lines) is measured (B). The percentage porosity is calculated by taking that ratio of pore surface area over total implant area. Scale bars in images A and B = 300 μm.

4.3 Results and Discussion

4.3.1. Dose Dependence Study

Previous dose estimates from the literature suggested that an effective adenosine dose would be in the range of about 200 ng per day (Huber *et al*., 2001; Boison *et al*., 1999). Silk implants were designed to administer varying doses (ranging from 40 ng/day to 1000 ng/day) to determine effective local dose and to test the hypothesis that different target release rates would suppress kindling epileptogenesis in a dose-dependent manner.

Cumulative release of adenosine from varied adenosine dose releasing silk implants is shown in Figure 4.6A. Over 14 days, the 40 ng/day target implants released 467.35 ng (average release rate = 33.38 ng per day), the 200 ng/day target implants released 2387.42 ng (average release rate = 170.53 ng per day) and the 1000 ng/day target implants released 11,465.48 ng (average release rate = 818.96 ng per day). Though average release rate is lower than the original

target, this *in vitro* release data confirms that implants designed to deliver varied doses are achieving varied daily adenosine release rates.

To test *in vivo* dose dependence, four groups of rats received infrahippocampal implants with target release rates of 0 ng (control, n= 5), 40 ng (n=5), 200 ng (n=6) and 1000 ng (n=6) adenosine per day. Four days after implantation, hippocampal kindling was initiated with each rat receiving a total of eight kindling sessions (each session consisting of six stimulations delivered every 30 minutes), with sessions 1–8 corresponding to days 4, 6, 8, 11, 13, 15, 18, and 20 following implantation.. Figure 4.6B shows the kindling curves (average seizure score versus stimulation number) of animals receiving the various dosage silk implants.

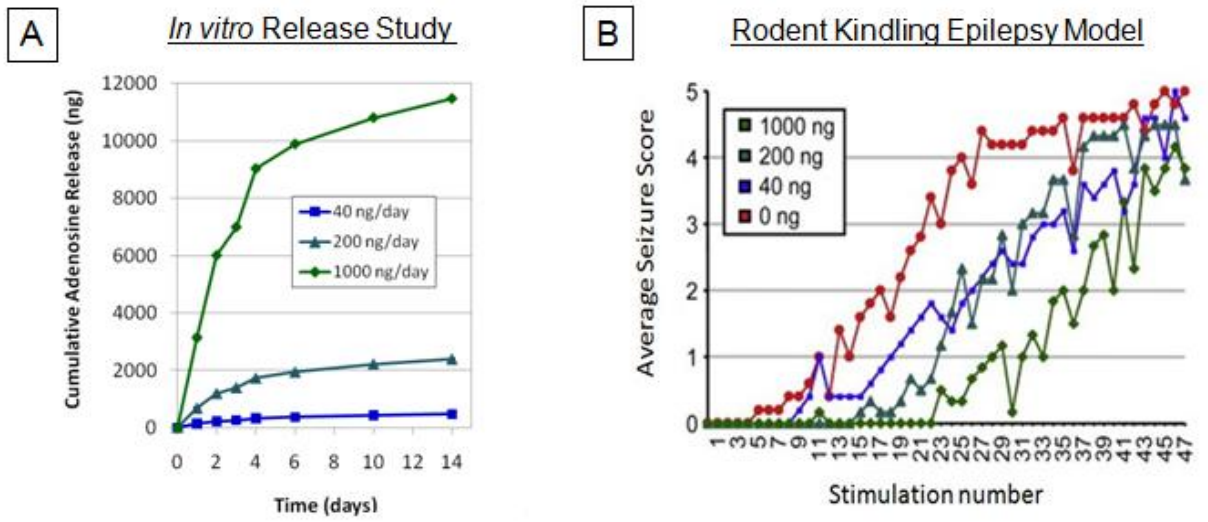

Figure 4.6. Varied adenosine dose releasing silk implants: *in vitro* release study and *in vivo* dose dependence study results (A) Cumulative release of adenosine from silk implants designed to release varied doses. N=3, error bars represent standard deviations, where error bars are not shown they fall into the background. (B) Retardation of kindling after infrahippocampal implantation of adenosine releasing polymers. Seizure stages averaged across the animals from each group for each individual stimulation. Kindling curves are shifted to the right with increasing doses of adenosine. Note that recipients of a target dose of 1000 ng adenosine per day are completely protected from any seizure during the first 23 stimulations.

Animals receiving empty control silk implants exhibit first partial seizures during session 2 (around stimulation 10), while first emergence of partial seizures was markedly delayed with

increasing doses of released adenosine. Recipients of a target dose of the highest dose (target dose = 1000 ng of adenosine per day) needed 2.5 times as many stimulations to reach the same kindling state as the control group (Figure 4.7)

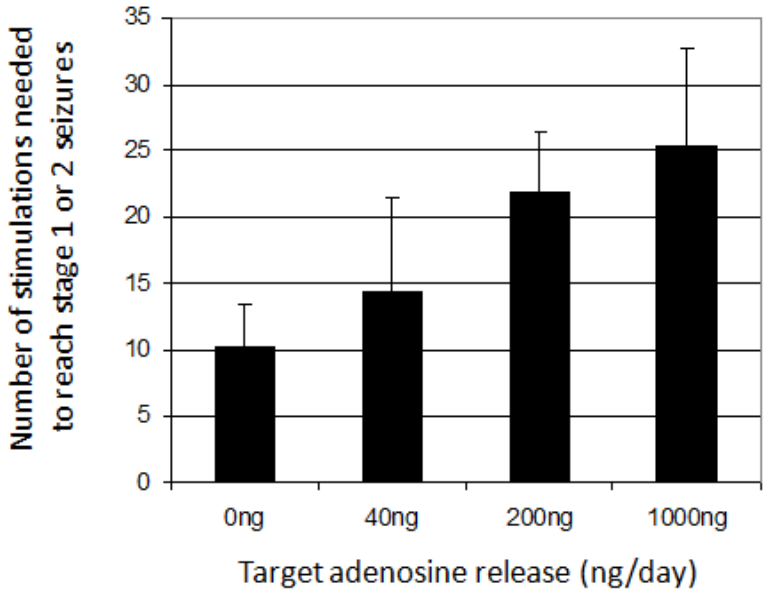

Figure 4.7. Number of kindling stimulations needed to elicit partial stage 1 or 2 seizures. Data were averaged from seizure score tables from the animals of Figure 4.7. Errors are given as ± SD.

4.3.2. Seizure Suppression

Based on the results of the dose-dependence study, the highest target dose (1000 ng/day) was selected for future study. Cumulative release from second generation silk implants designed to release 1000 ng/day is shown in Figure 4.8A. *In vitro* release (as daily release rate rather than cumulative release) is also represented in Figure 4.9A. *In vitro* release study results show that the second generation implants sustain release longer than previous implants and achieve release rates closer to the target (approx. 1000 ng/day from day 4 to day 10). Results of kindling experiments in rats receiving control and 1000 ng adenosine per day silk implants are shown in Figure 4.8B.

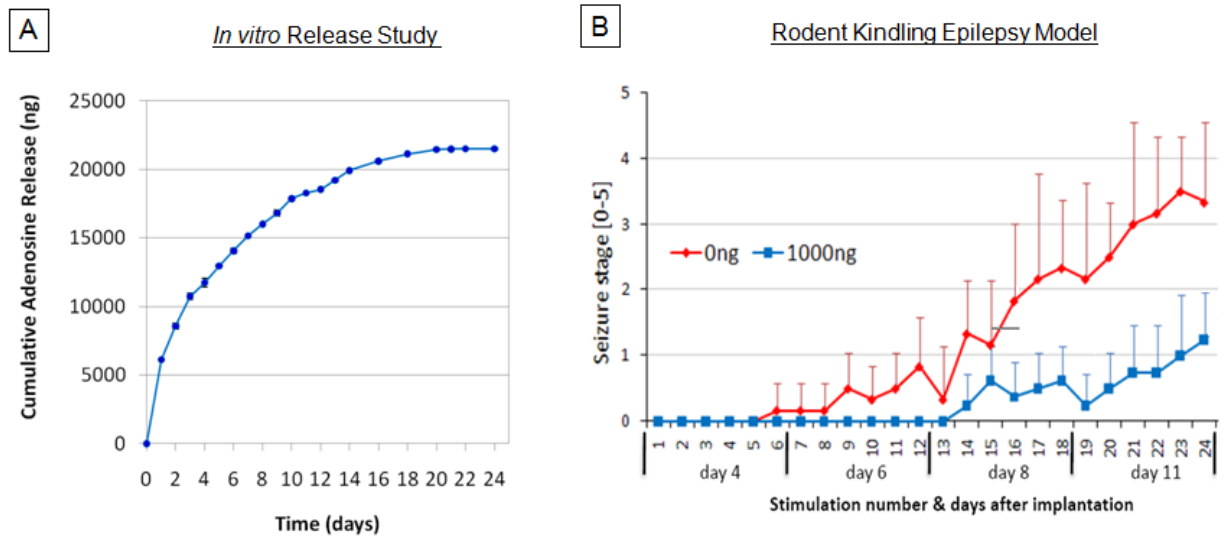

Figure 4.8. Adenosine releasing implants for seizure suppression *in vitro* and *in vivo* results (A) Cumulative release of adenosine from silk implants (B) Four days after infrahippocampal implantation of silk-based polymers with daily target release rates for adenosine of 0 ng (N=5, red), or 1000 ng (N=8, blue) kindling stimulations were delivered at a rate of 6 stimulations per day on days 4, 6, 8, and 11 following implantation. A total of 24 kindling stimulations were delivered. Seizure stages were averaged across animals from each group for each individual stimulus. Note that recipients of a target dose of 1000 ng adenosine per day display significant protection from kindling development. Errors are given as ±SD.

Animals receiving 1000 ng/day implants exhibit complete suppression of kindling development during the first 13 stimulations, and continue to display a suppression of seizures compared to control animals through the stimulation 24. Only at day 11, when *in vitro* results indicate implant-derived adenosine release drops off, does kindling development start to progress in animals receiving adenosine releasing implants. At stimulation 24 the averaged seizure response of the adenosine implant recipients was stage 1.25±0.7, while the averaged seizure response observed in the control group was stage 3.3±1.2, a statistically significant difference (two tailed t-test, df = 7, $p < 0.01$).

4.3.3. *In vivo* – Anti-epileptogenesis

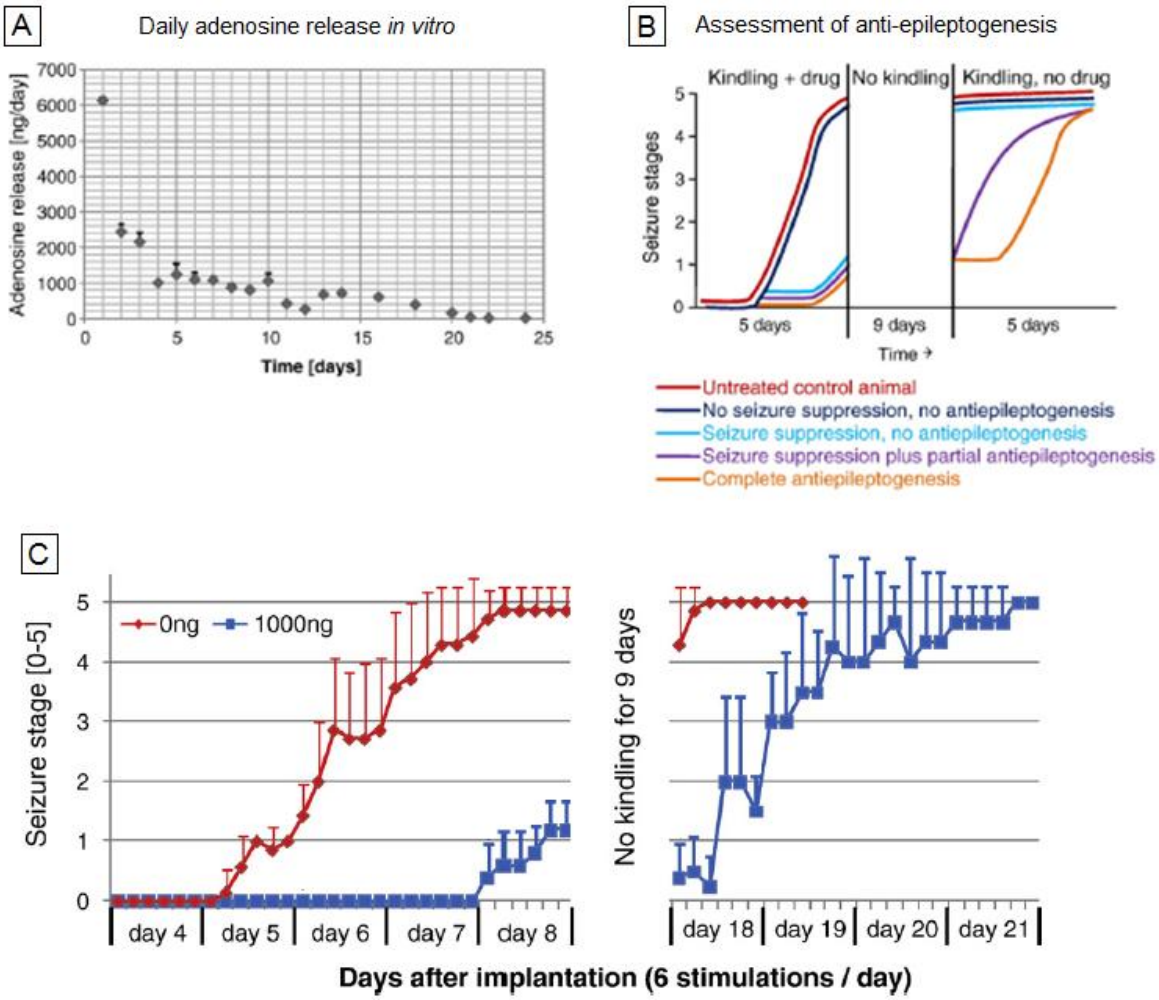

Figure 4.9. Anti-epileptogenesis study design and results (A) Daily release of adenosine from silk-based polymers. Adenosine release *in vitro* was determined for each day shown, based on averaged values from N=3 polymers. Note the stable release rate of around 1000 ng adenosine per day from day 4 to 10, corresponding to the pre-designed target release rate. Errors are given as ±SD. (B) Assessment of anti-epileptogenesis in the rat kindling model according to Silver *et al*., 1991: kindling is initiated during drug delivery followed by a washout period of the drug; subsequently, kindling is resumed in the absence of the drug. Five potential kindling outcomes are shown: red, normal kindling development of an untreated or sham-treated animal; dark blue, kindling in the presence of a drug with no effects on seizure expression and epileptogenesis; light blue, kindling development under the influence of a drug that suppresses seizures, but not epileptogenesis; violet, kindling development under the influence of a drug that exerts partial anti-epileptogenic effects; orange, kindling under the influence of a drug that completely suppresses epileptogenesis. Note that the criterion for complete suppression of epileptogenesis compared with partial epileptogenesis is a shift of the kindling curve to the right; the number of drug-free kindling stimulations needed to trigger a specific seizure stage should be the same as in control animals. (C) Four days after implantation of silk-based polymers with daily target release rates for adenosine of 0 ng (N=7, red), or 1000 ng (N=5, blue) kindling stimulations were delivered at a rate of 6 stimulations per day on days 4, 5, 6, 7, and 8 following implantation. A total of 30 kindling stimulations were delivered. After the 30th kindling stimulation, kindling was discontinued for 9 days to allow silk polymers to exhaust their adenosine release. Kindling stimulations were resumed at day 18. Seizure stages were averaged across animals from each group for each individual stimulus. Note that recipients of a target dose of 1000 ng

adenosine per day resumed kindling at day 18 at a level at which kindling was discontinued at day 8. After 7 consecutive stage 5 seizures kindling was discontinued in control animals due to animal welfare considerations. Errors are given as ±SD.

Consistent with the results shown in Figure 4.8B, animals receiving adenosine-releasing silk implants show robust suppression of seizures during the first 5 days of stimulation and exhibit protection from convulsive seizures through 30 stimulations (average seizure score = 1.3 ±0.5). Recipients of control silk implants that receive the same kindling stimulation exhibit an average seizure score of 4.9 ±0.4 at stimulation 30 (day 8 post implantation). After stimulation 30/day 8, kindling was discontinued 9 days to allow the silk implants to exhaust their adenosine release (Figure 4.9A) and resumed at day 18.When kindling was resumed at day 18, all control animals continued to display stage 4 and 5 seizures, while recipients of adenosine-releasing silk implants resumed at stages similar to the levels recorded prior to kindling discontinuation (average score of 0.5±0.6), then gradually increased in seizure severity until stage 4 and 5 seizures were reached at days 20 and 21 post implantation.

This kindling curve resembled the kindling curve of recipients of control implants, but the number of stimulations required to produce comparable seizure responses to animals receiving control implants is lower than in those control rats. This suggests that focal adenosine delivery exerts partial anti-epileptogenic effects (Silver *et al*., 1991). This is significant because currently available antiepileptic drugs are largely limited to seizure suppression (anti-ictogenesis), failing to prevent disease progression (anti-epileptogenesis) (Boison and Stewart, 2009). The traditional symptomatic treatment approach has little prospect to affect the underlying causes of the disease. The focal adenosine delivery from silk implants has potential not only for seizure suppression, but also for preventative use in patients with high risk of developing epilepsy. For example, following a traumatic brain injury, implantation of adenosine

releasing silk scaffolds into the traumatized brain area could improve therapeutic outcomes for these patients.

4.3.4. Histology

Figure 4.11 shows a crystal violet stain of rat brain sections 4 weeks post-implantation. Signs of degradation are visible based on some loss in structural integrity of the scaffolds (Figure 4.10 A and B). Some pores have been filled by invading cells (especially pores near the outer walls of the scaffold), while other pores remain unfilled (Fig. 4.10 C and D). Comparison of implant morphology before and after implantation allows additional assessment of scaffold degradation (Figure 4.11).

Prior to implantation, the average silk implant porosity based on surface area analysis was 41.07%, and this increased to 50.92% after implantation. The silk implants on average exhibited 9.85% more surface area after 4 weeks *in vivo*, suggesting that degradation was occuring in the rat brain. This rate of degradation is considerably slower than any of the *in vitro* sponge mass loss results reported in the literature (see Chapter 3, Table 3.1: Kim *et al*. report 70-80% mass loss after 22 days (Kim *et al*., 2005-1); Makaya *et al*. report ~88.6% mass loss after 4 days (Makaya *et al*., 2009); Wongpanit *et al*. report >80% mass loss after 17 days in 0.05 mg/mL proteinase type XIV(Wongpanit *et al*., 2010), etc.) This suggests that previous *in vitro* models represent more aggressive proteolytic degradation than actually occurs in the brain.

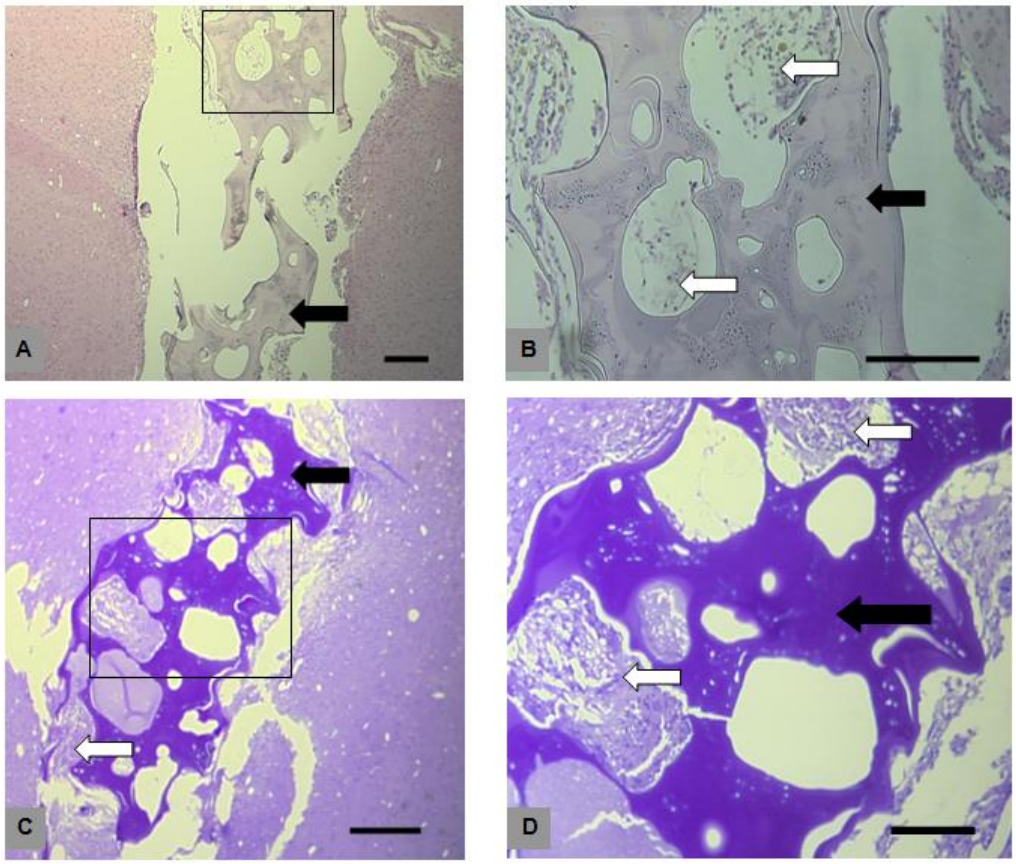

Figure 4.10. Morphologies of infrahippocampusly implanted aqueous-derived adenosine-loaded silk fibroin implants after 4 weeks. Images A and B are for implants in the brain of Rat #8 and H&E stained. Images C and D are for implants in the brain of Rat #27 and stained with crystal violet. Images B and D are enlarged views of images A and C, respectively. Scale bars in images A, B and C = 300 μm and in image D = 150 μm. Solid arrows = remaining scaffold. Blank arrows = cell ingrowth.

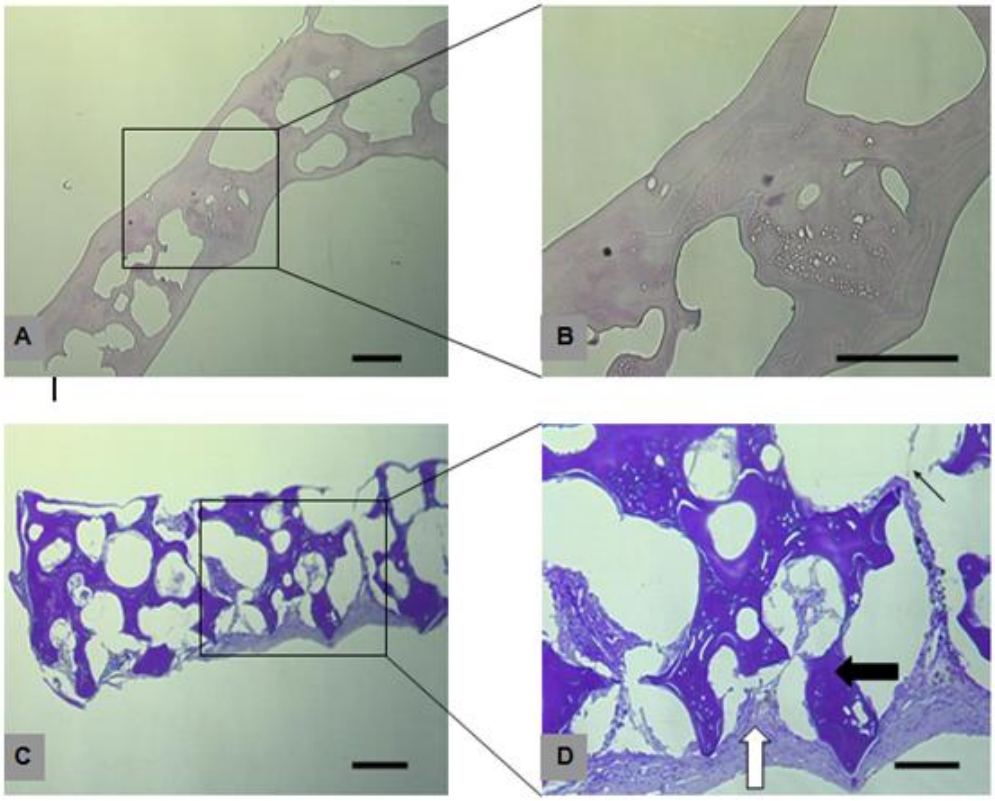

Figure 4.11. Morphologies of aqueous-derived adenosine-loaded silk fibroin implants before and after infrahippocampal implantation. Images A and B are H&E stained. Images C and D are for explants from Rat #28 and stained with crystal violet. Images B and D are enlarged views of images A and C, respectively. Scale bars in images A, B and C = 300 μm and in image D = 150 μm. Solid arrows = remaining scaffold. Blank arrows = cell ingrowth

The degradation of the scaffolds demonstrated here suggests the presence of silk-degrading proteases in rat brain. For example, chymotrypsin has been shown to degrade silk (Li *et al*., 2003) and a number of chymotrypsin-like proteases have been identified in rat brain. For example, caldecrin (α chymotrypsin-like protease) was demonstrated to be highly expressed within the hippocampus of adult rat brain (Tomomura *et al.,* 2002). Further investigation will be needed to assess the specific proteases involved in the process and modes to regulate the degradation lifetime of this type of implant. The biodegradability of silk-based polymeric implants demonstrated here constitutes a major advantage for the preventive use of this type of brain implants.

Conclusions

These studies demonstrate that silk systems can deliver therapeutically relevant drug loads *in vivo*. Polymers prepared in different doses were shown to induce dose-dependent retardation of seizure acquisition, validating the therapeutic potential of implants and the ability to control dosing. Adenosine-releasing silk implants were found not only to suppress seizures in a rat kindling model of epilepsy, but were also found to induce partial anti-epileptogenesis. Histological analysis showed ingrowth of local tissue and degradation of the scaffolds after 4 weeks *in vivo*. These studies have also demonstrated excellent agreement between *in vitro* release study predictions and *in vivo* response. Taken together, these results confirm the safety and efficacy of silk drug delivery implants for local delivery of neurological drugs, and suggest that these degradable, implantable biomaterial systems could potentially be applied to a range of therapeutics.

5. Silk biomaterials for antibiotic delivery and stabilization

5.1 Introduction

Antibiotics (defined as chemicals that act on specific targets to kill or limit the growth of micro-organisms) are an essential component of the treatment of infection (Englander and Friedman, 2010). Conventional systemic antibiotic delivery for both prevention and curing suffers from the drawbacks of tissue toxicity associated with renal and liver complications and poor penetration into ischemic and necrotic tissue (typical of post-traumatic and postoperative tissue) and the necessity of hospitalization to monitor drug levels and effects (Price *et al*., 1996; Ruszczak *et al*., 2003).

A simple system is therefore needed for antibiotic delivery that restricts delivery to a specific target site to minimize side-effects and maximize efficacy of dose. Ideally, the system must also degrade *in vivo* to avoid surgical retrieval and be easily built into existing treatments. As such, many systems based on degradable polymers have been explored for antibiotic delivery, including synthetic biodegradable polymers like poly-(lactide-co-glycolide), polycaprolactone and polyanhydrides and natural polymers like collagen and chitosan, though these systems suffer from the drawbacks described in previous chapters (harsh processing conditions, poor biocompatibility or material properties, etc.) (Zilberman and Elsner, 2008).

Antibiotic-loaded silk biomaterials injected or applied directly to wound sites would deliver antibiotics locally, thereby achieving therapeutic efficacy while avoiding the side-effects of large systemic doses of antibiotics. Unlike gauze, silk degrades naturally over time, so surgical removal would be unnecessary. In addition, maximizing antibiotic dose efficacy could also potentially slow development of antibiotic resistance, the rapid emergence of which is often

attributed to widespread overuse of systemic and topical antibiotics (Englander and Friedman, 2010; White *et al*., 2006).

Several potential applications that are especially attractive for silk-based implantable, controlled-release antibiotic delivery have been identified, including tuberculosis, biofilms, implant infections, osteomyletis and abscesses:

- Tuberculosis: In 1993, it was estimated that one-third of the world population was infected with *Mycobacterium tuberculosis* (Quenelle *et al.*, 2001). Treatment of tuberculosis requires continuous and repeated administration of large drug doses over long periods. Traditional treatment also has the disadvantages of contributing to microbial drug resistance and inducing toxic side-effects (Bartybekov *et al*., 1997). Controlled release delivery could potentially alleviate these problems by achieving localized delivery of antimycobacterial drugs and allowing programmed controlled release over a prolonged period (enhancing the efficacy of drugs that target actively multiplying mycobacteria) (Quenelle *et al*., 2001).
- Biofilms: Biofilms form when a collection of micro-organisms attached to a surface secrete an extracellular polymer matrix that prevents antibiotic diffusion. The composition of the biofilm matrix is highly variable (containing various proteins, polymers, complex carbohydrates and water) (Kennedy *et al*., 2010). The function of the biofilm is unknown, but bacteria encased in this extracellular biofilm matrix become highly resistant to antibiotics: the mimimum inhibitory concentration can increase 100- to 1000- fold for biofilm-embedded organisms compared to their planktonic free-floating counterparts (Aslam and Darouiche, 2009).
- Implant infections: The incidence of orthopedic implant related infection is 1.5% - 2.5% for primary hip or knee replacements and 3.2%- 5.6% for revision surgeries. The cost of treating

such an infection is estimated at more than $50,000 per episode (Aslam and Darouiche, 2009). The annual infection rate for cardiovascular implants is even higher: 7.4% (Hetrick and Schoenfisch, 2006). Implant infections often form biofilms, making systemic antibiotic delivery ineffective for the reasons described above. Therefore treatment frequently includes implant removal and/or amputation, which is both difficult and costly (direct medical costs associated with implant infections are estimated to exceed $3 billion annually in the U.S. alone (Hetrick and Schoenfisch, 2006)). The number of device-associated infections is expected to continue to rise as more patients receive biomedical implants, meaning the threat posed by implant-associated infections will affect a larger percentage of the populace (Hetrick and Schoenfisch, 2006). The serious medical complications of implant infections and the expense and difficulty in treating them have prompted considerable interest in exploring innovative preventative approaches, including antibiotic-eluting polymer coatings on implants (Daroiche and Mansouri, 2004). In addition to adding antibiotic-eluting silk coatings to implants to prevent infection, antibiotic-releasing silk biomaterials could be applied at the site of implant removal to aid in wound healing.

- Osteomyeletis: Treatment of osteomyelitis (bone infection) remains a challenge; even with aggressive systemic antibiotic therapy there are still significant relapse rates. To address this need, local delivery of antibiotics capable of achieving high drug concentrations at the infection site without inducing side effects has been investigated (Nandi *et al*., 2009). Nondegradable polymethylmathacrylate (PMMA) beads containing gentamicin have been approved for treatment of osteomyletits in Europe, but despite their efficacy these beads suffer from the major drawback of requiring subsequent removal. Biodegradable implants can provide high local antibiotic concentration for the prolonged time needed to eradicate

infection and (depending on the implant material properties) can be used as filler/support materials to guide tissue repair where infection requires bone removal. Though widespread research is currently being conducted in the area of local drug delivery systems to treat osteomyelitis, much work is still desired in the areas of biodegradable and biocompatible materials and the kinetics of antibiotic release (Nandi *et al*., 2009).

- Abscesses: Abscesses form when the tissue surrounding an infection site forms a dense capsule to isolate the infection from healthy tissue. Penetration of antibiotics into abscesses is limited by both the lack of vascularity and the dense biofilm-like capsule wall (Sauermann *et al*., 2005; Gerding *et al*.,1980; Han *et al*., 2009). Studies have shown that poor drug penetration (rather than inactivation or binding) is responsible for low levels of antibiotic within abscesses (Gerding *et al*., 1980). The difficulty of successfully treating abscesses with systemic antibiotic therapy is further compounded by high inter-individual variability in abscess permeability and the high variety of pathogens found in abscess fluid (Sauerman *et al*., 2005). Sauermann *et al.* report that the gradient from C_p (concentration in the plasma) to C_a (concentration in the pus within the abscess) is the driving force and only factor that can be influenced in increasing drug transport into the abscess. They therefore suggest that to overcome the abscess penetration barrier, high plasma levels be administered (Sauermann *et al.*, 2005. Note that successful treatment of brain abscesses must overcome not only all of these limitations, but also the added difficulty of penetrating the blood brain barrier (Brook, 1995; Raza *et al*., 2005). Because systemic antibiotic treatment alone is insufficient for treating abscesses, incision and drainage is the primary therapy for abscess management (Fitch *et al*., 2007; Stearne *et al*., 2002). Following drainage, cutaneous abscesses are packed with a non-degradable filler material to prevent wound collapse (Figure 5.1). This filler

material must eventually be retrieved and contains no antibiotics to aid in the healing process (Fitch *et al*., 2007). Packing and removal of the filler-material is a painful process that may need to be repeated multiple times until the infection resolves (O'Malley *et al.*, 2009).

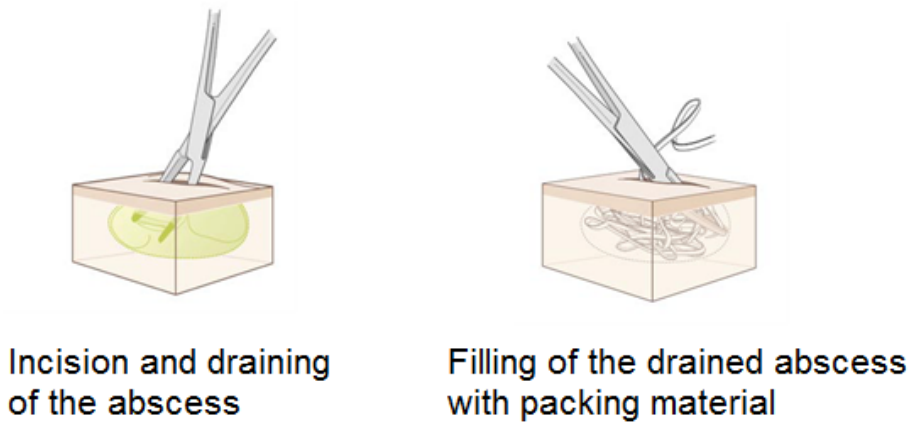

Figure 5.1. Schematic representation of traditional abscess treatment. Infected abscesses are drained, then filled with non-degradable packing materials (adapted from Fitch *et al*., 2007)

This broad range of applications suggests that characterizing a wide array of material formats and delivery strategies would be advantageous. For example, implants are particularly susceptible to infection during what is termed the 6 hour post-implantation "decisive period;" an ideal implant coating must rapidly release high levels of prophylactic antibiotics initially to combat the initial bacterial shock, followed by sustained release at a lower concentration to prevent latent infection (Zilberman and Elsner, 2008). For tuberculosis, release duration must persist at constant levels for months. The safety and efficacy of various antibiotic delivering devices is strongly dependent on achieving tight control over the rate and manner in which the drug is released. Because describing an "ideal release profile" for the various applications of antibiotic-eluting devices is impossible, having a system that is tunable for each application is paramount.

The objective of these studies is therefore to demonstrate loading and release of various antibiotics from a range of silk biomaterials, based on bacterial clearance of *Escherichia coli* ATCC 25922 and *Staphylococcus aureus* ATCC 25923, prevalent pathogens isolated from surgical site infections.

Model antibiotics tested include cefazolin, gentamicin, penicillin, ampicillin, rifampicin, erythromycin and tetracycline. Silk material formats tested include bulk loaded silk films, 3D porous sponges (loaded via nanofilm coatings and methanol-assisted adsorption), bulk and microsphere loaded hydrogels and degummed silk fibers.

Antibiotics were also considered a good model for testing controlled release of drugs with low water solubility. Many drugs are difficult to administer systemically due to their low water solubility. However, once loaded into polymer delivery systems the low water-solubility of these drugs can be used to limit daily release rate, thereby sustaining release. To impregnate silk biomaterials with drugs that possess low water solubility and high alcohol solubility, a high-concentration drug solution is prepared in methanol, and then the silk biomaterial for loading is immersed in the drug-saturated methanol. During the methanol soaking, drug is able to diffuse into the silk matrix and crosslinks the silk carrier as previously described. Once the drug loaded biomaterial is immersed in an aqueous solution, the adsorbed drug is "trapped" in the silk and diffusion out of the silk is limited by the drug's solubility in water. As a result, slow, sustained, zero-order release is achieved. To test hydrophobic drug loading and delivery from silk biomaterials, rifampicin and erythromycin (antibiotics with high methanol solubility and low water solubility) were chosen for study.

Another serious problem for many therapeutics, including antibiotics, is stabilization. Dating back to Fleming's original 1929 paper on penicillin (Fleming, 1929), the literature reports

that penicillin is unstable in solution, breaking down within weeks at room temperature (25^{o}C) and within 24 hours at 37^{o}C (Benedict *et al*. 1945). Breakdown of penicillin at body temperature represents a serious problem for any implantable delivery system designed to release over a time period longer than 24 hours.

The tetracycline class of antibiotics has been a mainstay in the treatment of bacterial infections due to its broad spectrum of antimicrobial activity and relatively low cost. Tetracycline is also widely used for agricultural applications, including treatment of bacterial infections of plants, in aquaculture, and in animal growth (Yang *et al*., 2004). Despite its broad clinical and agricultural utility, tetracycline suffers from severe instability as it is susceptible to multiple degradation pathways (Xuan *et al*., 2010). Sigma recommends tetracycline be stored at -20^{o}C and protected from light, as it is highly susceptible to photo-degradation. Tetracycline solutions will also become turbid on standing due to hydrolysis and precipitation of the degradation product.

Instability of antibiotics at temperatures $\geq$ 25^{o}C represents a problem in transporting and storing antibiotics (particularly in third world countries where refrigeration is limited). Numerous studies have demonstrated that immobilization in silk films via bulk loading exerts a stabilizing effect on encapsulated proteins. To determine if incorporation into silk films would have a similar stabilizing effect on light and temperature sensitive antibiotics, stability studies were carried out comparing the residual activity of penicillin and tetracycline stored in 8% (w/v) silk films and various other storage formats stored at various temperatures.

5.2 Materials and Methods

5.2.1 Materials

The bacteria strains used were *Escherichia coli* ATCC 25922 and *Staphylococcus aureus* ATCC 25923 (American Type Culture Collection, Manassas, VA). Antibiotics (penicillin G sodium salt, ampicillin sodium salt, cefazolin, gentamicin, rifampicin, erythromycin and tetracycline) were purchased from Sigma Aldrich (St. Louis, MO). Bacterial culture dishes, BD brand Luria-Bertani broth, Miller (formula per liter = 10 g tryptone, 5 g yeast extract, 10 g sodium chloride, 15 g agar), BD brand Luria-Bertani agar, Miller (formula per liter = 10 g tryptone, 5 g yeast extract, 10 g sodium chloride) were purchased from Fisher Scientific.

5.2.2. Silk film fabrication

Silk fibroin solution was prepared from *Bombyx mori* cocoons as previously described. Bulk loaded antibiotic impregnated silk films were prepared as previously described. Briefly, drug solution was mixed with silk solution to a final silk concentration of 6% (w/v), this mixture was aliquoted into Teflon lined molds (200 µL per film) and dried overnight at ambient conditions. Two loading concentrations were studied: for ampicillin-loaded films concentrations tested were 2 mg/mL, approx. 0.4 mg per film (designated “high loading”) and 1 mg/mL, approx. 0.2 mg per film (designated “low loading”), for penicillin concentrations tested were 4 mg/mL, approx. 0.8 mg per film (designated “high loading”) and 2 mg/mL, approx. 0.4 mg per film (designated “low loading”). To assess the effects of methanol on incorporated antibiotics, films were either treated with methanol for 5 minutes or left untreated.

To determine the minimum inhibitory penicillin loading concentration in silk films, penicillin was suspended in distilled water and was mixed to a final concentration of 8% (w/v) silk solution in penicillin concentrations ranging from 100 mg/mL down to 0.013 mg/mL. 200

µL of silk + penicillin solution were aliquoted into each well of a 48 well plate, dried overnight at ambient conditions, methanol treated for 5 minutes and dried again.

5.2.3. Microsphere fabrication

Microspheres were prepared according to the phospholipid template protocol previously described (Wang *et al*., 2007-3). Briefly, 200 mg of 1,2-dioleoyl-sn-glycero-3-phosphocholine (DOPC) phospholipid was dissolved in 1 mL of chloroform, then dried under N_2 to a film on the interior of a glass test tube. 2 mL of drug solution in 8% (w/v) silk containing 100 mg/mL penicillin or ampicillin were added to hydrate the phospholipid film, which forms microspheres upon exposure to the aqueous solution. Microspheres prepared with 8% silk with no drug added served as controls. The suspension of microspheres was repeatedly freeze-thawed, diluted in 100 mg/mL antibiotic solution in distilled water, then lyophilized. Once lyophilized, the material was treated with methanol containing 100 mg/mL antibiotic for 30 minutes to remove the lipids and induce β-sheet physical crosslinks to stabilize the structure. Methanol and microspheres were separated by centrifugation at 10,000 rpm for 5 min at 4^{o}C. The pellet was dried overnight at ambient conditions. Prior to hydrogel loading, the microsphere pellet was resuspended in the desired buffer and any clustered microspheres are dispersed by brief ultrasonication (5-10 seconds at 20% amplitude) using a Branson 450 ultrasonicator (Branson Ultrasonics Co., Danbury, CN). Antibiotic loading in the microspheres was determined by degrading a sample of microspheres overnight in a 1.0 mg/mL proteinase K solution at 37^{o}C and assayed using the zone of inhibition lawn clearance technique.

5.2.4. Fabrication and nanofilm coating of porous 3D silk sponges

Water-based porous scaffolds were prepared as previously described (Kim *et al*., 2005-1) using the mixture of microspheres and silk solution to imbed the microspheres in the final porous scaffold. Briefly, 4 g of 500–600 mm granular NaCl were added to 2 mL of 6% (w/v) silk solution mixed with microspheres in a plastic container and incubated at room temperature for over 24 h. The scaffolds were then washed for 24 h to leach out the sodium chloride. Scaffolds were punched out with an 8 mm Miltex biopsy punch and then trimmed with a scalpel on either end. Prior to coating, the average mass of silk scaffolds was 25.08 +/- 3.38 mg for the gentamicin coated scaffolds and 24.98 +/- 4.77 mg for cefazolin coated scaffolds.

Nanofilm coatings were applied using the previously described protocol (Wang *et al*., 2007-1), modified to accommodate the coating of a 3D porous scaffold. Scaffolds were first dipped in a 1 mg/mL antibiotic solution for 3 minutes, then dried at 37^{o}C for 30 min. Next, scaffolds were dipped in a diluted 0.2% (w/v) silk fibroin solution for 3 min, then dried at 37^{o}C for 30 min, rinsed in 90:10 (v/v) MeOH/water solution for 1 min and dried again. This process was repeated twice, for a total of three antibiotic layers. For the final silk layer, 4% (w/v) silk solution was used to provide a thicker capping layer.

5.2.5. Hydrogel fabrication

Silk hydrogels were prepared using sonication-induced gelation as previously described. Bulk loaded gels were prepared by sonicating silk solution of the desired concentration (either 4% (w/v) or 8% (w/v)) using a Branson Digital Sonifier 450 at 15% amplitude for 60-90 seconds, then mixing in antibiotic solution, then waiting for gelation to occur, entrapping the drug. Final antibiotic loading in the gels was 3 mg per gel. Microspheres were prepared according to the previously described lipid-template protocol. As with the bulk loading, silk was

sonicated and mixed with a microsphere suspension just prior to gelation. Final microsphere loading in the gels was 6 mg of microspheres per gel (3 mg of antibiotic per gel).

5.2.6. Methanol-assisted adsorption loading of silk biomaterials with poorly water soluble antibiotics

Silk films were prepared by casting 100 µL of 8% (w/v) silk into 5 mm diameter Teflon coated mold, dried overnight at ambient conditions, then demolded without methanol treatment. Degummed fibers were prepared by boiling *B. mori* cocoons for 60 minutes in a solution of 0.02 M Na_2CO_3, then rinsing (four rinses, 20 min each, in distilled water). The degummed rinsed silk was dried overnight at ambient conditions. Aqueous-derived silk fibroin sponges were prepared as described by Sofia *et al*. (2001). Briefly, 4 g of granular NaCl (particle size 660-710 microns) was added slowly to 2 mL of 8% (w/v) silk fibroin solution in cylindrical Teflon container. The containers were covered and left at room temperature for 24 hours, then immersed in water to leech the NaCl for approx. 48 hours. Scaffolds were punched out with a 6 mm biopsy punch and cut to 4 mm height.

To load biomaterials with antibiotics, dried samples were immersed in methanol solutions of the desired drug concentration (5, 50 and 500 mg/mL for erythromycin; 20 mg/mL rifampicin) 24 hours. Control samples were prepared by immersing in methanol for 24 hours.

5.2.7. Storage stability testing

For long term stability studies, tetracycline and penicillin loaded silk films were prepared as previously described. Briefly, drug solution was mixed with silk solution to a final silk concentration of 6% (w/v), this mixture was aliquoted (250 µL per film) into Teflon lined molds and dried films overnight at ambient conditions. Penicillin concentrations tested were 50 mg/mL

(for the 4°C, 25°C and 37°C study) and 25 mg/mL (for the 60°C study), for a final film loading of 12.5 mg and 6.25 mg per film, respectively. Tetracycline concentration used was 15 mg/mL for a final loading of 3.75 mg per film. Relatively high film loadings were selected for longterm storage studies to maximize the duration of detectable drug levels (i.e., if 10% of the stored drug was active after a certain storage duration, total initial loading would have to be at least 10 times the detection limit for that amount of drug to register when assayed). However, preliminary studies suggest that lower drug loadings may enhance storage stability compared with higher initial drug loadings (data not shown). Initial loading was decreased for the 60°C penicillin and then futher decreased for the tetracycline studies due to the observation that high percentages of drug activity were retained for long storage durations in silk films.

Tetracycline films and penicillin films for the 60°C study were untreated after drying, while penicillin films for the 4°C, 25°C and 37°C study were treated with 90%/10% methanol/H_2O for 5 minutes. Treatment conditions were changed between studies due to the observation in small scale scoping experiments that untreated films exhibited a greater stabilizing effect than methanol-treated silk films (additional work to optimize stabilizing conditions is still needed).

For comparison of different storage conditions, 1 mL aliquots of equivalent concentration were prepared in sterile ultrapure water and stored in 1.5 mL Eppendorf tubes. Dry powder aliquots were also measured out and stored in 1.5 mL Eppendorf tubes and dissolved in sterile ultrapure water just prior to testing. For penicillin storage, collagen films were prepared by dissolving Avitene® Microfibrillar Collagen Flour (Bard Davol, Warwick, RI) in sterile ultrapure water in a weight/volume concentration equal to the silk solution used for film preparation, then mixing with antibiotic solution and casting films as described.

Storage temperatures tested were 4°C (refrigeration), 25°C (room temperature), 37°C (body temperature) and 60°C. For tetracycline studies, all samples were wrapped in foil to protect from light exposure, except a group of 25°C (room temperature) storage samples were stored unwrapped and exposed to ambient light.

5.2.8. Bacteria culture

LB Broth was prepared according to manufacturer's instructions (25 grams/L). LB Agar was prepared according to manufacturer's instructions (40 grams/L) and aliquoted into 100 mm diameter Fisherbrand cell culture plates (15-20 mL per plate).

Lyophilized bacteria cultures were reconstituted and expanded according to manufacturer instructions. To test susceptibility, liquid cultures were grown for 18-24 hours to an optical density (OD_{600}) between 0.8 and 1 (corresponding to a viable count of approx. 10^8-10^9 CFU/mL (Chadfield *et al.*, 2005)). These cultures are referred to hereafter as overnight cultures.

To test the effect of the varied concentration penicillin and ampicillin silk film coated 48 well plate, 400 µL of overnight *S. aureus* or *E. coli* culture diluted 1 in 100 in LB broth were added to each well. The cultures were grown at 37°C for 48 hours, and then the optical density at 600 nm was measured for each sample with a UV spectrophotometer to estimate bacterial growth.

5.2.9. Susceptibility testing

Active antibiotic release was quantified using a direct zone of inhibition assay. This assay (based on the principle of the Kirby-Bauer Susceptibility Test (Bauer *et al*., 1959; Boyle *et al*.,1973)) determines active antibiotic present by comparing zones of clearance in bacterial

lawns with the lawns generated by standards of known concentration. Samples (either silk films directly or sterile filter paper disks soaked with known volumes of a standard solution or experimental solution of unknown concentration) are applied directly to agar plates coated with a mixture of dilute agar (20 g/L) and *S. aureus* overnight culture (5:1 volume:volume ratio), which grows to lawns overnight at 37°C. After 24 hours zone of inhibiton was measured using Image J image analysis software (Figure 5.2). Amount of drug released over 24 hours is then determined by comparison of sample zones of inhibition to the zones of inhibition of known standards on filter paper disks. Extended release studies were carried out by transferring test materials to new plates every 24 hours.

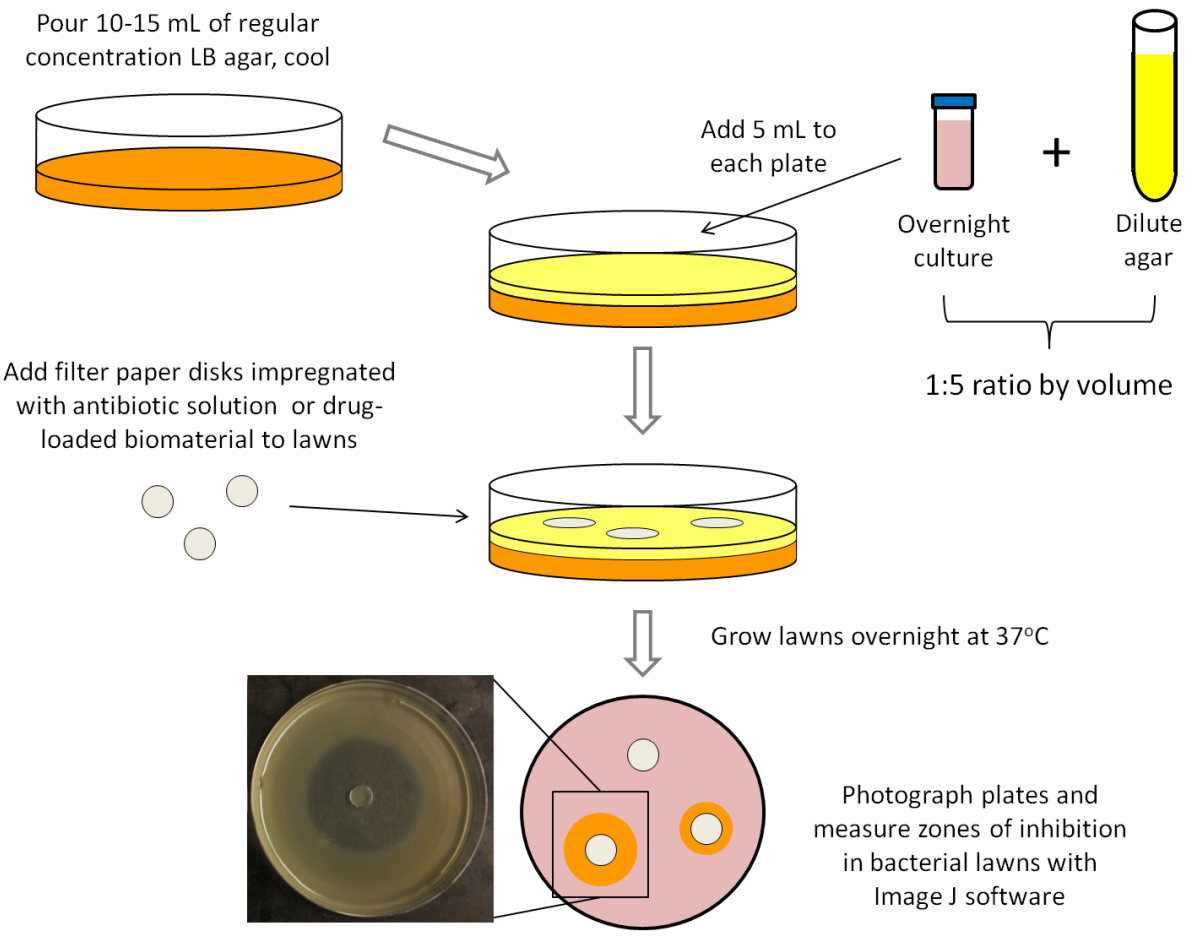

Figure 5.2. Schematic of the zone of inhibition assay protocol for determining antibiotic activity.

5.3. Results and Discussion

5.3.1. Short-term release of penicillin and ampicillin from silk films

While longer term release profiles were studied for many of the material formats studies, only the first 24 hours of penicillin and ampicillin release from silk films were characterized due to the literature reporting a 6-h post-implantation "decisive period" during which implants are particularly susceptible to surface bacterial colonialization (Zilberman and Elsner, 2008). The first 24 hours of release from silk films were therefore considered most critical in prevention of bacterial adhesion and long-term implant success.

Two loading concentrations were studied: 0.4 mg/film and 0.2 mg/film for amipicillin loaded films and 0.8 mg/film and 0.4 mg/film for penicillin loaded films. To assess the effects of methanol on incorporated antibiotics, films were either treated with methanol for 5 minutes or left untreated. Results of ampicillin and penicillin release from silk films are reported in Tables 5.1 and 5.2, respectively. Fraction of total load released in 24 hours is shown in Figure 5.3

Table 5.1. Ampicillin Film Release:

	High Loading/ Methanol treated	High Loading/ Untreated	Low Loading/ Methanol treated	Low Loading/ Untreated
Average active ampicillin Release (in µg)	213.84 ± 50.52	176.14 ± 45.49	68.47 ± 9.25	68.33 ± 22.96
Fraction of total theoretical film load released in the first 24 hours	0.53	0.44	0.34	0.34

High loading = 2 mg/mL ampicillin in a 6% (w/v) silk solution (theoretical load = 0.4 mg per film)
Low loading = 1 mg/mL ampicillin in a 6% (w/v) silk solution (theoretical load = 0.2 mg per film)

Table 5.2. Penicillin Film Release:

	High Loading/ Methanol treated	High Loading/ Untreated	Low Loading/ Methanol treated	Low Loading/ Untreated
Average active penicillin Release (in µg)	345.87 ± 140.94	167.08 ± 24.82	193.98 ± 5.03	205.88 ± 22.58
Fraction of total theoretical film load released in the first 24 hours	0.43	0.21	0.48	0.51

High loading = 4 mg/mL penicillin in a 6% (w/v) silk solution (theoretical load = 0.8 mg per film)
Low loading = 1 mg/mL penicillin in a 6% (w/v) silk solution (theoretical load = 0.4 mg per film)

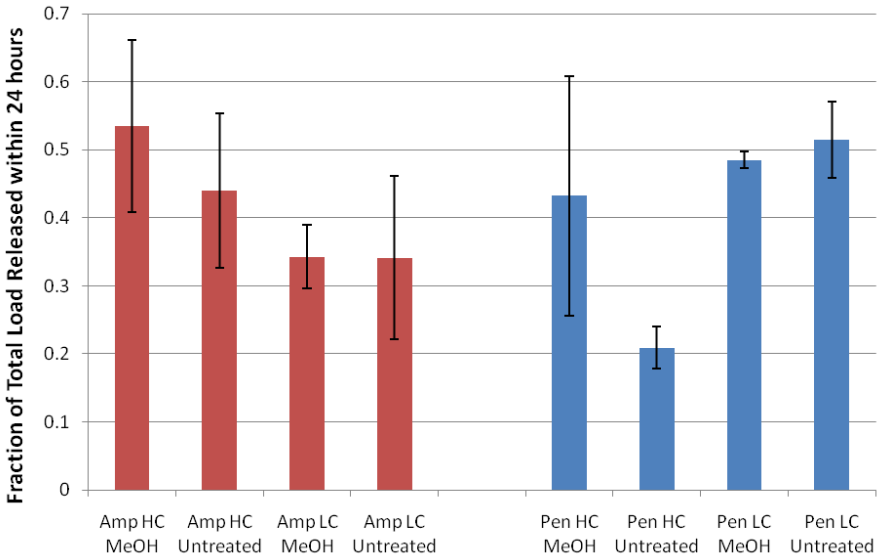

Figure 5.3. Fraction of total antibiotic release from silk films prepared with various loadings and post-drying treatments. HC= high concentration (10 mg/mL, 0.8 mg per film). N=3, error bars represent standard deviations.

These results suggest that methanol treatment does not degrade the incorporated antibiotic, as no reduction in activity is seen in the methanol treated films compared to the untreated films. The results also show that films deliver approximately half of their initial load within the first 24 hours of bacterial exposure. The fraction of the total load recovered is lower in untreated high loading films than in methanol treated films, possibly because some drug is lost when the film is resolubilized on the agar law (as opposed to eluting slowly from methanol

treated films). Films with lower loading do not exhibit any difference in recovery from methanol treated versus untreated silk films, so this may only be a problem for higher loading values.

Optical density measurements for liquid cultures of *S. aureus* and *E. coli* grown in wells coated with silk films prepared with varying penicillin concentrations are shown in Figure 5.4

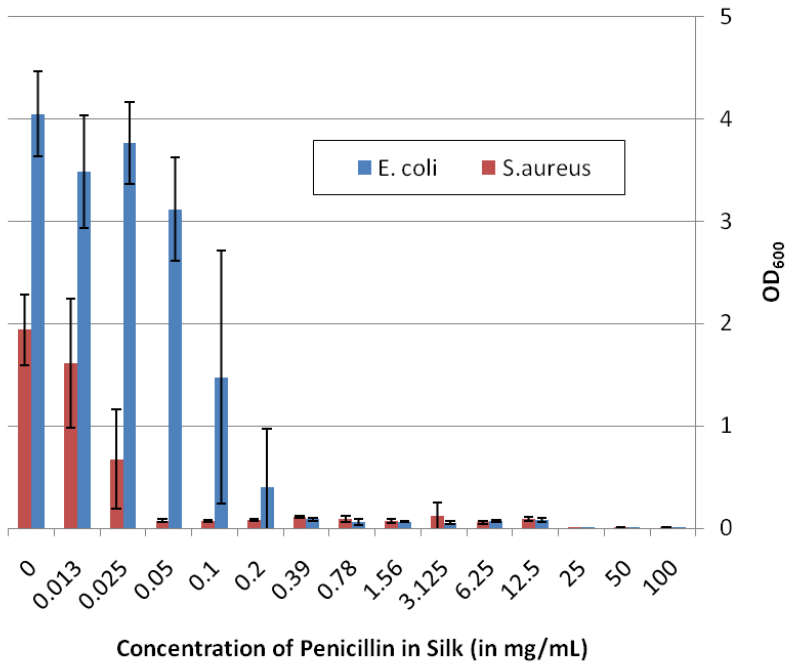

Figure 5.4. Optical density of *S. aureus* and *E. coli* liquid cultures at 600 nm (OD_{600}) relative to the concentration of penicillin used in the preparation of antibiotic silk films after 24 hours incubation at 37°C

For both bacteria tested, total inhibition was seen in films prepared with 25, 50, or 100 mg or penicillin per mL of silk (5, 10 and 20 mg of penicillin per film respectively). 0.39 mg/mL and 0.05 mg/mL were the minimum concentrations required to induce near total inhibition in *E. coli* and *S. aureus*, respectively. These results suggest that, prepared in sufficient drug concentrations, these films can be used to prevent infection and totally suppress bacterial growth.

5.3.2. Nanofilm Coatings of Gentamicin and Cefazolin on Porous Silk Scaffolds

Layer-by-layer nanofilm coating was studied as a potential loading strategy for water-soluble antibiotics and porous three-dimensional substrates. Cefazolin levels were too low to be detected on *E.coli* plates after the first 24 hours, so only cefazolin release data determined on *S. aureus* plates is shown. Gentamicin release data is shown based on both *S. aureus* and *E. coli* inhibition. Release duration was 5 days for gentamicin loaded sponges and 4 days for cefazolin loaded sponges. Data for cumulative gentamicin release is reported in the table inset of Figure 5.5 and shown in Figure 5.5; cumulative cefazolin release is reported in the table inset of Figure 5.6 and shown in Figure 5.6.

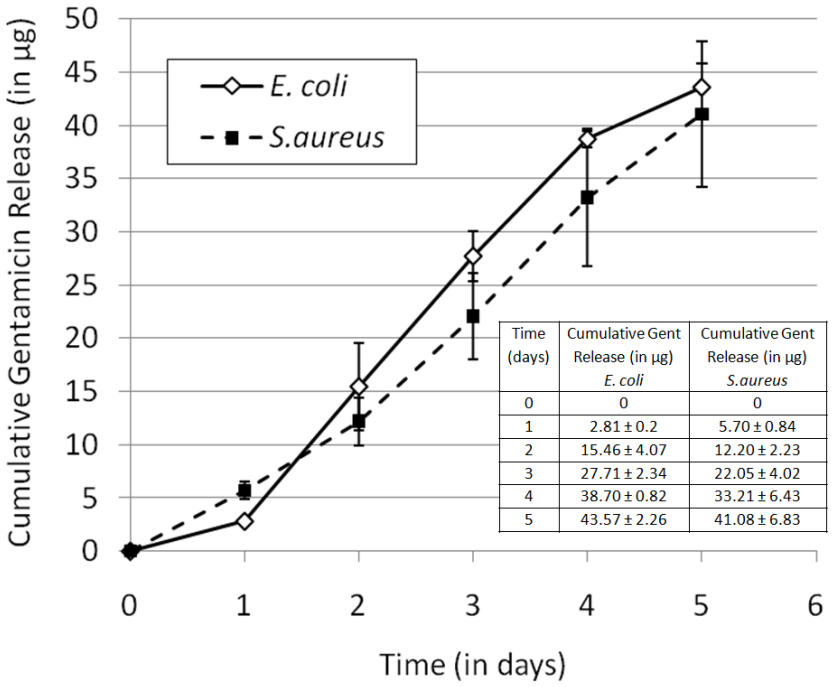

Time (days)	Cumulative Gent Release (in µg) *E. coli*	Cumulative Gent Release (in µg) *S.aureus*
0	0	0
1	2.81 ± 0.2	5.70 ± 0.84
2	15.46 ± 4.07	12.20 ± 2.23
3	27.71 ± 2.34	22.05 ± 4.02
4	38.70 ± 0.82	33.21 ± 6.43
5	43.57 ± 2.26	41.08 ± 6.83

Figure 5.5. Cumulative release of gentamicin from nanofilm coated porous silk scaffolds on *S. aureus* and *E. coli* lawns (note the close agreement between the gentamicin values determined for the two different bacteria). N=3, error bars represent standard deviation.

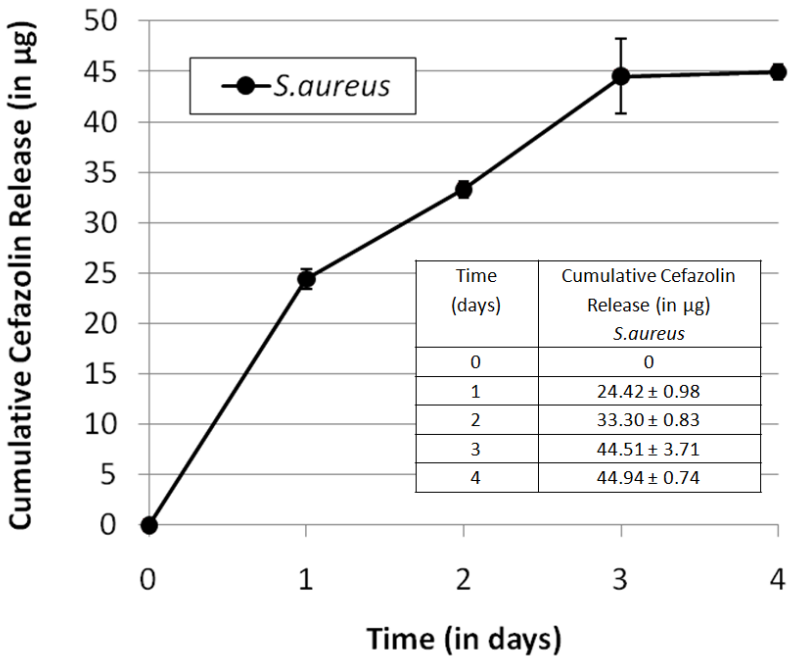

Figure 5.6. Cumulative release of cefazolin from nanofilm coated porous silk scaffolds on *S. aureus* lawns. N=3, error bars represent standard deviation.

Total loading was determined by degrading finished coated scaffolds in 0.1 mg/mL proteinase k solution at 37^{o}C overnight. For gentamicin loaded scaffolds, total loading was found to be 107.5 ± 30.95 µg (n = 4 samples) and for cefazolin loaded scaffolds, total loading was found to be 55.5 ± 6.98 µg (n =3 samples). The gentamicin loaded scaffolds released between 40 and 45 µg over 5 days and the cefazolin loaded scaffolds released approx. 45 µg over 3 days.

These results demonstrate that nanofilm coating can be used to achieve fairly linear, sustained release of water-soluble drugs from porous substrates to produce antibiotic-releasing silk sponges. This silk nanofilm coating process could also be useful for building antibiotic release into other biomaterials that would benefit from microbe resistance.

5.3.3. Injectable antibiotic delivery - bulk loaded silk hydrogels and silk microspheres suspended in silk hydrogels

Systems for injectable delivery of antibiotic releasing silk biomaterials were also studied. Drug release from both bulk loaded gels and gels loaded with drug releasing silk microspheres were characterized For penicillin loaded gels, 8% (w/v) and 4% (w/v) silk hydrogel was studied to examine the effects of silk concentration on drug release. As no noticeable effect was observed (likely due to the high solubility and small size of the antibiotics loaded), ampicillin release studies were carried out only using 8% (w/v) silk. Total loading of the microspheres was found to be approx. 0.5 mg of antibiotic per mg of silk microspheres. We attribute this high loading to the use of antibiotics in rinsing solutions during microsphere fabrication to prevent premature leeching.

Results of the zone of inhibition study in *S. aureus* lawns for penicillin and ampicillin loaded gels are shown in Figure 5.7.

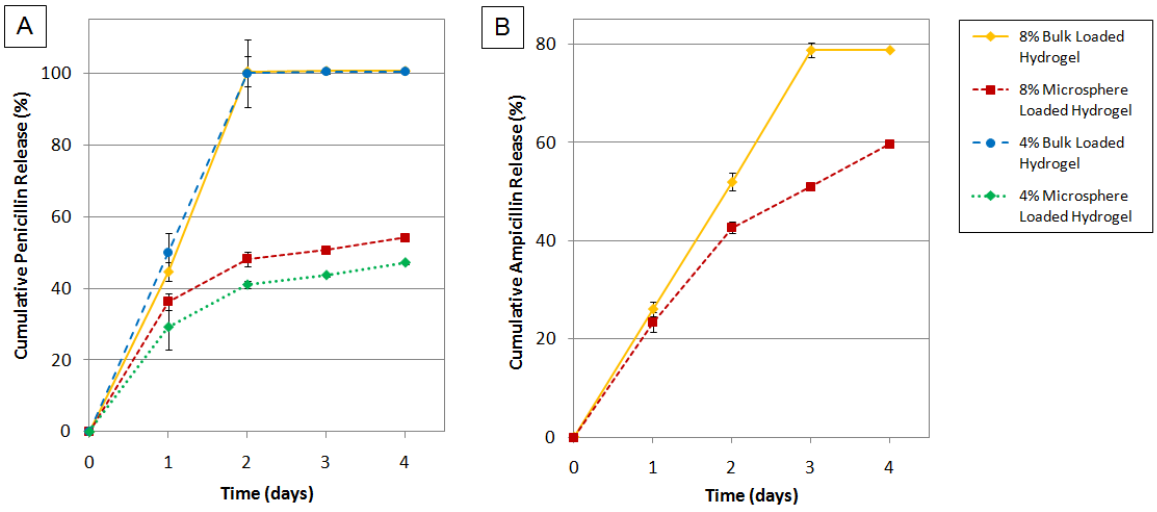

Figure 5.7. Cumulative drug release from penicillin and ampicillin loaded silk gels (A) Cumulative drug release from penicillin loaded silk hydrogels over 4 days, prepared from either 4% or 8% (w/v) silk solution either bulk loaded with penicillin by mixing penicillin into the silk solution prior to sonication (bulk) or loaded with microspheres by mixing penicillin silk microspheres into the silk solution prior to sonication (spheres). Cumulative drug release from ampicillin loaded 8% (w/v) silk gels over 4 days Silk hydrogels are either bulk loaded with ampicillin by mixing ampicillin into the silk solution prior to gelling (bulk loading) or loaded with microspheres by mixing ampicillin silk microspheres into the silk solution just after sonication. N=3, error bars represent standard deviations. Where error bars are not shown, they fall into background.

Bulk loaded gels exhausted their penicillin drug load within 48 hours and their ampicillin load within 72 hours. Microsphere loaded gels released at a lower daily release rate than bulk loaded but continued to release for 4 days for both penicillin and ampicillin. Loading of drug into silk microspheres sustained release and delayed burst compared to bulk loaded gels. This suggests that bulk loading could be used to deliver a large initial burst dose, with microspheres incorporated for sustained release of a lower maintenance antibiotic dose. These results also show that injectable formats can effectively deliver active antibiotics.

5.3.4. Methanol-assisted adsorption loading and release of poorly water soluble antibiotics from silk biomaterials

Hydrophobic drugs are difficult to administer due to their low water solubility. However, once loaded into polymer delivery systems the low water-solubility of these drugs can be used to limit daily release rate, thereby sustaining release. To test hydrophobic drug loading and delivery from silk biomaterials, rifampicin and erythromycin (antibiotics with high methanol solubility and low water solubility) were chosen for study.

To deliver hydrophobic, alcohol soluble drugs from silk biomaterials a high-concentration drug solution is prepared in methanol, then the silk biomaterial for loading is immersed in the drug-saturated methanol. During the methanol soaking, drug is able to move into the silk until equilibrium is reached (total drug loading scales linearly with the concentration of drug in the methanol). Once the drug loaded biomaterial is immersed in an aqueous solution, drug is “trapped” in the silk and diffusion out of the silk is limited by the drug’s solubility in water. As a result, slow, sustained, zero-order release is achieved.

Figure 5.8 shows cumulative release of erythromycin from porous silk sponges soaked for 24 hours in 5 mg/mL, 50 mg/mL and 500 mg/mL solutions of erythromycin in methanol. The sponges were dried, rinsed to remove any antibiotic stuck to the surface, and release was characterized with the zone of inhibition assay on *S. aureus* lawns.

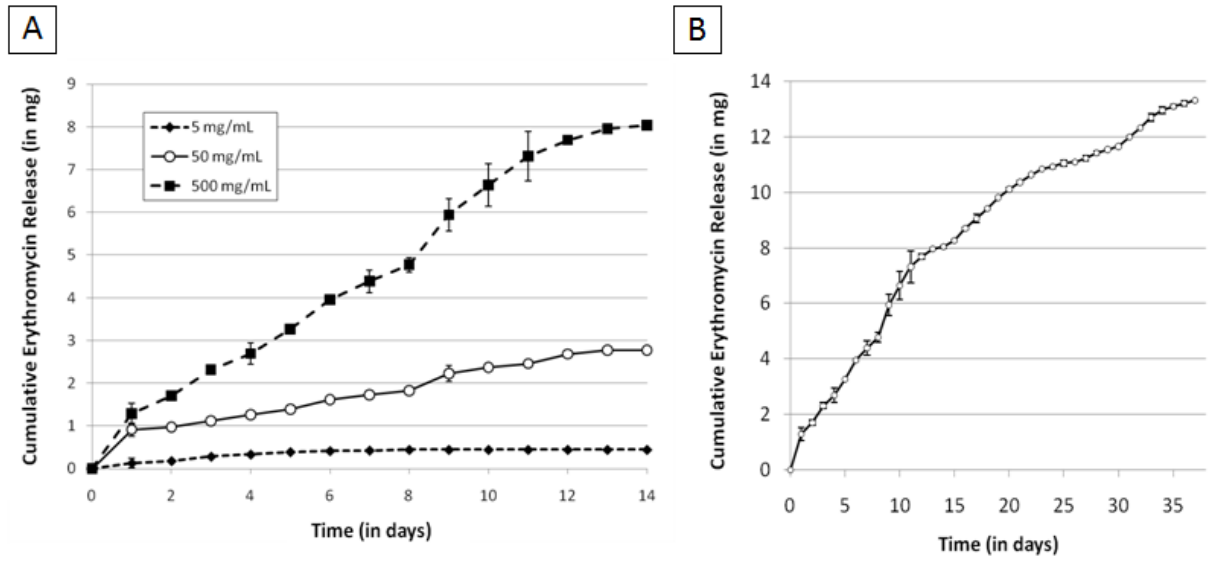

Figure 5.8. Cumulative erythromycin release from porous silk sponges. Sponges were loaded loaded by soaking in 5 mg/mL, 50 mg/mL and 500 mg/mL erythromycin in methanol solutions. (A) Comparison of cumulative release from sponges prepared using various loading concentrations over 14 days (B) Release from sponges prepared using the highest loading concentration (500 mg/mL) over 35 days. N=3, error bars represent standard deviations.

Zero-order release is sustained for at least two weeks from the scaffolds prepared from 50 mg/mL and 500 mg/mL. Note that release rate does not scale linearly with preliminary erythromycin concentration because drug release is limited by the solubility of erythromycin in water. However, differences in loading do produce different rates and some amount of early burst release is observed, suggesting that intial drug can affect the diffusion gradient and impact release behavior (though presumably a maxima would be reached where increased loading had no further effect on release rate because the water solubility of the drug would be rate limiting).

In the highest erythromycin loading (500 mg/mL initial methanol solution), continuous release is sustained for 35 days.

Cumulative rifampicin release (determined by both the zone of inhibition (ZOI) assay and by measuring UV absorbance at 475 nm) for methanol-assisted adsorption loaded sponges and films is shown in Figure 5.9.

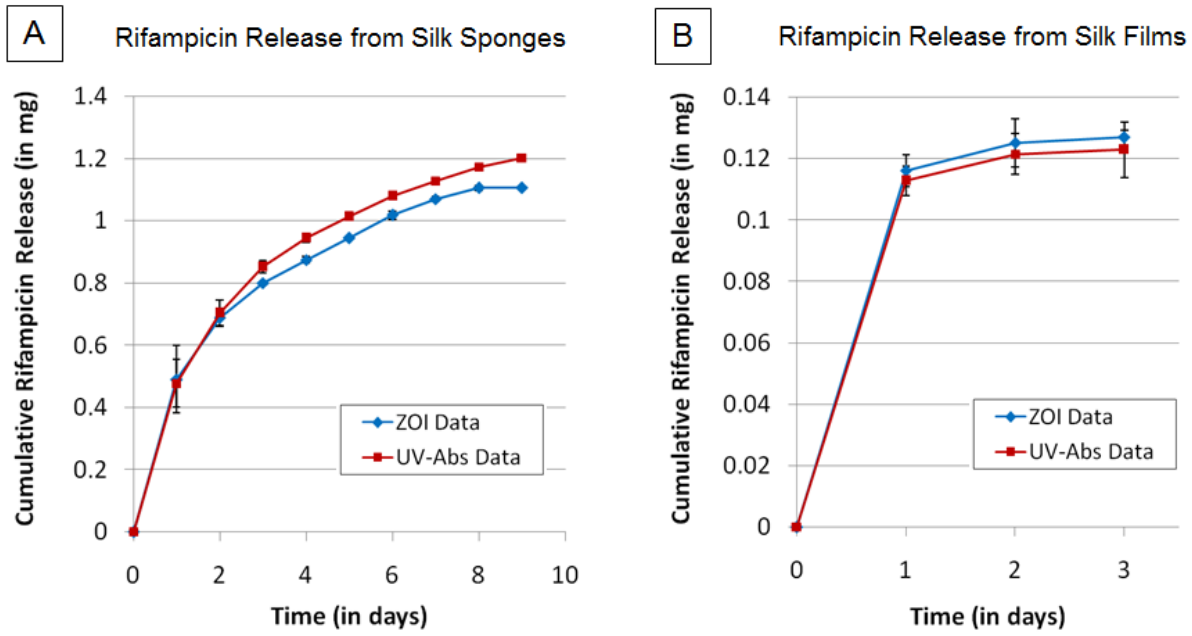

Figure. 5.9. Rifampicin release from silk sponges and silk films. N=3, error bars represent standard deviations, where error bars are not shown they fall into background.

Rifampicin loaded sponges exhibit release duration of 8-9 days, while films exhibit burst release (>85% release within the first 24 hours). Good agreement is observed between the cumulative release curves generated using ZOI data and UV-Absorbance data. Release from films is faster than from sponges or fibers due to the short path length/difference in material format. Rifampicin release from sponges (20 mg/mL initial loading) is comparable to erythromycin release (50 mg/mL initial loading).

Rifampicin-loaded silk fibroin fibers were able to produce a zone of inhibition in *S. aureus* lawns for 8 days (Figure 5.10).

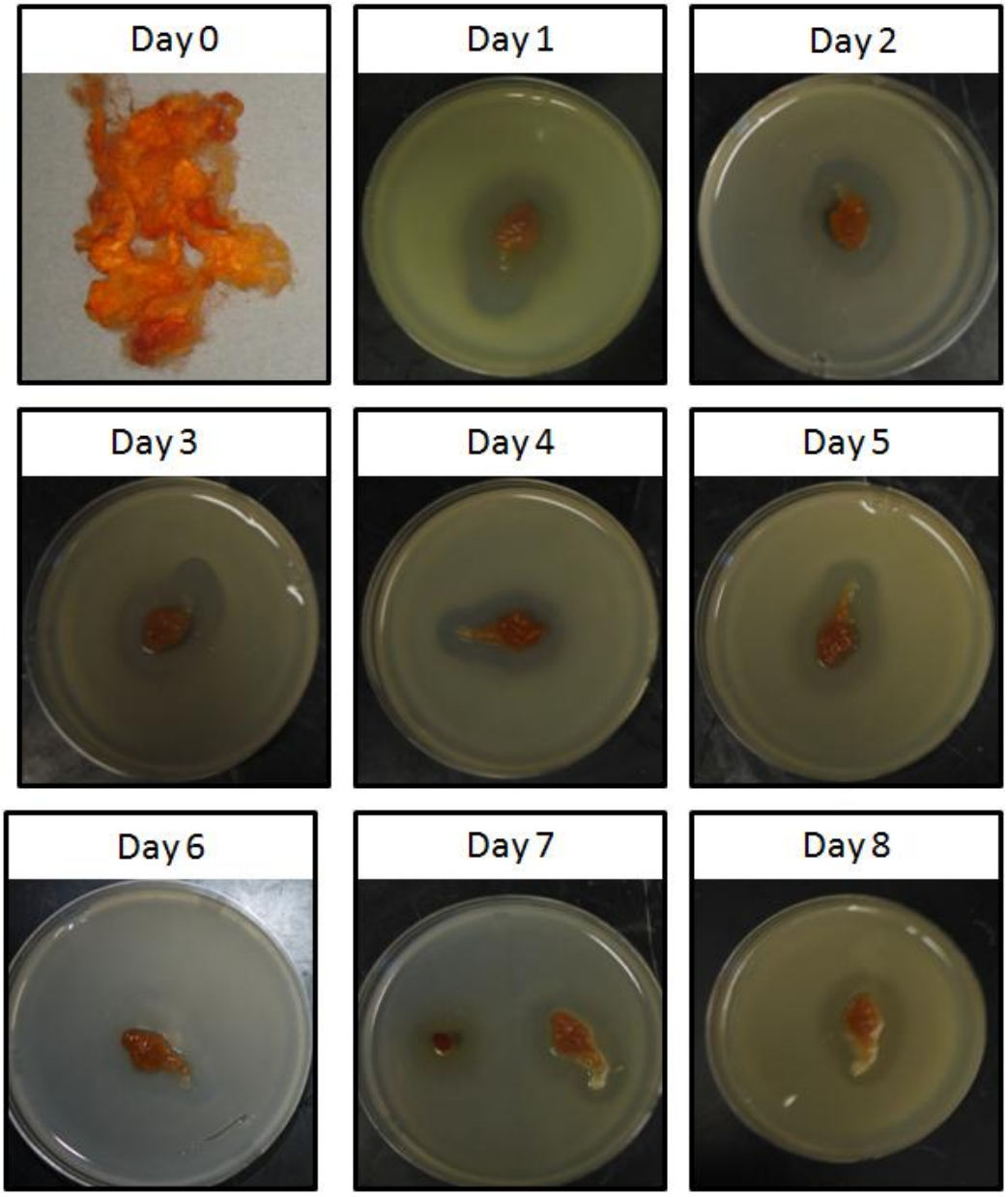

Figure 5.10. Agar plates showing the zones of inhibition in *S.*aureus lawns produced by rifampicin-releasing silk fibers over 8 days. Silk fibers were loaded with rifampicin by immersion in a 20 mg/mL rifampicin in methanol solution overnight. As the zones of inhibition around fiber masses show, the fiber is able to repress local bacterial growth for 8 days.

5.3.5. Antibiotic stabilization in silk films

5.3.5.1. Stability of penicillin in silk films and in solution at various storage temperatures (4°C, 25°C, and 37°C (body temp) over 6 months (183 days)

To determine if incorporation into silk films would have a stabilizing effect on sensitive antibiotics, a long-term stability study was carried out comparing the residual activity of penicillin stored in 8% (w/v) silk films or in solution at 4°C (refrigeration), 25°C (room temperature) and 37°C (body temperature). Results of the 6 month stability study are shown below in Figure 5.11.

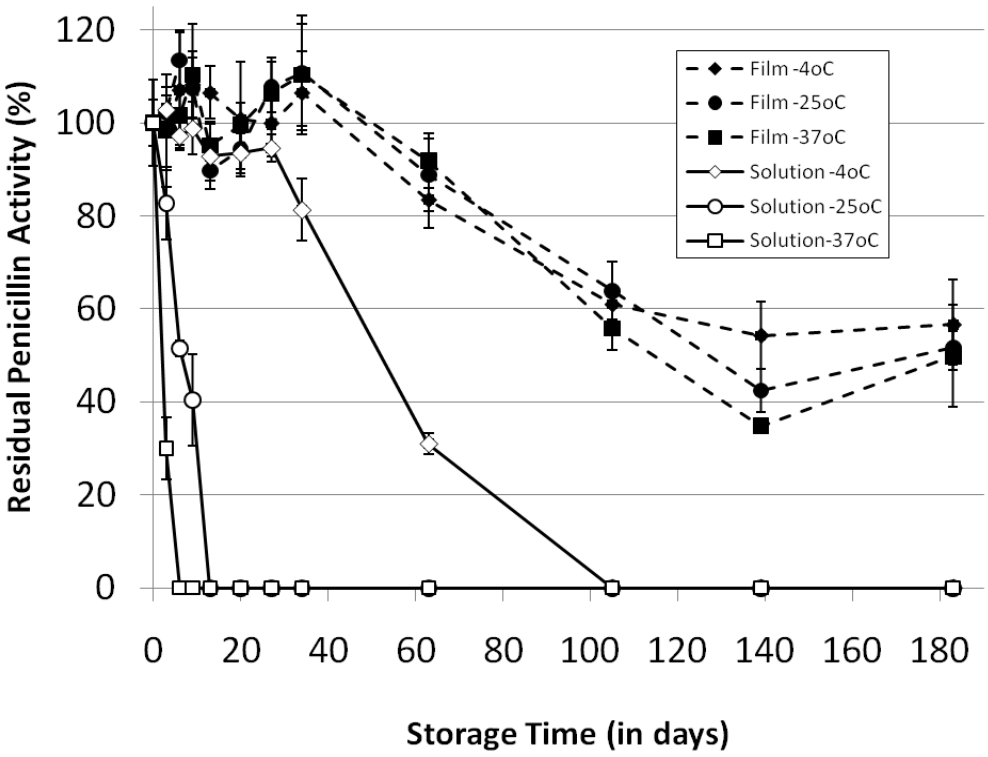

Figure 5.11. Stability over 183 days (6 months) of penicillin stored in solution or in 8% (w/v) silk films at 4°C (refrigeration), 25°C (room temperature) and 37°C (body temperature). N=3, error bars represent standard deviations.

While stability rapidly declines for penicillin in solution stored at 25°C and 37°C, temperature appears to have little to no effect on stability in silk films: approx. 50% of the initial

activity observed after 183 days of storage for all storage temperatures tested. Note that for the first 40 days of storage, incubation enhances activity above 100% of the initial value, a phenomenon also observed for the published enzyme storage data. Increasing temperature of storage has a much less pronounced effect on penicillin stored in silk films than stored in solution.

5.3.5.2. Comparison of storage stability in silk films versus other storage formats at 4^{o}C (refrigeration), 25^{o}C (room temp) and 37^{o}C (body temp)

Stability was also characterized for dry penicillin powder stored at 4^{o}C, 25^{o}C and 37^{o}C. Comparison of the stability of penicillin stored in silk films, in solution and in dry powder format over 6 months (183 days) is shown below in Figure 5.12. Comparison of the stability of penicillin stored in silk films and in collagen films (180 days) is shown in Figure 5.13.

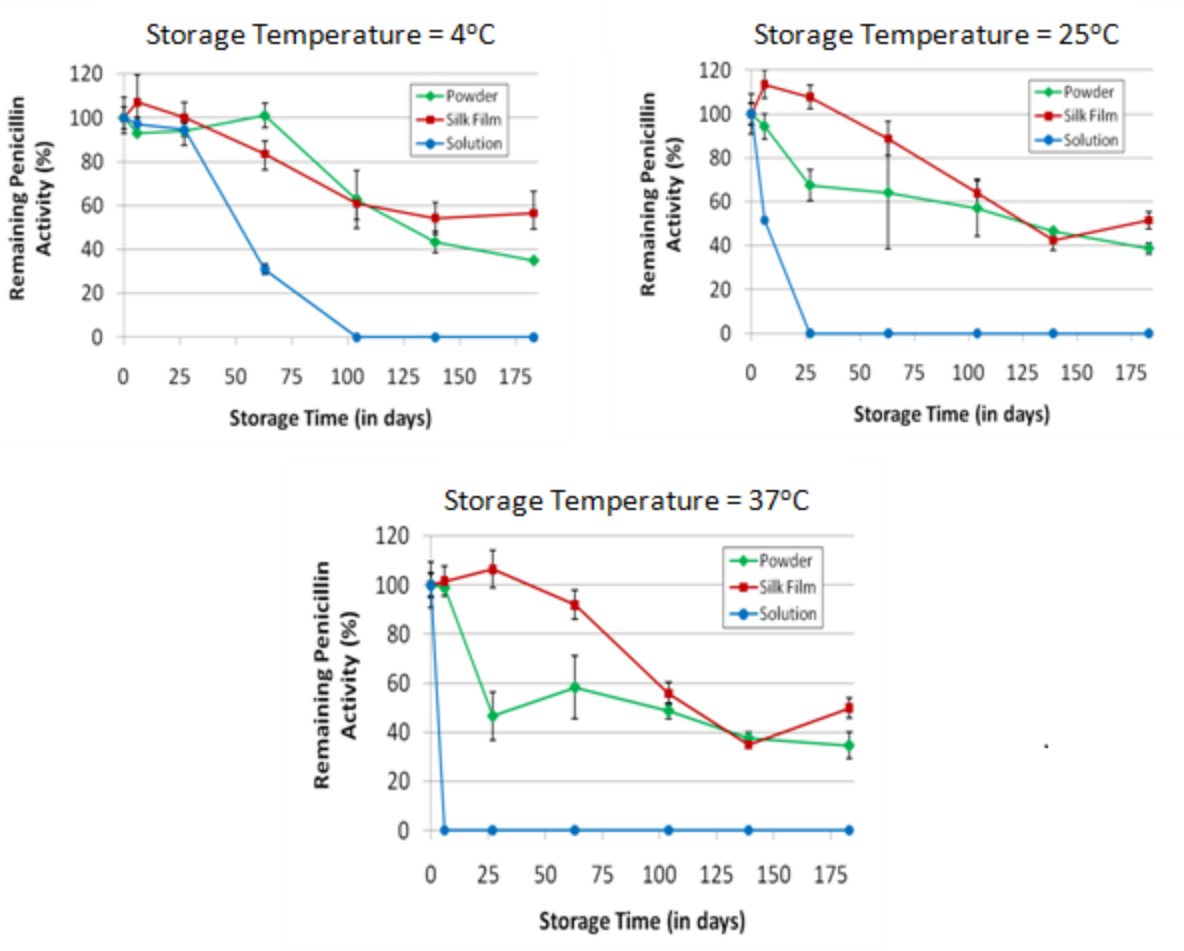

Figure 5.12. Comparison of stability for penicillin stored in 8% (w/v) silk films (red), in solution (blue) and as dry powder (green) at 4°C (refrigeration), 25°C (room temperature) and 37°C (body temperature) over 183 days (6 months). N=3, error bars represent standard deviations.

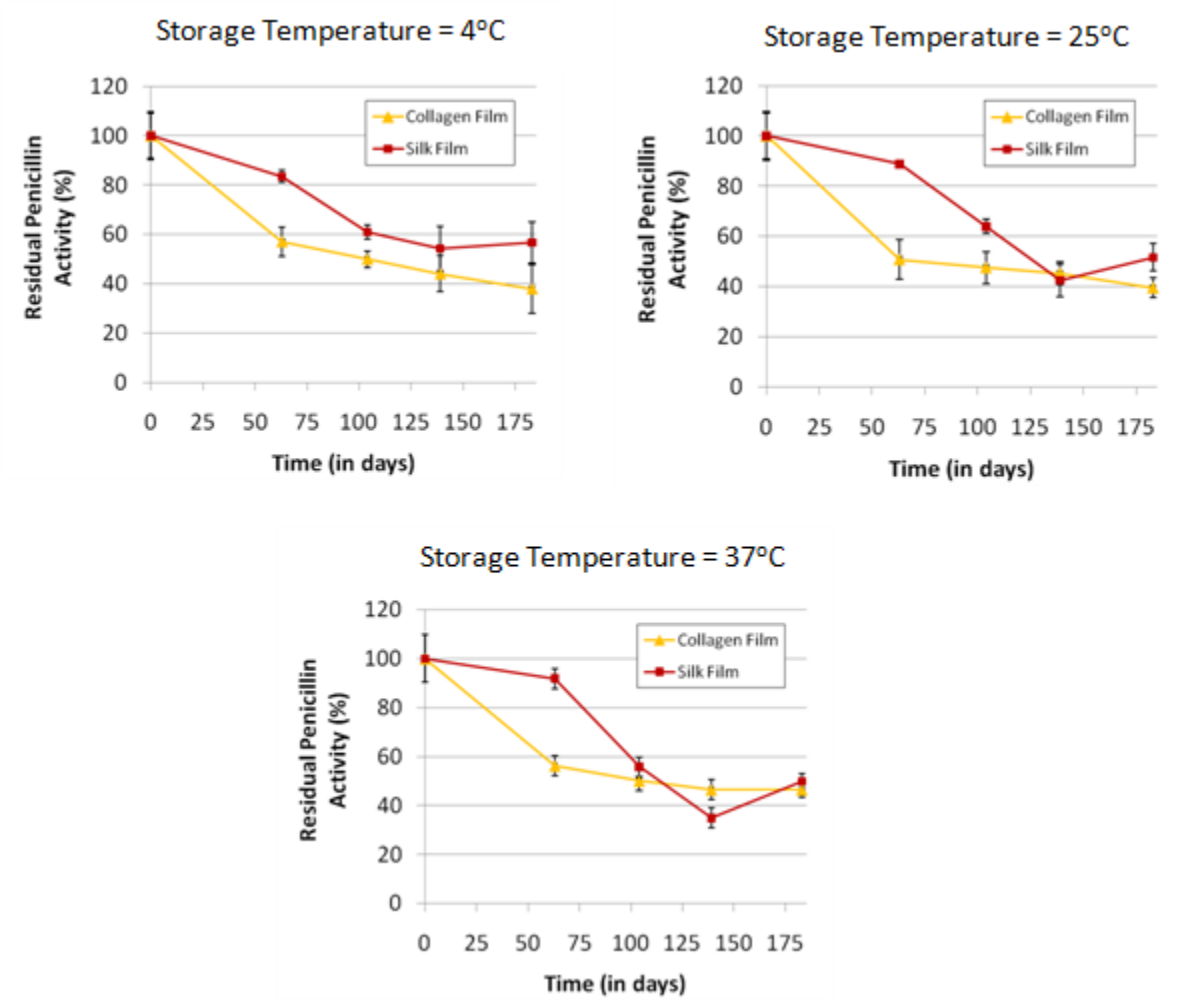

Figure 5.13. Comparison of stability for penicillin stored in 8% (w/v) silk films (red) and stored in collagen films (yellow) at 4°C (refrigeration), 25°C (room temperature) and 37°C (body temperature) over 183 days (6 months). N=3, error bars represent standard deviations.

With a few exceptions (25°C and 37°C on Day 140), we observe that the stability of penicillin incorporated into silk films is either as good or better than storage in dry powder form, including the recommended storage state (powder, 4°C). As with the powder storage format, excepting the Day 140 time points for 25°C and 37°C, penicillin exhibits equal or better stability in silk films as in collagen films.

5.3.5.3. Stability of penicillin in silk films at 60°C over 30 days

Finally, stability of penicillin incorporated into silk films at 60°C was characterized for 30 days. Because preliminary study observations suggested it would improve stability, a lower concentration of penicillin was loaded (from 50 mg/mL in the previous study to 25 mg/mL for the 60°C study) and films were untreated post drying rather than methanol treated. Results of a the 30 day stability study shown in Figure 5.14, with a dotted red line to emphasize which data points fall above or below 100%.

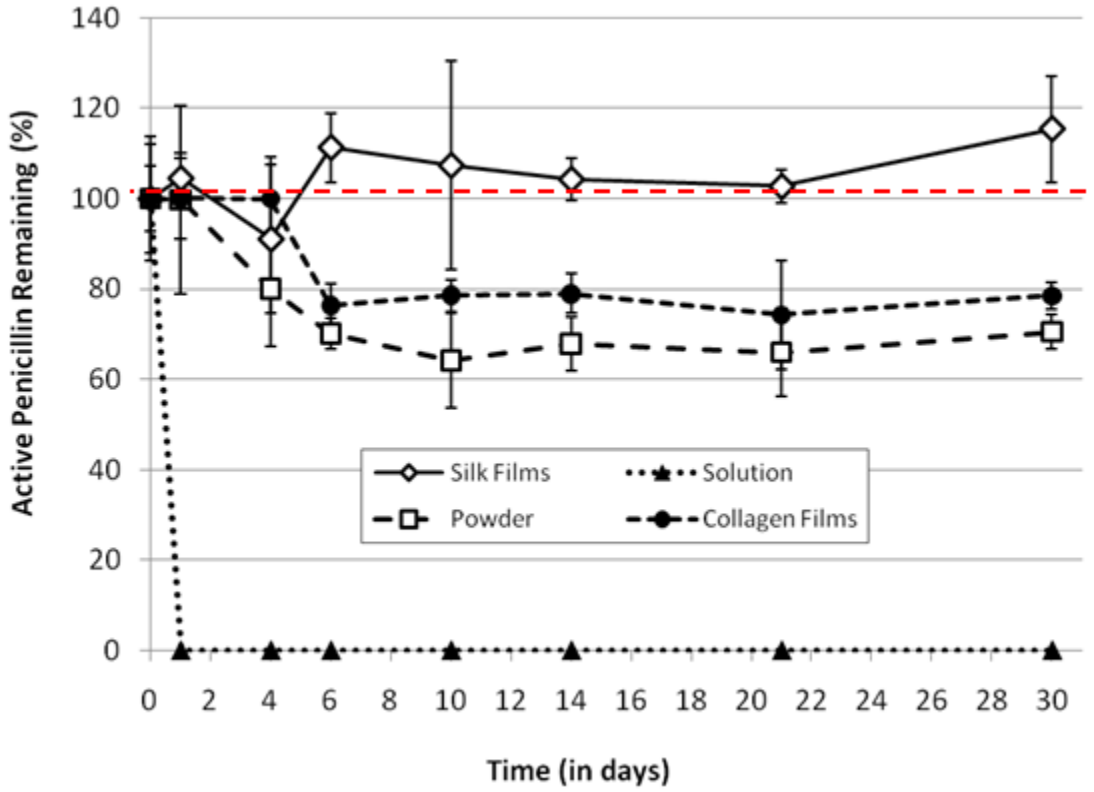

Figure 5.14. Comparison of stability over 30 days for penicillin stored at 60°C in various storage formats: in silk films, in collagen films, in solution and in dry powder form. Red dotted line indicates 100% activity. N=3, error bars represent standard deviations.

Penicillin loses 100% of its initial activity within 24 hours when stored in solution at 60°C (filled triangles). After 30 days of storage at 60°C, penicillin stored in dry powder form (empty squared) or incorporated into collagen films (filled circles) loses approx. 20-25% of its

initial activity. Penicillin stored in silk films loses little to no activity over 30 days (empty diamonds), with only a few data points dropping below 100% initial activity. After initial losses (days 1-6), drug stability is relatively constant for storage in silk films, collagen films and dry powder, but the reason for this phenomena is unknown and requires further investigation of the mechanisms and time-course of penicillin degradation.

5.3.5.4. Stability of tetracycline in silk films and in solution at various storage conditions over 4 weeks (28 days)

As expected, after 2 weeks in solution tetracycline solutions became turbid, even at 4°C due to hydrolysis and precipitation of the degradation product (Figure 5.15)

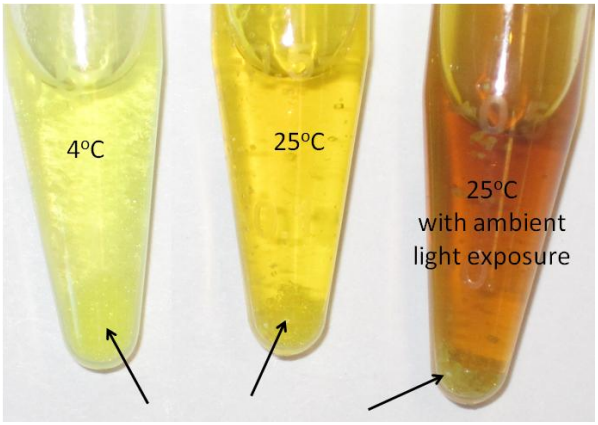

Figure 5.15. Photographs of 15 mg/mL tetracycline solutions stored for 2 weeks at 4°C and 25°C with light protection and 25°C with ambient light exposure. A precipitated hydrolysis product is observable for all the solutions, even those stored at 4°C (black arrows).

Figure 5.16 shows samples collected at 1 week, 2 weeks and 4 weeks storage.

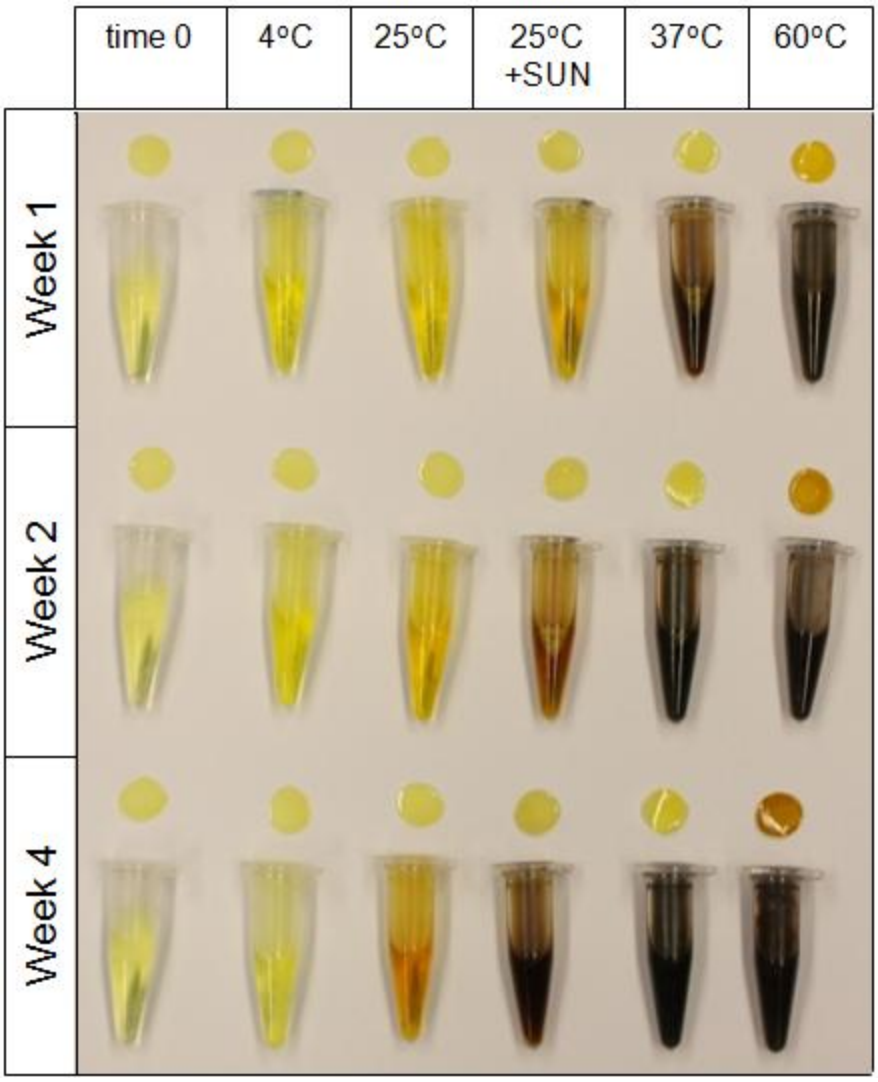

Figure 5.16. Tetracycline solutions and silk films stored at 4°C, 25°C, 37°C and 60°C and 25°C with ambient light exposure at 1, 2 and 4 weeks.

The darkening of the tetracycline solutions with increasing time, temperature and exposure to light exposure is an indicator of drug degradation (Yang *et al.*, 2004). This degradation product can be measured via absorbance at 450 nm, but other degradation pathways (like hydrolysis) can inactivate the tetracycline without generating the dark degradation product. Note that, except for the silk films stored at 60°C, no color change is seen in the silk films and even the 60°C films exhibit relatively slight darkening compared to the solutions. This suggests

that immobilization in silk films partially protects tetracycline from this degradation pathway. Figure 5.17 shows tetracycline activity remaining in solution or in silk film over 4 weeks for the various storage conditions tested.

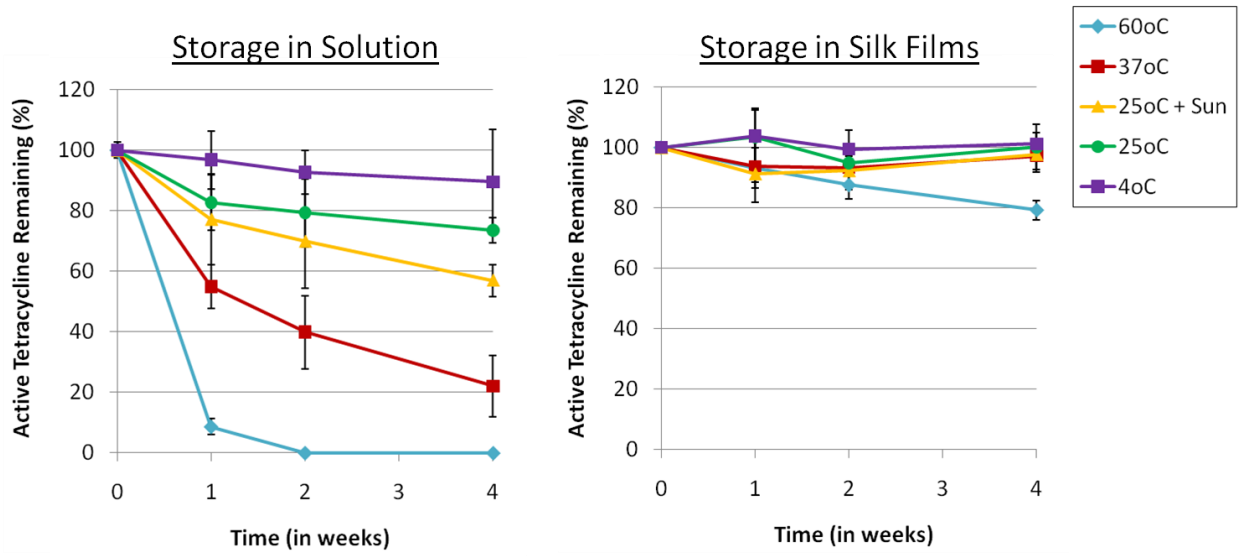

Figure 5.17. Stability over 4 weeks of tetracycline stored in solution or in 6% (w/v) silk films at 4°C, 25°C, 37°C, 60°C and 25°C with sunlight exposure. Activity measured using a zone of inhibition assay in S. aureus lawns. N=4, error bars represent standard deviations.

In solution, loss of activity is observed at all storage temperatures, even with refrigeration (4°C). In silk films, activity loss is only seen for films stored at 60°C, and even at this temperature, activity loss is relatively low: only approx. 10% and 20% activity loss at 2 and 4 weeks, compared to 100% loss at 2 weeks for tetracycline stored in solution. Storage at body temperature (37°C) results in no activity loss for storage in silk films, compared to 80% lost within 4 weeks for storage in solution.

5.4. Conclusions

Though considerable work still remains to be done, these studies provide preliminary proof-of-principle data suggesting antibiotics can be both stored in silk biomaterials and effectively released to repress local bacteria growth. Multiple loading approaches are demonstrated for a broad range of silk material formats, including bulk loading, microsphere imbedding, methanol impregnation and nanofilm coating. The stabilization effects of silk films previously reported for enzymes were also validated for light and/or temperature sensitive antibiotics. These systems could be especially useful in third world clinical settings as they are stable without refrigeration, would be easy to administer and could efficiently release antibiotics locally over sustained timeframes without constant reapplication, multiple repeated injections or surgical retrieval of implants, thereby avoiding complex, multi-step, expensive procedures that are difficult to carry out in many third world clinical settings.

6. Silk biomaterials for building drug delivery into tissue engineering scaffolds

Controlled release technologies have the potential to achieve precise spatial and temporal control of signaling through delivery of bioactive agents from the same tissue-engineering matrices designed to support cells (Saltzman and Olbricht, 2002). Despite the potential advantages, the ability to generate controlled-release scaffolds for tissue engineering remains a major challenge due to the lack of biomaterials with the necessary material properties. Due to its biocompatibility, mechanical strength, controllability and biodegradation, silk fibroin is uniquely suited to meet this need. The utility of silk as a vehicle for drug delivery (Numata and Kaplan, 2010-1) and a tissue engineering scaffold (Vepari and Kaplan, 2007; Wang *et al*., 2006), has been extensively studied.

Because of its mild processing conditions and protein-stabilization capabilities, silk is particularly attractive for growth factor delivery. Studies investigating growth factor delivery from silk tissue engineering scaffolds are summarized in Table 6.1. In this chapter, silk based small molecule drug delivery systems for tissue engineering using human mesenchymal stem cells (hMSCs) are presented. Signaling molecules studied include desferrioxamine (DFO) releasing silk microspheres for enhanced angiogenesis and dexamethasone releasing 3D porous sponges for enhanced osteogenesis (chemical structures shown in Figure 6.1.)

Table 6.1. Studies of Growth Factor Delivery from Silk Tissue Engineering Scaffolds

Growth Factor	***Silk Scaffold Material Format***	***Reference***
insulin growth factor I (IGF-I)	Porous bulk loaded sponge (porogen leeching + freeze-drying technique)	Uebersax *et al*., 2008
IGF-I	Silk microspheres (laminar jet break-up of an aqueous silk solution)	Wenk *et al.,* 2008

Bone morphogenetic protein 2 (BMP-2)	Bulk loaded electrospun nanofiber mats	Li *et al*., 2006
BMP-2	Silk films loaded via adsorption or covalent coupling	Karageorgiou *et al*., 2004
BMP2 and IGF-I	silk microspheres loaded using the lipid-template technique and incorporated them into aqueous-derived silk porous scaffolds using a gradient process	Wang *et al*., 2009
BMP-2, -9 and -14	Silk microspheres (ethanol precipitation technique)	Bessa *et al.,* 2010-1 and Bessa *et al.*, 2010-2
Basic fibroblast growth factor (bFGF)	3D porous silk sponges using either the aqueous or HFIP salt-leeching loaded via adsorption	Wongpanit *et al*., 2010
Parathyroid hormone (PTH)	Silk films loaded via covalent coupling	Sofia *et al*., 2001
Fibroblast growth factor 2 (FGF-2)	Silk films decorated with a sulfonated FGF-2 binding moiety using diazonium coupling	Wenk *et al*., 2010-1
Glial cell line-derived neurotrophic factor (GDNF) and nerve growth factor (NGF)	Bulk loaded silk films decorated with aligned silk nanofibers to provide topographical guidance cues, rolled up and glued into tubes, and coated with PLGA to reduce drug release through the exterior of the guidance conduit	Madduri *et al*., 2010
NGF	Porous tube-shaped scaffolds (freeze-drying technique)	Uebersax *et al*., 2007

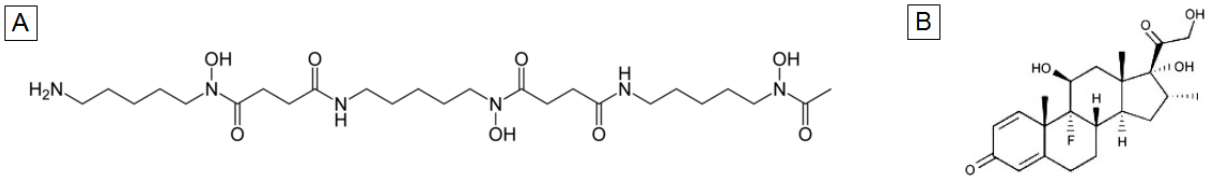

Figure 6.1. (A) Chemical structure of desferrioxamine (DFO) (MW = 560.68) (B) Chemical structure of dexamethasone (MW = 392.46)

6.1 Desferrioxamine (DFO) releasing silk mcrospheres for enhanced VEGF production

6.1.1. Introduction

Therapeutic application of VEGF may prove problematic and expensive (Shen *et al.*, 2006). As an alternative approach the use of small molecules that target the hypoxia inducible factor (HIF) pathway to activate angiogenesis have been explored. HIF is the master regulator of response to low oxygen, and has been shown to be activated in skeletal repair. The pathway through which HIF increases angiogenesis is shown in Figure 6.2. Small molecule inhibitors have been shown to activate the HIF pathway by blocking HIF-α degradation. In general, proposed molecules interfere with the required cofactors for prolyl hydroxylase enzymes PHDs: dimethyloxalylglycine (DMOG) and L-mimosine (L-mim) act as 2-oxyglutarate analogues and desferrioxamine (DFO) chelates the required iron (Figure 6.2). Studies have shown that use of these small molecule inhibitors to activate the HIF pathway can effectively increase vascularization in skeletal repair model. DFO was selected for study because it was more effective at increasing vascularization *in vitro* than other inhibitors studied (Shen *et al*., 2006) and its sustained release from gelatin microspheres has been previously demonstrated (Ulubayram *et al.*, 2005). It was hypothesized that sustained release of DFO from silk microspheres would effectively increase VEGF production in a dose-dependent manner *in vitro*.

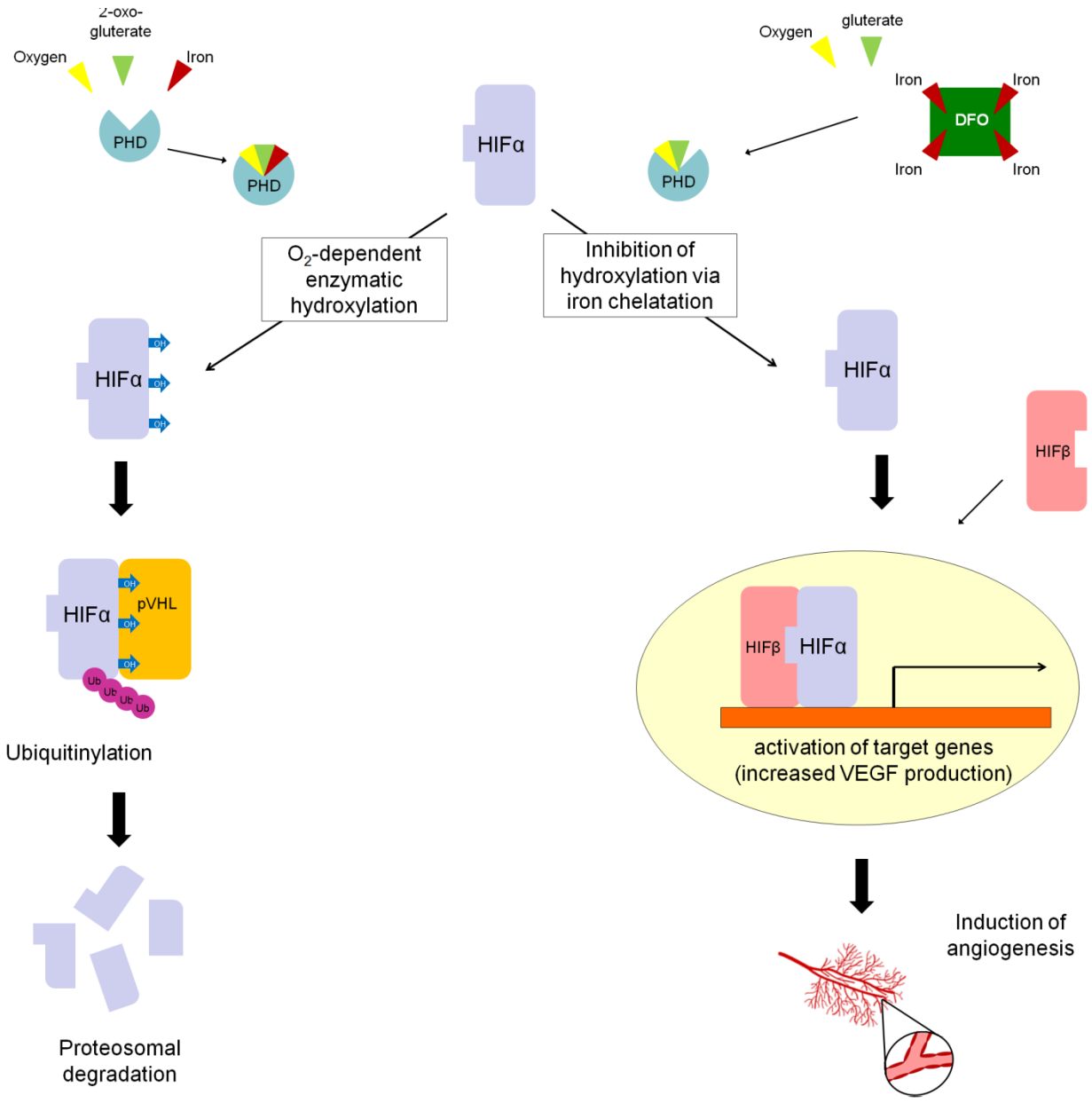

Figure 6.2. Schematic diagram of HIF regulation by enzymatic hydroxylation and proposed mechanism and consequences of protein hydroxylase inhibition. In the presence of the necessary cosubstrates (2-oxoglutarate and molecular oxygen) and the cofactor iron, the prolyl hydroxylase enzymes (PHDs) are active and able to hydroxylate HIFα (hydroxyl groups represented by blue arrows labeled "OH"). The von Hippel-Lindau protein (pVHL, in orange) is able to interact with the hydroxylated HIFα, which is ubiquitylated (ubiquitin represented by fuchsia circles labeled "Ub") and subsequently degraded. Hypoxic conditions (i.e., absence of the necessary oxygen cosubstrate) or, as shown here, the addition of inhibitors like DFO (which chelates the necessary iron cofactor) inhibit the activity of PHDs (right, inhibition of hydroxylation), thereby preventing hydroxylation of the HIFα . HIFa accumulates and translocates to the nucleus where it dimerizes with HIF-β to activate hypoxic responsive elements in the proximal promoter regions of HIF responsive genes (Shen *et al*., 2006; Chau *et al*., 2005; Warnecke *et al*., 2003; Ivan *et al*., 2001; Huang *et al*., 1998; Wang *et al*., 1993).

6.1.2. Materials and Methods

6.1.2.1. Materials

Cocoons of *Bombyx mori* silkworm silk were purchased from Tajima Shoji Co., LTD (Sumiyoshicho, Naka-ku, Yokohama, Japan). 1,2-Dioleoyl-*sn*-glycero-3-phosphocholine (DOPC) was purchased from Avanti Polar Lipids (Alabaster, AL). DFO salt and manganese dioxide were purchased from Sigma Aldrich (St. Louis, MO).

6.1.2.2. DFO-releasing silk microspheres preparation

Silk fibroin solution was prepared as we have previously described using a 60 minute degumming time (Sofia *et al*., 2001). Microspheres were prepared according to the phospholipid template protocol previously described (Wang *et al*., 2007-3). Briefly, 200 mg of 1,2-dioleoyl-sn-glycero-3-phosphocholine (DOPC) phospholipid was dissolved in 1 mL of chloroform, then dried under N_2 to a film on the interior of a glass test tube. 1 mL of drug solution in 8% (w/v) silk (25 mg DFO/mL silk) was added to hydrate the phospholipid film, which forms microspheres upon exposure to the aqueous solution. Microspheres prepared with 8% (w/v) silk with no drug added served as controls. The suspension of microspheres is repeatedly freeze-thawed, diluted in distilled water, then lyophilized. Once lyophilized, the material is treated with methanol (MeOH) for 30 minutes to remove the lipids and induce β-sheet physical crosslinks to stabilize the structure. Methanol and microspheres are separated by centrifugation at 10,000 rpm for 5 min at 4^{o}C. The pellet is dried overnight at ambient conditions. Prior to gel imbedding or release testing, the microsphere pellet is resuspended in the desired buffer and any clustered

microspheres are dispersed by brief ultrasonication (10-15 seconds at 20% amplitude) using a Branson 450 ultrasonicator (Branson Ultrasonics Co., Danbury, CN).

6.1.2.3. Loading and release studies for DFO loaded silk microspheres

10 mg of DFO microspheres were used to determine DFO loading (initial loading 312.5 µg/ mg of silk). To determine loading, the microspheres were treated with hexafluoroisopropanol (HFIP) and dissolved in 1 mL of PBS as previously described (Wang *et al*., 2009).

To determine drug release from silk microspheres, silk microspheres were resupended in 0.5 mL of Dulbecco's PBS at 37^{o}C with shaking. DFO microspheres were suspended at a concentration of 30 mg/mL (15 mg in 0.5 mL). At desired time points, the microspheres were centrifuged at 10,000 RPM for 5 minutes and the buffer was removed and replaced with fresh buffer. The buffer removed periodically from the system was assayed for DFO content as previously described (Beyer and Fridovich, 1989). Briefly, removed buffer samples were treated with excess MnO_2 (approx. 500 mg/mL) and allowed to react for 3-4 hours. Unchanged MnO_2 was removed by centrifugation and the supernatant was filtered through 0.45 µm-pore-size Millipore filters. DFO content was determined by spectrophotometric analysis at 640 nm. For determining DFO release from microspheres, n = 6.

6.1.2.4. Human mesenchymal stem cell (hMSC) isolation and culture

Human mesenchymal stem cells (hMSCs) were isolated from bone marrow aspirate (Lonza, Gaithersburg, MD) using a modified version of the method described by Altman *et al*. 2001. Briefly, the bone marrow aspirate was diluted in Dulbecco's phosphate-buffered saline (DPBS) then cultured at 37^{o}C in 5% CO_2 for 10 days in expansion medium (Dulbecco's

modified Eagle medium supplemented with 10% fetal bovine serum, 100 U/ml penicillin, 100 mg/ml streptomycin, 0.25 mg/ml amphotericin, 0.1 mM non-essential amino acids, and 1 ng/ml basic fibroblast growth factor). Expansion media was added twice a week until the cells reached 50% confluence, at which point non-adherent hematopoietic cells were removed by washing with PBS.

6.1.2.4. DFO bioactivity study

The bottom of the wells of a 24-well plate were coated with 200 µL of 4% (w/v) sonication-induced silk hydrogel containing 8, 4, 2 and 1 mg of DFO-releasing silk microspheres per gel or containing no microspheres for controls. Microsphere loaded hydrogels were prepared by sonicating a sterile 4% (w/v) silk solution with a Branson Digital Sonifier 450 at 15% amplitude for 60-90 seconds, mixing in a suspension of microspheres of the desired concentration in sterile ultrapure water, aliquoting into the wells (200 µL per well), and incubating at room temperature for 15 minutes to allow gelation to occur.

Passage 4 (p4) hMSCs were seeded at a density of 100,000 cells per well and cultured in 1 mL of control media consisting of Dulbecco's modified Eagle medium (DMEM) supplemented with 10% fetal bovine serum, 100 U/ml penicillin, 100 mg/ml streptomycin, 0.25 mg/ml amphotericin, 0.1 mM non-essential amino acids. Negative control cells were untreated (i.e., cultured in control media on hydrogel that released no DFO) and positive control cells were treated with 50 µM DFO every other day (i.e, cultured in control media supplemented with 50 µM DFO on silk hydrogel that released no DFO). DFO supplementation to the positive controls was discontinued after day 5 to mimic microsphere release profiles. Media was replaced every

other day. Collected media was assayed for VEGF content using a human VEGF ELISA kit (R&D Systems Inc., Minneapolis, MN).

6.1.3. Results

6.1.3.1. DFO loading and release from silk microspheres

Total DFO loading was determined to be approx. 190 µg per mg of silk microspheres (encapsulation efficiency approximately 60%). Cumulative release of DFO *in vitro* is shown in Figure 6.3.

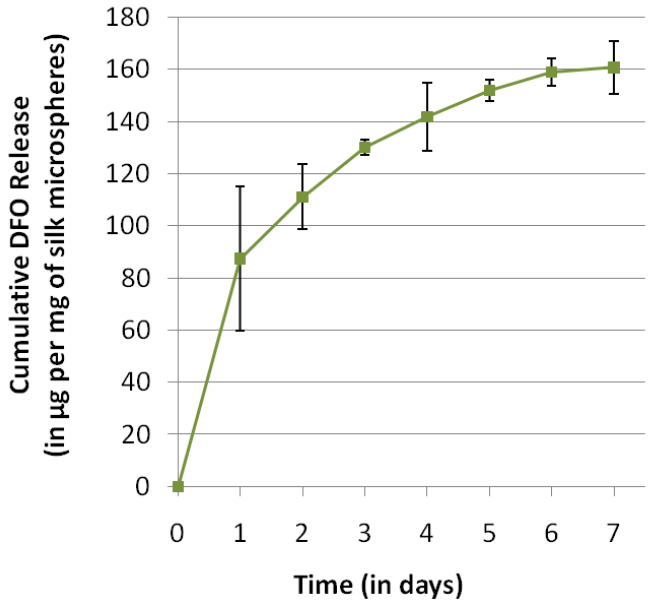

Figure 6.3. Cumulative *in vitro* release of DFO from silk microspheres.

Slightly higher release is observed for the first 24 hours of release, followed by continuous release for a total of 6 days. Very little DFO release is observed between days 6 and 7 and no detectable release is observed after day 7 (limit of detection = 0.16 mg/mL). The lowest release rate within the first 5 days occurs from days 3 to 5 (approx. 20 µg per day).

6.1.3.2. Effect of sustained release DFO-eluting silk microspheres on VEGF expression

To confirm that DFO was being released from silk microspheres in an active form (i.e. maintains the ability to increase VEGF expression), the effect of DFO releasing silk microspheres on VEGF production by hMSCs was studied. Results are shown broken down by day (Figure 6.4) and treatment type (Figure 6.5).

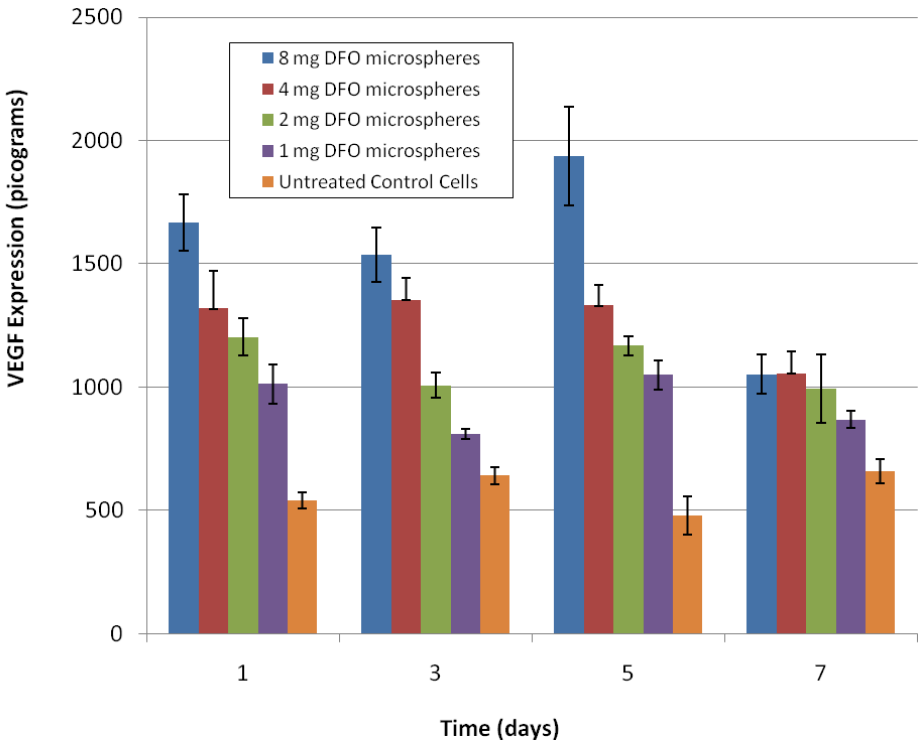

Figure 6.4. VEGF expression over 7 days (broken down by day). N=4, error bars represent standard deviations.

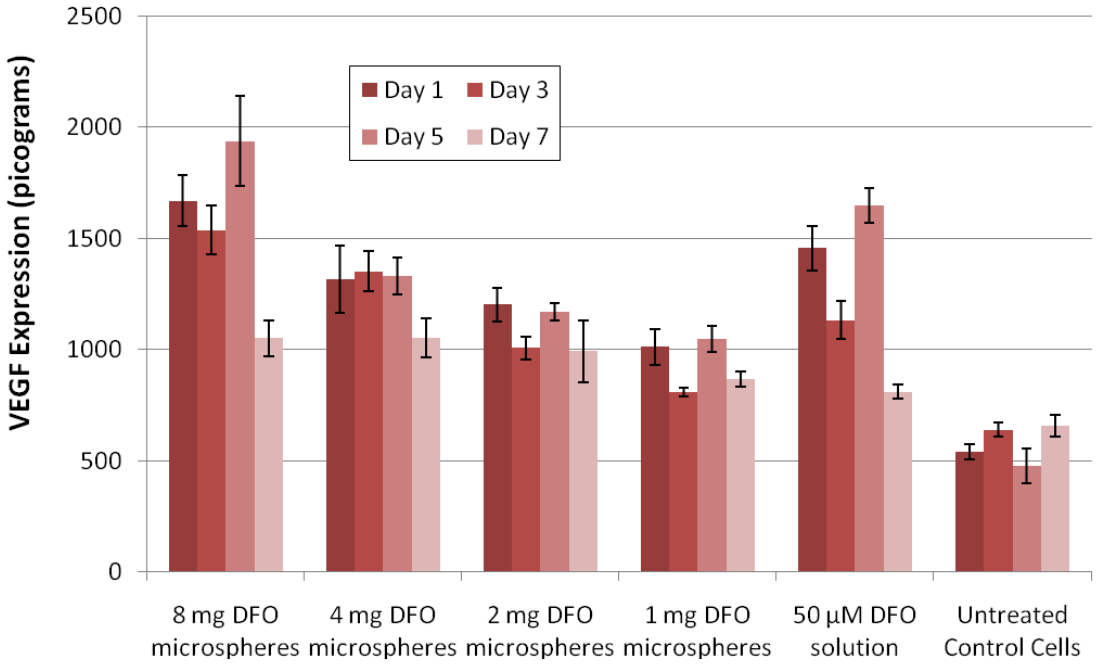

Figure 6.5. VEGF expression over 7 days (broken down by type of cell treatment). N=4, error bars represent standard deviations.

For cells cultured with DFO-releasing silk microspheres, VEGF expression remains elevated through day 5, then drops off on day 7, which is consistent with the *in vitro* release behavior (Figure 6.2), which shows that release drops off after day 5 and is essentially exhausted by day 7. This is supported by the behavior of cells receiving 50 µM DFO in their media through day 5, then receiving control media. In addition, Figure 6.3 clearly shows a dose-dependent response (i.e., as microsphere loading increases, VEGF expression increases). This suggests that the increase in VEGF expression is caused by the DFO eluted by the microspheres.

6.1.4 Conclusions

These studies demonstrate loading, sustained release and bioactivity of DFO from silk microspheres. Currently, tissue engineering is severely limited by the inability to adequately

vascularize tissue. Without intrinsic vascularization, development of tissue of clinically relevant size is prevented by mass transport limitations, nutrient perfusion and oxygen diffusion (Jain *et al*., 2005; Rouwkema *et al*., 2008). Dose-dependent increases in VEGF production by hMSCs were induced by DFO microspheres suspended in silk hydrogels. The DFO-releasing silk microspheres described here therefore represent a promising potential strategy to enhance the vascularization of tissue engineering implants.

6.2. Controlled release of dexamethasone from porous 3D silk sponges for enhanced osteogenetic differentiation

6.2.1. Introduction

There is a major clinical need for new bone tissue to restore the function of damaged or lost bone. Autologous bone graft is the treatment of choice for bone defects, but is restricted by donor site morbidity and limited availability (Jäger *et al*., 2010; Kim *et al.*, 2005-2). Bone-tissue engineering has been studied as an alternative treatment for bone regeneration, and bone marrow stromal cells (hMSCs) represent a potential cell source for autologous bone-tissue engineering. Dexamethasone is a glucocorticoid, which is used extensively *in vitro* as an osteogenic factor, and *in vivo* for the treatment of inflammatory and autoimmune diseases (Nuttleman *et al*., 2006). Dexamethasone has been shown to be required for osteogeneic differentiation of hMSCs *in vitro* (Cheng *et al*. 1994). Dexamethasone offers advantages over bone morphogenetic proteins (BMPs), including anticarcinogenic effects and lower costs (Kim *et al*., 2005-2). Studies of other dexamethasone-releasing polymer scaffolds have demonstrated successful *in vitro* osteogenesis, including poly(lactic-co-glycolic acid) (PLGA) scaffolds (Shi *et al*., 2010; Kim *et al*., 2005-2), electrospun polycaprolactone (PCL) nanofibers (Martins *et al*., 2010) and poly(ethylene glycol) (PEG)-based hydrogel (Nuttelman *et al*., 2006). The unique material properties of silk (including

its slow degradation and mechanical strength) make it an excellent scaffold for bone tissue engineering (Wang *et al*., 2006). Dexamethasone is also soluble in alcohol, with limited aqueous solubility, making it a good candidate for a silk-based sustained release delivery. It was hypothesized that scaffolds loaded with dexamethasone and seeded with hMSCs and cultured in dexamethasone-absent media would exhibit greater osteogenic differentiation than unloaded control scaffolds.

6.2.2. Materials and methods

6.2.2.1. Materials

Cocoons of *Bombyx mori* silkworm silk were purchased from Tajima Shoji Co., LTD (Sumiyoshicho, Naka-ku, Yokohama, Japan). Dexamethasone was purchased from Sigma Aldrich (St. Louis, MO).

6.2.2.2. Preparation and dexamethasone loading of porous scaffolds

Aqueous-derived silk fibroin scaffolds were prepared as previously described (Sofia *et al*., 2001). Briefly, 4 g of granular NaCl (particle size 600-710 microns) was added slowly to 2 mL of 8% (w/v) silk fibroin solution in cylindrical Teflon container. The containers were covered and left at room temperature for 24 hours, then immersed in water to leech the NaCl for approx. 48 hours. Scaffolds were punched out with a 6 mm biopsy punch and cut to 4 mm height. To load scaffolds with dexamethasone, dried 6 mm x 4 mm scaffolds were immersed in 10 mL of 0.025 mg/mL dexamethasone in methanol for 24 hours. Control scaffolds were immersed in methanol for 24 hours.

For release studies, dexamethasone scaffolds were prepared by soaking in 10 mL of 25 mg/mL dexamethasone in methanol. A higher loading concentration was used in order to achieve detectable release concentrations, but studies have demonstrated that loading scales linearly with initial loading concentration (data not shown), so it was anticipated that these scaffolds would accurately reflect release behavior of the sponges used in tissue culture studies.

6.2.2.3. Dexamethasone loading and release study

To determine drug release, scaffolds were immersed in 1 mL of PBS and incubated at 37^{o}C. At desired time points, the buffer was removed and replaced with fresh buffer. The amount of released dexametheasone was determined using UV-Vis spectroscopy at 266 nm. The amount of released compound in each sample was summed with the amounts at each previous time point and divided by the total amount to obtain cumulative release values. Four samples were tested per release buffer type (n=4) and each sample was assayed in triplicate.

Total dexamethasone loading was determined by dissolving silk scaffolds in a 0.1 mg/mL proteinase k solution overnight. Dexamethasone content was determined by measuring absorbance at 266 nm.

6.2.2.4. Scaffold seeding and 3D culture

Human mesenchymal stem cells (hMSCs) were isolated and cultured as described above (6.1.2.4). Passage 4 hMSCs were seeded at a density of 1 x 10^6 hMSCs per scaffold as previously described (Meinel *et al.*, 2004). Briefly, each scaffold was pre-wetted by incubating for 30 minutes in DMEM supplemented with 200 U/mL penicillin, 200 μg/mL streptomycin, and 0.5 μg/mL fungizone, blotted dry, and seeded by adding 1 x 10^6 cells (p4 hMSC) suspended in

50 µL DMEM. The seeded constructs were placed in 24-well plates (one construct per well) and incubated at 37^{o}C for 2 h to allow cell attachment. To maintain moisture, 30 µl DMEM was added to each construct every 30 min. After 2 h, 1 mL of medium was added into each well. All scaffolds (dexamethasone-releasing and control) received dexamethasone-deficient osteogenic media consisting of α-MEM supplemented with 10% FBS, 0.1 mM nonessential amino acids, 0.5 mg/ml ascorbic acid-2-phosphate, 10 mM β-glycerolphosphate, 200 U/mL penicillin, 200 µg/mL streptomycin, and 0.5 µg/mL fungizone.

6.2.2.5. Biochemical analysis

To determine alkaline phosphatase activity, scaffolds were immersed 1mL 0.2% Triton X-100 and 5mM $MgCl_2$ solution, minced with microscissors, incubated for 30 min at room temperature and centrifuged for 3 minutes at 1200 rpm. Alkaline phosphatase (ALP) activity in the supernatant was determined using an ALP assay kit (Stanbio Laboratory, Boerne, TX) according to the protocol of the manufacturer. To determine total calcium content, calcium was extracted by immersing the scaffolds in 1 mL 5% trichloroacetic acid, mincing the scaffolds with microscissors and centrifuging for 3 minutes at 1200 rpm. Calcium content was determined using a Total Calcium assay kit (Stanbio Laboratory, Boerne, TX) according to the protocol of the manufacturer. To determine DNA content, scaffolds were immersed 1mL 0.2% Triton X-100 and 5mM $MgCl_2$ solution and minced with microscissors. DNA content was measured using the PicoGreen Assay (Molecular Probes, Eugene, OR), according to the protocol of the manufacturer. Samples were assayed at week 2 and week 4.

6.2.2.6. Histology

After 4 weeks in culture, samples were washed in PBS and fixed in 10% neutral buffered formalin, dehydrated through a series of graded alcohols, embedded in paraffin and sectioned at 5 µm thickness. Calcium staining was performed according to von Kossa.

6.2.3. Results

6.2.3.1. Dexamethasone release from porous silk sponges

Total dexamethasone loading in the release study scaffolds was found to be approx. 30 µg per scaffold (scaffold loading for the cell culture study is assumed to be approx. 0.03 µg per scaffold or 30 ng per scaffold).

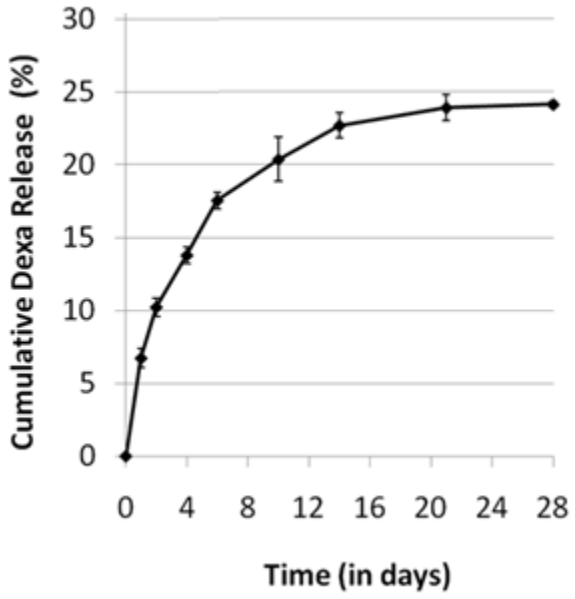

Figure 6.6. Cumulative dexamethasone release from porous silk scaffolds. N=4, error bars represent standard deviations.

Dexamethasone release is sustained approximately 21 days. After 21 days, no additional release is detected. Cumulative release after 21 days is slightly less than 25% of the total drug

load. Further work is needed to confirm, but this suggests approximately 75% of the total drug load is adsorbed to the silk and cannot freely diffuse into the release buffer.

6.2.3.2. Bioactivity of dexamethasone-releasing porous silk sponges

Results of biochemical assays of dexamethasone releasing scaffolds compared with control scaffolds are shown in Figure 6.7

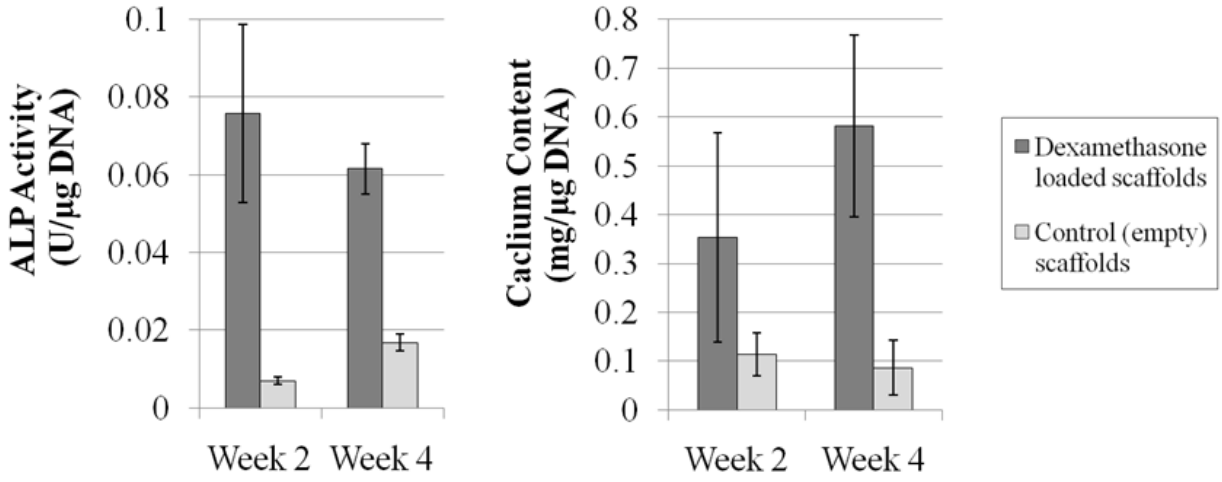

Figure 6.7. Alkaline phosphate (ALP) and calcium content for dexamethasone releasing and control silk sponges at 2 and 4 weeks. N=6, error bars represent standard deviations.

Scaffolds that are loaded with dexamethasone exhibit increased ALP activity and increased calcium deposition at week 2 and week 4. The difference in ALP activity between cultures seeded on control scaffolds and dexamethasone releasing scaffolds was found to be statistically significant (two-tailed t-test, df = 10, $p<0.001$). The difference in calcium deposition between cultures seeded on control scaffolds and dexamethasone releasing scaffolds was not significant at week 2, but was statistically significant at week 4 (two-tailed t-test, df = 10, $p<0.001$).

Calcium deposition increases from week 2 to week 4, despite dexamethasone release exhaustion around day 14. This may be the result of dexamethasone adsorbed to the silk scaffold

that is not able to freely diffuse from the scaffold (approx. 75% of the total load) being released as the scaffold is degraded by the hMSCs. This is consistent with studies of bFGF release from silk scaffolds (Wongpanit *et al*., 2010) and the theory that tissues sequester growth factors, storing them in the extracellular matrices (ECM) to protect their potency and deliver them on demand (Wenk *et al*., 2010-1; Vlodavsky *et al*., 1991; Benoit and Anseth, 2005). Alternately, 14 days of dexamethasone exposure may be sufficient to induce osteogenic differentiation of the hMSCs. This is consistent with the hypothesis that even a transient exposure of stem cells to dexamethasone (particularly during the first week) may be effective in induction and maintenance of the osteoblastic phenotype (Martins *et al*., 2010). Further studies with scaffolds loaded with fluorescein-labeled dexamethasone and proteinase-induced degradation are needed to assess the fate of the unreleased dexamethasone. Future work must also include comparison studies of cells cultured on dexamethasone-releasing scaffolds and cells cultured on silk scaffolds in media supplemented with dexamethasone.

6.2.3.3. Histology

Histology sections of dexamethasone-releasing scaffolds seeded with hMSCs and cultured for 4 weeks in dexamethasone-absent media are shown in Figure 6.8.

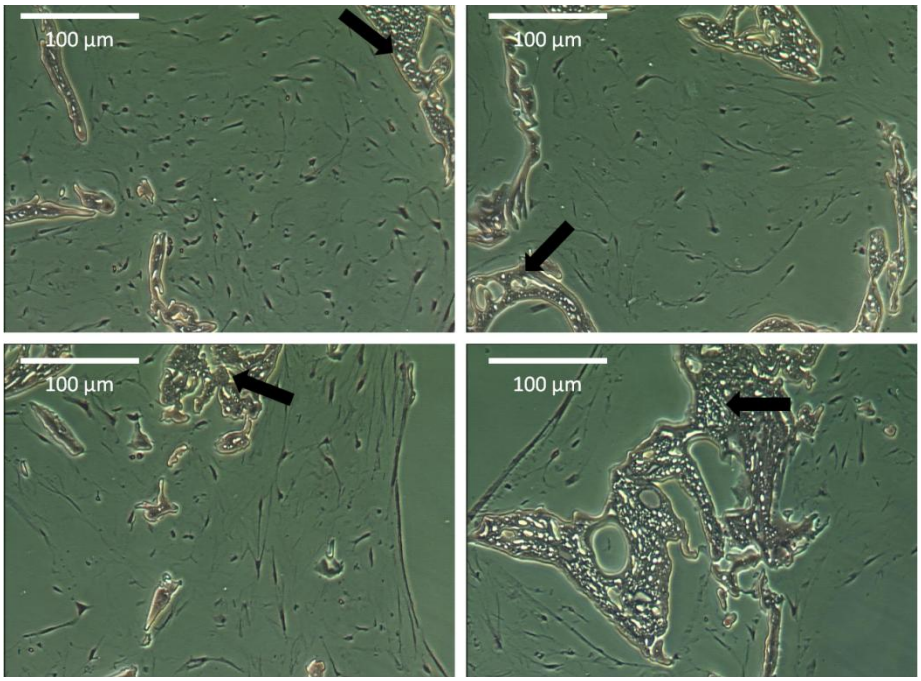

Figure 6.8. Histology sections of hMSCs cultured on dexamethasone releasing 3D porous silk scaffolds after 4 weeks in culture. Scale bars = 100 µm. Solid black arrows = remaining scaffold.

Calcium deposition (which would be indicated by black staining) is not apparent at 4 weeks (this time point may be too early to observe calcium deposition (Kim *et al.*, 2007)). However, histology does show that seeded hMSCs are uniformly distributed and fill the scaffold pores, suggesting the silk scaffolds provide sufficient support for cell growth.

6.2.4. Conclusions

These studies demonstrated that dexamethasone loaded silk sponges are able to enhance the osteogeneic differentiation of hMSCs seeded in 3D. These scaffolds were able to induce osteogenesis *in vitro* without BMP2 or dexamethasone provided in soluble form in the media (as measured by increased ALP activity and increased calcium deposition compared with control scaffolds). In addition to the biochemical analysis, histology demonstrated even cell distribution within the scaffold pores, demonstrating that dexamethasone-loaded silk scaffolds are able to

function both as a support for cell attachment, proliferation and differentiation as well as a carrier to release bioactive signaling molecules.

Note that some of the strategies for adenosine delivery described in previous chapters may also have utility in future tissue engineering applications. Adenosine has been found to increase glial cell line-derived neurotrophic factor (GDNF) production by astrocytes (Yamagata et al., 2007), which could have therapeutic potential in the treatment of peripheral nerve injury and neurodegenerative disorders (Willerth and Sakiyama-Elbert, 2007). Additionally, adenosine has been shown to downregulate cellular metabolic demands (Buck, 2004; Staples and Buck, 2009), which could potentially improve the survival rates of larger tissue implants by reducing their oxygen and nutrient needs until the requisite host vasculature is established.

7. Conclusion and Future Directions

Silk fibroin possesses unique properties that are particularly well suited to meet the unmet clinical need for controlled, sustained release from full degradable implants. In this thesis we demonstrate the controllability and versatility of silk based drug delivery systems. A thorough investigatation of the basic material features involved in small molecule diffusion from silk encapsulated reservoirs allowed us to achieve precise control of release behavior through manipulation of the implant characteristics. Zero-order release is observed, suggesting these tunable implants will be able to maintain therapeutic drug concentrations within narrow windows, maximizing therapeutic efficacy and safety.

We also demonstrate how use of modeling informs our understanding of the system, to the point where we were able to develop an integrated model that accurately predicted the results of path length and degumming time. This precise, consistent control of release behavior is significant in that it represents a drug delivery system that can be customized to meet the specific demands of a target application. The model presented is drug-specific, but similar models could easily be developed for other small molecules using the approach described here as a template. This would reduce the amount of empirical, trial-and-error data required to achieve target release kinetics. We were able to develop an accurate model from a relatively small amount of initial data (path length versus volume of silk hydrogel/mass of silk coating, diffusion coefficient versus degumming time, and release behavior of adenosine from reservoirs of known path length and known degumming time).

It is worth noting that the model tested describes one of the simplest possible systems, and predictions will become more complicated for larger drugs and proteins, which may not be able to freely diffuse from the silk and will rely on a combination of degradation and diffusion.

Preliminary data was presented on the relationship between release and degradation and strategies for controlling degradation via manipulation of the material properties and controlled release of proteinase inhibitors to reduce local degradation and proteolytic enzymes to increase local degradation. However, substantial future work will need to be done to understand the complex relationships between material properties, diffusion, degradation and drug kinetics. Investigations of the proteolytic degradation at various implantation sites and development of consistent *in vitro* models to represent these sites will be especially important.

Future work will also include expanding silk based drug delivery to other clinical applications which have shown promise in preliminary studies, including delivery of analgesics, vaccines and chemotherapy drugs. The applications presented in this thesis demonstrate the diversity of material formats available for therapeutic applications and provide promising *in vitro* and *in vivo* data. Studies of adenosine delivery for epilepsy are particularly encouraging, as they demonstrate good agreement between *in vitro* release data and *in vivo* therapeutic efficacy (dose dependence, comparable time frames, etc.). We anticipate that the ever-expanding biomaterial "tool kit" silk provides will eventually allow the simultaneous optimization of implant structure, material properties and drug release behavior that is needed to maximize the cost-efficiency, convenience, efficacy and safety of many new and existing therapeutics, especially those which cannot be delivered via traditional administration approaches.

8. References

Abletshauser CB, Schneider R, Rupprecht H. Film coating of pellets with insoluble polymers obtained in situ crosslinking in the fluidized bed. J Control Release 1993;21:149-156.

Acharya G, Park K. Mechanisms of controlled drug release from drug-eluting stents. Adv Drug Deliver Rev 2006;58:387-401.

Acharya C, Ghosh S, Kundu S. Silk fibroin protein from mulberry and non-mulberry silkworms: cytotoxicity, biocompatibility and kinetics of L929 murine fibroblast adhesion. J Mater Sci Mater Med 2008;19:2827–2836.

Acharya C, Kumar V, Sen R, Kundu S C. Performance evaluation of a silk protein-based matrix for the enzymatic conversion of tyrosine to L-DOPA. Biotechnol J 2008; 3:226–233.

Aigner T, Stöve J. Collagens—major component of the physiological cartilage matrix, major target of cartilage degeneration, major tool in cartilage repair. Adv Drug Deliv Rev 2003;55:1569-1593.

Altman GH, Horan RL, Martin I, Farhadi J, Stark PRH, Volloch V, Richmond JC, Vunjak-Novakovic G, Kaplan DL. Cell differentiation by mechanical stress. FASEB J 2001;16:270-272.

Altman GH, Horan RL, Lu H, Moreau J, Martin I, Richmond JC, Kaplan DL. Silk matrix for tissue engineered anterior cruciate ligaments. Biomaterials 2002;23:4131–4141.

Altman GH, Diaz F, Jakuba C, Calabro T, Horan RL, Chen J, *et al*. Silk-based biomaterials. Biomaterials 2003;24:401–416.

Arai T, Freddi G, Innocenti R, Tsukada M. Biodegradation of *Bombyx mori* silk fibroin fibers and films. J Appl Polym Sci 2004;91:2383–2390.

Aslam S, Darouiche RO. Antimicrobial therapy for bone and joint infections. Curr Infect Dis Rep 2009;11:7-13.

Batyrbekov EO, Rukhina LB, Zhubanov BA. Drug delivery systems for tuberculosis treatment. Polym Int 1997;43:317-320.

Bauer AW, Perry DM, Kirby WMMM. Single disc antibiotic sensitivity testing of *Staphylococci*. Arch Int Med 1959;104:208-216.

Bayraktar O, Malay O, Özgarip Y, Batigün A. Silk fibroin as a novel coating material for controlled release of theophylline. Eur J Pharm Biopharm 2005;60:373–381.

Benedict RG, Schmidt WH, Coghill RD, Oleson PA. The stability of penicillin in aqueous solution. J Bacteriol 1945;49:85–95.

Benoit DSW, Anseth KS.Heparin functionalized PEG gels that modulate protein adsorption for hMSC adhesion and differentiation. Acta Biomaterialia 2005;1:461–470.

Bernstein, H-G. Proteases and Alzheimer's disease: present knowledge and emerging concepts of therapy. In: Lendeckel U, Hooper NM, editors. Proteases in the brain. New York: Springer, 2005.

Bessa PC, Balmayor ER, Azevedo HS, Nürnberger S, Casal SM, van Griensven M, Reis RL, Redl H. Silk fibroin microparticles as carriers for delivery of human recombinant BMPs physical characterization and drug release. J Tissue Eng Regen Med 2010-1;4:349-355.

Bessa PC, Balmayor ER, J. Hartinger, G. Zanoni, D. Dopler, A. Meinl, A. Banerjee, M. Casal, H. Redl, R.L. Reis, M. van Griensven. Silk fibroin microparticles as carriers for delivery of human recombinant bone morphogenetic protein-2: *in vitro* and *in vivo* bioactivity. Tissue Eng Part C Methods. 2010-2;16:937-945.

Beyer Jr. WF, Fridovich I. Characterization of a superoxide dismutase mimic prepared from desferrioxamine and MnO_2. Arch Biochem Biophys. 1989;271: 149-156.

Beynon R, Bond JS. Proteolytic enzymes: a practical approach. Oxford: Oxford University Press, 2001.

Bilati U, Allémann E, Doelker E. Strategic approaches for overcoming peptide and protein instability within biodegradable nano- and microparticles. Eur J Pharm Biopharm 2005;59:375–388.

Boison D, Scheurer L, Tseng JL, Aebischer P, Mohler H. Seizure suppression in kindled rats by intraventricular grafting of an adenosine releasing synthetic polymer. Exp Neurol 1999;160:164–174.

Boison D, Huber A, Padrun V, Deglon N, Aebischer P, Mohler H. Seizure suppression by adenosine-releasing cells is independent of seizure frequency. Epilepsia 2002;43(8):788–796.

Boison D. Adenosine kinase, epilepsy and stroke: mechanisms and therapies. Trends in Pharm Sci 2006;27**:**653-658.

Boison D. The adenosine kinase hypothesis of epileptogenesis, Prog Neurobiol 2008;84:249–262.

Boison D, Stewart KA. Therapeutic epilepsy research: From pharmacological rationale to focal adenosine augmentation. Biochem Pharmacol 2009;78:1428–1437.

Boison D, Chen J-F, Fredholm BB. Adenosine signaling and function in glial cells. Cell Death Differ 2010;17:1071-1082.

Boyle VJ, Fancher ME, Ross RW. Rapid, modified Kirby-Bauer susceptibility test with single, high-concentration antimicrobial disks. Antimicrob Ag Chemother 1973**;**3:418-424.

Brem H, Piantadosi S, Burger PC, Walker M, Selker R, Vick NA, Black K, Sisti M, Brem S, Mohr G, Muller P, Morawetz R, Schold SC. Placebo-controlled trial of safety and efficacy of intraoperative controlled delivery by bio- degradable polymers of chemotherapy for recurrent gliomas. Lancet 1995;345:1008–1012.

Brook, I. Topical review: brain abscess in children: microbiology and management. J Child Neurol 1995;10: 283-288.

Buck LT. Adenosine as a signal for ion channel arrest in anoxia-tolerant organisms. Comp Biochem Physiol B 2004;139:401–414.

Burrell MM. Enzymes of Molecular Biology. Totowa: Humana Press, 1994. p.271-276.

Cao Z, Chen X, Yao J, Huang L, Shao Z. The preparation of regenerated silk fibroin microspheres. Soft Matter, 2007;3:910–915.

Cao Y, Wang B. Biodegradation of silk biomaterials. Int J Mol Sci 2009;10:1514-1524.

Cacchio A, de Blasis E, de Siati P, Spacca G, Santilli V, de Paulis F. Effectiveness of treatment of calcific tendinitis of the shoulder by disodium EDTA. Arthritis & Rheum 2009;61:84–91

Cappello J, Crissman JW, Crissman M, Ferrari FA, Textor G, Wallis O, Whitledge JR, Zhou X, Burman D, Aukerman L, Stedronsk ER. In-situ self-assembling protein polymer gel systems for administration, delivery, and release of drugs. J Control Release 1998;53:105-117.

Castaneda-Agullom M, Del Castilla LM, Whitaker JR, Tappel AL. Effect of ionic strength on the kinetics of trypsin and alpha chymotrypsin. J Gen Physiol 1962;44:1103-1120.

Chadfield MS, Bojesen AM, Christensen JP, Juul-Hansen J, Saxmose Nielsen S, Bisgaard M. Reproduction of sepsis and endocarditis by experimental injection of chickens with *Streptococcus gallinaceus* and *Enterococcus hirae*. Avian Pathol. 2005;34:238-247.

Chang S, Dai Y, Kang B, Han W, Chen D. Fabrication of silk fibroin coated ZnSe:Mn^{2+} quantum dots under gamma-radiation and their magnetic properties. Solid State Commun 2009;149:1180-1183.

Chau NM, Rogers P, Aherne W, Carroll V, Collins I, McDonald E, Workman P, Ashcroft M. Identification of novel small molecule inhibitors of hypoxia-inducible factor-1 that differentially block hypoxia-inducible factor-1 activity and hypoxia-inducible factor-1alpha induction in response to hypoxic stress and growth factors. Cancer Res 2005;65:4918–4928.

Cheng SL, Yang JW, Rifas L, Zhang SF, Aviol LV. Differentiation of human bone marrow osteogenic stromal cells *in vitro*: induction of the osteoblast phenotype by dexamethasone. Endocrinology 1994;134**:** 277–286.

Cheema SK, Gobin AS, Rhea R, Lopez-Berestein G, Newman RA, Mathur AB. Silk fibroin mediated delivery of liposomal emodin to breast cancer cells. Int J Pharm 2007;341: 221–229.

Chen J, Minoura N, Tanioka A. Transport of pharmaceuticals through silk fibroin membrane. Polymer 1994;35:2853-2856.

Chen W, He J, Olson JJ, Lu DR. Direct intracerebral delivery of carboplatin from PLGA microspheres against experimental malignant glioma in rats. Drug Delivery 1998;5:101-110.

Chen J, Altman GH, Karageorgiou V, Horan R, Collette A, Volloch V, *et al*. Human bone marrow stromal cell and ligament fibroblast responses on RGD-modified silk fibers. J Biomed Mater Res A 2003;67:559–70.

Chen JL, Yin Z, Shen WL, Chen X, Heng BC, Zou XH, Ouyang HW. Efficacy of hESC-MSCs in knitted silk-collagen scaffold for tendon tissue engineering and their roles. Biomaterials 2010-1;31:9438-9451.

Chen B, Yin C, Cheng Y, Li W, Zhu-an Cao, Tianwei Tan. Using silk woven fabric as support for lipase immobilization: The effect of surface hydrophilicity/hydrophobicity on enzymatic activity and stability. Biomass Bioenerg. 2010-2; article in press.

Chintala SK, Tonn JC, Rao JS. Matrix metalloproteinases and their biological function in human gliomas. Int J Devl Neuroscience 1999;17:495-502.

Choi H-M, Bide M, Phaneuf M, Quist W, Logerfo F. Antibiotic treatment of silk to produce novel infection-resistant biomaterials. Text Res J 2004; 74; 333-342.

Danckwerts M, Fassih A. Implantable controlled release drug delivery systems: a review. Drug Dev Ind Pharm 1991;17:1465–1502.

Dang W, Davlau T, Ying P, Zhao Y, Nowotmk D, Clow CS, Tyler B, Brem H. Effects of GLIADEL® wafer initial molecular weight on the erosion of wafer and release of BCNU. J Control Release 1996;42:83-92.

Daroiche RO, Mansouri MD. *In vitro* activity and *in vivo* efficacy of antimicrobial-coated vascular grafts. Ann Vasc Surg. 2004;18:497-501.

Daugherty AL, Cleland JL, Duenas EM, Mrsny RJ. Pharmacological modulation of the tissue response to implanted polylactic-co-glycolic acid microspheres. Eur J Pharmacol Biopharm 1997;44**:**89– 102.
Daugherty AL, Mrsny RJ. Formulation and delivery issues for monoclonal antibody therapeutics. Adv Drug Deliv Rev 2006;58:686-706
Dehdashti AR, Muster M, Reverdi A, de Tribolet V, Ruefenacht DA. Preoperative silk suture embolization of cerebral and dural arteriovenous malformations. Neurosurg Focus. 2001;11:e6
Demura M, Asakura T, Kuroo T. Immobilization of biocatalysts with *Bombyx mori* silk fibroin by several kinds of physical treatment and its application to glucose sensors. Biosensors 1989;4:361-372.
Demura M, Asakura T. Porous membrane of Bombyx mori silk fibroin: structure characterization, physical properties and application to glucose oxidase immobilization. J Membrane Sci 1991;9:39-52.
Dinerman AA, Cappello J, Ghandehari H, Hoa SW .Solute diffusion in genetically engineered silk–elastinlike protein polymer hydrogels. J Control Release 2002;82:277-287.
De Paoli Lacerda SH, Ingber B, Rosenzweig N. Structure-release rate correlation in collagen gels containing fluorescent drug analogs. Biomaterials 2005;26:7164–7172.
Dorta M, Santoveña A, Llabrés M, Fariña JB. Potential applications of PLGA film-implants in modulating *in vitro* drugs release. Int J Pharm 2002;248:149-156.
Dunwiddie TV. Adenosine and suppression of seizures. Adv Neurol 1999;79:1001-1010.
Ellis MR, Kane KY. Lightening the lead load in children. Am Fam Physician 2000;62:545-54.
Englander L, Friedman A. Nitric oxide nanoparticle technology: a novel antimicrobial agent in the context of current treatment of skin and soft tissue infection. J Clin Aesthet Dermatol. 2010;3:45-50.
Enomoto S, Sumi M, Kajimoto K, Nakazawa Y, Takahashi R, Takabayashi C, Asakura T, Sata M. Long-term patency of small-diameter vascular graft made from fibroin, a silk-based biodegradable material. J Vas Surg 2010;51:155-164.
Fang J-Y, Chen J-P, Leu Y-L, Wang H-Y. Characterization and evaluation of silk protein hydrogels for drug delivery. Chem Pharm Bull 2006;54:156-162.
Farris W, Mansourian S, Chang Y, Lindsley L, Eckman EA, Frosch MP, Eckman CB, Tanzi RE, Selkoe DJ, Guénette S. Insulin-degrading enzyme regulates the levels of insulin, amyloid β-protein, and the β-amyloid precursor protein intracellular domain *in vivo*. Proc Natl Acad Sci USA 2003;100:4162-4167.
Farris W, Mansourian S, Leissring MA, Eckman EA, Bertram L, Eckman CB, Tanzi RE, Selkoe DJ. Partial loss-of-function mutations in insulin-degrading enzyme that induce diabetes also impair degradation of amyloid β –protein. Am J Pathol 2004;164:1425–1434.
Fitch MT, Manthey DE, McGinnis HD, Nicks BA, Pariyadath M: Abscess incision and drainage. N Engl J Med. 2007;357:e20
Fleming, A. On the antibacterial action of cultures of a penicillium with special reference to their use in the isolation of B. influenza. Brit J Exp Pathol 1929; 3: 226-236.
Friess W. Collagen – biomaterial for drug delivery. Eur J Pharm Biopharm 1998;45:113–136.
Friess W, Zhou W, Groves MJ. *In vivo* activity of collagen matrices containing PS1, an anti-neoplastic glycan, against murine sarcoma cells. Pharm Sci 1996;2:1–4.
Fu Y, Kao WJ. Drug release kinetics and transport mechanisms of non-degradable and degradable polymeric delivery systems. Expert Opin. Drug Deliv. 2010;7:429-444.

Fung LK, Ewend MG, Sills A, Sipos EP, Thompson R, Watts M, Colvin OM, Brem H, Saltzman WM. Pharmacokinetics of interstitial delivery of carmustine, 4-hydroperoxycyclophosphamide, and paclitaxel from a biodegradable polymer implant in the monkey brain. Cancer Res 1998;58:672–684.

Furia T. EDTA in foods- a technical review. Food Technol 1964;18:1874-1882.

Gerding DN, Kozak AJ, Peterson LR, Hall WH. Failure of single doses of cefazolin and cefamandole to penetrate experimental chronic *Escherichia coli* abdominal abscesses. Antimicrob agents ch 1980;17:1023-1029.

Girish KS, Kemparaju K. Inhibition of *Naja naja* venom hyaluronidase: role in the management of poisonous bite. Life Sci 2006;78:1433-1440.

Gobin, A.S., Rhea, R., Newman, R.A., Mathur, A.B., 2006. Silk-fibroin-coated liposomes for long-term and targeted drug delivery. Int J Nanomed. 1, 81–87.

Gouder N, Fritschy JM, Boison D. Seizure suppression by adenosine A1 receptor activation in a mouse model of pharmacoresistant epilepsy. Epilepsia 2003;44:877–85

Gracia RC, Snodgrass WR. Lead toxicity and chelation therapy. Am J Health Syst Pharm. 2007;64:45-53.

Graven-Nielsen T, Jansson Y, Segerdahl M, Kristensen JD, Mense S, Arendt-Nielsen L, Sollevi A. Experimental pain by ischaemic contractions compared with pain by intramuscular infusions of adenosine and hypertonic saline. Eur J Pain 2003;7:93-102.

Greish K, Araki K, Li D, O'Malley Jr. BW, Dandu R, Frandsen J, Cappello J, Ghandehari H. Silk-elastinlike protein polymer hydrogels for localized adenoviral gene therapy of head and neck tumors, Biomacromolecules 2009;10:2183–2188.

Gupta RK, Chang AC, Siber GR. Biodegradable polymer microspheres as vaccine adjuvants and delivery systems. Dev Biol Stand 1998;92**:** 63–78.

Gustafson J, Greish K, Frandsen J, Cappello J, Ghandehari H. Silk-elastinlike recombinant polymers for gene therapy of head and neck cancer: from molecular definition to controlled gene expression. J Control Release 2009;140:256–261.

Gustafson JA, Ghandehari H. Silk-elastinlike protein polymers for matrix-mediated cancer gene therapy. Adv Drug Deliv Rev 2010;62:1509-1523.

Güttinger M, Padrun V, Pralong W, Boison D. Seizure suppression and lack of adenosine A1 receptor desensitization after focal long-term delivery of adenosine by encapsulated myoblasts. Exp Neurol 2005;193:53–64.

Gutman RL, Peacock G, Lu DR. Targeted drug delivery for brain cancer treatment. J Control Release 2000;65:31–41.

Guziewicz N, Best A, Perez-Ramirez B, Kaplan DL. Lyophilized silk fibroin hydrogels for the sustained local delivery of therapeutic monoclonal antibodies. Biomaterials 2011;in press

Haider M, Megeed Z, Ghandehari H. Genetically engineered polymers: status and prospects for controlled release. J Control Release 2004;95:1–26.

Han G, Martinez LR, Mihu MR, Friedman AJ, Friedman JM, Nosanchuk JD. Nitric oxide releasing nanoparticles are therapeutic for S*taphylcoccus aureus* abscesses in a murine model of infection. PLoS One. 2009;4:e7804

Hanawa T, Watanabe A, Tsuchiya T, Ikoma R, Hidaka M, Sugihara M. New oral dosage form for elderly patients. II. release behavior of benfotiamine from silk fibroin gel. Chem Pharm Bull 1995;43:872-876.

Hardy JG, Römer LM, Scheibel TR. Polymeric materials based on silk proteins. Polymer 2008;49:4309–4327.

Hardy JG, Scheibel TR. Composite materials based on silk proteins. Prog Poly Sci 2010;35:1093-1115.
Heller, J and Hoffman, AS. Drug Delivery Systems. In: Ratner, B.D., Hoffman AS, Schoen, FJ, Lemons, JE, editors. Biomaterials science: an introduction to materials in medicine. New York: Elsevier, 2004
Hemming ML, Patterson M, Reske-Nielsen C, Lin L, Isacson O, Selkoe DJ. Reducing amyloid plaque burden via ex vivo gene delivery of an Aβ-degrading protease: a novel therapeutic approach to Alzheimer's disease PLoS Med 2007;4:1405-1416.
Hetrick EM, Schoenfisch MH. Reducing implant-related infections: active release strategies. Chem Soc Rev 2006;35:780–789.
Hewitt CW, Black KS. Overview of a 10-year experience on methods and compositions for inducing site-specific immunosuppression with topical immunosuppressants. Transplant Proc 1996;28:922–923.
Hicker T, Kreutzer D, Burgess DJ, Moussy F. Dexamethasone/PLGA microspheres for continuous delivery of an anti-inflammatory drug for implantable medical devices. Biomaterials 2002;23:1649-1656.
Higuchi T. Mechanism of sustained-action medication. Theoretical analysis of rate of release of solid drugs dispersed in solid matrices. J Pharm Sci 1963;52:1145-1149.
Higuchi M, Iwata N, Saido TC. Understanding molecular mechanisms of proteolysis in Alzheimer's disease: Progress toward therapeutic interventions. *Biochimica et Biophysica Acta* **1751** (2005) 60–67.
Hines DJ, Kaplan DL. Mechanisms of Controlled Release from Silk Fibroin Films. Biomacromolecules 2011;in press.
Hino T, Shimabayashi S, Nakai A. Silk microspheres prepared by spray-drying of an aqueous system. Pharm Pharmacol Commun 2000;6:335–339.
Hino T, Tanimoto M, Shimabayashi S. Change in secondary structure of silk fibroin during preparation of its microspheres by spray-drying and exposure to humid atmosphere. J Colloid Interf Sci 2003;266:68–73.
Hochberg F, Pruitt A. Assumptions in the radiotherapy of glioblastoma. Neurology 1980;30: 907-911.
Hofmann S, Wong Po Foo CT, Rossetti F, Textor M, Vunjak-Novakovic G, Kaplan DL, Merkle HP, Meinel L. Silk fibroin as an organic polymer for controlled drug delivery. J Control Release 2006;111: 219–227.
Holy CE, Cheng C, Davies JE, Shoichet MS. Optimizing the sterilization of PLGA scaffolds for use in tissue engineering. Biomaterials 2001;22:25-31
Horan RL, Antle K, Collette AL, Wang Y, Huang J, Moreau JE, Volloch V, Kaplan DL, Altman GH. *In vitro* degradation of silk fibroin. Biomaterials 2005;26:3385–3393
Horan RL, Collette AL, Lee C, Antle K, Chen J, Altman GH. Yarn design for functional tissue engineering. J Biomech 2006;39:2232–2240.
Hu X, Kaplan D, Cebe P. Determining beta-sheet crystallinity in fibrous proteins by thermal analysis and infrared spectroscopy. Macromolecules 2006;39:6161-6170.
Hu X, Lu Q, Sun L, Cebe P, Wang X, Zhang X, Kaplan DL. Biomaterials from ultrasonication-induced silk fibroin−hyaluronic acid hydrogels. Biomacromolecules 2010; 11:3178-3188.
Hu X, Wang X, Rnjak J, Weiss AS, Kaplan DL, Biomaterials derived from silk-tropoelastin protein systems. Biomaterials 2010;31:8121-813.

Huang LE, Gu J, Schau M, Bunn HF. Regulation of hypoxia-inducible factor 1alpha is mediated by an O_2-dependent degradation domain via the ubiquitin-proteasome pathway. Proc Natl Acad Sci USA 1998;5:7987–7992.

Huang F, Sun L, Zheng J. *In vitro* and *in vivo* characterization of a silk fibroin-coated polyester vascular prosthesis. Artif. Organs 2008;32:932–941

Huber A, Padrun V, Deglon N, Aebischer P, Mohler H, Boison D. Grafts of adenosine-releasing cells suppress seizures in kindling epilepsy. Proc Natl Acad Sci USA 2001;98:7611–7616.

Ihedioha JI, Ochiogu IS, Ihedioha TE. Co-administration of Na-EDTA and diminazene aceturate (DA). J Comp Path 2007;136: 206-211.

Imsombut T, Srisuwan Y, Srihanam P, Baimark Y. Genipin-cross-linked silk fibroin microspheres prepared by the simple water-in-oil emulsion solvent diffusion method. Powder Technol 2010;203:603-608.

Ivan M, Kondo K, Yang H, Kim W, Valiando J, Ohh M, Salic A, Asara JM, Lane WS, Kaelin WG Jr. HIF alpha targeted for VHL-mediated destruction by proline hydroxylation: implications for O_2 sensing. Science 2001; 292:464–468.

Iwata N, Mizukami H, Shirotani K, Takaki Y, Muramatsu S, Lu B, Gerard NP, Gerard C, Ozawa K, Saido TC. Presynaptic localization of neprilysin contributes to efficient clearance of amyloid-β peptide in mouse brain. J Neurosci 2004;24**:** 991–998.

Jäger M, Hernigou P, Zilkens C, Herten M, Fischer J, Krauspe R. Cell therapy in bone-healing disorders. Orthopade 2010; 39:449-462.

Jain RA. The manufacturing techniques of various drug loaded biodegradable poly(lactide-*co*-glycolide) (PLGA) devices. Biomaterials 2000;21:2475-2490.

Jain RK, Au P, Tam J, Duda DG, Fukumura D. Engineering vascularized tissue. Nat Biotechnol 2005;23:821-823.

Jeong J, Hur W. Even-numbered peptides from a papain hydrolysate of silk fibroin. J Chromatogr 2010;B878**:**836–840.

Jiang P, Liu H, Wang C, Wu L, Huang J, Guo C. Tensile behavior and morphology of differently degummed silkworm (*Bombyx mori*) cocoon silk fibres. Mater Lett 2006;60:919-925.

Jin H-J, Chen J, Karageorgiou V, Altman GH, Kaplan DL. Human bone marrow stromal cell responses on electrospun silk fibroin mats. Biomaterials 2004;25:1039–1047.

Jin H-J, Park J, Karageorgiou V, Kim UJ, Valluzzi R, Cebe P, Kaplan DL. Water-insoluble silk films with reduced β-sheet content. Adv Funct Mater 2005;15:1241–1247.

Kaplan DL, Mello CM, Arcidiacono, Fossey S, Senecal K, Muller W. Silk. In: McGrath K, Kaplan D, editors. Protein-Based Materials. Boston: Birkhäuser, 1997

Karageorgiou V, Meinel L, Hofmann S, Malhotra A, Volloch V, Kaplan DL. Bone morphogenetic protein-2 decorated silk fibroin films induce osteogenic differentiation of human bone marrow stromal cells. J Biomed Mater Res A 2004;71:528-537.

Katayama H, Issiki M, Yoshitomi H. Application of fibroin in controlled release tablets containing theophylline. Biol Pharm Bull 2000;10:1229-34.

Kennedy P, Brammah S, Willis E. Burns, biofilm and a new appraisal of burn wound sepsis. Burns 2010;36:49-56.

Kikuchi J, Mitsui Y, Asakura T, Hasuda K, Araki H, Owaku K. Spectroscopic investigation of tertiary fold of staphylococcal protein A to explore its engineering application. Biomaterials 1999;20:647-654.

Kim U-J, Park J, Li C, Jin H-J, Valluzzi R, Kaplan DL. Structure and properties of silk hydrogels. Biomacromolecules 2004;5:786-792.
Kim UJ, Park J, Kim HJ, Wada M, Kaplan DL. Three dimensional aqueous-derived biomaterial scaffolds from silk fibroin. Biomaterials 2005-1;26:2775-2785.
Kim H, Suh H, Jo SA, Kim HW, Lee JM, Kim EH, Reinwald Y, Park S-H, B-H, Jo I. *In vivo* bone formation by human marrow stromal cells in biodegradable scaffolds that release dexamethasone and ascorbate-2-phosphate. Biochem Bioph Res Co 2005-2;332:1053–1060.
Kim HJ, Kim U-J, Leisk GG, Bayan C, Georgakoudi I, Kaplan DL. Bone regeneration on macroporous aqueous-derived silk 3-D scaffolds. Macromol Biosci 2007;7:643-655.
Kincl FA, Ciaccio LA. Suppression of immune responses by progesterone. Endocrinol Exp 1980;14: 27–33.
Kluge JA, Rosiello NC, Leisk GG, Kaplan DL, AL Dorfmann. The consolidation behavior of silk hydrogels. J Mech Behav Biomed Mater 2010;3:278-89.
Kundu J, Chung YI, Kim YH, Tae G, Kundu SC. Silk fibroin nanoparticles for cellular uptake and control release. Int J Pharm 2010;388:242-50.
Kurioka A, Yamazaki M, Hirano H. Primary structure and possible functions of a trypsin inhibitor of Bombyx mori. Eur J Biochem 1999;259:120-126.
Kurisawa M, Chung JE, Yang YY, Gao SJ, Uyama H. Injectable biodegradable hydrogels composed of hyaluronic acid-tyramine conjugates for drug delivery and tissue engineering. Chem Commun 2005;4312-4314
Lamas GA, Hussein SJ. EDTA chelation therapy meets evidence-based medicine. Complemen Ther Clin Pract 2006;12:213–215.
Lambert RJW, Hanlon GW, Denyer SP. The synergistic effect of EDTA/antimicrobial combinations on *Pseudomonas aeruginosa.* J Appl Microbiol 2004;96:244–253.
Lammel AS, Hu X, Park S-H, Kaplan DL, Scheibel TR. Controlling silk fibroin particle features for drug delivery. Biomaterials 2010;31:4583-4591.
Langer R. Invited review: polymeric delivery systems for controlled drug release. Chem Eng Commun 1980;6:1-48
Langer RS, Peppas NA. Present and future applications of biomaterials in controlled drug delivery systems. Biomaterials 1981;2:201-214.
Lavelle EC, Yeh MK, Coombes AG, Davis SS. The stability and immunogenicity of a protein antigen encapsulated in biodegradable microparticles based on blends of lactide polymers and polyethylene glycol. Vaccine 1999;17:512–529.
Lawrence BD, Cronin-Golomb M, Georgakoudi I, Kaplan DL, Omenetto FG. Bioactive Silk Protein Biomaterial Systems for Optical Devices. Biomacromolecules 2008;9:1214–1220
Leal-Egaña A, Scheibel T. Silk-based materials for biomedical applications. Biotechnol Appl Biochem 2010;55:155–167.
Lebovits AH, Strain JJ, Messe MR, Schleifer SJ, Tanaka JS, Bhardwaj S. Patient noncompliance with self-administered chemotherapy. Cancer 1990;65:17-22.
Leissring MA, Farris W, Chang AY, Walsh DM, Wu X, Sun X, Frosch MP, Selkoe DJ. Enhanced proteolysis of β-amyloid in APP report transgenic mice prevents plaque formation, secondary pathology, and premature death. *Neuron* 2003;40: 1087–1093.
Lesniak MS, Upadhyay U, Goodwin R, Tyler B, Brem H. Local delivery of doxorubicin for the treatment of malignant brain tumors in rats. Anticancer Res 2005;25:3825–3831.

Li M, Ogiso M, Minoura N. Enzymatic degradation behavior of porous silk fibroin sheets. Biomaterials 2003;24:357–365.
Li C, Vepari C, Jin H-J, Kim HJ, Kaplan DL. Electrospun silk-BMP-2 scaffolds for bone tissue engineering. Biomaterials 2006;27: 3115–3124.
Li T, Steinbeck JA, Lusardi T, Koch P, Lan JQ, Wilz A, Segschneider M, Simon RP, Brüstle, Boison D.. Suppression of kindling epileptogenesis by adenosine releasing stem cell-derived brain implants. Brain 2007;130:1276–88.
Li T, Ren G, Lusardi T, Wilz A, Lan JQ, Iwasato T, Itohara S, Simon RP, Boison D. Adenosine kinase is a target for the prediction and prevention of epileptogenesis in mice. J Clin Invest 2008;118:571–82.
Licastro F, Davis LJ, Morini MC, Cucinotta D, Savorani G. Cerebrospinal fluid of patients with senile dementia of Alzheimer's type shows an increased inhibition of alpha-chymotrypsin. Alzheimer Dis Assoc Disorder 1994;8:241-249.
Lieb WR, Stein WD, Biological membranes behave as non-porous polymeric sheets with respect to the diffusion of non-electrolytes. Nature 1969;224:240-243.
Lin W-J, Lee H-G. Design of a microporous controlled delivery system for theophylline tablets J Control Release 2003;89:179–187.
Liu H, Fan H, Wang Y, Toh SL, Goh JCH. The interaction between a combined knitted silk scaffold and microporous silk sponge with human mesenchymal stem cells for ligament tissue engineering. Biomaterials 2008;29:662–674.
Liu X-Y, Zhang C-C, Xu W-L, Ouyang C. Controlled release of heparin from blended polyurethane and silk fibroin film. Materials Letters 2009;63: 263–265.
Lovett M, Cannizzaro C, Daheron L, Messmer B, Vunjak-Novakovic G, Kaplan DL. Silk fibroin microtubes for blood vessel engineering. Biomaterials 2007;28:5271–5279.
Lu TK, Collins JJ. Dispersing biofilms with engineered enzymatic bacteriophage. PNAS 2007;104:11197-11202.
Lu S, Wang X, Lu Q, Hu X, Uppal N, Omenetto FG, Kaplan DL. Stabilization of enzymes in silk films. Biomacromolecules 2009;10:1032–1042.
Lu Q, Wang X, Hu X, Cebe P, Omenetto F, Kaplan DL. Stabilization and release of enzymes from silk films. Macromol Biosci 2010-1;10:359–368.
Lu Q, Hu X, Wang X, Kluge JA, Lu S, Cebe P, Kaplan DL. Water-insoluble silk films with silk I structure. Acta Biomaterialia 2010-2;6:1380–1387.
Liu Y, Guan H, Beckett TL, Juliano MA, Juliano L, Song ES, Chow KM., Murphy MP, Hersh LB. *In vitro* and *in vivo* degradation of Aβ peptide by peptidases coupled to erythrocytes. Peptides 2007;28: 2348-2355.
Luo Y, Kirker KR, Prestwich GD. Cross-linked hyaluronic acid hydrogel films: new biomaterials for drug delivery. J Control Release 2000;69:169 –184.
Madduri S, Papaloïzos M, Gander B. Trophically and topographically functionalized silk fibroin nerve conduits for guided peripheral nerve regeneration. Biomaterials 2010;31:2323–2334.
Makaya K, Terada S, Ohgo K, Asakura T. Comparative study of silk fibroin porous scaffolds derived from salt/water and sucrose/hexafluoroisopropanol in cartilage formation. J Biosci Bioeng 2009;108:68–75.
Mandal BB, Kundu SC. Calcium alginate beads embedded in silk fibroin as 3D dual drug releasing scaffolds. Biomaterials 2009;30:5170–5177.

Mandal BB, Mann JK, Kundu SC. Silk fibroin/gelatin multilayered films as a model system for controlled drug release. Eur J Pharm Sci 2009;37:160-71

Maniscalco BS, Taylor KA. Calcification in coronary artery disease can be reversed by EDTA–tetracycline long-term chemotherapy. Pathophysiology 2004;11:95–101.

Mathur AB, Gupta V. Silk fibroin-derived nanoparticles for biomedical applications. Nanomedicine 2010;5:807-820.

Matsumoto A, Chen J, Collette AL, Kim U-J, Altman GH, Cebe P, Kaplan DL. Mechanisms of silk fibroin sol-gel transitions. J Phys Chem B 2006;110:21630-21638.

Marr RA, Rockenstein E, Mukherjee A, Kindy MS, Hersh LB, Gage FH, Verma IM, Maslia E. Neprilysin gene transfer reduces human amyloid pathology in transgenic mice. J Neurosci 2003;23:1992-1996.

Martins A, Duarte ARC, Faria S, Marques AP, Reis RL, Neves NM. Osteogenic induction of hBMSCs by electrospun scaffolds with dexamethasone release functionality Biomaterials 2010;31:5875-5885.

Maysinger D, Morinville A. Drug delivery to the nervous system. Trends Biotechnol 1997;15:410-418.

Megeed Z, Haider M, Li D, O'Malley Jr. BW, Cappello J, Ghandehari H. *In vitro* and *in vivo* evaluation of recombinant silk-elastinlike hydrogels for cancer gene therapy. J Control Release 2004;94: 433– 445.

Menei P, Daniel V, Montero-Menei C, Brouillard M, Pouplard-Barthelaix A, Benoit JP. Biodegradation and brain tissue reaction to poly(D,L-lactide-co-glycolide) Biomaterials 1993;14: 470-478

Meinel L, Karageorgiou V, Fajardo R, Snyder B, Shinde-Patil V, Zichner L, Kaplan DL, Langer R, Vunjak-Novakovic G. Bone tissue engineering using human mesenchymal stem cells: effects of scaffold material and medium flow. Ann Biomed Eng 2004;32:112–22

Meinel L, Hofmann S, Karageorgiou V, Zichner L, Langer R, Kaplan D, Vunjak-Novakovic G. Engineering cartilage-like tissue using human mesenchymal stem cells and silk protein scaffolds. Biotechnol Bioeng 2004;88:379-391.

Meinel L, Hofmann S, Karageorgiou V, Kirker-Head C, McCool J, Gronowicz G, Zichner L, Langer R, Vunjak-Novakovic, Kaplan DL.The inflammatory responses of silk films *in vitro* and *in vivo*. Biomaterials 2005;26:147-155.

Minoura N, Tsukada M, Nagura M. Physico-chemical properties of silk fibroin membrane as a biomaterial. Biomaterials 1990;11:430-434

Miller BC, Eckman EA, Sambamurti K, Dobbs N, Chow KM., Eckman CB, Hersh LB, Thiele DL. Amyloid--β peptide levels in brain are inversely correlated with insulysin activity levels *in vivo*. Proc Natl Acad Sci USA 2003;100:6221-6226.

Miners JS, Baig S, Palmer J, Palmer LE, Kehoe PG, Love S. Aβ-degrading enzymes in Alzheimer's disease. Brain Pathology 2008;18: 240–252.

Mittal G, Sahana DK, Bhardwaj V, Ravi Kumar MNV. Estradiol loaded PLGA nanoparticles for oral administration: effect of polymer molecular weight and copolymer composition on release behavior *in vitro* and *in vivo*. J Control Release 2007;119:77–85.

Miyairi S, Sugiura M, Fukui S. Immobilized β-glucosidase in fibroin membrane. Agric Biol Chem 1978;42:1661-1667.

Moioli EK, Hong L, Guardado J, Clark PA, Mao JJ. Sustained release of TGFβ3 from PLGA microspheres and its effect on early osteogenic differentiation of human mesenchymal stem cells. Tissue Eng 2006;12:537-546.

Murphy AR, Kaplan DL. Biomedical applications of chemically-modified silk fibroin. J Mater Chem 2009;19:6443-50.
Nagarkar S, Nicolai T, Chassenieux C, Lele A. Structure and gelation mechanism of silk hydrogels. Phys Chem Chem Phys 2010;12:3834–3844.
Nandi SK, Mukherjee P, Roy S, Kundu B, De DK, Basu D. Local antibiotic delivery systems for the treatment of osteomyelitis – a review. Mater Sci Eng 2009;C29:2478–2485.
Nathwani BB, Jaffari M, Juriani AR, Mathur AB, Meissner KE. Fabrication and characterization of silk-fibroin-coated quantum dots. IEEE Transactions on Nanobioscience 2009;8:72-77.
Nazarov R, Jin HJ, Kaplan DL. Porous 3-D scaffolds from regenerated silk fibroin. Biomacromolecules 2004;5:718–26.
Nuanchai K, Prasong S, Wilaiwan S. *In vitro* degradation of *Bombyx mori* silk fibroin films exposed to protease XXIII. Biotechnology 2009;8:468-472.
Numata K, Kaplan DL. Silk-based delivery systems of bioactive molecules. Adv Drug Deliv Rev. 2010;62:1497-1508.
Numata K, Kaplan DL. Mechanisms of enzymatic degradation of amyloid β microfibrils generating nanofilaments and nanospheres related to cytotoxicity. Biochemistry 2010;49:3254-3260.
Nuttelman CR, Tripodi MC, Anseth KS. Dexamethasone-functionalized gels induce osteogenic differentiation of encapsulated hMSCs. J Biomed Mater Res A 2006;76:183-195.
O'Hagan DT, Rahman D, McGee JP, Jeffery H, Davies MC, Williams P, Davis SS, Challacombe SJ. Biodegradable microparticles as controlled release antigen delivery systems. Immunology 1991;73: 239– 242.
O'Hara TM, Bennett L, McCoy CP, Jack SW, Fleming S. Lead poisoning and toxicokinetics in a heifer and fetus treated with $CaNa_2EDTA$ and thiamine. J Vet Diagn Invest 1995;7:531-537.
O'Malley GF, Dominici P, Giraldo P, Aguilera E, Verma M, Lares C, Burger P, Williams E. Routine packing of simple cutaneous abscesses is painful and probably unnecessary. Acad Emerg Med 2009;16:470–473.
Omenetto FG, Kaplan DL. SnapShot: silk biomaterials. Biomaterials 2010-1;23:6119-6120
Omenetto FG, Kaplan DL. New Opportunities for an Ancient Material, Science 2010-2;329: 528-31.
Omelczuk MO, McGinity JW. The influence of polymer glass transition temperature and moelcuar weight on drug release from tablets containing poly(DL-lactic acid). Pharmaceut Res 1992;9:26-32.
Østergaard J, Larsen SW, Parshad H, Larsen C. Bupivacaine salts of diflunisal and other aromatic hydroxycarboxylic acids: aqueous solubility and release characteristics from solutions and suspensions using a rotating dialysis cell model. Eur J Pharm Sci 2005;26:280–287.
Pandit MW, Sagar AJ, Rao MSN. Studies on silk fibroin. Molecular weight, sedimentation coefficient, viscosity and optical rotation of silk fibroin from carbonate-extracted silk fiber. Arch Biochem Biophys 1972;149:259-268.
Panilaitis B, Altman G, Chen J, Jin HJ, Karageorgiou V, Kaplan, DL. Macrophage responses to silk. Biomaterials 2003;24:3079–3085.
Park TG. Degradation of poly(D,L-lactic acid) microspheres: effect of molecular weight. J Control Release 1994;30:161-173.

Park S-H, Gil ES, Shi H, Kim HJ, Lee K, Kaplan DL. Relationships between degradability of silk scaffolds and osteogenesis. Biomaterials 2010;31:6162-6172.
Patil SD, Papadmitrakopoulos F, Burgess DJ. Concurrent delivery of dexamethasone and VEGF for localized inflammation control and angiogenesis. J Control Release 2007;117: 68–79.
Petrini P, Parolari C, Tanzi MC. Silk fibroin-polyurethane scaffolds for tissue engineering. J Mater Sci-Mater M 2001;12:849-853.
The Practice Committee of the American Society for Reproductive Medicine. Hormonal contraception: recent advances and controversies. Fertil Steril 2004;82:520-526.
Price, JS, Tencer AF, Arm DM, Bohach GA. Controlled release of antibiotics from coated orthopedic implants, J Biomed Mater Res 1996;30:281–286.
Price Evans DA, Tariq M, Sujata B, McCann G, Sobki S. The effects of magnesium sulphate and EDTA in the hypercholesterolaemic rabbit. Diabetes Obes Metab 2001;3:417-422.
Pritchard EM, Szybala C, Boison D, Kaplan DL. Silk fibroin encapsulated powder reservoirs for sustained release of adenosine. J Control Release 2010;144: 159–167.
Puppi D, Chiellini F, Piras AM, Chiellini E. Polymeric materials for bone and cartilage repair. Prog Polym Sci 2010;35:403–440.
Putthanarat S, Eby RK, Naik RR, Juhl SB, Walker MA, Peterman E, Ristich S, Magoshi J, Tanaka T, Stone MO, Farmer BL, Brewer C, Ott D. Nonlinear optical transmission of silk/green fluorescent protein (GFP) films. Polymer 2004;45:8451–8457.
Quenelle DC, Winchester GA, Staas JK, Barrow ELW, Barrow WL. Treatment of tuberculosis using a combination of sustained-release rifampicin-loaded microspheres and oral dosing with isoniazid. Antimicrob agents ch 2001;45:1637-1644.
Racine R. Kindling: the first decade. Neurosurgery 1978;3:234–252.
Rajkhowa R, Wang L, Kanwar JR, Wang X. Molecular weight and secondary structure change in eri silk during alkali degumming and powdering. J Appl Poly Sci 2011;119:1339-1347.
Ramkissoon-Ganorkar C, Liu F, Baudys M, Kim SW. Modulating insulin-release profile from pH/ thermosensitive polymeric beads through polymer molecular weight. J Control Release 1999;59:287–298.
Raza MW, Shad A, Pedler SJ, Karamat KA. Penetration and activity of antibiotics in brain abscess. J Coll Physicians Surg Pak 2005;15:165-167.
Ribeiro JA, Sebastião AM, de Mendonça A. Adenosine receptors in the nervous system: pathophysiological implications. Prog Neurobiol 2003;68:377–392.
Ritger PL, Peppas NA. A simple equation for description of solute release I. Fickian and non-fickian release from non-swellable devices in the form of slabs, spheres, cylinders or discs. J Control Release 1987;5:23–36.
Roberts, MH, Bentley MD, Harria JM. Chemistry for peptide and protein PEGylation. Adv Drug Delivery Rev 2002;54:439-476.
Rosenfeld SS, Taylor EW. Reactions of 1-N^6-ethenoadenosine nucleotides with myosin subfragment 1 and acto-subfragment 1 of skeletal and smooth muscle.J Biol Chem 1984;259:11920–11929.
Rouwkema J, Rivron NC, van Blitterswijk CA. Vascularization in tissue engineering. Trends Biotechnol 2008;26:434-441
Rucavado A, Escalante T, Franceschi A, Chaves F, Leon G, Cury Y, *et al*. Inhibition of local hemorrhage and dermonecrosis induced by *Bothrops asper* snake venom: effectiveness of early in situ administration of the peptidomimetic metalloproteinase inhibitor batimastat and the chelating agent $CaNa_2EDTA$. Am J Trop Med Hyg 2000;63:313–319.

Ruszczak Z, Friess W. Collagen as a carrier for on-site delivery of antibacterial drugs. Adv Drug Deliv Rev 2003;55:1679–1698.
Saltzman WM. Drug Delivery: Engineering principles for drug therapy. Oxford: Oxford University Press, 2001.
Saltzman WM, Olbricht WL. Building drug delivery into tissue engineering. Nat Rev Drug Discov 2002;1:177-186.
Sauermann R, Karch R, Langenberger H, Kettenbach J, Mayer-Helm B, Petsch M, Wagner C, Sautner T, Gattringer R, Karanikas G, Joukhadar C. Antibiotic abscess penetration: fosfomycin levels measured in pus and simulated concentration-time profiles. Antimicrob agents ch 2005;49:4448-4454.
Schmitt EA, Flanagan DR, Linhardt RJ. Importance of distinct water environments in the hydrolysis of poly(DL-lactide-co-glycolide). Macromolecules 1994;27:743-748.
Schmutz F, McAuliffe W, Anderson DM, Elliott JP, Eskridge JM, Winn HR. Embolization of cerebral arteriovenous malformations with silk: histopathologic changes and hemorrhagic complications. Am J Neuroradiol 1997;18:1233-1237.
Seo,Y, Yoon H, Song K, Kwon S, Lee H, Park Y, Park J. Increase in cell migration and angiogenesis in a composite silk scaffold for tissue-engineered ligaments. J. Orthop. Res.2009;27:495–503.
Shen X, Wan C, Ramaswamy G, Mavalli M, Wang Y, Duvall CL, Deng LF, Guldberg RE, Eberhart A, Clemens TL, Gilbert SR. Prolyl hydroxylase inhibitors increase neoangiogenesis and callus formation following femur fracture in mice. J Orthop Res 2009;27:1298-1305.
Shi X, Wang Y, Varshney RR, Gong LRY, Wang D-A. Microsphere-based drug releasing scaffolds for inducing osteogenesis of human mesenchymal stem cells *in vitro*. Eur J Pharm Sci 2010;39:59–67.
Siepmann F, Siepmann J, Walther M, MacRae RJ, Bodmeier R. Polymer blends for controlled release coatings. J Control Release 2008;125:1–15.
Silver JM, Shin C, McNamara JO. Antiepileptogenic effects of conventional anticonvulsants in the kindling model of epilespy. Ann Neurol 1991;29:356–363.
Sofia S, McCarthy MB, Gronowicz G, Kaplan DL. Functionalized silk-based biomaterials for bone formation. J Biomed Mater Res 2001;54:139-148.
Sorensen K. An easy microtiter plate-based chromogenic assay for ethylenediaminetetraacetic acid and similar chelating agents in biochemical samples. Anal Biochem 1992;206:210-211.
Stamatialis DF, Papenburg BJ, Gironés M, Saiful S, Bettahalli SNM, Schmitmeier S, Wessling M. Medical applications of membranes: drug delivery, artificial organs and tissue engineering. J Membrane Sci 2008;308:1-34.
Staples JF, Buck LT. Matching cellular metabolic supply and demand in energy-stressed animals. Comp Biochem Physiol A 2009;153:95–105.
Stearne LE, Buijk SL, Mouton JW, Gyssens IC. Effect of a single percutaneous abscess drainage puncture and imipenem therapy, alone or in combination, in treatment of mixed-infection abscesses in mice. Antimicrob Agents Chemother. 2002;46:3712–3718.
Steendam R, van Steenbergen MJ, Hennink WE, Frijlink HW, Lerk CF. Effect of molecular weight and glass transition on relaxation and release behavior of poly(DL-lactic acid) tablets. J Control Release 2001;70:71-82.

Sterchi EE, Stocker W, editors. Proteolytic enzymes: tools and targets. New York: Springer-Verlag, 1999.
Szybala C, Pritchard EM, Lusardi TA, Li I, Wilz A, Kaplan DL, Boison D. Antiepileptic effects of silk-polymer based adenosine release in kindled rats. ExpNeurol 2009;219:126–135.
Tang X, Ding F, Yang Y, Hu N, Gi X. Evaluation of *in vitro* biocompatibility of silk fibroin-based biomaterials with primarily cultured hippocampal neurons. J Biomed Mater Res A 2009;91A:166-174.
Tanzi RE, Moir RD, Wagner SL. Clearance of Alzheimer's Aβ peptide: the many roads to perdition. Neuron 2004;43:605-608.
Tomomura A, Yamada H, Itagaki K, Fujimoto K, Katoh S. Rat brain expresses serum calcium-decreasing factor (caldecrin). Neurosci Lett 200;317:17–20.
Tsukada M, Freddi G, Minoura N, Allara G. Preparation and application of porous silk fibroin materials. J Appl Polym Sci 1994;54:507–514.
Uebersax L, Fedele DE, Schumacher C, Kaplan DL, Merkle HP, Boison D, Meinel L. The support of adenosine release from adenosine kinase deficient ES cells by silk substrates. Biomaterials 2006;27:4599–4607.
Uebersax L, Mattotti M, Papaloïzos M, Merkle HP, Gander B, Meinel L. Silk fibroin matrices for the controlled release of nerve growth factor (NGF). Biomaterials. 2007;28:4449–4460.
Uebersax L, Merkle HP, Meinel L. Insulin-like growth factor I releasing silk fibroin scaffolds induce chondrogenic differentiation of human mesenchymal stem cells. J Control Release 2008;127;12–21.
Uhrich KE, Cannizzaro SM, Langer RS, Shakesheff KM. Polymeric systems for controlled drug release. Chem Rev 1999;99:3181-3198.
Ulubayram K, Kiziltay A, Yilmaz E, Hasirci N. Desferrioxamine release from gelatin-based systems. Biotechnol Appl Biochem 2005;42: 237–245.
Vandamme TF, Ngombo Mukendi J-F. Controlled release of levamisole from poly-(E-caprolactone) matrices: III. Effects of molecular weight and polymer coating on drug release. Int J Pharm 1996;145:77-86.
Varde NK, Pack DW. Influence of particle size and antacid on release and stability of plasmid DNA from uniform PLGA microspheres. J Control Release 2007;124:172–180.
Vekrellis K, Ye Z, Qiu WQ, Walsh D, Hartley D, Chesneau V, Rosner MR, Selkoe DJ. Neurons regulate extracellular levels of amyloid β-protein via proteolysis by insulin-degrading enzyme. J Neurosci 2000;20:1657–1665.
Vepari CP, Kaplan DL. Covalently immobilized enzyme gradients within three-dimensional porous scaffolds. Biotechnol Bioeng 2006;93:1130–1137.
Vepari C, Kaplan DL. Silk as a biomaterial. Prog Polym Sci 2007;32:991-1007.
Vlodavsky I, Fuks Z, Ishai-Michaeli R, Bashkin P, Levi E, Korner G, Bar-Shavit R, Klagsbrun M. Extracellular matrix-resident basic fibroblast growth factor: implication for the control of angiogenesis. J Cell Biochem 1991;45:167-176.
Wang GL, Semenza GL. Desferrioxamine induces erythropoietin gene expression and hypoxia-inducible factor 1 DNA-binding activity: implications for models of hypoxia signal transduction. Blood 1993;82:3610–3615.
Wang J, Chua KM, Wang CH. Stabilization and encapsulation of human immunoglobulin G into biodegradable microspheres. J Colloid Interface Sci 2004;271**:** 92– 101.

Wang X, Kim HJ, Xu P, Matsumoto A, Kaplan DL. Biomaterial coatings by stepwise deposition of silk fibroin. Langmuir 2005;21:11335–11341.
Wang Y, Kim H-J, Vunjak-Novakovic G, Kaplan DL. Stem cell-based tissue engineering with silk biomaterials. Biomaterials 2006;2:6064–6082.
Wang X, Hu X, Daley A, Rabotyagova O, Cebe P, Kaplan DL. Nanolayer biomaterial coatings of silk fibroin for controlled release. J Control Release 2007-1; 121: 190–199.
Wang X, Wenk E, Hu X, Castro GR, Meinel L, Wang X, Li C, Merkle H, Kaplan DL. Silk coatings on PLGA and alginate microspheres for protein delivery. Biomaterials 2007-2;28:4161–4169.
Wang X, Wenk E, Matsumoto A, Meinel L, Li C, Kaplan DL. Silk microspheres for encapsulation and controlled release. J Control Release 2007-3;117: 360–370.
Wang Y, Rudym DD, Walsh A, Abrahamsen L, Kim HJ, Kim HS. *In vivo* degradation of three-dimensional silk fibroin scaffolds. Biomaterials 2008-1;29: 3415-3428.
Wang X, Zhang X, Castellot J, Herman I, Iafrati M, Kaplan DL Controlled release from multilayer silk biomaterial coatings to modulate vascular cell responses. Biomaterials 2008-2;29:894–903.
Wang X, Kluge JA, Leisk GG, Kaplan DL. Sonication-induced gelation of silk fibroin for cell encapsulation. Biomaterials 2008-3;29:1054–1064.
Wang X, Wenk E, Zhang X, Meinel L, Vunjak-Novakovic G, Kaplan DL. Growth factor gradients via microsphere delivery in biopolymer scaffolds for osteochondral tissue engineering. J Control Release 2009;134:81–90.
Wang X, Yucel T, Lu Q, Hu X, Kaplan DL. Silk nanospheres and microspheres from silk/pva blend films for drug delivery. Biomaterials 2010;31:1025–1035.
Wang X, Kaplan DL. Functionalization of silk fibroin with neutravidin and biotin. Macromol Biosci 2011;11:100-10.
Ward DR, Lathrop LB, Lynch MJ. Dissolution and compatibility considerations for the use of mannitol in solid dosage forms. J Pharm Sci 1969;58**:** 1464-1467.
Warnecke C, Griethe W, Weidemann A, Jürgensen JS, William C, Bachmann S, Ivashchencko Y, Wagner I, Frei U, Wiesenet M, Eckardt KU. Activation of the hypoxia-inducible factor-pathway and stimulation of angiogenesis by application of prolyl hydroxylase inhibitors. Faseb J 2003;17:1186–1188.
Wenk E, Wandrey AJ, Merkle HP, Meinel L. Silk fibroin spheres as a platform for controlled drug delivery. J Control Release 2008;132: 26–34.
Wenk E, Meinel AJ, Wildy S, Merkle HP, Meinel L. Microporous silk fibroin scaffolds embedding PLGA microparticles for controlled growth factor. Biomaterials 2009;30:2571–2581.
Wenk E, Murphy AR, Kaplan DL, Meinel L, Merkle HP, Uebersax L. The use of sulfonated silk fibroin derivatives to control binding, delivery and potency of FGF-2 in tissue regeneration. Biomaterials 2010;31:1403–1413
Wenk E, Merkle HP, Meinel L. Silk fibroin as a vehicle for drug delivery applications. J Control Release 2010; in press
White RJ, Cutting K, Kingsley A. Topical antimicrobials in the control of wound bioburden. Ostomy Wound Manage. 2006;52:26–58.
Willerth SM, Sakiyama-Elbert SE. Approaches to neural tissue engineering using scaffolds for drug delivery. Adv Drug Deliv Rev 2007;59:325–338.

Wojcik WJ, Neff NH. Adenosine measurement by a rapid HPLC-fluorometric method: induced changes of adenosine content in regions of rat brain. J Neurochem 1982;39:280–2.
Wooley RE, Jones MS. Action of EDTA-Tris and antimicrobial agent combinations on selected pathogenic bacteria. Vet Microbiol 1983;8:271-280.
Woolfon AD, Malcolm RK, Gallagher RJ. Design of a silicone reservoir intravaginal ring for the delivery of oxybutynin. J Control Release 2003;91:465-476.
Wongpanit P, Ueda H, Tabata Y, Rujiravanit R. *In vitro* and *in vivo* release of basic fibroblast growth factor using a silk fibroin scaffold as delivery carrier. Journal of Biomaterials Science 2010;21: 1403–1419.
Wu Y, Shen Q, Hu S. Direct electrochemistry and electrocatalysis of heme-proteins in regenerated silk fibroin film. Analytica Chimica Acta 2006;558:179–186.
Xuan R, Arisi L, Wang Q, Yates SR, Biswas KC. Hydrolysis and photolysis of oxytetracycline in aqueous solution. J Environ Sci Heal B. 2010;45:73-78.
Yamada H, Nakao H, Takasu Y, Tsubouchi K. Preparation of undegraded native molecular fibroin solution from silkworm cocoons. Mater Sci Eng 2001;C14:41–46.
Yamagata K, Hakata K, Maeda A, Mochizuki C, Matsufuji H, Chino M, Yamori Y. Adenosine induces expression of glial cell line-derived neurotrophic factor (GDNF) in primary rat astrocytes. Neurosci Res 2007;59:467–474
Yang W, Moore IF, Koteva KP, Bareich DC, Hughes DW, Wright GD. TetX Is a Flavin-dependent Monooxygenase Conferring Resistance to Tetracycline Antibiotics. J Biol Chem. 2004;279:52346-52352.
Yang Y, Chen X, Ding F, Zhang P, Liu J, Gu X. Biocompatibility evaluation of silk fibroin with peripheral nerve tissues and cells *in vitro*. Biomaterials 2007-1;28:1643-1652.
Yang Y, Ding F, Wu J, Hu W, Liu W, Liu J, Gu X. Development and evaluation of silk fibroin-based nerve grafts used for peripheral nerve regeneration. Biomaterials 2007-2;28:5526-5535.
Yang Y, Zhao Y, Gu Y, Yan X, Liu J, Ding F, Gu X. Degradation behaviors of nerve guidance conduits made up of silk fibroin *in vitro* and *in vivo*. Polym Degrad Stabil 2009;94:2213–2220
Yeo J-H, Lee K-G, Lee Y-W, Kim SY. Simple preparation and characteristics of silk fibroin microsphere. Eur Polym J 2003;39:1195–1199.
Yoshioka T, Kawazoe N, Tateishi T, Chen G. *In vitro* evaluation of biodegradation of poly(lactic-co-glycolic acid) sponges. Biomaterials 2008;29:3438–3443.
Young S, Wong M, Tabata Y, Mikos AG. Gelatin as a delivery vehicle for the controlled release of bioactive molecules. J Control Release 2005;109:256-274.
Yucel T, Cebe P, Kaplan DL. Vortex-induced injectable silk fibroin hydrogels. Biohys J 2009;97: 2044-2050.
Zhang X, McAuley KB, Goosen MFA. Towards prediction of release profiles of antibiotics from coated poly (DL-lactide) cylinders. J Control Release 1995;34: 175-179.
Zhang Y-Q, Shen W-D, Gu R-A, Zhu J, Xue R-Y. Amperometric biosensor for uric acid based on uricase-immobilized silk fibroin membrane. Analytica Chimica Acta 1998;369: 123-128.
Zhang X, Reagan MR, Kaplan DL. Electrospun silk biomaterial scaffolds for regenerative medicine. Adv Drug Deliv Rev 2009;61: 988–1006.

Zhou S, Deng X, Li X, Jia W, Liu L. Synthesis and characterization of biodegradable low molecular weight aliphatic polyesters and their use in protein-delivery systems. J Appl Polym Sci 2004;91:1848–1856.
Zhou Y, Chu JS, Li JX, Wu XY. Theoretical analysis of release kinetics of coated tablets containing constant and non-constant drug reservoirs. Int J Pharm 2010;385:98–103.
Zilberman M, Elsner JJ. Antibiotic-eluting medical devices for various applications. J Control Release 2008;130: 202-215.
Zolnik BS, Burgess DJ. Effect of acidic pH on PLGA microsphere degradation and release. J Control Release 2007;122:338-344.
Zolnik BS, Leary PE, Burgess DJ. Elevated temperature accelerated release testing of PLGA microspheres. J Control Release 2006;112:293-300.